INSTYTUT PODSTAWOWYCH PROBLEMÓW TECHNIKI
POLSKA AKADEMIA NAUK

ROZPRAWA DOKTORSKA

Termowrażliwe hydrożele napełniane bioaktywnymi nanowłóknami jako rusztowania dla inżynierii tkankowej

Thermosensitive hydrogels loaded with bioactive nanofibers as scaffolds for tissue engineering

mgr inż. Beata Niemczyk-Soczyńska

Praca wykonana w Samodzielnej Pracowni Polimerów i Biomateriałów
pod kierunkiem Prof. dr hab. inż. Pawła Łukasza Sajkiewicza
Promotor pomocniczy: dr inż. Arkadiusz Gradys

WARSZAWA 2023

Badania prowadzone w ramach niniejszej pracy doktorskiej były częścią projektu PRELUDIUM o numerze 2018/29/N/ST8/00780 finansowanego przez Narodowe Centrum Nauki oraz projektu POWER Och! DOK o numerze POWR.03.02.00-00-1028/17-00 realizowanego w ramach Programu Operacyjnego Wiedza Edukacja Rozwój 2014-2020 oraz współfinansowanego ze środków Europejskiego Funduszu Społecznego.

Składam serdeczne podziękowania

Prof. Pawłowi Sajkiewiczowi za podjęcie się opieki, cierpliwość, wyrozumiałość oraz nieocenioną pomoc merytoryczną podczas przygotowywania rozprawy.

Dr Arkadiuszowi Gradysowi za przekazaną wiedzę, poświęcony czas, cenne uwagi oraz zaangażowanie w realizację badań.

Wyrazy wdzięczności koleżankom i kolegom z Samodzielnej Pracowni Polimerów i Biomateriałów za wsparcie merytoryczne, jak również wszelką życzliwość.

Pracę dedykuję Mężowi oraz Rodzicom, którzy do końca we mnie wierzyli i zawsze mnie wspierali.

Spis treści

Abstract

The following thesis summarizes the studies on thermosensitive injectable hydrogel systems loaded with short electrospun bioactive nanofibers as scaffold for tissue engineering applications/3-D cell culture model. The hydrogel system is based on two polysaccharides, consisting of methylcellulose/agarose (MC/AGR) solution. The MC crosslinks physically while heating near the physiological temperature, while AGR increases the MC thermal crosslinking rate and mechanical properties of the hydrogel system. In order to provide both, the extracellular matrix (ECM)-mimicking fibrous structure, injectability and biochemical cues, short bioactive electrospun poly-L-lactic acid (PLLA)/laminin nanofibers were added to the hydrogel system. Differential scanning calorimetry (DSC) and dynamic mechanical analysis (DMA) provided information on the MC physical crosslinking mechanism which is, undoubtedly, crucial for fundamental knowledge. Additionally, both of these methods showed that AGR addition increases the MC crosslinking rate. Addition of AGR also improves MC viscoelastic properties, i.e., the final G' value. Moreover, biocompatibility studies revealed AGR contribution in an increased *in vitro* cellular response and confirmed its non-toxic effect. Optimizing the concentration and ratio between MC and AGR enabled the selection of two compositions that showed the crosslinking rate, viscoelastic properties, and structure adequate for the best support for cell adhesion, proliferation, and differentiation.

PLLA/laminin nanofibers were obtained via electrospinning, and fibers fragmentation took place via ultrasonication. Biochemical cues of short fibers were acquired due to laminin incorporation via physical adsorption. In this part, not only obtained fibers were investigated but also the short fibers fabrication process was optimized and thoroughly investigated in terms of applying different ultrasonication parameters, sonication media and duration of the process. Optimizing the short fibers fabrication process allowed the selection of an adequate sonication medium and the relevant fragmentation time. A gel permeation chromatography (GPC) demonstrated that electrospinning and ultrasonic fragmentation do not cause polymers' molecular weight degradation, while wide-angle x-ray scattering (WAXS) results showed the ultrasonication process could influence PLLA crystallinity. The obtained short PLLA fibers morphology was characterized via Scanning Electron Microscopy (SEM) and the fibers' average length was in the range of 40-60 μm.

The short PLLA fibers were functionalized with laminin - native ECM protein - via physical adsorption. Water contact angle (WCA) measurements and bicinchoninic acid assay showed

that the greatest amount of the protein was incorporated into the PLLA short fibers that had previously been treated with ethanol.

The ultimate MC/AGR hydrogel loaded with short PLLA/laminin fibers was characterized in terms of viscosity, injection ability, morphology and the cellular morphology of L929 fibroblasts, LN-18, and WG-4 glioma cells. The viscosity tests indicated the shear-thinning character of the MC/AGR systems, which increases its tendency with the thermal crosslinking of the hydrogels. Higher viscosity was also observed after short fibers addition to the hydrogel. The injection ability measurements of dynamic glide forces and maximum forces indicate that, depending on the injection rate, hydrogels loaded with short fibers could be injectable via 23G needle. Morphology of the system mimics the native ECM. This result is consistent with the biocompatibility studies, which showed that short PLLA/laminin fibers increase the cells-hydrogel interactions, indicated by fast growth and proliferation of fibroblasts and WG4 glioma cells.

The results of the study provide indications that the obtained composite hydrogel is a very promising system as a scaffold or a 3-D cell culture model from the perspective of tissue engineering.

1. Introduction

Tissue engineering is an interdisciplinary field of science focused on implementing modern technologies and on the progress of medicine to improve, regenerate or maintain desired tissues and restore their functions. Biomaterial scaffolds play a key role in applications dedicated to tissue engineering by providing an appropriate environment and support for cell adhesion, proliferation, as well as directing cell fate to new tissue formation [1]. The biomaterial scaffold should meet specified requirements imposed by tissue engineering. The general ones demand materials biocompatibility, controlled biodegradability, desired morphology that allows efficient cell infiltration and nutrient transportation, appropriate biochemical and mechanical properties that correspond to dedicated tissue. Depending on the type of dedicated tissues and their complexity, there could be more specific requirements. For instance, biomaterials dedicated to cartilage, bone or neural tissue engineering should provide a faithfully extracellular matrix (ECM) imitating environment to withstand newly formed cells' viability, enable vascularization, and facilitate proper structural support for cells.

The contemporary state of the art in clinical therapies dedicated to such complicated tissues as the brain, spinal cord, or cartilage injuries are mainly founded on stimulating surgeries and transplantation [2,3]. Nevertheless, they usually are complex, and expensive and lead to long-term and painful rehabilitation. Furthermore, such surgeries mostly relieve the pain, but regeneration of such tissues as the brain, spinal cord or cartilage still remains quite a challenge.

A substantial potential alternative of surgeries could be injectable scaffolds, for instance, injectable hydrogels. They are introduced into the body using the minimally invasive method to get to the hardly available sites such as cartilage, or to avoid damage to especially such delicate tissues as the brain and spinal cord, but also to decrease patients' discomfort [4,5]. Such injectable approaches could minimize scarring, be more affordable, and accelerate patients' convalescence.

In recent years, extensive studies on cell-biomaterial relations indicated that cell-ECM interactions have an enormous impact on cell fate. It has been found that ECM has inductive properties and enables soft tissue reconstruction.

Structurally native ECM consists of a highly hydrated structure consisting of glycosaminoglycans (GAGs), associated with them proteoglycans so called interstitial network. The interstitial network is loaded with dense protein fiber meshes, i.e., the basement membrane.

From the chemical point of view, the major components of ECMs are hyaluronic acid belonging to the group of glycosaminoglycans and proteins such as collagen, fibronectin or laminin. From a biochemical perspective, a crucial role in cell signaling plays particular peptide sequences interacting with integrins present on the cell membrane's surface. In this respect, arginine–glycine–aspartate (RGD) found naturally in collagen or fibronectin, and valine–alanine–valine (IKVAV) occurring in laminin are those sequences, so-called binding sites, that support cell-ECM integrity, and further tissue regeneration [6 ,7 ,8].

Considering the current needs of tissue engineering and the ECM nature, the combination of hydrogels and bioactive nanofibers seems to be an attractive approach in the area of scaffold for tissue regeneration.

Hydrogels are polymers that form 3-D highly hydrated polymeric networks by the unique ability of water absorption and retention in the structure. They are highly attractive from the biomedical perspective due to excellent biocompatibility, easy processing ability, and structural resemblance to native ECM, to the interstitial network particularly. Moreover, some

of them could be rapidly introduced into injured tissue (up to 5 minutes) by injection filling the irregular shape of lesions and increasing effective integration with host tissue. Hydrogels could be crosslinked chemically or physically depending on their desired properties and potential application. Although chemically crosslinked by chemical reactions, materials form permanent junctions providing improved mechanical properties, the crosslinking agents are usually cytotoxic for living cells. The physical crosslinking based on ionic bonds, hydrogen bonds, molecular entanglements, or hydrophobic interactions is impermanent and weaker than chemical one, but on the other hand, safe for living cells [9,10].

One of the hydrogels' drawbacks is the lack of fibrous structure, which is undoubtedly important support for cell activity. A proper hydrogel functionalization, for instance by the addition of short electrospun fibers is a natural way to overcome that problem. For many years, electrospun fibers enjoyed a great interest in biomedical applications. The fibrous scaffolds seeded with cells could be implanted to the site of damaged tissue providing its regeneration or fibrous mats could serve as drug carriers for drug delivery system applications. It is the result of their attractive properties, i.e., the ECM mimicking fibrous structure, biodegradability, porosity supporting cell attachment, proliferation and differentiation [11]. Additionally, the electrospinning method allows immobilizing signaling molecules easily, obtaining a wide range of fiber size from a few manometers to tens of microns, controlling fibers alignment as well as using electrospinning methods allows scaling up production rate which is crucial from the industry points of view [12].

Nevertheless, electrospun fibers could be introduced into the organism by surgery only, which narrows their application scope in some fields of tissue engineering. Electrospun fibers fragmentation might provide them new properties such as dispersity in liquids, for instance in not crosslinked hydrogels, and injection ability at the same time keeping the fibrous structure mimicking native ECM fibers.

Although there are some publications of the conjugation of short electrospun fibers into injectable hydrogels, e.g., [13,14], there is still a lack of thorough and systematic investigations using such composites. Additionally, most of the short electrospun fibers fabrication techniques require some improvements.

In this PhD dissertation systematic investigation of unique, yet not described in the literature injectable hydrogel/electrospun fibers composite consisting of MC/AGR hydrogel loaded with PLLA/laminin short nanofibers was performed. The obtained composite material

combined injection ability, thermally induced physical crosslinking, mechanical stability and structure mimicking native ECM supporting cell attachment and proliferation.

2. Aim of the study

The study was aimed at designing a smart injectable thermosensitive hydrogel system loaded with short fibers that could serve as a scaffold for tissue engineering applications. The composition and fabrication process should provide material properties, which not only assures injectability and *in situ* crosslinking after injection, but also mimics the ECM. To accomplish this goal, it was necessary to select adequate components, their concentration, and ratio, the fabrication process and its parameters as well as the methods and methodology of materials characterization:

1. Systematic investigation of MC hydrogel at various solution concentrations in order to select optimal MC hydrogel concentrations from the perspective of the crosslinking rate, viscoelastic properties, and cellular response.

2. Systematic investigations of various concentrations and ratios of MC and AGR solutions and selection of optimal proportions of MC/AGR systems. Characterizing the hydrogel system in terms of thermal effects, crosslinking rate, viscoelastic properties, as well as biological properties.

3. Electrospinning of PLLA nanofibers, their ultrasonic fragmentation, and subsequent functionalization with laminin. Characterization of short bioactive electrospun nanofibers as regards structure, wettability, amount of immobilized protein, and distribution in hydrogel solution.

4. Optimization of the proportions, i.e., concentrations and contributions in the solution, between particular components of hydrogel, i.e., MC and AGR, as well as short bioactive PLLA/laminin fibers to obtain the injectable material with proper ECM-mimicking structure that was the best support and environment for the functioning and proliferation of cells. Characterization of the composite in terms of viscosity, injectability, and biological properties, to assess its value from the perspective of tissue engineering and 3-D tumor culturing model.

3. Hypothesis

The following scientific hypothesis was stated: there exists an optimal chemical composition and a fabrication process to obtain a smart thermosensitive injectable hydrogel composite made of MC/AGR solution with the addition of PLLA/laminin short electrospun fibers, which fairly mimics the native extracellular matrix and may be suitable for tissue engineering applications and their derivatives, e.g., 3-D cell culture models.

4. Materials

The hydrogel system consists of two polysaccharides: methylcellulose and agarose. MC is a well-known smart stimuli-responsive material that under the change of temperature undergoes a reversible sol-gel transition. Moreover MC is nontoxic, easily processable, stable in physiological conditions, FDA-approved and biocompatible. In MC, methylated cellulose, hydroxyl groups are substituted with methoxy groups (-OCH_3). Such modification, contrary to classic cellulose, makes MC water soluble and results in physical crosslinking during heating. MC shows an inverse thermal crosslinking nature, manifested by the Lower Critical Solution Temperature (LCST). While the material is below the LCST, it is fully miscible with the solvent in all proportions, forming a homogeneous solution (sol). On the other hand, while the material is heated above the LCST, it shows only partial liquid miscibility, and the phase separation occurs due to changes in molecular interactions.

Thermodynamically, the separation between the two phases results from the negative entropy of mixing between the polymer and the solvent. This entropy component increases with temperature, counteracting the favorable enthalpy contribution that is caused by formation of the hydrogen bonds between hydrophilic components of the polymer and the surrounding water molecules. Upon reaching the temperature at which the entropic term predominates, the hydrated conformation, present at low temperature, changes to a contracted conformation, minimizing contact with water, and the contracted polymer coils start aggregating into larger structures. In a result, polymer-polymer interactions dominate in the solution and form a three-dimensional hydrogel network resulting in the formation of gel [15, 16, 17].

Depending on materials properties, i.e., substitution degree of -OCH_3 groups, materials concentration, or additives such as salts but also on the heating rate, the LCST occurs for MC in the range of c.a. 30-80 °C [9].

While the MC solution is heated up near 37 °C, the two-staged crosslinking occurs as a consequence of physical interactions. At room temperature, the MC hydrophilic -OH groups interact strongly with water molecules, i.e., polymer-solvent interactions. The -OCH_3 groups are surrounded by so-called “water cages" providing hydrophobic hydration around hydrophobic parts of MC [18, 19]. This results in weak polymer-solvent interactions, and strong solvent-solvent interactions prevent MC crosslinking at ambient temperature. While MC solution is heated to c.a. 37 °C the water cages are destroyed, which expose -OCH_3 groups that start to interact with each other increasing the contribution of polymer-polymer interactions in the solution. These dependencies characterize the 1st MC crosslinking stage. The subsequent heating leads to formation of hydrophobic aggregates and afterward a three-dimensional fibril hydrogel network. These interactions are referred to as the 2nd MC crosslinking stage [20, 21].

MC has no bioactive receptors providing effective cell-material suitability and interactions. Moreover, it needs a long period of time to form a fully thermally crosslinked 3-D network, thus, AGR was selected as an additive for improving the crosslinking rate and viscoelastic properties of MC.

AGR is a linear polymer made up of repeating agarose units consisting of D-galactose and 3,6-anhydro-L-galactopyranose, isolated and purified from agar or agar-bearing marine algae. AGR shows diverse thermal crosslinking in comparison to MC, it crosslinks upon cooling below room temperature as a consequence of the double helices formation and their subsequent aggregation into microcrystalline junctions [22].

According to the literature [23], the effect of AGR addition resulting in the increased MC crosslinking rate may be explained by a strong attraction to the AGR chains of the water molecules, which detach from the MC chains during the water cages breakage. Additionally, the interpenetrating MC and AGR chains lead to higher density of the hydrogel network enhancing the polymer-to-polymer chains interactions and mechanical properties.

a)

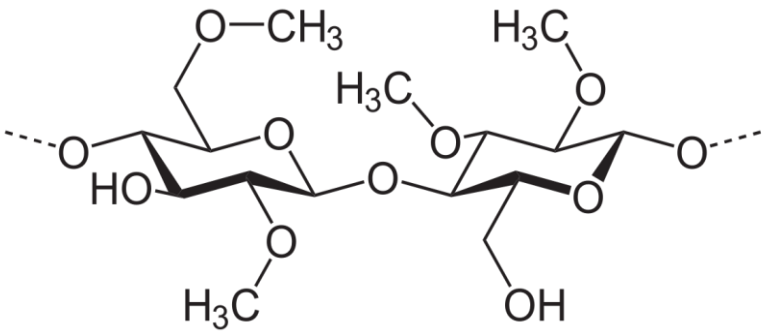

b)

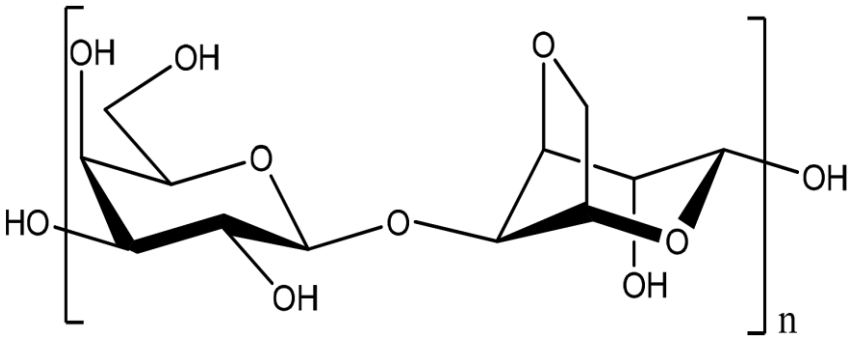

Figure 1. Chemical structure of a) methylcellulose [24], b) agarose [25].

The third component, which was loaded into the hydrogel system, consisted of short electrospun PLLA/laminin fibers. The PLLA is an aliphatic polyester, which is broadly used for electrospinning of scaffolds for tissue engineering applications. This polymer and PLLA-based scaffolds characterize great biocompatibility, biodegradability, structure, and stiffness similar to some types of native tissues, e.g., nerve tissue [26]. Moreover, PLLA is characterized by glass transition temperature (T_g) above room temperature, thus, the electrospun PLLA fibers were selected for the study due to their relative brittleness, which enables efficient fiber fragmentation by ultrasonication. Additionally, PLLA fibers' surface could be easily functionalized with proteins containing signaling molecules allowing overcoming the biochemical inertia characteristic for unfunctionalized aliphatic polyesters. For this purpose, one of the key ECM components of laminin providing IKVAV (Ile-Lys-Val-Ala-Val) signaling molecules was immobilized to the surface of fibers. Laminin, as a major compound of ECM basement membrane, by the presence of IKVAV groups, strongly affects cellular adhesion, morphology, growth, migration, and proliferation [27]. The presence of the protein on PLLA short fibers surface furthermore increases their hydrophilicity. It is well-known that laminin

presence efficiently regenerates nerves, i.e., injured axons and efficiently binds Schwann cells [28, 29]. Moreover, some recent findings suggest laminin natively occurring in cartilage is responsible for tuning such chondrocyte activities as adhesion, migration and proliferation [30]. Literature reports, e.g., [31, 32] suggest the scaffolds' functionalization with laminin could provide their increased bioactivity through increased activity of cartilage-forming cells.

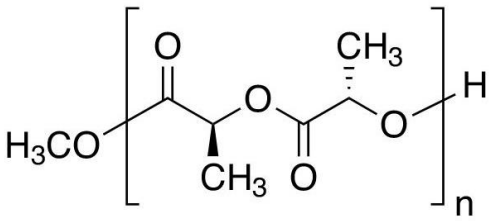

Figure 2. Chemical structure of PLLA.

5. Methods

5.1. MC and MC/AGR characterization

5.1.1. Differential scanning calorimetry (DSC)

DSC is a method that registers changes in the heat flow that come to/from a sample as a function of time/temperature, enabling detection of thermal effects accompanying a phase transition. It was used to detect the thermal effects during the MC crosslinking in order to investigate the process, including its kinetics along with the effect of AGR addition. The details of the DSC procedures were described in particular papers.

5.1.2. Dynamic mechanical analysis (DMA)

DMA is a method that characterizes the polymer's viscoelastic properties by measuring the materials response to applied sinusoidal oscillatory force (stress σ) in the form of materials strain (ε). In DMA two main parameters are measured: the storage modulus (E') and the loss modulus (E"). The first one is characteristic of elastic materials and measures the energy stored by materials. The second one is characteristic of viscous materials and measures energy dissipated by the material.

DMA allowed for estimating the dependence between MC concentration, its crosslinking rate and the hydrogels' final viscoelastic properties (stiffness). The storage and loss modulus were defined for shearing as G' and G", respectively. Usually, the G' and G" curves

intersection followed with G’ advantage over G”, indicates the crosslinking point of the materials [33]. Since intersection points have not been registered but the G’ dominance over G” was visible, the crosslinking rate was determined from the time derivative of G’. Additionally, the method allowed to evaluate the material's stiffness as the final G’ of the hydrogel.

5.1.3. Biocompatibility studies

The biocompatibility studies were conducted to evaluate materials cytotoxicity, cellular morphology and distribution on Mouse Fibroblasts (L929) and Human Bone-Marrow Derived Mesenchymal Stem/Stromal Cells (hBM-MSCs) after 1, 3 and 5 days to assess MC hydrogels value as biomaterials.

The cytotoxicity test was conducted on extracts using Presto Blue assay. In this respect, various hydrogels extracts were added to wells with cells and after 1-3 days cellular viability in comparison to TCP was analyzed. The obtained cell viability was analyzed according to the EU ISO 10993-5:2009 “Biological evaluation of medical devices: —Tests for in vitro cytotoxicity” standard for biological safety assessments for medical devices and their intended use.

The morphology of cells seeded on hydrogels via scanning electron microscopy (SEM) and fluorescence microscopy (FM) showed fibroblasts infiltrated the hydrogels at some point. The infiltration was particularly evident from FM images, where cell density and viability were increased in comparison to the control. Depending on FM focusing and hydrogel depth, different cell infiltration has been observed.

5.1.4. Degradation rate

Degradation tests were performed on selected samples to evaluate whether materials are biodegradable, stable in physiological conditions, and whether degradation time is compatible with dedicated tissue regeneration. In order to mimic the physiological conditions, the tests were performed in PBS at 37 °C .

5.2. Fabrication of short electrospun PLLA fibers, their modification with laminin and characterization

5.2.1. Electrospinning

Electrospinning is a fibrous materials formation method widely used for many kinds of polymers in many fields of science and industry. During electrospinning, a syringe pump

polymer solution is extruded through the syringe. While achieving the applied high voltage, the pendant drop of polymer forms a highly electrified cone jet. Consequently, electrostatic forces overcome the polymer solutions' surface tension, and the liquid jet extrudes from the cone. The polymer solution jet is stretched, the polymer solvent evaporates, and the polymer micro-/nanofibers are collected on a collector, which is usually grounded [11].

The electrospinning method was used for fabrication of aligned PLLA fibers.

PLLA with various molecular weights of Mw ~ 217− 225 kDa, Mw ~ 260 kDa, and Mw ~ 330 kDa was used for electrospinning. The PLLA samples were dissolved in 1,1,1,3,3,3, -hexafluoro-2-propanol (HFIP) and electrospun using Bioinicia horizontal setup (Valencia, Spain), with the flow rate in the range of 1-2 ml/h and applied high voltage in the range of 12-14 kV. The fibers were collected on a grounded rotational collector with an electric potential of -2kV, achieving high speeds up to 1000 rpm to obtain ultimately aligned fibers.

5.2.2. Ultrasonic fragmentation of electrospun fibers

Ultrasonic homogenization is a method that uses high-quality ultrasonic vibration and cavitation to generate strong shear forces to break down molecules and droplets, leading to the reduction of agglomerates in the liquid suspensions and provide homogeneous dispersions in the solutions [34]. Besides homogenization of solid and liquid suspensions, particle size reduction, or intensification of soluble dissolution, the method is perfect for some electrospun fibers fragmentation, which was used and described in this study.

5.2.3. Morphology

Scanning electron microscopy (SEM) is widely used to image microstructures' surfaces. Through the interaction of the electron beam with the atoms of investigated material, a virtual image is created that reflects the sample's topography or determines the elemental composition depending on the detector used.

The method was used to study electrospun fibers and fragmented fibers morphology, i.e., alignment, average diameter and length as well as corresponding distributions.

Additionally, the ImageJ software with the Fiji directions plugin was used to evaluate fiber alignment, average diameter, and length distribution. The plugin generated fiber orientation histograms showing the number of fibers in a given direction in the analyzed SEM image using

the Fourier image analysis method [35]. While the parameters of average diameter and length distributions were calculated by means of 100 fibers measurements, the histograms were generated and subsequently fitted with Gaussian/biphasic dose-response functions, of which a half-width was designated.

5.2.3. Wide-angle x-ray scattering (WAXS)

The WAXS was used for the evaluation of the crystallinity degree of each PLLA fibers.

In the study, a CuKα radiation (λ=1.5418 Å) at a voltage of 40 kV, a current of 20 mA, in coupled theta, and 2Theta mode was used to register the radial profiles. A diffraction angle of 2θ was in the range of 6-30 degrees, the results collection time at the angular point was 1 s. From the obtained results, a background scan was subtracted via Bruker evaluation software. Subsequently, the scans were analyzed numerically via PeakFit software. The results were deconvoluted using Gauss functions for amorphous scattering, while for crystal scattering diffraction a Pearson VII function was used. The crystallinity degree was determined as a ratio of the area of crystalline diffraction peaks and the overall area in the analyzed range of scattering.

5.2.4. Gel permeation chromatography (GPC)

GPC, also called Size Exclusion Chromatography (SEC), is a high-performance liquid chromatography type that provides information on molecular weight distribution for a particular material. GPC involves the relationship between the logarithm value of the molecular weight of separated molecules and the volume of elution from the column as a linear correlation.

The GPC studies led to evaluate whether number average (M_n) and weight average (M_w) molecular weights of PLLA changes after electrospinning and subsequent ultrasonic fragmentation.

5.2.5. Water contact angle (WCA) measurements via goniometer

The WCA measurements allow to analyze of the materials' surface properties, such as wettability or surface energy [36]. The most common analysis is sessile drop contact angle measurement, in which a droplet is dispensed from the syringe placed perpendicularly to the sample surface.

The WCA measurements allowed determining the fibers' surface wettability change before and after the hydrophilic functionalization via physical adsorption of laminin. The studies were carried out with the sessile drop method, dispensing 2 µl of a deionized water drop. The contact angles were measured at 1 s and 3 s.

5.2.6. Bicinchoninic acid assay (BCA) assay

A BCA protocol assumes the reduction of Cu 2^+ to Cu^+ by residues of cysteine, cystine, tryptophan, and tyrosine as well as peptide bonds in proteins while being in an alkaline solution [37]. The chelation reaction of two bicinchoninic acid molecules with Cu^+ generates purple-colored products with an intensity adequate to the protein concentration, which presents a strong absorbance at 562 nm. The absorbance increases linearly with the protein concentration at a wide range of 5-2000 µg/mL.

In this study, the BCA assay led to quantitatively determining the amounts of laminin after its adsorption to the PLLA fibers. The details were described in one of the publications included in the cycle.

5.3. MC/AGR /PLLA/laminin system characterization

5.3.1. Viscosity measurements via rotational viscometer

The use of a viscometer allowed for measuring and evaluating studied liquids' viscosity during liquid flow conditions. The viscosity could be investigated via U-tube, falling-ball, falling-piston, vibrational and rotational viscometers [38]. In our studies, the rotational viscometer was used. Rotational viscometer provides the value of the torque that is required to rotate a spindle immersed in a fluid at an applied constant speed. The continuous spindles' rotation allows proper calculations and time-dependent fluid analysis.

The measurements via rotational viscometer at two constant temperatures of 22 °C and 37 °C and various shear rates allowed to study the viscosity of solutions before and after physical crosslinking, as well as register changes after short fibers addition.

The viscosity studies were conducted with applied constant shear rates of 50, 100, 200, 300, 400, 500, and 500 s^{-1}. The viscosities being out of the measuring range were extrapolated numerically using the Carreau regression model, which was well-approximated to the experimental values [39].

5.3.2. Injection ability

Injectability was studied to evaluate the practical usability of a hydrogel system loaded with short fibers by measuring the force at applied flow rates of 1 ml/min and 0.125 ml/min. The maximum force needed to inject the composite material was taken into account during further analysis. This maximum force during injection was determined as the value averaged from three measurements. The obtained values were compared with the literature value considered as reasonable forces to make an injection by humans.

Injectability studies were conducted using an electronically controlled servo hydraulic loading actuator. The measurements were conducted using two measuring ranges of max. 125 N and max. 1000 N. The syringe loaded with hydrogel solution was attached to a dedicated holder, where the tip of the piston touched the dynamometer, while the syringe targeted downwards. The hydrogel solutions were extruded through the syringe into hydrogel-simulated human tissue, i.e., thermally crosslinked MC hydrogel with mechanical properties similar to the native human spinal cord [40].

All of the measurements were received using an individually prepared dedicated electronic code (MTS Systems testing environment).

5.3.3. Morphology

The MC/AGR/PLLA/laminin systems morphologies were investigated using a SEM to determine the morphology of short fibers in hydrogels with emphasis on the similarity of the composite structure to the native ECM.

Prior to imaging, the samples were stored at -70 °C overnight and subsequently freeze-dried. The freeze-dried samples were sputtered with 8 nm of gold. The images were captured at an acceleration voltage of 7 kV.

5.3.4. Biocompatibility studies

The MC/AGR /PLLA/laminin hydrogel/short fibers systems were investigated similarly to previous biocompatibility studies. In this respect, the cytotoxicity of the composites and cellular morphology of L929 fibroblasts were tested after 1, and 3 days according to the EU ISO 10993-5:2009 standard to evaluate the biological safety of the proposed approach.

Additionally, LN18 and WG4 glioma cell lines were used to evaluate the morphology of the cells seeded on the hydrogel system via FM.

6. Articles included in the publication cycle of the dissertation

1. Niemczyk B., Sajkiewicz P., Kołbuk D., Injectable hydrogels as novel materials for central nervous system regeneration, *Journal of Neural Engineering*, Vol.15, No.5, pp.051002-1-15, 2018.

2. Niemczyk-Soczyńska B., Gradys A., Kołbuk D., Krzton-Maziopa A., Sajkiewicz P., Crosslinking kinetics of methylcellulose aqueous solution and its potential as a scaffold for tissue engineering, *Polymers*, Vol.11, No.11, pp.1772-1-17, 2019.

3. Niemczyk-Soczyńska B., Gradys A., Sajkiewicz P., Hydrophilic surface functionalization of electrospun nanofibrous scaffolds in tissue engineering, *Polymers*, Vol.12, No.11, pp.2636-1-20, 2020.

4. Niemczyk-Soczyńska B., Dulnik J., Jeznach O., Kołbuk D., Sajkiewicz P., Shortening of electrospun PLLA fibers by ultrasonication, *Micron*, Vol.145, pp.103066-1-8, 2021.

5. Niemczyk-Soczyńska B., Sajkiewicz P., Gradys A., Toward a Better Understanding of the Gelation Mechanism of Methylcellulose via Systematic DSC Studies, *Polymers*, Vol.14, No.9, pp.1810-1-13, 2022.

6. Niemczyk-Soczyńska B., Gradys A., Kołbuk D., Krztoń-Maziopa A., Rogujski P., Stanaszek L., Lukomska B., Sajkiewicz P., A methylcellulose/agarose hydrogel as an innovative scaffold for tissue engineering, *RSC Advances*, Vol.12, No.41, pp.26882-26894, 2022.

7. Niemczyk-Soczyńska B., Kołbuk D., Mikułowski G., Ciechomska I., Sajkiewicz P., Methylcellulose/agarose hydrogel loaded with short electrospun PLLA/laminin fibers as injectable scaffold for tissue engineering/3D cell culture model for tumour therapies, *RSC Advances*, Vol. 13, No.18, pp. pp.11889-11902, 2023.

Table 1. Summary of bibliographic data included in the dissertation.

Publication number	**IF**	**Scores MNiSW 2019**	**Scores divided by the number of co-authors**	**Citation number (Scopus)**	**Citation number (Web of Science)**
1	4.551	35	11.7	42	39
2	3.426	100	20	20	18
3	4.329	100	33.3	48	42
4	2.39	100	20	7	7
5	4.967	100	33.3	5	5
6	4.036	100	12.5	1	1
7	4.036	100	20	0	0
			Σ= 150.8		

7. Summary of articles included in the publication cycle of the dissertation

7.1. Injectable hydrogels as novel materials for central nervous system regeneration

The experimental studies were preceded by a thorough literature review related to various smart scaffolds dedicated to central nervous system (CNS) regeneration. The publication discusses a major problem of central nervous system tissue engineering arising from the complex anatomical structure and poor self-regenerating capabilities of the brain and spinal cord. Then, the specific neural ECM architecture and mechanical properties of the brain and spinal cord are described to note which material properties are being sought for those applications. Afterward, the various current scaffold-dedicated neural regeneration approaches are discussed considering the fabrication techniques, advantages and disadvantages. The literature experimental cited in this review describing materials-neural cell response were compared and summarized.

This review discussed the current trends in polymeric scaffolds for central nervous system regeneration: their pros and cons, and the potential to provide brain or spinal cord regeneration. The publication put a particular emphasis on smart injectable and non-injectable hydrogels but also their modifications with different types of micro- and nano-additives.

In the review it is concluded that using a single material for such a sophisticated application as CNS tissue engineering is insufficient. Thus, combining various materials, for instance, hydrogels with nanoadditives may provide synergistic improved effects and new properties in previously known and well-described individual materials. This publication allowed particular materials selection with specified properties crucial from the central nervous system perspective, which was subsequently implemented in the current Ph.D. thesis. In this respect, thermosensitive MC/AGR hydrogels loaded with short bioactive electrospun PLLA/laminin nanofibers have been chosen as a promising material combination.

7.2. Crosslinking kinetics of methylcellulose aqueous solution and its potential as a scaffold for tissue engineering

Since current surgeries can carry the risk of complications, are expensive and in many cases lead to a painful recovery and long rehabilitation, injectable hydrogel scaffolds are considered to be an interesting transplanting surgery alternatives. Thus, the state-of-the-art in tissue engineering is directed toward minimally invasive "smart" approaches [41,42].

A notable representative of smart injectable hydrogels is methylcellulose (MC), which presents a unique property - an invertible thermal crosslinking occurring upon the heating at c.a. physiological temperature. Such thermally triggered crosslinking is beneficial from the tissue engineering point of view because it eliminates the use of chemical crosslinking agents or UV light that could be cytotoxic [23]. The crosslinking rate and viscoelastic (mechanical) properties of MC could be easily adjusted by tuning its concentration in a way that could be adequate from the perspective of injectability into the body, mimicking native ECM, and is mechanically suitable for particular tissues.

The aim of this study was to assess the effect of MC concentration on its crosslinking rate, viscoelastic and biological properties to evaluate its significance as a thermosensitive hydrogel for tissue engineering applications.
For this purpose, a wide range of MC concentrations were systematically studied as regards crosslinking using two complementary methods, differential scanning calorimetry (DSC) and dynamic mechanical analysis (DMA), as well as biocompatibility studies using Presto blue cytotoxicity assay and cell morphological characteristics via SEM and FM.

The DSC results showed a multi-staged thermal crosslinking of MC with complex changes in the thermal effects depending on MC concentration. The registered thermograms during heating showed two endotherms corresponding to the two stages of MC crosslinking. The prevalent low-temperature effect accompanies the destruction of water cages, while the high-temperature effect decreases, and both effects shift toward lower temperatures. Additionally, during heating at very low MC concentrations of <2 wt.%, exothermic effects were observed before low- temperature endotherm. This unexpected effect was explained as delayed water cages formation around -OCH_3 groups. Its absence at higher MC concentrations was described as inaccessible space in the solution as an effect of more tightly packed polymer chains.

The thermal effects registered during cooling showed two exotherms, where the high-temperature exotherm was most likely the effect of hydrophobic network destruction, while the low-temperature exotherm was an effect of the formation of water cages around hydrophobic molecules of MC. The exotherms registered during cooling indicated the complex thermoreversible nature of MC crosslinking.

The phase diagram showed that below the T_{onset} of water cages' breaking (the low-temperature endotherm) the MC was in the single-phase sol form, while during water cages' breaking and hydrophobic domains formation (the low- and high-temperature endotherm) the sol-gel transition occurred. Above the temperature of hydrophobic domains formation (the high-temperature endotherm), the fully crosslinked MC hydrogel has occurred.

The DSC results showed that a low MC concentration, the rates of water cages' formation, of their further breaking and hydrophobic interactions formation, they follow different trends. The water cages' formation rate increased with MC concentration to some extent (<2 wt.%), as a result of the increased contribution of MC molecules. Above 2 wt.% MC, the formation of water cages does not occur. The water cages' destruction followed by hydrophobic aggregates formation are the only processes that take place at higher MC concentrations during heating.

The rate of water cages' destruction and hydrophobic aggregates formation decreased with MC concentration as a consequence of decreased molecular mobility of MC chains. Furthermore, the temperature also influenced the crosslinking rate. The destruction of water cages and subsequent hydrophobic domains formation occurring at higher temperatures is faster than at lower ones.

The DSC results outlined here were preliminary, and the further, more systematic DSC studies on some points, e.g., on the formation of water cages (exothermic effect), provided a new perspective on MC crosslinking. The details are described in Section 7.6.

The DMA results indicated complex and approximately sigmoidal G' growth, allowing determination of the final G' of crosslinked hydrogel. For low MC concentrations, the G' changes were ambiguous and not clear, while at higher MC concentrations the curves showed smooth G' growth with an evident plateau.

The analysis of dG'/dt dependencies showed that the maximum rate of crosslinking is highly dependent on applied temperature, heating time, and MC concentration. The complex crosslinking observed at small MC concentrations is most likely the effect of relatively large distances between methoxy groups, making crosslinking process more difficult. For the higher MC concentrations, the time and temperature used were sufficient to create a fully crosslinked

network. The high MC concentrations showed rapid initiation and a very stable course of crosslinking. It was the effect of more tightly packed MC chains, in which fewer water cages were to break and more already formed hydrophobic interactions occurred.
Similarly to DSC studies, the crosslinking rate k from DMA was determined from half-time of transition. The k vs MC concentration showed two local maxima of crosslinking rate at c.a. 3 and 8 wt.%.

As expected, the ultimate viscoelastic properties, determined from G' vs time dependencies, increased with MC concentrations. According to the literature reports [43, 44], biomaterials' mechanical (viscoelastic properties) should correspond to the native tissues. Thus, obtained values were compared with the viscoelastic properties of human tissues. The concentrations being in the range of c.a. 2-3.5 wt.% corresponds to the values of the human spinal cord. On the other hand, viscoelastic properties of higher MC concentrations, i.e., above 6.5 wt.% could be applied as scaffolds for human meniscus or cartilage regeneration.

For MC concentrations up to 5 wt.% cell viabilities were at acceptable levels as nontoxic materials according to EU ISO 10993-5 standard. The biocompatibility studies generally showed that fibroblasts seeded on the MC hydrogels stayed viable throughout the whole culturing duration. Nevertheless, the MC concentrations and higher added hydrogel volumes influenced the metabolic activity and morphology of the L929 cell line. Similarly to cytotoxicity tests above 5 wt.% MC hydrogels occurred to be toxic to the cells: it could be an effect of limited access to oxygen and nutrients as a result of too high hydrogel viscosity.

To sum up, the DSC studies of a wide range of MC concentrations revealed a reversible complex MC thermal crosslinking through the occurrence of two endotherms representing water cages destruction providing the release of hydrophobic -OCH_3 groups and subsequent formation of the 3-D hydrophobic network between released -OCH_3 groups. **Considering investigated viscoelastic and biological properties the MC concentrations being in the range of 2-5 wt.% could be considered to be attractive from the tissue engineering point of view. These concentration ranges were chosen for further more advanced biocompatibility studies.**

7.3. Hydrophilic surface functionalization of electrospun nanofibrous scaffolds in tissue engineering

Since one of the assumed goals was the functionalization of short electrospun PLLA nanofibers with bioactive protein, i.e., laminin, the preparation of the proper theoretical background was required. Most of the aliphatic polyesters including PLLA are hydrophobic and biochemically inert, which is an undesirable property from the perspective of tissue engineering. Hydrophobic polyester fibers do not provide the biochemical cues, i.e., functional groups recognized by cell-binding receptors, that are necessary to provide cell-material interaction leading to efficient cell mobility, proliferation, differentiation and then recreating the cell's ECM. Hydrophilic functionalization and functional group activation on materials surfaces allow overcoming polyester materials bioinertia. The hydrophilic surface functionalization could be divided into pre-, during, and post-electrospinning methods. The first one is based on bulk blending with bioactive polymers or proteins, while the second one is coaxial electrospinning. The last one, i.e., post-electrospinning functionalization methods only refer to the fiber's surface and could be divided into wet chemical and physical treatments.

The review aimed at the discussion of the chemical and physical post-electrospinning hydrophilic surface functionalization strategies of polyester nanofibers and their subsequent functionalization with bioactive material providing bioactive sites of RGD, and IKVAV sequences. In this respect, the pros and cons and the relevance of tissue engineering applications of each method were described.

Wet chemical methods are strong treatments that involve acids or basics or organic substances as diamines, that lead to partial breakage of polymeric chain at the place of particular groups, e.g., ester bonds in polyesters. Taking into account that chemical functionalization can seriously affect deeper layers of the materials, the condition for chemical reactions, e.g., pH, temperature, chemical concentration, and the duration of the reaction, need to be strictly controlled to avoid changes in polymer bulk properties resulting in a deterioration of materials mechanical properties.

The chemical methods could be classified into aminolysis, hydrolysis, covalent grafting, and plasma treatment. As a result of the wet chemical modification method, various reactive groups, e.g., –COOH, –OH, and $–NH_2$ can be formed. Each of these methods were described thoroughly highlighting pros, cons and their potential for particular needs.

Other types of hydrophilic functionalization methods described in this publication were physical ones. They were classified into physical adsorption and layer-by-layer assembly (LBL).

In the publication it was concluded that using a single functionalization method could be insufficient for such complex and demanding applications as tissue engineering. Combining a few functionalization methods, e.g., aminolysis and subsequent biomolecule immobilization or hydrolysis followed with LBL could bring a synergistic effect to improve fibers hydrophilicity and biocompatibility by providing biological activity on the surfaces.

The described topic enabled systematization of the knowledge and was helpful particularly during short PLLA fibers modification with laminin via physical adsorption (described in detail in 7.7. subsection).

7.4. Shortening of electrospun PLLA fibers by ultrasonication

Electrospun nanofibers provide many advantages including high surface-to-volume ratio, mimicking of ECM protein fibers and decent mechanical properties. However, their morphology is rather 2-D than 3-D, and they could be placed inside the body, by surgery only. To overcome those limitations electrospun nanofibers could be shortened to an adequate length and mixed with other injectable materials. For instance, the fragmentation of electrospun fibers and combining them with injectable hydrogels could provide fibers homogeneous dispersion, materials system injectability, adequate mechanical support for cells and ECM-mimicking structure.

This study was aimed at fabrication of electrospun fibers and their subsequent fragmentation using ultrasonication. In this publication, a thorough investigation of the ultrasonication process parameters and polymer properties on the effectiveness of PLLA fibers fragmentation was presented. Specifically, effects of various sonication media, duration of fragmentation, and PLLA molecular weight and fiber crystallinity have been studied. To refine fibers length distribution, the post-fragmentation process, that was, the additional filtration through 40 μm cell strainers, was carried out.

Electrospinning conditions were tuned in such a way to obtain non-woven allowing for the most effective fibers fragmentation.

Various sonication media - water, ethanol, and isopropanol were chosen to study the effect of the sonication medium on ultrasonic fragmentation efficiency. The results indicated isopropanol as the optimal sonication medium, allowing to get the lowest average fiber lengths. The analysis of dependencies between polymer media was supported by molecular polymer-solvent interactions calculations using Hansen solubility parameters.

Analysis of the effect of PLLA molecular weight and the duration of the ultrasonication process on fiber fragmentation confirmed effectiveness of the method showing that the average fiber length decreased with the duration of the process reaching the range of $58 - 70$ μm.

WAXS studies revealed that electrospun PLLA fibers were amorphous, showing clearly two amorphous halos indicating two characteristic inter-chain spacings. Moreover, it was found the ultrasonication induced crystallization in the fragmented fibers. It was most likely due to some heating observed as an increase in the sonication medium's temperature up to c.a. 40 °C. Although the sonication medium was cooled with ice, after longer time its temperature eventually increased, inducing the crystallization of the higher molecular mobility of polymer chains.

The GPC results showed PLLA molecular weight distribution peaks were equivalent before and after electrospinning as well as after subsequent ultrasonic fragmentation. The results indicated those processes do not lead to the polymer degradation providing important information from the perspective of polymers post-electrospinning functionalization.

Viscosity studies of the hydrogel system, both pure and loaded with PLLA fibers, showed hydrogel stability and slight increase in viscosities after fibers addition. The comparison of viscosities values with the viscosity limit of liquid injection via 22G needle, showed all of the studied samples were considered to be injectable [45].

This research allowed the optimization of the fabrication of relatively short PLLA fibers by selecting adequate electrospinning and subsequent fragmentation parameters using ultrasonic methods without affecting the polymer's molecular weight. On the other hand, the ultrasonication increased the fibers' crystallinity, which could be prevented by more thorough control of cooling during the process, e.g., by cooling with a dry ice instead of ice.

The ultrasonic fragmentation method expanded the possibilities of potential use of electrospun fibers, for instance additives to the hydrogel that provide mechanical support and

improve hydrogels morphological similarity to native ECM.

7.5. Toward a Better Understanding of the Gelation Mechanism of Methylcellulose via Systematic DSC Studies

Although all of the scientists confirm LCST multistep character of MC thermal crosslinking (details are described in Section 4), the mechanism alone is still under debate. There are many theories explaining MC crosslinking mechanisms such as three gel occurrences in phase diagrams, fibrils formation by primary nucleation, and subsequent crystallization or destruction of water cages and subsequent hydrophobic three-dimensional hydrogel network formation.

MC crosslinking could be investigated using rheological methods (DMA), macroscopic methods such as the inversion of the test tube or thermal analysis techniques, e.g., DSC. Rheological method seems to give the most clear information related to the crosslinking process from the intersection of storage (G') and loss modulus (G''). This intersection corresponds to a transition from a fluid-like (viscous) behavior where G">G' to a solid-like (elastic) behavior where G'>G". For polymers that do not show the intersection point, the crosslinking rate could be determined as time or temperature derivative of G'. Generally the method gives clear information on materials crosslinking rate but it is challenging to provide hermetic conditions preventing hydrogels solvent evaporation. Although there are methods that could help to overcome this problem such as using solvent traps, e.g., silicone oil or covering plates, they do not work for every polymer risking unreliable results especially during the long-term measurements at higher temperatures. The inversion test tube method, although it allows macroscopic observation of hydrogel mobility, does not give the possibility to obtain information about the structure of the hydrogel (whether the hydrogel is partially or fully crosslinked) or the mechanism of cross-linking.

In the case of DSC method hermetic conditions avoiding water evaporation can be provided by using special hermetic rubber sealed pans. **The aim of this study was to explain the thermally-induced crosslinking mechanism via systematic studies of DSC measurements for a wide spectrum of MC concentrations.** The aim was achieved by systematic DSC investigation of materials with various MC concentrations. Additionally, those investigations

provided the answer to the question of whether or not MC is relevant as a thermosensitive scaffold for tissue engineering application.

Our DSC results showed several endotherms during heating and several exotherms during cooling. Generally for heating mode two peaks were observed, named as the medium-temperature (MT) and the high-temperature (HT), but for smaller MC concentrations, i.e., <9 wt.%, there was an additional low-temperature (LT) shoulder, which was taken into account as the third peak during numerical deconvolution. This additional peak, although registered by other groups, e.g., [46] has not been analyzed and explained in literature reports. The LT peak corresponds to the water molecules reorganization in the vicinity of polymer chains at c.a. 50 ℃, i.e., thermally induced spanning water network breaking into smaller water clusters. The MT endotherm in the temperature range of 55-70 ℃ corresponds to the polymer-solvent interactions, i.e., specific dehydration. So called "water cages" around hydrophobic methoxy groups interact with MC hydrophilic parts. At ambient conditions, on the one hand, water molecules interact with -OH groups in MC via hydrogen bonding, but on the other hand water cages surround hydrophobic $-OCH_3$ groups in MC. The temperature increase induces destruction of the hydrogen bonds and subsequent exposure to the $-OCH_3$ groups. The HT endotherm occurring at c.a. 65-72 ℃ is related to the intra- and intermolecular polymer-polymer interactions resulting in formation of the 3-D hydrophobic fibril-like hydrogel network.

In the earlier paper (Section 7.2), the LT peak was not detected. In the present paper, the peak was revealed using a much broader temperature range for the DSC measurements and improved data analysis. Thus, current results provide an update and amendment of the earlier preliminary ones.

For cooling mode at all of the studied concentrations there were always two exothermic peaks. The measurements showed similarly as observed for heating mode, decreasing trends of transition heat normalized to the MC mass as a function of MC concentration. The heats of both effects normalized to the sample mass mostly increase with the increasing MC concentration and both heats extrapolated to zero MC content lead to the same heat. For the heats normalized to the MC content, the range of the lowest MC contributions in the solution showed MT and HT decrease with increasing MC concentration.

Those dependencies suggest the LT peak observed during heating is most likely included into the MT peak during cooling. In addition, for the MT and HT peaks during cooling, oppositely than for heating, the heat of the HT peak prevailed over the MT peak, indicating the complexity of MC gelation.

Moreover, the results showed that during heating the MT and HT peaks shift toward lower temperatures with increasing MC content, but the position of the LT peak remains unchanged. Additionally, the heat of the MT and HT transitions increased, while the heat of the LT transition slightly decreased with increase of MC content, supporting the conclusion that the MT and HT peaks correspond to MC molecular interactions, while the LT peak relates to the solvent-solvent interactions. Additionally, those observations were supported with the advantage of the LT heat over the MT and HT for small MC concentrations. An evident proof that LT effect corresponds to water molecules interactions only, while MT and HT effects correspond to MC molecules interaction, resulted from the comparison of the ΔH using alternative normalizations - to water and MC content instead of the whole sample mass. The ΔH of LT peak increases with the increase of water content approaching the extrapolated value at zero MC content, which is practically the same irrespective of the type of normalization. While the heats of MT and HT showed more complex dependencies without a clear trend.

In summary, our DSC systematic analysis showed multistage, reversible MC crosslinking arising from LCST nature. Depending on MC concentration, the two or three endotherms accompanied the crosslinking effect. The LT has not been previously reported, and most likely corresponds to the molecular interactions in a solvent, that are destructions of spanning water networks into smaller water clusters. The MT and HT effects accompany changes in polymer-solvent and polymer-polymer interactions, respectively. For polymer-solvent interactions, it is the water cages destruction, while for polymer-polymer interactions, it is the formation of three dimensional hydrophobic fibril networks.

7.6. A methylcellulose/agarose hydrogel as an innovative scaffold for tissue engineering

Although MC has many benefits such as thermally sensitive crosslinking ability near 37 ℃, low costs of material and manufacturing technology, and mechanical properties that are easy to adjust by changing its concentration to meet the requirements of the native tissues, like

every material it has some disadvantages. One of them is an insufficient crosslinking rate, while another is a non-cell-adhesive character [47]. The blending of MC with another biomaterial that has greater affinity to water and cell-adhesive nature accelerating MC crosslinking and increasing cell-material interactions effectively overcomes this problem. According to the literature reports, for this purpose AGR is a suitable candidate [23,48].

Therefore, this study was aimed at investigating the AGR addition effect on the MC mechanism and rate of crosslinking, and viscoelastic properties of the hydrogel system. Additionally, various concentrations and proportions of MC/AGR hydrogels were studied in terms of biological properties to assess their usefulness from the perspective of requirements imposed on scaffolds for tissue engineering applications.

The various proportions and concentrations of the MC/AGR systems were prepared, and the thermal effects and crosslinking rate were investigated in a heating mode (-5–100 ℃) using DSC and in isothermal conditions at 37 ℃ using DMA. Similarly to the previous studies (7.5 subsection), a few endotherms of LT, MT, and HT corresponding to MC crosslinking have been observed. It was shown that AGR addition increases especially the heat effects of LT as a result of AGR's higher affinity to water than pure MC. The unclear trend of MT and HT dependencies after AGR addition is the effect of mutual interactions between MC and AGR that decrease the molecular mobility of polymeric chains and consequently could hamper the kinetics of MC crosslinking. The isothermal DMA measurements showed that AGR addition provides faster initiation of MC crosslinking and its faster dehydration, but does not increase the rate of further steps, i.e., hydrophobic network formation. Additionally, the higher AGR contribution in the MC/AGR system ultimately forms stronger hydrophobic interactions leading to higher viscoelastic properties of the hydrogel systems at 37 ℃.

Cytotoxicity Presto Blue assay showed the non-toxic character of the studied materials. The cell number determined from the calibration curve showed similar amounts of cells in comparison to the control, indicating good potential of MC/AGR hydrogel as scaffold for tissue engineering applications.

Additionally the 2-D and 3-D morphological fibroblasts and mesenchymal stem cell observations via fluorescent microscope showed their various distribution and shape depending on the MC/AGR concentration, on which surface the cells were seeded. The 3-D images allows to see cell distribution in the whole hydrogel volume. On most of the hydrogels, the fibroblasts

were equally distributed, except for two concentrations with high content of MC and AGR, where round shape aggregates were visible. The viability tests of mesenchymal stem cells (hMSCs) showed the cells were alive throughout the whole time of culturing. Most of the concentrations show comparable viability with the control. The highest number of the dead cells was found for the highest MC/AGR concentrations indicating its negative effect on the cell viability. Morphological distribution of the MSCs showed their homogenous suspension in all volumes of the hydrogels. In the first day of cell culturing in the hydrogels volume they showed a spherical morphology, which according to the literature, e.g., [49] is beneficial for embedding cells in hydrogel matrix approaching as a potential injectable cell delivery system. It appears that most of the studied hydrogels provide mechanically protecting conditions for the cells during the transplantation procedure. Additionally, the viscosity of the MC/AGR hydrogel systems enables cell migration within the scaffold providing the settlement of transplanted cells in the host tissue. After a longer time of cell culturing, cells showed flattened morphology; some of the cells migrated to the bottom of the well, and the time of migration was dependent on hydrogel concentration, and thus viscosity.

Similarly to the L929, the MSCs showed a different round-shaped aggregate morphology, while seeded on MC5/AGR5. The reason for the unfavorable morphology of both cell lines for higher hydrogels concentration is uneven distribution of the crosslinking, resulting in more and less crosslinked areas. In the denser crosslinked areas there could be insufficient oxygen availability and decreased possibilities for nutrients and oxygen transportation.

This study demonstrated that AGR addition initiates MC crosslinking resulting in a faster crosslinking rate and increased viscoelastic properties of the hydrogel system. Additionally, AGR addition led to obtaining of non-toxic nature of MC/AGR systems and good cellular response and adhesion in selected variants of MC/AGR hydrogels. Besides the potential of these materials as injectable scaffolds for tissue engineering, they could also be used as the injectable cells delivery systems.

The study allowed to narrow down the research area and select for further studies those MC/AGR concentrations that provide a supportive environment for the cells by adequate crosslinking rate, mechanical support, good cell adhesion, morphology as well as nutrients and oxygen transportation.

7.7. Methylcellulose/agarose hydrogel loaded with short electrospun PLLA/laminin fibers as injectable scaffold for tissue engineering/3D cell culture model for tumour therapies

The general aim of this study was to design and fabricate a thermosensitive injectable hydrogel system loaded with short fibers that provides an ECM-mimicking hospitable environment providing adequate biochemical and mechanical cues for cell proliferation and differentiation. The potential application of such an approach was considered as an injectable scaffold for tissue engineering that could provide cell regeneration or a three-dimensional brain tumor culture model for designing innovative anti-cancer treatments.

On the way to the goal of the work, biological modification of short fibers with laminin, tuning the hydrogel/short bioactive fibers proportions, evaluation of viscosities, injectability, morphology, and most importantly biological properties were carried out.

Two previously selected MC/AGR concentrations of 3 wt.% MC/3 wt.% AGR and 5 wt.% MC/3.5 wt.% AGR have been chosen for this study. Additionally, electrospun short PLLA fibers with the average fiber length 40-60 μm were functionalized with the native ECM protein of laminin via physical adsorption.

Despite small differences in degradability between samples of different concentrations at short times, the complete degradation occurred after 18 days of the observation.

The BCA assay showed clearly that the highest amount of laminin has been attached to the short fibers treated with EtOH. It was the effect of the higher surface area, increased surface roughness, and lower surface tension after EtOH treatment as also indicated by the WCA analysis.

The viscosity studies showed the shear-thinning behavior of the hydrogel system which was even stronger for thermally crosslinked hydrogel at 37 °C. Shear-thinning is the effect seen in polymers as the viscosity decreasing upon applying high shear rates, as a consequence of molecular disentanglement and chain alignment along flow direction. As expected, the addition of short PLLA fibers to the MC/AGR hydrogel solution increased the viscosity of hydrogel systems.

Injectability was estimated from the force needed to extrude the solution. The detailed parameters of the process were described in subsection 5.3.2. The solution was assumed injectable if the maximum force recorded during extrusion was less than 30N, which is assumed from literature as the reasonable force used by a human making injection through a 23 G needle. In general, the measurements showed an increase of the force with increasing the injection rate, particularly at higher flow rates, as well as with increasing the hydrogels concentration and addition of short PLLA fibers. The results showed that as expected in the case of hydrogels loaded with fibers, an injection with reasonable force needs reduction of the flow rate.

SEM images showed that fiber-loaded hydrogels were morphologically similar to the native ECM of a rats spinal cord [50], or a porcine cartilage [51]. Considering the morphological perspective such hydrogels may provide a topographical cues for increased cellular adhesion.

Biocompatibility studies on L929 fibroblasts showed the non-toxic character. The significantly increased cell viability was observed for cells seeded on hydrogel loaded with fibers with the highest amounts of laminin in comparison to control. The highest cell number and the best spindle-like morphology was observed in laminin-rich hydrogels in comparison to the control which is consistent with cellular viability studies.

The morphologies of LN18 and WG4 glioma cells seeded on hydrogels loaded with short fibers and functionalized with laminin showed different shapes. The LN18 cells showed round morphology, while WG4 cells showed spindle-like morphology after 1 and 3 days of culturing. All of the samples were nontoxic for both cell lines and they infiltrated homogeneously to the whole hydrogel volume. The best morphology and distribution of the WG4 cells was observed for hydrogel with the highest amounts of laminin. On this hydrogel sample cells well-developed lamellipodia with filopodia in comparison to other samples and the control. This particular sample could be used as a 3-D cell culture model for studies of glioma cell signalization pathways and anticancer therapies.

To sum up, in this study smart thermosensitive injectable MC/AGR hydrogel loaded with short bioactive PLLA/laminin fibers was designed, formed and characterized. The laminin was successfully attached to the short electrospun PLLA fibers treated with EtOH resulting in bioactive fibers.

The hydrogel system showed the shear-thinning character. Injectability tests showed that by tuning the applied injection rate, the highly concentrated hydrogels loaded with large amounts of fibers could be injected by humans via a 23 G needle in a reasonable manner.

The hydrogel loaded with short fibers, thanks to the appropriate morphology and biochemical cues mimicking native ECM, enhances the cellular response and cell proliferation by increasing adhesion to the material.

8. Conclusions

The doctoral thesis allowed for the following conclusions:

1) The method of formation of a smart thermosensitive injectable hydrogel composite made of MC/AGR aqueous solution reinforced with short PLLA/laminin fibers obtained by electrospinning, ultrasonication and functionalization with laminin was found feasible.
2) At the optimal chemical composition, the MC/AGR/PLLA/laminin hydrogel system simultaneously provided appropriate injectability, timely in-situ thermal crosslinking, fair mimicking of the native ECM, and good cellular response, suggesting the approach could be useful for tissue engineering applications or 3-D tumour culture models.
3) The obtained results provide fundamental knowledge of composite material which could be valuable for both materials science and tissue engineering:
    a. The MC crosslinking process was determined as a reversible physical and thermal phenomena consisting of two consecutive stages: water cages destruction followed by formation of a 3-D hydrophobic network.
    b. Addition of AGR was found to increase the MC crosslinking rate, enhance the mechanical properties, and cell-material interactions.
    c. Fabrication method of short PLLA/laminin fibers via electrospinning, ultrasonication, and functionalization with laminin, in general, occurred to be highly prospective for application in injectable reinforced biological hydrogel systems.

9. References

[1] Mo X., Sun B., Wu T., Li, D., Electrospun nanofibers for tissue engineering. In Electrospinning: Nanofabrication and Applications; Ding, B., Wang, X., Yu, J., Eds.; William Andrew Publishing: Norwich, NY, USA, 2019, pp. 719–734.

[2] Li X., Katsanevakis E., Liu X., Zhang N., Wen X., Engineering neural stem cell fates with hydrogel design for central nervous system regeneration, Prog. Polym. Sci., 2012, 37, pp.1105-1129.

[3] Wu J., Chen Q., Deng C., Xu B., Zhang Z., Yang, Y., Lu, T, Exquisite design of injectable hydrogels in cartilage repair, Theranostics, 2020, 10(21), 9843.

[4] Pérez-Garnes M., Barcia J. A., Gómez-Pinedo U., Monleon Pradas M., Vallés-Lluch A. Materials for central nervous system tissue engineering, In Cells and Biomaterials in Regenerative Medicine, Eberli, D., Ed., InTech: Rijeka, Croatia, 2014, pp. 201-259.

[5] Rył A., Owczarz P. Injectability of Thermosensitive, Low-Concentrated Chitosan Colloids as Flow Phenomenon through the Capillary under High Shear Rate Conditions, Polymers, 2020, 12(10), 2260.

[6] Bignami A., Hosley M., Dahl D., Hyaluronic acid and hyaluronic acid-binding proteins in brain extracellular matrix, Anat. Embryol., 1993,188, pp. 419–433.

[7] Buzanska L., Zychowicz M., Sarnowska A., Domanska- Janik K. Bioengineering of neural stem cell niche, Postepy Biochem. 2013, 59, pp. 175–86.

[8] Llacua L. A., Faas M. M., de Vos P ., Extracellular matrix molecules and their potential contribution to the function of transplanted pancreatic islets, Diabetologia, 2018, 61, pp. 1–12.

[9] Khaing Z.Z., Seidlits S.K., Hyaluronic acid and neural stem cells: Implications for biomaterial design, J. Mater. Chem. B, 2015, 3, pp. 7850–7866.

[10] Aurand E.R., Lampe K.J., Bjugstad K.B., Defining and designing polymers and hydrogels for neural tissue engineering, Neurosci. Res., 2012, 72, pp. 199–213.

[11] Ramakrishna S., Fujihara K., Teo W.E., Lim T.C. and Ma Z. An Introduction to Electrospinning and Nanofibers, World Scientific Publishing, Singapore, 2005.

[12] Chen S., John J. V., McCarthy A., Xie J. New forms of electrospun nanofiber materials for biomedical applications, J. Mater. Chem. B, 2020, 8(17*)*, pp. 3733–3746.

[13] Li M., Wu Y., Li H., Tan C., Ma S., Gong, J., Deng H., Nanofiber reinforced alginate hydrogel for leak-proof delivery and higher stress loading in nucleus pulposus, Carbohydr. Polym., 2023, 299, pp. 120193.

[14] Wang L., Li T., Wang Z., Hou J., Liu S., Yang Q., Wu, Y., Injectable remote magnetic nanofiber/hydrogel multiscale scaffold for functional anisotropic skeletal muscle regeneration, Biomaterials, 2022, 285, pp.121537.

[15] Charlet G., Delmas G., Thermodynamic properties of polyolefin solutions at high temperature: 1. Lower critical solubility temperatures of polyethylene, polypropylene and ethylene-propylene copolymers in hydrocarbon solvents, Polymer, 1981, 22(9), pp. 1181-1189.

[16] Charlet G., Ducasse R., Delmas, G., Thermodynamic properties of polyolefin solutions at high temperature: 2. Lower critical solubility temperatures for polybutene-1, polypentene-1 and poly (4-methylpentene-1) in hydrocarbon solvents and determination of the polymer-solvent interaction parameter for PB1 and one ethylene-propylene copolymer, Polymer, 1981, 22(9), pp. 1190-1198.

[17] Wu D., Cheng J., Su X., Feng Y., Hydrophilic modification of methylcellulose to obtain thermoviscosifying polymers without macro-phase separation, Carbohydr. Polym., 2021, 260, pp. 117792.

[18] Haque A., Morris, E. R., Thermogelation of methylcellulose. Part I: molecular structures and processes, Carbohydr. Polym., 1993, 22(3), pp. 161-173.

[19] Joshi S.C., Lam Y.C., Modeling heat and degree of gelation for methyl cellulose hydrogels with NaCl additives, J. Appl. Polym. Sci., 2006, 101, pp.1620–1629.

[20] Li L., Thangamathesvaran P.M., Yue C.Y., Tam K.C., Hu X., Lam Y.C. Gel Network Structure of Methylcellulose in Water, Langmuir, 2001, 17, pp. 8062–8068.

[21] Kobayashi K., Huang C.I., Lodge T.P., Thermoreversible gelation of aqueous methylcellulose solutions, Macromolecules, 1999, 32, pp. 7070–7077.

[22] Fernández E., López D., Mijangos C., Duskova-Smrckova M., Ilavsky M., Dusek K. Rheological and thermal properties of agarose aqueous solutions and hydrogels, J. Polym. Sci., Part B: Polym. Phys., 2008, 46(3), pp. 322-328.

[23] Martin B. C., Minner E. J., Wiseman S. L., Klank R. L., Gilbert R. J., J. Neural Eng., 2008, 5(2), pp. 221.

[24] Chłądzyński S., Malata G., Składniki zapraw klejowych do płytek. Część II-Metyloceluloza, Izolacje, 2008, 3, pp. 30-34.

[25] Tohidinia M., Biabangard A., Noroozifar M., Platinized agarose microspheres as a new modifier in graphite paste electrodes for the electrochemical determination of 4-aminophenol, RSC Adv., 2020, 10(5), pp. 2944-2951.

[26] Yang Y., Yin X., Wang H., Qiu W., Li L., Li F., Zhao, Y., Engineering a wirelessly self-powered and electroconductive scaffold to promote peripheral nerve regeneration. Nano Energy, 2023, 107, pp. 108145.

[27] Horacek M. J., Thompson J. C., Dada M. O., Terracio L. The extracellular matrix components laminin, fibronectin, and collagen IV are present among the epithelial cells forming Rathke's pouch, Cells Tissues Organs, 1993, 147(2), pp. 69-74.

[28] Koh H. S., Yong T., Chan C. K., Ramakrishna S., Enhancement of neurite outgrowth using nano-structured scaffolds coupled with laminin, Biomaterials, 2008, 29(26), pp. 3574-3582.

[29] Milner R., Wilby M., Nishimura S., Boylen K., Edwards G., Fawcett J., Pytela, R., Division of labor of Schwann cell integrins during migration on peripheral nerve extracellular matrix ligands, Dev. Biol., 1997, 185(2), pp. 215-228.

[30] Sun Y., Wang T. L., Toh W. S., Pei, M., The role of laminins in cartilaginous tissues: from development to regeneration, Eur. Cells Mater, 2017, 34, pp. 40.

[31] Francisco A. T., Hwang P. Y., Jeong C. G., Jing L., Chen J., Setton L. A. Photocrosslinkable laminin-functionalized polyethylene glycol hydrogel for intervertebral disc regeneration, Acta Biomater, 2014, 10, pp. 1102–1111.

[32] Gilchrist C. L., Darling E. M. , Chen J., Setton L. A. Extracellular matrix ligand and stiffness modulate immature nucleus pulposus cell-cell interactions, PLoS One, 2011, 6(11), e27170.

[33] Li L., Shan H., Yue C.Y., Lam Y.C., Tam K.C., Hu X., Thermally induced association and dissociation of methylcellulose in aqueous solutions, Langmuir, 2002, 18, pp. 7291–7298.

[34] Kusters K. A., Pratsinis S. E., Thoma S. G., Smith D. M. Ultrasonic fragmentation of agglomerate powders. Chem. Eng. Sci., 1993, 48(24), pp. 4119-4127.

[35]Clemons T. D., Bradshaw M., Toshniwal P., Chaudhari N., Stevenson A. W., Lynch J., Iyer K. S., Coherency image analysis to quantify collagen architecture: implications in scar assessment, RSC Adv., 2018, 8(18), pp. 9661-9669.

[36] Williams D., Kuhn A., O'Bryon T., Konarik M., Huskey, J., Contact angle measurements using cellphone cameras to implement the Bikerman method, Galvanotechnik, 2011, 102(8), pp. 1718.

[37] Ahanotu A., Hynds D., Hanson L. Contribution of Infection with Cytomegalovirus (CMV) to the Production of Amyloid Precursor Protein (APP) and Alzheimer's Disease-associated Beta Amyloid, 2022.

[38] Barnes H. A., Hutton J. F., Walters K., An introduction to rheology, Elsevier, 1989, 3.

[39] Bodnár T., Sequeira A., Prosi M., On the shear-thinning and viscoelastic effects of blood flow under various flow rates., Appl. Math. and Comput., 2011, 217(11), pp. 5055–5067.

[40] Niemczyk-Soczyńska B., Gradys A., Kołbuk D., Krztoń-Maziopa A., Sajkiewicz P. Crosslinking kinetics of methylcellulose aqueous solution and its potential as a scaffold for tissue engineering, Polymers, 2019, 11(11), pp. 1772.

[41] Eslahi N., Abdorahim M., Simchi A., Smart polymeric hydrogels for cartilage tissue engineering: a review on the chemistry and biological functions, Biomacromolecules, 2016, 17(11), pp. 3441-3463.

[42] Ravichandran R., Venugopal J. R., Sundarrajan S., Mukherjee S., Sridhar R., Ramakrishna, S., Minimally invasive injectable short nanofibers of poly (glycerol sebacate) for cardiac tissue engineering, Nanotechnology, 2012, 23(38), pp. 385102.

[43] King R. E., Lau H. K., Zhang H., Sidhu I., Christensen M. B., Fowler E. W., Li L., Jia X., Kiick K. L., Thibeault S. L., Biocompatibility and Viscoelastic Properties of Injectable Resilin-Like Polypeptide and Hyaluronan Hybrid Hydrogels in Rabbit Vocal Folds, Regen Eng Transl Med., 2019, 5(4), pp. 373-386.

[44] Wu D. T., Jeffreys N., Diba M., Mooney D. J., Viscoelastic Biomaterials for Tissue Regeneration, Tissue Eng. Part C Methods, 2022, 28(7), pp. 289-300.

[45] Jezek J., Rides M., Derham B., Moore J., Cerasoli E., Simler R., Perez-Ramirez B., Viscosity of concentrated therapeutic protein compositions, Adv. Drug Deliv. Rev., 2011, 63(13), pp. 1107-1117.

[46] Nishinari K., Hofmann K. E., Moritaka H., Kohyama K., Nishinari, N. Gel-sol transition of methylcellulose. Macromol. Chem. Phys., 1997, 198(4), pp. 1217-1226.

[47] Bonetti L., De Nardo L., Fare S., Thermo-responsive methylcellulose hydrogels: From design to applications as smart biomaterials, Tissue Eng., Part B, 2021, 27(5), pp. 486–513.

[48] Stabenfeldt S. E., Garcia A. J. and LaPlaca M. C., Thermoreversible laminin-functionalized hydrogel for neural tissue engineering, J. Biomed. Mater. Res., Part A, 2006, 77(4), pp. 718–725.

[49] Kim E. J., Choi J. S., Kim J. S., Choi Y. C. and Cho Y. W., Injectable and thermosensitive soluble extracellular matrix and methylcellulose hydrogels for stem cell delivery in skin wounds, Biomacromolecules, 2015, 17(1), pp. 4–11.

[50] Ban D. X., Liu Y., Cao T. W., Gao S. J., Feng, S. Q., The preparation of rat's acellular spinal cord scaffold and co-culture with rat's spinal cord neuron in vitro, Spinal cord, 2017, 55(4), pp. 411-418.

[51] Chen Y. C., Chen R. N., Jhan H. J., Liu D. Z., Ho H. O., Mao Y., Sheu M. T., Development and characterization of acellular extracellular matrix scaffolds from porcine menisci for use in cartilage tissue engineering, Tissue Eng. Part C Methods, 2015, 21(9), pp. 971-986.

ARTICLES INCLUDED IN THE PUBLICATION CYCLE OF THE DISSERTATION

IOP Publishing Journal of Neural Engineering
J. Neural Eng. **15** (2018) 051002 (15pp) https://doi.org/10.1088/1741-2552/aacbab

Topical Review

Injectable hydrogels as novel materials for central nervous system regeneration

B Niemczyk, P Sajkiewicz and D Kołbuk

Institute of Fundamental Technological Research, Polish Academy of Sciences, Pawinskiego 5b St., 02-106 Warsaw, Poland

E-mail: bniem@ippt.pan.pl

Received 8 November 2017, revised 30 May 2018
Accepted for publication 11 June 2018
Published 11 July 2018

Abstract

Approach. Injuries of the central nervous system (CNS) can cause serious and permanent disability due to limited regeneration ability of the CNS. Presently available therapies are focused on lesion spreading inhibition rather than on tissue regeneration. Recent investigations in the field of neural tissue engineering indicate extremely promising properties of novel injectable and non-injectable hydrogels which are tailored to serve as biodegradable scaffolds for CNS regeneration. *Objective*. This review discusses the state-of-the-art and barriers in application of novel polymer-based hydrogels without and with nanoparticles for CNS regeneration. *Main results*. Pure hydrogels suffer from lack of similarities to natural neural tissue. Many of the biological studies indicated nano-additives in hydrogels may improve their topography, mechanical properties, electroconductivity and biological functions. The most promising biomaterials which meet the requirements of CNS tissue engineering seem to be injectable thermosensitive hydrogels loaded with specific micro-and nanoparticles. *Significance*. We highlight injectable hydrogels with various micro-and nanoparticles, because of novelty and attractiveness of this type of materials for CNS regeneration and future development perspectives.

Keywords: hydrogels, nanoparticles, injectable, microparticles, nanofibers, central nervous system

(Some figures may appear in colour only in the online journal)

1. Introduction

The human nervous system is the organ system that, in cooperation with the endocrine system monitors and controls most of automatic processes and activities [1]. Nervous system consists of the central nervous system (CNS)-the brain and the spinal cord, and the peripheral nervous system (PNS)—somatic and autonomic nerves [2, 3]. CNS might be classified in terms of: main functions, the type of neural cells and the anatomy. The main functions of the brain are integration and processing external and internal information obtained from nerves (e.g. respiratory, sensory, cardiac, motor functions etc) [1]. Spinal cord is mainly responsible for communication between the brain and the peripheral nerves—transfers information from peripheral nerves about muscles activities to the brain and from the brain to the muscles) [1]. PNS somatic system transmits sensory information for CNS, while autonomic controls automatic functions (e.g. heart beating, blood pressure) [3]. The human brain and spinal cord are made up of the neurons and glial cells (glia, neuroglia) [4]. A typical neuron consists of a cell body—soma, dendrites, and axons. Neurons play the most important role in CNS—transmit impulses to other cells [5].

Neurons are the basic functional units of the nervous system, and they generate electrical signals called action potentials, which allow them to quickly transmit information over long distances [5]. Neuroglia cells consist of: astrocytes, oligodendrocytes and microglia [5]. Astrocytes are essential to nervous system function, but compared to neurons, they mostly play supportive role. They are the most common glial cells of the

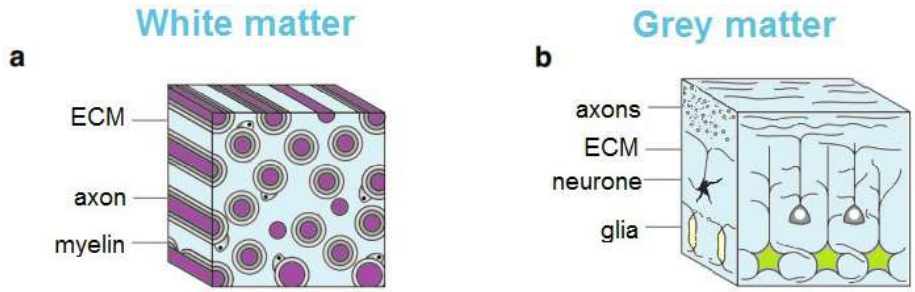

Figure 1. Schematic representation of: (a) white matter architecture, (b) grey matter architecture.

grey matter, possessing branched prolongations, which occupy the main piece of the interneuronal spaces. The oligodendrocytes provide the myelination of the axons within the CNS to enable the effective transmission of neural impulses. The microglia consists of few small cells, derived from the mesenchyme, which invade the CNS in the last stages of fetal development (during injury microglia transform into phagocytic cells [5, 6].

Traumatic brain injuries (TBI) and spinal cord injuries (SCI) are the most problematic injuries, because of the lack of the ability of the adult nervous system for spontaneous, functional regeneration. This leads to major socioeconomic problem throughout the world [7]. For instance, 577 cases of TBI per 100 000 people per year occurred in the US only, while, in Europe, the number of patients with diagnosed TBI is estimated at 262 per 100 000 [8].

SCI are predominantly associated with irreversible loss of motor function and happen mostly due to traffic accidents, pool jumping and falling from heights [9, 10]. In the US, 39 per 100 000people were estimated to be SCI victims every year, while in Europe the amount of SCI cases was 15 per 100 000 per year [11].

Regeneration of damaged neural tissue is a considerable challenge due to its complex anatomical and histological structure and poor self-healing capability. It is hindered by the presence of internal factors, which block its reconstruction. As a consequence of CNS injures, both traumatic injuries or damages such as tumor formation, scar tissue is formed, resulting in the inhibition of the regeneration process. TBI usually leads to permanent disability.

TBIs and SCIs often lead to death, and the patients who survived are suffering from permanent disability [12–15].

Up to this date, there is no effective therapy for TBI and SCIs (e.g.: [16]). Practiced surgery only inhibited lesion spreading, while drug therapies have been so far focused mostly on pain relief [17]. Hence, the goal of CNS tissue engineering is to design a biomaterial enabling for the effective outgrowth and differentiation of neural stem cells (NSCs) [18].

This review describes the current trends in polymeric scaffolds for CNS regeneration, with emphasis on the newest and most advanced solutions using injectable hydrogels containing different types of micro- and nanoparticles.

2. Requirements for biomaterials supporting CNS regeneration

Injury of CNS generates abundant alterations in cellular signalling and extracellular matrix (ECM) environment. The ECM creates 10%–20% of the CNS volume and can have inductive properties by promoting immune/neural stem cell infiltration to allow reconstruction of soft tissue [19, 20]. The effective scaffold should mimic the architecture, chemical composition and mechanical properties of natural ECM allowing for easy colonization by cells and the regeneration of axons, as well the reconstruction of damaged blood vessels without providing an immune response [14, 21].

Another role of the biomaterial used in regeneration is to avoid traumatic effects of glial scarring on CNS damage [10, 14, 15, 22]. From one side the glial scar inhibit a macrophages activity and oxidative stress extension [23], but, from another, the glial scar presence repairs a broken blood-brain barrier (BBB) and inhibits activity of inflammatory cells—the main factors providing degeneration of axons [22].

Scaffold morphology, mechanical properties, electrical conductivity and bioactive additives in nerve tissue regeneration are discussed below.

2.1. Architecture

Anatomically, the brain is composed of the cerebrum, the cerebellum, and the brainstem [1]. From macroscopic point of view, the human brain consists of two main regions: white matter and grey matter. Internal white matter is rather homogenous and composed of highly aligned, myelinated nerve fibers, while in external white matter fibers are more disorganized [24]. Grey matter consists mainly of cell bodies and unmyelinated axons and exhibits highly anisotropic structure/properties [24], what is presented in the figure 1.

The spinal cord is surrounded by bony spine and anatomically is made up of the spinal nerves which are classified into dorsal root and ventral root. Similarly to brain, spinal cord consists of white and grey matter. The composition of white matter is analogous to the brain, while grey matter consists of a sensory dorsal horn and a somatomotor ventral horn which both form a characteristic for spinal cord H-shaped structure [1].

Depending on the specificity of the injured area, material dedicated to CNS regeneration should follow soft tissue structure and topography [25–29]. A general consequence of neural disease or disorder is the disruption of the unidirectional architecture. Therefore bridging the lesion part should be the first step in CNS regeneration. A supportive structure mimicking the natural neural structure should be implanted and the

key functions should be provided (e.g. anisotropic structure is beneficial for SCI regeneration) [18, 26–29].

Under laboratory conditions, SCs are commonly used to confirm regeneration ability of the biomaterial [18, 30]. This is due to the ability of SCs to aid: conduction of nervous impulses along axons, neural development and regeneration, trophic support for neurons, production of the neural ECM, modulation of neuromuscular synaptic activity etc. It was proved that regenerating axons migrate along SCs, leading to bridging of nerve gaps [18]. Lack of SCs in the CNS is the most important barrier for regeneration [23]. Neural progenitor cells (NPCs) cultivation on a surface with anisotropic structure (biomaterial in form of aligned electrospun fibers) results in effective proliferation and differentiation into neurons [31].

The high scaffold porosity is responsible for cellular migration and controlled diffusion of cells metabolites and medium, being crucial point in cells organization, differentiation and survival [32]. Pores size might be adjusted in such a way to enable metabolite diffusion, but also appropriate cells adhesion to biomaterial. Dahlin *et al* [33] and Yang *et al* [34] reported that 90% porosity and pore size ranging 10–100 μm are the most suitable for neural cells (neurons) growth. Electrospinning process typically allows for the production of mats with 85%–90% porosity which is appropriate. Nevertheless in this case their pore size was insufficient (0.1–0.35 μm) [35]. Sponges obtained by the self-assembly technique are also characterized by high porosity and their pore size was appropriate for neural cells (100–400 μm) [36]. Materials formed using the freeze-casting technique have porosity in the range of 40%–97% and pore size from 10 μm to 50 μm [37]. These values do not characterize a desired environment for neural cells.

2.2. Mimicry of ECM

ECM has inductive properties and allows to reconstruct soft tissue (infiltrate of immune cells and its degradation products effectively entice host neural stem/progenitor cells) [19]. Beside neurons and glial cells, ECM creates 10%–20% volume of the CNS [20]. The effective scaffold for CNS regeneration should mimic natural ECM in terms of morphology, chemical composition and mechanical properties to obtain better cell integrity and environment which do not provide immune response [14, 21]. ECM structure consists of interstitial network -highly hydrated structure made of linear polysaccharide chains—glycosaminoglycans (GAGs) and proteoglycans, and the suitable biomaterial perhaps should mimic this structure [20, 38].

Chemically, in most of other systems ECM consists of various proteins such as fibronectin and laminin, but in CNS their amount is decreased [20]. Hyaluronic acid (HA), proteoglycans and linking proteins form most of ECM space [20]. An important role in communication between cells play short, specific peptide sequences which effectively interact with cell membrane integrin proteins. For instance, arginine–glycine–aspartate (RGD) derived from fibronectin, tyrosine–isoleucine–glycine–serine–arginine (YIGSR) and valine–alanine–valine (IKVAV) derived from laminin promote better ECM-cell integrity [20, 38, 39]. They might be found only in natural biomaterials and Ghuman *et al* [19] confirmed ECM hydrogel consisted of ECM proteins (laminin, fibronectin) effectively regenerated brain tissue after the stroke. In order to obtain binding sites in synthetic materials, their modification is necessary (e.g. by attaching RGD sequences) [40].

ECM mechanical properties (stiffness) are determined by amount of proteins and proteoglycans, hence might be adjusted by varying chemical composition [39]. Appropriate material should has mechanical properties suitable to health neural tissue to serve as structural support for cells infiltration. Too stiff material might press on tissue and in effect inhibit neural cells (axons) regeneration [10]. Ghuman *et al* [19] described biomaterial mimicking ECM which promoted chemotaxis, stem cells differentiation into neurons and were easily infiltrated by macrophages.

Another important issue is ECM signalling molecules activation—they attract specific neural cells of host and induce their regenerative response [19]. In natural neural tissue, electrical transmission between cellular synapses occurs when informational molecules can pass directly from the source to the target cell through gap junctions. Astroglia, interconnected via gap junctions, act as an electrical syncytium, which allows inter alia spatial buffering of K^+ and long-range Ca^{2+} waves. Ca^{2+} waves can affect the metabolism and excitability of the neurons embedded in the astrocyte network via Ca^{2+} induced mobilization of glucose from glial glycogen stores, and secretion of neurotransmitters through reduction of free Ca^{2+} in synaptic clefts, respectively. Overall, communication through gap junctions appears to be an integral component of the complex cell–cell interactions occurring in central neuronal–glial networks [31]. This phenomena is used in neural tissue engineering—signaling molecules are activated in proper ECM, where they attract specific neural cells of host and induce their regenerative response [19]. For example, laminin/$\alpha 6\beta 1$ receptor signalling provides human stem cells differentiation into neurons [41].

2.3. Mechanical properties

It is known that matching mechanical properties of an implanted biomaterial to that of the host tissue is crucial for the success of regeneration process (e.g.: [37, 42]).

Therefore, many investigations have been carried out to estimate mechanical properties of CNS tissues. Cheng *et al* [43] summed up literature data related to brain and spinal cord mechanical properties. They found mechanical properties dependent on gender, age, diseases etc. For example, *in vivo* studies have shown that with aging progress, the brain tissue become softer [43]. Several research were carried out to determine The mechanical properties (stiffness) of the human brain and spinal cord—are presented in table 1.

It is a great challenge to obtain material which structure and mechanical properties mimicking those of native tissues. Biomaterial, with the stiffness similar to brain, is resulting in

Table 1. Mechanical properties of the human brain and spinal cord.

	Shear modulus	Young's (elastic) modulus	Storage (elastic shear) modulus	Loss (viscous) modulus
Brain	0.4–1.4 kPa [24]	3–10 kPa [45]	1.18–2.22 kPa [47]	0.63–1.14 kPa [47]
Spinal cord	5–42 kPa [44]	1.02–1.37 MPa [46]	—	—

effective differentiation of neurons. *In vitro* studies of neural progenitor cell showed the best differentiation ability on scaffolds with similar stiffness to the brain [48]. In case of electrospun PLA fibers, mimicking native ECM architecture, elastic modulus was 38 MPa [49]. In general, better activity of neural cells was shown on materials with lower stiffness (for example in the range of 7.6–11 MPa) [49]. Young's modulus of self-assembled sponge was in the range of 0.01–1 kPa and under *in vitro* tests on NSCs, good NPCs activity on its surface was confirmed [50]. Various materials, formed via freeze-casting, showed Young's modulus in the range of 1–10 kPa [37] and according to the table 1. materials with the higher stiffness (10 kPa) could be appropriate for TBI therapies.

2.4. Electrical properties

Bioelectric stimulation plays a key role in maintaining biological functions such as muscle contraction and signal transferring in the nervous system [10]. The nervous system responds to electrical fields and the key component of neural communication is the action potential generated at the synapse. Neurons have evolved special abilities for sending electrical signals (action potentials) along axons. The term 'conduction' applies to how the cell body of a neuron communicates with its own terminals via the axon. Communication between neurons is achieved by the movement of chemicals or electrical signals across a synapse and it called neurotransmission [51]. The conduction mechanism is associated with neuronal membrane depolarization, which releases Ca^{2+} ions. This is an impulse for sending the mediator into the synapses and provide further impulse for transport to subsequent neurons [52]. Electrical conductivity in the human brain is in the range of 0.63–2.43 mS cm^{-1} while the signal transmission velocity is approximately 7000 m s^{-1} [53, 54].

SCI cause axons degeneration and electrical impulses cannot be transmitted. After injury the quantity of Ca^{2+} in cells is disrupted and with arising immune response, axons loss their functions. Electrical stimulation might overcome a transmission barrier and keep the all the lost function through stimulation of nerve-muscle system [55].

An *in vitro* and *in vivo* studies of human NPCs (rat spinal cord) showed electrical impulses stimulate NPCs to growth and differentiate after stroke. Such stimulation is caused by the change of gene expression in NPCs, which encourage their regenerative activity [56].

The time of electrical stimulation is also crucial in neurite regeneration [57]. Neurite growth under electrical stimulation was observed on: adult neurons in peripheral and CNS [58–60]. However, electrical activity has also been associated with neurite growth inhibition after K^+ induced depolarization of adult rat DRG cultures [61, 62].

In vivo electrical stimulation on rats DRG, in appropriate time, leads to obtain 2 fold increase neurons length and axonal regeneration after SCI. The most effective time of electrical stimulation was 1 h—it enhanced *in vivo* sensory axon growth after spinal cord injury [57].

Many electrically conductive materials have been investigated for CNS regeneration (e.g.: [63–65]). The main role of them is to enable cellular communication between neuronal cells incorporated into the material, enhance of electrical signals transmission to mimic neurotransmission in health neural tissue [57]. Conductive properties of the biomaterial used in CNS regeneration are essential because the amount of cells introduced during surgery is relatively low, and distances between them are higher than few nanometres required for electrical synapses communication. Electrically conductive materials can also allow application of electrical stimuli that can mimic the electrophysiological environment experienced by cells in a variety of biological processes, including muscle contraction, wound healing, and synaptic transmission [66].

Commonly used in neural tissue regeneration are carbon materials: carbon nanotubes (CNTs), carbon nanofibers (CNFs) and graphene [63, 64]. Especially interesting, from CNS point of view, are CNTs and CNFs which have shape, mechanical and electrical properties analogous to neurites [64]. However, there are reports also that CNTs may provide oxidative stress and negatively impact axons growth *in vitro* on DRG [63]. Another group of electroconductive materials are polymers, e.g. polypyrrole (PPy), polyaniline (PANI) and derivatives of polythiophene (PEDOT). George *et al* [56] produced electrically stimulated PPy scaffold with human NPCs as a therapy after stoke. *In vitro* studies (RNAseq analysis) showed improved gene expression in hNPCs and *in vivo* studies (rat cortex) confirmed their increased regenerative activity. PPy scaffolds are difficult processable, brittle and mechanically rigid [67].

Polyaniline (PANI) is great material or additive which increases electrical conductivity, but also is non-degradable and might cause chronic inflammation [67].

Poly(ethylene dioxythiophene) (PEDOT) shows high stability and electrical conductivity [65], but also poor solubility in water [68].

2.5. Scaffold fabrication techniques

Three main forms of materials for CNS regeneration can be distinguished: non-injectable and injectable hydrogels, sponges and nanofibers (e.g.: [69–75]). Table 2 summarizes the main advantages and disadvantages of the most common forms of scaffolds used in neural tissue regeneration together with corresponding techniques of their formation.

Table 2. Advantages and disadvantages of hydrogels, sponges, nanofibers for CNS tissue engineering [37, 48–50, 79–82].

	Advantages	Disadvantages
Nanofibers by electrospinning	∗Multifunctional process- broad spectrum of polymers (natural and synthetic)	∗Small pore size ∗2D structure ∗Limited ability of placing scaffold into lesion
	∗Controlled topography-e.g.: random versus aligned fibers ∗High porosity	∗Excessive mechanical properties
Sponges by self-assembly	∗3D structure ∗Biological activity ∗ Adequate mechanical properties ∗Adequate porosity and pores size	∗Rapid degradation ∗Limited ability of placing scaffold into lesion
Sponges by freeze-casting	∗Adequate mechanical properties ∗3D structure	∗2D porosity and small pores size ∗Limited selection of materials
Pure hydrogels (without additives)	∗Soft, multifunctional ∗3D structure ∗Minimally invasive due to injectability Fill the lesion shape by injection	∗Low mechanical properties ∗Lack of fibrous structure ∗Low stability *in vivo*

Natural and synthetic polymers dedicated to CNS and PNS regeneration, with wide range of electrical and mechanical properties are analyzed in the literature. The following paragraphs contain more information about the types of polymers for CNS regeneration discussed in the literature. Beside various polymers and techniques used for scaffold fabrication in neural regeneration, additional enhancement of CNS regeneration is achieved by the addition of drugs, neural cells (e.g.: NPCs) and neurotrophic growth factors (NGFs) [75–77]. Some of them appear to be particularly promising- enhanced cell proliferation is observed, also *in vivo* conditions (rat brain). For example, type I collagen as mesenchymal stem cells (MSC) delivery system was well tolerated *in vitro* and did not provide immune response in rat brain [78].

Beside of the technique of the substrate forming, cells-biomaterial interactions include cells adhesion, their migration, proliferation, differentiation [83]. Under laboratory conditions, dorsal roots ganglion (DRG) cells [63, 84, 85], Schwann cells (SCs) (glia of the peripheral nervous system) [18, 63], NPCs [84, 86] and NSCs [17, 87], MSCs are commonly used to confirm efficiency of the scaffold [88, 89].

3. Hydrogels

Hydrogels are 3D structures, in which polymer chains are crosslinked by either a physical or chemical method to form a network. They are characterized by a wide range of possibilities in tailoring their mechanical and electrical properties [42, 90] as well as architecture [36].

The main criteria for hydrogels classification relate to the nature of polymer (natural or synthetic), and the crosslinking method (physical or chemical) (e.g. [91]). The crosslinking method is crucial for final properties, as well as the stability of hydrogels. Physically crosslinked hydrogels have transient junctions that arise either from polymer chain entanglements or physical interactions such as ionic interactions, hydrogen bonds, hydrophobic interactions or crystal formation [90, 91]. In chemically crosslinked hydrogels, the junctions are permanent as a result of various chemical reactions, such as radical polymerization, Michael addition, Schiff-base reaction, or photo-polymerization. While chemical crosslinking results in higher stability and mechanical strength of hydrogels, their supplication in tissue engineering is limited by the toxicity of chemical crosslinkers. Due to this fact, hybrid crosslinking using both physical and chemical methods is also studied.

Discussion of hydrogels for CNS regeneration from the perspective of delivery method to the injury area is shown in the following paragraphs.

3.1. Non-injectable hydrogels

Non-injectable hydrogels are characterized by high viscosity in compared to injectable hydrogels. Generally, in tissue engineering they can be used as implants or for external applications, such as wound dressings.

In CNS regeneration the most common synthetic, non-injectable system is based on polyethylene glycol (PEG) which comprehensive modulus is in the range of 21–600 kPa [92, 93] and poly(2-hydroxyethyl methacrylate) (poly(HEMA))-based polymers, which mechanical properties were suitable for soft tissue (e.g. brain). Because of the lack of biological activity, synthetic polymers should be modified, for instance with RGD sequence or natural materials as agarose, alginate, gelatin, HA and chitosan in order to improve cellular adhesion on the hydrogels surface [53, 94].

The modification of polymers can lead to an additional increase in the electrical conductivity, which is crucial for CNS regeneration [14, 95, 96]. There are few examples of pure hydrogels which possess electroconductive properties. One of them is chemically crosslinked poly(3-thiophene acetic acid (PTAA), which has electrical conductivity equal to 0.01 S cm^{-1} and showed better C2C1 cell activity [65].

Another method to obtain electrically conductive hydrogels is by combining synthetic, insulating, 3D structured aqueous

hydrogel with electrical conductive polymers such as polyaniline (PANI) and polypyrrole (PPy) [65, 96, 97]. Examples of this type of non-injectable approaches will be discussed in the following section 4.1.

Relatively novel type of scaffolds are 3D-bioprinted hydrogels loaded with cells. Such scaffolds showed enhanced cellular growth and proliferation [98]. For CNS tissue engineering, alginate, fibrin, fibrinogen/ thrombin and thermosensitive polyurethane loaded with neural cells (e.g.: NSCs) are commonly used in bioprinting technique [98, 99]. There are plenty of advantages of bioprinting using hydrogels: simple processing, various bioprinter type and low costs [98]. Nevertheless, depending on the bioprinter, fabrication process can disrupt the soft integrated structure of the hydrogel, and cell aggregates can clog the nozzle tip [98]. Many bioprinted hydrogels are not suitable for tissue engineering because their crosslinking agents as UV radiation are toxic for cells immersed in the hydrogel matrix and degradation products of hydrogel (fibrin) cause an immune response. Moreover bioink materials as non—injectable materials do not map the irregular lesion shape [14].

Summing up, besides many advantages which are mentioned above of non-injectable hydrogels, such as: biomimetic properties, adequate mechanical and electrical properties, the main reason for searching for a new solution is a the possibility of direct delivery to the place of injury. Non-injectable hydrogels need to be introduced to the injury area by the means of open surgery, which increases the risk of after-surgery complications.

3.2. Injectable hydrogels

The idea of injectable hydrogels is to inject relatively low-viscosity polymer solution in the injury area, where it undergoes gelation. A very important characteristic is the rate of gelation, which should be on the one hand slow enough to allow for the injection to take place and fill the lesion completely, and on the other fast enough to prevent it from flowing out of the lesion site. The rate of crosslinking (gelation) can be tailored by the type of the polymer, its molecular weight, concentration and crosslinking type/degree-chemical or physical crosslinking (e.g.: UV light, pH and temperature changing). It is important to tailor the mechanical properties of the hydrogel to those of soft tissues of interests and degradation time to regeneration rate of injured tissue [100, 101]. This is especially significant case of structures like the human brain, which has compact and complex structure so the injury may be in the deep parts of the brain and not easy to localize [14].

Injectable hydrogels are mainly polysaccharides-based materials, such as HA or chitosan. HA, as a natural component of the ECM, easily interacts with cell receptors, which improves material and neural cells interactions [90]. There are many examples of HA modifications, like attaching RGD groups or adding another hydrogel, such as methylcellulose (MC), leading to the improvement its properties [100, 102].

Another type are the polyacrylamide PAM- and PEG-based hydrogels, e.g.: PEG hydrogel crosslinked with oximine [103]. Rheological analysis confirmed storage modulus was appropriate for brain tissue regeneration and was determined to be 0.5 kPa. *In vivo* studies on rats involving subcutaneous dorsal tissue, showed rapid gelation (20 min) which indicates a great potential of this material as minimally invasive approach for the CNS regeneration [103].

An interesting type in this group of materials are self-assembling hydrogels. They consist of natural, synthetic or hybrid hydrogels incorporated with proteins which are able to self-assembling. In their structure spontaneous organization is carried out as a consequence of non-covalent (physical) interactions (e.g.: double helix, proteins aggregation) [104]. An example of such approach in CNS tissue engineering is self-assembly peptide hydrogel conjugated with IKVAV sequence and NSCs. Increase of pH stimulate self-assembling of peptides and provide 3D network formation. Such approach provides NSCs differentiation into neurons and effectively supported elongation of axons [87], which was confirmed by *in vivo* studies on the mouse brains.

To our knowledge, in the literature, there are no reports of a single, injectable hydrogel with electroconductive properties. To obtain such electroconduction they are usually modified with various forms of electroconductive materials e.g. electroconductive fibers [97] or magnetic particles [105].

Compared to non-injectable hydrogels injectable materials avoid complex and long surgeries—they are rapidly introducing into the body (up to 5 min) and show improved integration with host tissue [63]. However, it must be taken into account that such injectable materials behave differently *in vitro* and *in vivo*. The complex internal environment of the body can significantly affect their mechanical properties and the gelation rate [103]. Moreover, agents used in chemical crosslinking (e.g.: glutaraldehyde) are very often toxic for cells [84, 106].

General schematics of non-injectable (a) and injectable (b) hydrogel-based drug delivery system strategies are presented in the figure 2.

3.3. Thermosensitive hydrogels

Thermosensitive hydrogels are a specific case of injectable hydrogels. These materials become a gel as a consequence of physical interactions, stimulated by changes in temperature. This crosslinking mechanism is connected to critical solution temperature (CST). Below and above CST hydrophilic polymers loose large amounts of water and become a gel with a domination of hydrophobic interactions [12]. The low viscosity solution can be easily injected by syringe inside the body and as a result of *in situ* crosslinking, its viscosity increases resulting in gel formation [107, 108].

An interesting type of thermosensitive hydrogels, which are made of natural components, are ECM hydrogels (e.g.: basement membrane and porcine urinary bladder) [19, 109]. At room temperature such material was in a liquid form and the storage modulus was 0.0001 kPa, but while temperature increased to 37 °C, it became a solid hydrogel with storage modulus 0.01–0.5 kPa after 5 min. Although, the gelation time was impressive, in these concentrations (0–8 mg ml^{-1}) the

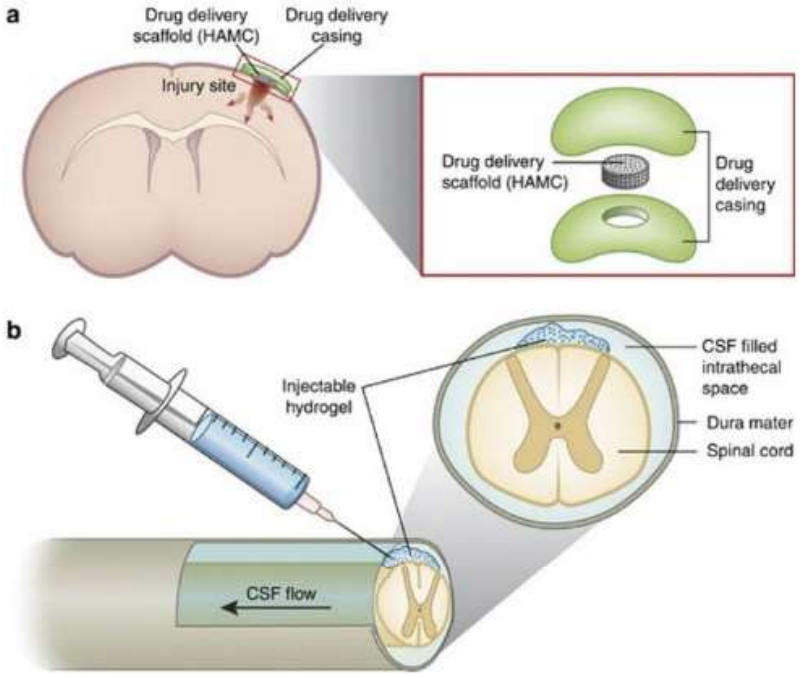

Figure 2. Strategy of drug delivery system using non-injectable (a) and injectable hydrogel (b) for TBI and SCI. HAMC non-injectable hydrogel loaded with drug is located on the cortex, allowing drug distribution into the brain (a). Injectable hydrogel (b) is injected between dura matter and intrathecal space, where crosslink rapidly and release the drug exactly at the injured site. Figure adapted with permission from Springer Customer Service Centre GmbH: Nature, Neuropsychopharmacology, Regenerative therapies for CNS diseases: a biomaterials approach, Tam *et al* [70]. Copyright 2014 American College of Neuropsychopharmacolog. With permission of Springer.

storage modulus was less than ideal (table 1) [109]. Ghuman *et al* [19] fabricated ECM hydrogel with elastic modulus (0.5–1 kPa) suitable for CNS regeneration. The studies showed such material induces rapid and effective infiltration of host cells (microglia, macrophages, NPCs) and provides regeneration of the tissue after stoke in rat brains. This reaction is probably caused by chemical composition mimicking ECM (laminin and fibronectin) and signal molecules inducing regenerative response.

Extensively studied natural thermosensitive hydrogels are agarose and cellulose derivatives, such as MC and some synthetic polymers based on polyacrylamide (PAM) (e.g. Poly(N-isopropylacrylamide) (P(NIPAAm)) [84, 110, 111].

Because of chemical treatment of cellulose, MC becomes water-soluble. The gelation temperature depends on MC concentration in aqueous solution, being usually around 40 °C–50 °C [110]. The storage modulus of MC gels is relatively low, for instance 0.1 kPa for 3% solution, being too low for CNS applications (according to table 1) [110]. In order to obtain improved properties for tissue regeneration, thermal-sensitive polymers can be blended with other natural polymers. However, Payene *et al* [112] described the collagen/MC and β glycerophosphate (β-GLC) blend as potential candidate for tissue engineering. The rheological measurements of MC/Col/β-GLC showed storage modulus G′ up to 0.07 kPa [112]. This value is too low for CNS tissue engineering scaffolds, but signifies the material could be useful as a delivery system. In turn, the viability and proliferation tests on stem cells (hMSCs) confirmed this composite is adequate for *in vivo* tissue engineering applications [112].

The increase of storage modulus of MC, as well as lowering the gelation temperature and improving stability in physiological environment was achieved by the addition of HA [100]. Many *in vitro* and *in vivo* studies, carried out by Pakulska *et al* [73], Sarkar *et al* [113], and Ballios *et al* [114], confirmed positive results in the brain healing process with the use of such blended systems.

Despite its huge potential, from economical and practical point of view, HA is unfavorable (poor mechanical properties and rapid degradation) [89, 115]. One of the most interesting approaches to replace HA is addition of agarose to MC. This composition has properties very similar to HA/MC and also crosslinks at physiological temperature. Studies performed by Martin *et al* [84] showed that elastic modulus of MC and agarose composite is approximately 1.3 MPa and the addition of agarose 3 fold decreased the gelation time. *In vitro* tests on neuronal cells (DRG) confirmed their good viability during the contact with hydrogel.

Thermal sensitivity is mostly the domain of natural polymers, however injectable synthetic PAM hydrogel showed these properties as well. In this matter, PAM-based materials, such as P(NIPAAm) with Young's modulus ca. 1.2 kPa are especially attractive [111]. Another example of a hydrogel for SCI treatment is P(NIPAAm)-PEG with compressive (elastic) modulus in the range of 2–4 kPa. *In vitro* tests showed great cells adhesion and the release tests also showed that growth factors (GFs) are released in up to 6 weeks, which indicate this approach is appropriate for long-term CNS therapies [116].

The next promising way for CNS therapies is modification of P(NIPAAm). For example, Brahima *et al* [117] described

Table 3. Non-injectable hydrogel with nanoparticles.

Cross linker	Nature of hydrogel matrix	Hydrogel	Particles	Advantages provided by nanoparticles	Function of composite	Ref.
Ammonium peroxydisulfate	Natural	Bacterial cellulose	PANI nanofibers	Topography, electroconductivity, 3D structure	Scaffold	[129]
UV light	Natural	HEC	PANI nanotubes	Electroconductivity, topography, mechanical properties	Scaffold/ delivery system	[97]
Bisazide	Synthetic	PVA	SWCNT	Electroconductivity	—	[119]
UV light	mixed	GelMa	MWCNT	Electroconductivity, slower degradation, mechanical	Scaffold	[120]
UV light	Synthetic	PEG and PEGPCL	PCL and core/shell PCL/ PEGPCL nanofibers	Topography	Fibrous scaffold	[121]
no indicated	Natural	Chitosan	MWCNT	Topography, electroconductivity	Scaffold	[128]
N, N′-methylene bis acrylamide	Synthetic	PAA-PVA	PANI nanoparticles	Electroconductivity	Scaffold	[130]

a delivery system consisting of poly(NIPAAm-co-AAc) interpenetrated polymer network (IPN) hydrogel which is also pH-responsive system. The release tests showed an increase in substance delivery with rising temperature and pH reduction. This results might be crucial for the future delivery systems design.

There are many [73, 117, 118] *in vitro* and *in vivo* studies demonstrating the effectiveness of hydrogels for CNS regeneration. For instance Wang *et al* [118] studied heparin-poloxamer thermosensitive hydrogel as growth factor delivery system. *In vivo* tests on rats with SCI showed a 8–10 fold increase in the number of axons, which proves the suitability of this approach in neural tissue engineering [118].

4. Hydrogels with micro- and nanoparticles

Hydrogels loaded with nanoparticles have unique properties, attractive for CNS regeneration due to combining the characteristics of hydrogel and nanoparticles. In CNS tissue engineering, particles addition to hydrogel matrix can provide many benefits related to electroconductivity, mechanical properties, topography, ECM similarities, as well as allows drugs, GFs and cells to be introduced [119–124]. This approach was helpful for delivery system applications and solved an issue of uncontrolled GFs release, as well as provided their protection from toxic crosslinking agents [103, 125].

The non-injectable and injectable hydrogels loaded with nanoparticles are compiled briefly in tables 3 and 4. Loaded additives are in the form of nanofibers and nanotubes as well as microspheres, micro- and nanoparticles [121, 126, 127].

4.1. Non-injectable hydrogels loaded with micro and nanoparticle

Han *et al* [123] fabricated photo-crosslinked PEG hydrogel loaded with electrospun poly(ε-caprolactone) (PCL) nanofibers, the main task of which was to supply the material in fibrillar form, which is favourable by cells. Such combination of synthetic PEG/PCL hydrogel with PCL nanofibers was beneficial for interactions with cells investigated i*n vitro* and *in vivo* (rat brain) conditions [121].

Electro-conductive additives to hydrogels like single- and multi-walled CNTs, metal nanoparticles and electroconductive polymeric nanoparticles [119, 128] appear to be extremely important in nervous system regeneration process. For instance Lee *et al* [119] prepared a PVA hydrogel with single-walled nanotubes (SWCNT), obtaining an essential electrical conductivity increase. Gupta *et al* [128] modified chitosan hydrogel using MWCNT nanotubes. Rheological measurements showed Young's modulus 1.4 fold increase, while electrical conductivity 106 fold increased after the addition of nanotubes [128]. Despite the obtained modulus was to high according to table 1, *in vivo* studies on rat brain showed this approach provides high viability of neural cells (HT-22) and confirmed scaffolds were supplying mechanical and electrical cues [128]. Similar investigation was carried out by Ahadian *et al* [120] where methacrylated gelatin (GelMa) was filled by MWCNT. Thanks to this additive, electrical properties increased by 1.5%–10% and Young's modulus 1.6–4 fold increased depending on MWCNT concentration [120].

However, according to some reports, CNTs are responsible for oxidative stress which leads to neural cells apoptosis [64]. Considering this fact, more research is directed towards the use of electroconductive polymers. For example, by combination of photo-crosslinkable, natural 2-hydroxyethylcellulose (HEC) hydrogel and polyaniline (PANI) nanotubes (HEC/PANI) [97]. The addition of nanotubes caused 0.15 fold increase of electrical properties. This increase was beneficial for cellular morphology and neural cells activity [97]. Shi *et al* [129] studying natural, *in situ* gelling of bacterial cellulose hydrogel filled by PANI nanofibers reported even a 1000 000 fold increase of the electrical conductivity of the composite. There is a potential for this biomaterial to be used in tissue engineering, but more *in vitro* and *in vivo* studies still need to be done [129].

Bajpai *et al* [130] formed an unique hydrogel, using PANI nanoparticles distributed in polyacrylic acid (PAA) and polyvinylalcohol (PVA) hydrogel. This composite showed good biocompatibility, mechanical properties, and electrical conductivity approximately 3–4 fold higher compared to pure hydrogel [130].

Nanoparticles introduced into non-injectable hydrogels provide many benefits similar to the above-mentioned: improved mechanical strength, appropriate topography or/and electrical properties, cells/GFs/drugs delivery. However, like the non-injectable hydrogels in stand-alone use, they do not fulfil the CNS tissue engineering requirements concerning minimally invasive insertion in the place of injury [123]. Therefore, investigations on injectable hydrogel composites are recently carried out. Current approaches are described below.

4.2. Injectable hydrogels with nano- and microparticles

Most of the investigations are related to the use of injectable hydrogels as delivery media of various active factors, such as glial cell-derived neurotrophic factor (GDNF), by encapsulation into nano- or microspheres. Nanoparticles are safe for neural tissue, can pass the BBB, and their small size allows them to move through cell membranes, increasing the availability of the carried substances and providing their sustained release [131]. However, too small nanoparticles can be absorbed by macrophages immediately after injection into the body. To solve this problem they are encapsulated inside the polymeric microspheres or suspended directly in hydrogel matrix [127].

Ansorena *et al* [124] was one of the first researchers who encapsulated GDNF in poly(lactide-co-glycolide) (PLGA) microspheres and dispersed it in ionic crosslinked alginate/fibrinogen hydrogel (table 4). GDNF release profile showed a rate 2.5 times slower in case of PLGA nanoparticles in hydrogel matrix in comparison to pure hydrogel. On the other hand, the results of *in vivo* studies indicated better neurite outgrowth for free GDNF-loaded compared to GDNF loaded in microparticles contained hydrogel. Rat spinal cord treated with hydrogels with free GDNF showed a complete recovery [124].

Some others publications describe PEG-based hydrogels and PLGA nanoparticles as delivery devices, which are listed in the table 4. For instance, photo-crosslinked PLGA-PEG-PLA hydrogel filled with GFs encapsulated in PLGA microparticles [122] or photo-crosslinked PEG hydrogel with PLGA microspheres as delivery system with controlled release rate [131].

Encapsulation in PLGA microspheres was also used for anti-tumor brain therapy. Polyethylene glycol dimethacrylate (PEG-DMA) hydrogel was filled by gradually sustained anti-tumor drug in PLGA nanoparticles. *In vivo* studies on mouse brains confirmed reduced weight in U87MG tumor cells as a response for drugs contained composite [132]. Current strategies employing nanoparticles loaded in hydrogel matrices are mainly focused on their multifunctionality. This is especially important from the point of view of neural tissue regeneration, because many requirements have to be fulfilled simultaneously in this case. Depending on intended function, nanoparticles implemented in different forms, and are made from various materials, including ceramics or polymers.

Lampe *et al* [133] described a PLGA-PEG-PLA hydrogel with PLGA microparticles, which provided controlled GFs release and an approximately 2 fold decrease in the number of glial scar cells (astrocytes and microglia).

A novel solution of this problem is the encapsulation of GFs in lipid microcapsules protecting them from direct contact with toxic crosslinking agents [134]. *In vitro* and *in vivo* studies on neural cells (axons) and rat brains confirm the effectiveness of this solution—an increase in cellular viability and proliferation was observed on hydrogel with such nanoparticles [134].

Glass nanofibers are another example of fillers used for the enhancement of topographical and biological properties of hydrogels. Novajra *et al* [135] used a chemically crosslinked hybrid, consisting of agarose hydrogel and glass nanofibers. In this case, the presence of nanofibers reduced 2 fold the release of GFs from hydrogel. *In vitro* tests on neonatal olfactory bulb ensheathing (NOBEC) cell line confirmed better cellular spreading on hydrogels with glass nanofibers [135].

A similar increase in cellular activity was observed for the ionic crosslinked alginate hydrogel filled with silk nanofibers [136]. It was shown that due to the addition of fibers, GFs release was 3 fold higher than from pure alginate hydrogel. They also leads to abundant cell adhesion on the surface of the material, which was confirmed via *in vivo* tests on SCI rat model [136].

A relatively new approach is injectable, self-assembling hydrogel with nanoparticles. Liu *et al* [137] fabricated cellulose acetoacetate (CAA)/hydroxypropyl chitosan (HPCS) modified with amino-cellulose nanocrystals (CNC-NH2). Nanocrystals were a kind of crosslinking agent leading to an improvement of hydrogel mechanical properties. Rheological analysis showed that CNC-NH2 effectively reinforced the hydrogel. Compared to pure hydrogel their storage modulus 2 fold increased to 2.3 kPa (according to table 1 this value is suitable for brain regeneration). Although the composite was tested *in vitro* on L929 cells only, the results show it can be potentially used in CNS tissue engineering.

Recently, an innovative approach for CNS regeneration seems to be magnetic gels (ferrogels). Ferrogels are made up of the colloidal magnetic particles loaded in polymeric matrix. They are stimuli-responsive materials which behavior is controlled with appropriate magnetic field [105]. Lopez-Lopez *et al* [138] fabricated an injectable fibrin hydrogel loaded with commercial magnetite nanoparticles (MagP-OH, 110 nm diameter), which modified microstructure of whole composite and significantly increased its storage modulus (up to 0.6 kPa) and functioned as additional crosslinking agent. Although, biocompatibility tests were carried out only on subcutaneous tissue of the forelegs of rats [138], such approach might be studied as promising material for CNS regeneration.

The concept of electroconductive, injectable hybrid hydrogels is also found in literature. Koppes *et al* [85] studied collagen hydrogel filled with SWCNT. AFM nanoindentation showed that Young's modulus 120 fold increase, while electric conductivity approximately 2 fold increase after the SWCNT addition to pure collagen hydrogel. During this study, a positive effect of electrical stimulation on neuronal cell (DRG line) activity was shown. The neurite outgrowth 3.3 fold increased in comparison to the pure hydrogel [85].

Table 4. Injectable hydrogels loaded with various particles for CNS regeneration.

Crosslinking factor	Nature of hydrogel matrix	Hydrogel	Particles	Particles functions (cells/GFs/drug type)	Ref.
Ca^{2+} ions	Natural	Alginate/fibrinogen	PLGA microspheres with GDNF	Controlled release of GFs	[124]
No indicated	Synthetic	PLA-PEG-PLA hydrogel	PLGA microparticles with neurotrophic factor	Controlled release of GFs	[122]
Photo-polimerization	Synthetic	PEG	PLGA microspheres with neurotrophic factor	Controlled release of GFs	[131]
UV light	Synthetic	PEG-DMA	PLGA nanoparticles with drug-temozolomide	Controlled drug release	[132]
UV light	Synthetic	PEG-based	PLGA microspheres with NGFs	Controlled release of GFs	[133]
Genipin	Natural	Collagen	Lipid microtubes with fibroblast growth factor (FGF-2)	Controlled release of GFs, protective role during chemical crosslinking	[134]
Genipin	Natural	Agarose/gelatin	Glass hollow fibers with neurotrophic factors	Controlled release of GFs	[135]
Ca^{2+} ions	Natural	Alginate microspheres	Silk fibers with NGFs	Controlled release of GFs, topography (scaffold and delivery system)	[136]
CNC-NH_2	Natural/ Synthetic	CAA/HPCS	CNC-NH_2	Crosslinking, mechanical improvement	[137]
Temperature	Natural	Collagen	Carbon nanotubes (SWCNT)	Electrical conductive	[85]
Temperature (local cooling)	Natural	Agarose	PLGA nanoparticles with drug-methylprednisolone	Sustained drug release	[140]
Temperature	Natural	HA/MC	PLGA microparticles with drug-cyclosporin A	Sustained drug release	[123]
Temperature	Natural	HA/MC	PLGA nanoparticles	Sustained drug release	[110]
Temperature	Natural	HA/MC	PLGA nanoparticles with neurotrophin NT-3	Controlled release of GFs	[141]
Temperature	Natural	Adipic acid dihydrazide-modified hyaluronic acid (ADH-HA)	Cellulose nanocrystals	Biological, structural, additional crosslinker fibrous scaffold	[139]
Temperature	Natural	HA/MC	Electrospun genipin-collagen or poly (3-caprolactone-co-D,L lactide) (P(CL:DLLA) nanofibers with NSPCs	Controlled release of cells, topography	[86]
Temperature	Natural	Agarose/MC	PLLA + fibronectin nanofibers	Topography fibrous scaffold	[142]

An addition of the particles may have a significant effect on the composite formation process and because of that it is important to precisely adjust all their properties, such as size and concentration [139]. Additionally it should be aware of the risks that added particles might be entrapped and entangled with hydrogel polymeric chains and disrupt the effective functioning (e.g. therapeutics release) [139].

4.2.1. Injectable thermo-sensitive with micro-, nano-particles. In CNS tissue engineering, emphasis is placed on drug delivery systems. In this field, hydrogels are commonly functionalized with PLGA particles, e.g.: PLGA drug-loaded microparticles dispersed in natural agarose hydrogel [140] (table 4). Immunofluorescence analysis showed that nanoparticles addition reduced lesion volume and hence led to effective therapeutic release [140]. The *in vivo* tests on SCI rat model also confirmed a decreased amount of injury factors and provided reduction size of the lesion.

Another popular approach is HA/MC hydrogel loaded with PLGA nanoparticles. In this composite there are factors influencing release profile, e.g.: reduced amount of HA in HA/MC composition increased the time of drug release [110], and reduced number of nanoparticles decreased the time of release [141].

An interesting approach was described by Domingues *et al* [139] who incorporated cellulose nanocrystals into HA-based hydrogel, resulting in an increase of mechanical properties. Rheological measurements using DMA technique showed that storage modulus approximately 2 fold increase in comparison to pure hydrogel. *In vitro* study confirmed better human adipose derived stem cells (ADSCs) viability on the surface of hydrogel enriched with cellulose nanoparticles. Cellulose nanocrystals affect hydrogel degradation rate- in hyaluronidase and PBS environment. The composite showed longer degradation time compared to pure HA hydrogel [139].

Longer release, biocompatibility and appropriate biodegradation rate was observed and described by Hsieh *et al* [86] for HA/MC filled with natural or synthetic electrospun fibers (collagen crosslinked with genipin or poly (3-caprolactone-co-D,L lactide)). *In vitro* study confirmed positive influence of

nanofibers filler on viability and proliferation of neural stem/progenitor cells (NSPCs) [86].

The addition of nanofibers to injectable hydrogels limits the injection ability. One of the possible solutions to this problem was proposed by Rivet *et al* [142] by using of cut PLLA electrospun fibers. They were added to agarose/MC hydrogel increasing proliferation and activity of neural cells [142].

According to our knowledge, there is no data about thermosensitive, injectable hydrogels loaded with electroconductive particles for CNS tissue engineering.

Thermally sensitive, injectable hydrogels loaded with nanoparticles are extremely promising to CNS regeneration due to their unique- hybrid properties. However, we should be aware that some of the nanoparticles might be entrapped in hydrogel after thermal crosslinking, which can seriously decrease composite functionality [126]. The presence of some particles also can induce immune response, leading to local rise in the body temperature and influences the gelation kinetics [126]. Finally, there is the problem of injectability when loaded with nanoparticles, particularly nanofibers which can be overcome by special techniques of fibers preparation.

5. Summary, conclusions and future directions

The newest trend in hydrogels formation for CNS tissue engineering is the use of hydrogels, particularly injectable hydrogels, loaded with various nano- and microparticles. The most important benefits from the introduction of nano- and microparticles are:

- increase of mechanical properties
- increase of electrical conductivity
- biomimetic topography
- enhancement of biological properties; controlled delivery of therapeutics, cells and GFs

Despite these advantages, we should be aware of some problems related to nano- and microparticles loaded hydrogels, of which the most important are:

- keeping the materials injectable (especially in the case of nanofibers loaded hydrogels)
- matching mechanical properties and electrical conductivity of native neural tissue
- providing appropriate biodegradation kinetics
- maintaining a non-toxic character of the whole system

While injectable hydrogels loaded with electroconductive nanoparticles are common, to our best knowledge there are no reports on thermosensitive, injectable hydrogels with such additives for CNS regeneration. We are deeply convinced that smart materials containing thermosensitive, injectable hydrogels as a matrix and nanoparticles as additives can fulfill the high requirements of CNS regenerative medicine. In this regard, there are still many investigations to be carried out, such as the optimization of hydrogel composition, the determination of micro- and nanoparticles size, shape and concentration, etc. Considerable attention should be directed toward the effect of used materials on living tissues, to be determined via *in vivo* studies. Such investigations are very needed considering that this approach is very attractive for clinical applications.

Currently, there are only few reports on the practical aspects of the injection procedure. Traditional injection carries a risk of unstable and inaccurate introduction of the hydrogel system into the body especially when microinjuries are dealt with [143]. Future strategies combining microinjections with stable, electronically controlled platform and hydrogel/nanoparticles systems of cells, GFs or therapeutics delivery might offer, expected for years, effective regeneration of CNS. We believe that this approach utilizing in CNS clinical applications is only a matter of time.

Additionally, it should be brought to attention that the mechanisms of neural tissue growth stimulation are not yet fully known. However, numerous publications concerning CNS regeneration, including *in vivo* tests, encourage researchers to continue investigations of the structure and properties of hydrogels.

ORCID iDs

B Niemczyk https://orcid.org/0000-0002-5836-1015

References

[1] Whalin M K and Arora S S 2018 Anatomy of the brain and spinal cord *Basic Sciences in Anesthesia* (Cham: Springer) pp 41–59
[2] Mosby Inc. 2009 *Human Nervous System Mosby's Medical Dictionary* 8th edn (St Louis, MO: Elsevier Health Sciences)
[3] Johnson B K 2018 Physiology of the autonomic nervous system *Basic Sciences in Anesthesia* (Cham: Springer) pp 355–64
[4] Bacon R L and Niles N R 1986 Nervous tissue *Medical Histology* (New York: Springer) pp 113–34
[5] Purves D, Augustine G J, Fitzpatrick D, Katz L C, LaMantia A S, McNamara J O and Williams S M 2001 *Neuroscience* 2nd edn (Sunderland, MA: Sinauer Associates)
[6] Gil V A 2012 *Functional neuroanatomy of the dog Universitat Autònoma de Barcelona* (Bellaterra: Servei de Publicacions)
[7] Taylor C A, Bell J M, Breiding M J and Xu L 2017 Traumatic brain injury–related emergency Department Visits, Hospitalizations, and Deaths—United States, 2007 and 2013 *MMWR Surveill. Summ.* **66** 1–16
[8] Adrian H, Marten K, Salla N and Lasse V 2016 Biomarkers of traumatic brain injury: temporal changes in body fluids *eNeuro* **3** ENEURO-0294
[9] Schwab M E and Bartholdi D 1996 Degeneration and regeneration of axons in the lesioned spinal cord *Physiol. Rev.* **76** 319–70
[10] Lis A, Szarek D and Laska J 2013 Biomaterials engineering strategies for spinal cord regeneration: state of the art *Polim. Med.* **43** 59–80
[11] Weidner N, Rudiger R and Tansey K E 2017 *Neurological Aspects of Spinal Cord Injury* vol 1 (Switzerland: Springer) pp 3–17
[12] Stabenfeldt S E, Garcia A J and LaPlaca M C 2006 Thermoreversible laminin-functionalized hydrogel for neural tissue engineering *J. Biomed. Mater. Res.* A **77** 718–25

[13] Delcroix G J R, Schiller P C, Benoit J P and Montero-Menei C N 2010 Adult cell therapy for brain neuronal damages and the role of tissue engineering *Biomaterials* **31** 2105–20
[14] Lis A, Szarek D and Laska J 2013 The outlook for the use of polymeric scaffolds in the reconstruction and the regeneration stimulation of traumatic brain injuries *Polim. Med.* **43** 302–12
[15] Park J H, Han J B, Kim S K, Park J H, Go D H, Sun B and Min B I 2010 Spinal GABA receptors mediate the suppressive effect of electroacupuncture on cold allodynia in rats *Brain Res.* **1322** 24–9
[16] Silva P A, Pereira P, Pinto R, Silveira F and Vaz R 2014 Bilateral sciatic neuropathy due to fibrous bands in a patient with severe traumatic brain injury *Clin. Neurol. Neurosurg.* **120** 93–5
[17] Li X, Katsanevakis E, Liu X, Zhang N and Wen X 2012 Engineering neural stem cell fates with hydrogel design for central nervous system regeneration *Prog. Polym. Sci.* **37** 1105–29
[18] Han D and Cheung K C 2011 Biodegradable cell-seeded nanofiber scaffolds for neural repair *Polymers* **3** 1684–733
[19] Ghuman H, Massensini A R, Donnelly J, Kim S M, Medberry C J, Badylak S F and Modo M 2016 ECM hydrogel for the treatment of stroke: characterization of the host cell infiltrate *Biomaterials* **91** 166–81
[20] Bignami A, Hosley M and Dahl D 1993 Hyaluronic acid and hyaluronic acid-binding proteins in brain extracellular matrix *Anat. Embryol.* **188** 419–33
[21] Guilak F, Cohen D M, Estes B T, Gimble J M, Liedtke W and Chen C S 2009 Control of stem cell fate by physical interactions with the extracellular matrix *Cell Stem Cell* **5** 17–26
[22] Cregg J M, DePaul M A, Filous A R, Lang B T, Tran A and Silver J 2014 Functional regeneration beyond the glial scar *Exp. Neurol.* **253** 197–207
[23] Gesteira T F, Coulson-Thomas Y M and Coulson-Thomas V J 2016 Anti-inflammatory properties of the glial scar *Neural Regen. Res.* **11** 1742
[24] Budday S *et al* 2017 Mechanical charakterization of human brain tissue *Acta Biomater.* **48** 319–40
[25] Mahairaki V, Lim S H, Christopherson G T, Xu L, Nasonkin I, Yu C and Koliatsos V E 2011 Nanofiber matrices promote the neuronal differentiation of human embryonic stem cell-derived neural precursors *in vitro Tissue Eng.* A **17** 855–63
[26] Harris G M, Madigan N N, Lancaster K Z, Enquist L W, Windebank A J, Schwartz J and Schwarzbauer J E 2017 Nerve guidance by a decellularized fibroblast extracellular matrix *Matrix Biol.* **60** 176–89
[27] Hyatt A J, Wang D, van Oterendorp C, Fawcett J W and Martin K R 2014 Mesenchymal stromal cells integrate and form longitudinally-aligned layers when delivered to injured spinal cord via a novel fibrin scaffold *Neurosci. Lett.* **569** 12–7
[28] Sensharma P, Madhumathi G, Jayant R D and Jaiswal A K 2017 Biomaterials and cells for neural tissue engineering: current choices *Mater. Sci. Eng.* C **77** 1302–15
[29] Mothe A J, Tam R Y, Zahir T, Tator C H and Shoichet M S 2013 Repair of the injured spinal cord by transplantation of neural stem cells in a hyaluronan-based hydrogel *Biomaterials* **34** 3775–83
[30] Kanno H, Pressman Y, Moody A, Berg R, Muir E M, Rogers J H and Bunge M B 2014 Combination of engineered Schwann cell grafts to secrete neurotrophin and chondroitinase promotes axonal regeneration and locomotion after spinal cord injury *J. Neurosci.* **34** 1838–55
[31] Parys B, Cote A, Gallo V, De Koninck P and Sik A 2010 Intercellular calcium signaling between astrocytes and oligodendrocytes via gap junctions in culture *Neuroscience* **167** 1032–43
[32] Alessandri M, Lizzo G, Gualandi C, Mangano C, Giuliani A, Focarete M L and Calzà L 2014 Influence of biological matrix and artificial electrospun scaffolds on proliferation differentiation and trophic factor synthesis of rat embryonic stem cells *Matrix Biol.* **33** 68–76
[33] Dahlin R L, Kasper F K and Mikos A G 2011 Polymeric nanofibers in tissue engineering *Tissue Eng.* B **17** 349–64
[34] Yang F, Murugan R, Ramakrishna S, Wang X, Ma Y X and Wang S 2004 Fabrication of nano-structured porous PLLA scaffold intended for nerve tissue engineering *Biomaterials* **25** 1891–900
[35] Wang Z, Crandall C, Sahadevan R, Menkhaus T J and Fong H 2017 Microfiltration performance of electrospun nanofiber membranes with varied fiber diameters and different membrane porosities and thicknesses *Polymer* **114** 64–72
[36] Zhang J, Du Y, Zhang L, Zheng X, Ma Y, Dong S and Zhou D 2017 Preparation of sponge carrier supported photocatalyst by self-assembly technique for phenol photodegradation in visible light *Mol. Catal.* **432** 1–7
[37] Wegst U G, Schecter M, Donius A E and Hunger P M 2010 Biomaterials by freeze casting *Phil. Trans.* A **368** 2099–121
[38] Llacua L A, Faas M M and de Vos P 2018 Extracellular matrix molecules and their potential contribution to the function of transplanted pancreatic islets *Diabetologia* **61** 1–12
[39] Buzanska L, Zychowicz M, Sarnowska A and Domanska-Janik K 2013 Bioenineering of neural stem cell niche *Postepy Biochem.* **59** 175–86
[40] Freudenberg U, Hermann A, Welzel P B, Stirl K, Schwarz S C, Grimmer M and Storch A 2009 A star-PEG–heparin hydrogel platform to aid cell replacement therapies for neurodegenerative diseases *Biomaterials* **30** 5049–60
[41] Ma W, Tavakoli T, Derby E, Serebryakova Y, Rao M S and Mattson M P 2008 Cell-extracellular matrix interactions regulate neural differentiation of human embryonic stem cells *BMC Dev. Biol.* **8** 90
[42] Khaing Z Z, Thomas R C, Geissler S A and Schmidt C E 2014 Advanced biomaterials for repairing the nervous system: what can hydrogels do for the brain? *Mater. Today* **17** 332–40
[43] Cheng S, Clarke E C and Bilston L E 2008 Rheological properties of the tissues of the central nervous system: a review *Med. Eng. Phys.* **30** 1318–37
[44] Bartlett R D, Choi D and Phillips J B 2016 Biomechanical properties of the spinal cord: implications for tissue engineering and clinical translation *Regen. Med.* **11** 659
[45] Taylor Z and Miller K 2004 Reassessment of brain elasticity for analysis of biomechanisms of hydrocephalus *J. Biomech.* **37** 1263–9
[46] Bilston L E and Thibault L E 1996 The mechanical properties of the human cervical spinal cord *in vitro Ann. Biomed. Eng.* **24** 67–74
[47] Weickenmeier J, Kurt M, Ozkaya E, Wintermark M, Pauly K B and Kuhl E 2018 Magnetic resonance elastography of the brain: a comparison between pigs and humans *J. Mech. Behav. Biomed. Mater.* **77** 702–10
[48] Seidlits S K, Khaing Z Z, Petersen R R, Nickels J D, Vanscoy J E, Shear J B and Schmidt C E 2010 The effects of hyaluronic acid hydrogels with tunable mechanical properties on neural progenitor cell differentiation *Biomaterials* **31** 3930–40
[49] Lins L C, Wianny F, Livi S, Hidalgo I A, Dehay C, Duchet-Rumeau J and Gérard J F 2016 Development of bioresorbable hydrophilic–hydrophobic electrospun scaffolds for neural tissue engineering *Biomacromolecules* **17** 3172–87
[50] Cunha C, Panseri S, Villa O, Silva D and Gelain F 2011 3D culture of adult mouse neural stem cells within

functionalized self-assembling peptide scaffolds *Int. J. Nanomed.* **6** 943
[51] Stufflebeam R 2008 Neurons, synapses, action potentials, and neurotransmission *Consortium on Cognitive Science Instruction*
[52] Berridge M J, Bootman M D and Lipp P 1998 Calcium-a life and death signal *Nature* **395** 645–8
[53] Akhtari M, Emin D, Ellingson B M, Woodworth D, Frew A and Mathern G W 2016 Measuring the local electrical conductivity of human brain tissue *J. Appl. Phys.* **119** 064701
[54] Sabzpoushan S H and Sabzpoushan S A 2014 L-sensors in aerospace sensor *Netw. Data Commun.* **3** 14
[55] Hamid S and Hayek R 2008 Role of electrical stimulation for rehabilitation and regeneration after spinal cord injury: an overview *Eur. Spine J.* **17** 1256–69
[56] George P M, Bliss T M, Hua T, Lee A, Oh B, Levinson A and Steinberg G K 2017 Electrical preconditioning of stem cells with a conductive polymer scaffold enhances stroke recovery *Biomaterials* **142** 31–40
[57] Goganau I, Sandner B, Weidner N, Fouad K and Blesch A 2018 Depolarization and electrical stimulation enhance *in vitro* and *in vivo* sensory axon growth after spinal cord injury *Exp. Neurol.* **300** 247–58
[58] Wood M and Willits R K 2006 Short-duration, DC electrical stimulation increases chick embryo DRG neurite outgrowth *Bioelectromagnetics* **27** 328–31
[59] Geremia N M, Gordon T, Brushart T M, Al-Majed A A and Verge V M 2007 Electrical stimulation promotes sensory neuron regeneration and growth-associated gene expression *Exp. Neurol.* **205** 347–59
[60] Udina E, Furey M, Busch S, Silver J, Gordon T and Fouad K 2008 Electrical stimulation of intact peripheral sensory axons in rats promotes outgrowth of their central projections *Exp. Neurol.* **210** 238–47
[61] Andre S, Boukhaddaoui H, Campo B, Al-Jumaily M, Mayeux V, Greuet D and Scamps F 2003 Axotomy-induced expression of calcium-activated chloride current in subpopulations of mouse dorsal root ganglion neurons *J. Neurophysiol.* **90** 3764–73
[62] Sleeper A A, Cummins T R, Dib-Hajj S D, Hormuzdiar W, Tyrrell L, Waxman S G and Black J A 2000 Changes in expression of two tetrodotoxin-resistant sodium channels and their currents in dorsal root ganglion neurons after sciatic nerve injury but not rhizotomy *J. Neurosci.* **20** 7279–89
[63] Wu D, Pak E S, Wingard C J and Murashov A K 2012 Multi-walled carbon nanotubes inhibit regenerative axon growth of dorsal root ganglia neurons of mice *Neurosci. Lett.* **507** 72–7
[64] Fraczek-Szczypta A 2014 Carbon nanomaterials for nerve tissue stimulation and regeneration *Mater. Sci. Eng.* C **34** 35–49
[65] Mawad D, Gilmore K, Molino P, Wagner K, Wagner P, Officer D L and Wallace G G 2011 Anerodible polythiophenebased composite for biomedical applications *J. Mater. Chem.* **21** 5555–60
[66] Landers J, Turner J T, Heden G, Carlson A L, Bennett N K, Moghe P V and Neimark A V 2014 Carbon nanotube composites as multifunctional substrates for *in situ* actuation of differentiation of human neural stem cells *Adv. Health Mater.* **3** 1745–52
[67] Balint R, Cassidy N J and Cartmell S H 2014 Conductive polymers: towards a smart biomaterial for tissue engineering *Acta Biomat.* **10** 2341–53
[68] Xiao Y, Cui X, Hancock J M, Bouguettaya M, Reynolds J R and Martin D C 2004 Electrochemical polymerization of poly (hydroxymethylated-3, 4 ethylenedioxythiophene) (PEDOT-MeOH) on multichannel neural probes *Sensors Actuators* B **99** 437–43
[69] Saracino G A, Cigognini D, Silva D, Caprini A and Gelain F 2013 Nanomaterials design and tests for neural tissue engineering *Chem. Soc. Rev.* **42** 225–62
[70] Tam R Y, Fuehrmann T, Mitrousis N and Shoichet M S 2014 Regenerative therapies for central nervous system diseases: a biomaterials approach *Neuropsychopharmacology* **39** 169
[71] Zhong Y and Bellamkonda R V 2008 Biomaterials for the central nervous system *J. R. Soc. Interface* **5** 957–75
[72] Orive G, Anitua E, Pedraz J L and Emerich D F 2009 Biomaterials for promoting brain protection, repair and regeneration *Nat. Rev. Neurosci.* **10** 682
[73] Pakulska M M, Ballios B G and Shoichet M S 2012 Injectable hydrogels for central nervous system therapy *Biomed. Mater.* **7** 024101
[74] Cao H, Liu T and Chew S Y 2009 The application of nanofibrous scaffolds in neural tissue engineering *Adv. Drug Deliv. Rev.* **61** 1055–64
[75] Sulejczak D, Andrychowski J, Kowalczyk T, Nakielski P, Frontczak-Baniewicz M and Kowalewski T 2014 Electrospun nanofiber mat as a protector against the consequences of brain injury *Folia Neuropathol.* **52** 56–69
[76] Shyu W C, Lin S Z, Chiang M F, Yang H I, Thajeb P and Li H 2004 Neuregulin-1 reduces ischemia-induced brain damage in rats *Neurobiol. Aging* **25** 935–44
[77] Han J, Wang B, Xiao Z, Gao Y, Zhao Y, Zhang J and Dai J 2008 Mammalian target of rapamycin (mTOR) is involved in the neuronal differentiation of neural progenitors induced by insulin *Mol. Cell. Neurosci.* **39** 118–24
[78] Hoban D B, Newland B, Moloney T C, Howard L, Pandit A and Dowd E 2013 The reduction in immunogenicity of neurotrophin overexpressing stem cells after intra-striatal transplantation by encapsulation in an *in situ* gelling collagen hydrogel *Biomaterials* **34** 9420–9
[79] Sundberg L M, Herrera J J and Narayana P A 2011 Effect of vascular endothelial growth factor treatment in experimental traumatic spinal cord injury: *in vivo* longitudinal assessment *J. Neurotrauma* **28** 565–78
[80] Tysseling-Mattiace V M, Sahni V, Niece K L, Birch D, Czeisler C, Fehlings M G and Kessler J A 2008 Self-assembling nanofibers inhibit glial scar formation and promote axon elongation after spinal cord injury *J. Neurosci.* **28** 3814–23
[81] Nune M, Krishnan U M and Sethuraman S 2016 PLGA nanofibers blended with designer self-assembling peptides for peripheral neural regeneration *Mater. Sci. Eng.* C **62** 329–37
[82] Buchholz F L and Graham A T 1998 *Modern Superabsorbent Polymer Technology* (New York: Wiley) p 279
[83] Mahoney M J and Anseth K S 2006 Three-dimensional growth and function of neural tissue in degradable polyethylene glycol hydrogels *Biomaterials* **27** 2265–74
[84] Martin B C, Minner E J, Wiseman S L, Klank R L and Gilbert R J 2008 Agarose and methylcellulose hydrogel blends for nerve regeneration applications *J. Neural Eng.* **5** 221
[85] Koppes A N, Keating K W, McGregor A L, Koppes R A, Kearns K R, Ziemba A M and Thompson D M 2016 Robust neurite extension following exogenous electrical stimulation within single walled carbon nanotube-composite hydrogels *Acta Biomater.* **39** 34–43
[86] Hsieh A, Zahir T, Lapitsky Y, Amsden B, Wan W and Shoichet M S 2010 Hydrogel/electrospun fiber composites influence neural stem/progenitor cell fate *Soft Matter* **6** 2227–37
[87] Cheng T Y, Chen M H, Chang W H, Huang M Y and Wang T W 2013 Neural stem cells encapsulated in a

functionalized self-assembling peptide hydrogel for brain tissue engineering *Biomaterials* **34** 2005–16
[88] Carriel V, Garrido-Gomez J, Hernández-Cortés P, Garzon I, Garcia-Garcia S, Saez-Moreno J A and Alaminos M 2013 Combination of fibrin-agarose hydrogels and adipose-derived mesenchymal stem cells for peripheral nerve regeneration *J. Neural Eng.* **10** 026022
[89] Lei Y, Gojgini S, Lam J and Segura T 2011 The spreading, migration and proliferation of mouse mesenchymal stem cells cultured inside hyaluronic acid hydrogels *Biomaterials* **32** 39–47
[90] Khaing Z Z and Seidlits S K 2015 Hyaluronic acid and neural stem cells: implications for biomaterial design *J. Mater. Chem.* B **3** 7850–66
[91] Aurand E R, Lampe K J and Bjugstad K B 2012 Defining and designing polymers and hydrogels for neural tissue engineering *Neurosci. Res.* **72** 199–213
[92] Kim Y S, Cho K, Lee H J, Chang S, Lee H, Kim J H and Koh W G 2016 Highly conductive and hydrated PEG-based hydrogels for the potential application of a tissue engineering scaffold *React. Funct. Polym.* **109** 15–22
[93] Alexander A, Khan J, Saraf S and Saraf S 2014 Polyethylene glycol (PEG)–poly (N-isopropylacrylamide) (PNIPAAm) based thermosensitive injectable hydrogels for biomedical applications *Eur. J. Pharm. Biopharm.* **88** 575–85
[94] Guiseppi-Elie A 2010 Electroconductive hydrogels: synthesis, characterization and biomedical applications *Biomaterials* **31** 2701–16
[95] Kuzmenko V, Kalogeropoulos T, Thunberg J, Johannesson S, Hägg D, Enoksson P and Gatenholm P 2016 Enhanced growth of neural networks on conductive cellulose-derived nanofibrous scaffolds *Mater. Sci. Eng.* C **58** 14–23
[96] Dadsetan M, Knight A M, Lu L, Windebank A J and Yaszemski M J 2009 Stimulation of neurite outgrowth using positively charged hydrogels *Biomaterials* **30** 3874–81
[97] Petrov P, Mokreva P, Kostov I, Uzunova V and Tzoneva R 2016 Novel electrically conducting 2-hydroxyethylcellulose/polyaniline nanocomposite cryogels: Synthesis and application in tissue engineering *Carbohydr. Polym.* **140** 349–55
[98] Hospodiuk M, Dey M, Sosnoski D and Ozbolat I T 2017 The bioink: A comprehensive review on bioprintable materials *Biotechnol. Adv.* **35** 217–39
[99] Hsieh F Y and Hsu S H 2015 3D bioprinting: a new insight into the therapeutic strategy of neural tissue regeneration *Organogenesis* **11** 153–8
[100] Hou S, Xu Q, Tian W, Cui F, Cai Q, Ma J and Lee I S 2005 The repair of brain lesion by implantation of hyaluronic acid hydrogels modified with laminin *J. Neurosci. Methods* **148** 60–70
[101] Lee K Y, Bouhadir K H and Mooney D J 2004 Controlled degradation of hydrogels using multi-functional cross-linking molecules *Biomaterials* **25** 2461–6
[102] Li L M, Han M, Jiang X C, Yin X Z, Chen F, Zhang T Y and Ou-Yang H W 2017 Peptide-tethered hydrogel scaffold promotes recovery from spinal cord transection via synergism with mesenchymal stem cells *ACS Appl. Mater. Interfaces* **9** 3330–42
[103] Grover G N, Braden R L and Christman K L 2013 Oxime cross-linked injectable hydrogels for catheter delivery *Adv. Mater.* **25** 2937–42
[104] Xu C and Kopecek J 2007 Self-assembling hydrogels *Polym. Bull.* **58** 53–63
[105] Cremer P, Heinen M, Menzel A M and Lowen H 2017 A density functional approach to ferrogels *J. Phys.: Condens. Matter.* **29** 275102
[106] Lee C R, Grodzinsky A J and Spector M 2001 The effects of cross-linking of collagen-glycosaminoglycan scaffolds on compressive stiffness, chondrocyte-mediated contraction, proliferation and biosynthesis *Biomaterials* **22** 3145–54
[107] Kim M S, Park S J, Chun H J and Kim C H 2011 Thermosensitive hydrogels for tissue engineering *Tissue Eng. Regen. Med.* **8** 117–23
[108] Xu Y, Li Z, Li X, Fan Z, Liu Z, Xie X and Guan J 2015 Regulating myogenic differentiation of mesenchymal stem cells using thermosensitive hydrogels *Acta Biomater.* **26** 23–33
[109] Massensini A R, Ghuman H, Saldin L T, Medberry C J, Keane T J, Nicholls F J and Modo M 2015 Concentration-dependent rheological properties of ECM hydrogel for intracerebral delivery to a stroke cavity *Acta Biomater.* **27** 116–30
[110] Baumann M D, Kang C E, Tator C H and Shoichet M S 2010 Intrathecal delivery of a polymeric nanocomposite hydrogel after spinal cord injury *Biomaterials* **31** 7631–9
[111] Haq M A, Su Y and Wang D 2017 Mechanical properties of PNIPAM based hydrogels: a review *Mater. Sci. Eng.* C **70** 842–55
[112] Payne C, Dolan E B, O'Sullivan J, Cryan S A and Kelly H M 2017 A methylcellulose and collagen based temperature responsive hydrogel promotes encapsulated stem cell viability and proliferation in vitro *Drug Deliv. Trans. Res.* **7** 132–46
[113] Sarkar N 1995 Kinetics of thermal gelation of methylcellulose and hydroxypropylmethylcellulose in aqueous solutions *Carbohydr. Polym.* **26** 195–203
[114] Ballios B G, Cooke M J, Donaldson L, Coles B L, Morshead C M, van der Kooy D and Shoichet M S 2015 A hyaluronan-based injectable hydrogel improves the survival and integration of stem cell progeny following transplantation *Stem Cell Rep.* **4** 1031–45
[115] Chong B F, Blank L M, Mclaughlin R and Nielsen L K 2005 Microbial hyaluronic acid production *Appl. Microbiol. Biotechnol.* **66** 341–51
[116] Comolli N, Neuhuber B, Fischer I and Lowman A 2009 In vitro analysis of PNIPAAm-PEG, a novel, injectable scaffold for spinal cord repair *Acta Biomater.* **5** 1046–55
[117] Brahima S, Boztepe C, Kunkul A and Yuceer M 2017 Modeling of drug release behavior of pH and temperature sensitive poly (NIPAAm-co-AAc) IPN hydrogels using response surface methodology and artificial neural networks *Mater. Sci. Eng.* C **75** 425–32
[118] Wang Q *et al* 2017 A thermosensitive heparin-poloxamer hydrogel bridges aFGF to treat spinal cord injury *ACS Appl. Mater. Interfaces* **9** 6725–45
[119] Lee E, Park J, Im S G and Song C 2012 Synthesis of single-walled carbon nanotube-incorporated polymer hydrogels via click chemistry *Polym. Chem.* **3** 2451–5
[120] Ahadian S *et al* 2014 Hybrid hydrogels containing vertically aligned carbon nanotubes with anisotropic electrical conductivity for muscle myofiber fabrication *Sci. Rep.* **4** 4271
[121] Han N, Johnson J K, Bradley P A, Parikh K S, Lannutti J J and Winter J O 2012 Cell attachment to hydrogel-electrospun fiber mat composite materials *J. Funct. Biomater.* **3** 497–513
[122] Donaghue I E, Tam R, Sefton M V and Shoichet M S 2014 Cell and biomolecule delivery for tissue repair and regeneration in the central nervous system *J. Control. Release* **190** 219–27
[123] Tuladhar A, Morshead C M and Shoichet M S 2015 Circumventing the blood-brain barrier: local delivery of cyclosporin A stimulates stem cells in stroke-injured rat brain *J. Control. Release* **215** 1–11
[124] Ansorena E *et al* 2013 Injectable alginate hydrogel loaded with GDNF promotes functional recovery in a hemisection model of spinal cord injury *Int. J. Pharm.* **455** 148–58

[125] Toh W S and Loh X J 2014 Advances in hydrogel delivery systems for tissue regeneration *Mater. Sci. Eng.* C **45** 690–7
[126] Koetting M C, Peters J T, Steichen S D and Peppas N A 2015 Stimulus-responsive hydrogels: theory, modern advances, and applications *Mater. Sci. Eng.* R **93** 1–49
[127] Ordikhani F, Sheth S and Zustiak S P 2017 Polymeric particle-mediated molecular therapies to treat spinal cord injury *Int. J. Pharm.* **516** 71–81
[128] Gupta P, Sharan S, Roy P and Lahiri D 2015 Aligned carbon nanotube reinforced polymeric scaffolds with electrical cues for neural tissue regeneration *Carbon* **95** 715–24
[129] Shi Z, Zang S, Jiang F, Huang L, Lu D, Ma Y and Yang G 2012 *In situ* nano-assembly of bacterial cellulose–polyaniline composites *RSC Adv.* **2** 1040–6
[130] Bajpai A K, Bajpai J and Soni S N 2009 Designing polyaniline (PANI) and polyvinyl alcohol (PVA) based electrically conductive nanocomposites: preparation, characterization and blood compatible study *J. Macromol. Sci.* A **46** 774–82
[131] Burdick J A, Ward M, Liang E, Young M J and Langer R 2006 Stimulation of neurite outgrowth by neurotrophins delivered from degradable hydrogels *Biomaterials* **27** 452–9
[132] Fourniols T, Randolph L D, Staub A, Vanvarenberg K, Leprince J G, Préat V and Danhier F 2015 Temozolomide-loaded photopolymerizable PEG-DMA-based hydrogel for the treatment of glioblastoma *J. Control. Release* **210** 95–104
[133] Lampe K J, Kern D S, Mahoney M J and Bjugstad K B 2011 The administration of BDNF and GDNF to the brain via PLGA microparticles patterned within a degradable PEG-based hydrogel: protein distribution and the glial response *J. Biomed. Mater. Res.* A **96** 595–607
[134] Macaya D J, Hayakawa K, Arai K and Spector M 2013 Astrocyte infiltration into injectable collagen-based hydrogels containing FGF-2 to treat spinal cord injury *Biomaterials* **34** 3591–602
[135] Novajra G, Tonda-Turo C, Vitale-Brovarone C, Ciardelli G, Geuna S and Raimondo S 2014 Novel systems for tailored neurotrophic factor release based on hydrogel and resorbable glass hollow fibers *Mater. Sci. Eng.* C **36** 25–32
[136] Jiao G, Pan Y, Wang C, Li Z, Li Z and Guo R 2017 A bridging SF/Alg composite scaffold loaded NGF for spinal cord injury repair *Mater. Sci. Eng.* C **76** 81–7
[137] Liu H, Li C, Wang B, Sui X, Wang L, Yan X and Mao Z 2018 Self-healing and injectable polysaccharide hydrogels with tunable mechanical properties *Cellulose* 1–13
[138] Lopez-Lopez M T, Rodriguez I A, Rodriguez-Arco L, Carriel V, Bonhome-Espinosa A B, Campos F and Duran J D G 2017 Synthesis, characterization and *in vivo* evaluation of biocompatible ferrogels *J. Magn. Magn. Mater.* **431** 110–4
[139] Domingues R M, Silva M, Gershovich P, Betta S, Babo P, Caridade G and Gomes M E 2015 Development of injectable hyaluronic acid/cellulose nanocrystals bionanocomposite hydrogels for tissue engineering applications *Bioconjug. Chem.* **26** 1571–81
[140] Kim Y T, Caldwell J M and Bellamkonda R V 2009 Nanoparticle-mediated local delivery of methylprednisolone after spinal cord injury *Biomaterials* **30** 2582–90
[141] Stanwick J C, Baumann M D and Shoichet M S 2012 Enhanced neurotrophin-3 bioactivity and release from a nanoparticle-loaded composite hydrogel *J. Control. Release* **160** 666–75
[142] Rivet C J, Zhou K, Gilbert R J, Finkelstein D I and Forsythe J S 2015 Cell infiltration into a 3D electrospun fiber and hydrogel hybrid scaffold implanted in the brain *Biomatter* **5** e1005527
[143] Zadroga A, Jezierska-Wozniak K, Czarzasta J, Barczewska M, Wojtkiewicz J and Maksymowicz W 2017 Therapeutic potential of olfactory ensheathing cells and mesenchymal stem cells in spinal cord injuries *Stem Cells Int.* **2017** 3978595

polymers

MDPI

Article

Crosslinking Kinetics of Methylcellulose Aqueous Solution and Its Potential as a Scaffold for Tissue Engineering

Beata Niemczyk-Soczynska [1,*], Arkadiusz Gradys [1], Dorota Kolbuk [1], Anna Krzton-Maziopa [2] and Pawel Sajkiewicz [1]

[1] Institute of Fundamental Technological Research, Polish Academy of Sciences, Pawinskiego 5b St., 02-106 Warsaw, Poland; argrad@ippt.pan.pl (A.G.); dkolbuk@ippt.pan.pl (D.K.); psajk@ippt.pan.pl (P.S.)

[2] Faculty of Chemistry, Warsaw University of Technology, Noakowskiego 3 St., 00-664 Warsaw, Poland; anka@ch.pw.edu.pl

* Correspondence: bniem@ippt.pan.pl

Received: 27 September 2019; Accepted: 24 October 2019; Published: 28 October 2019

Abstract: Thermosensitive, physically crosslinked injectable hydrogels are in the area of interests of various scientific fields. One of the representatives of this materials group is an aqueous solution of methylcellulose. At ambient conditions, methylcellulose (MC) is a sol while on heating up to 37 °C, MC undergoes physical crosslinking and transforms into a gel. Injectability at room temperature, and crosslinkability during subsequent heating to physiological temperature raises hopes, especially for tissue engineering applications. This research work aimed at studying crosslinking kinetics, thermal, viscoelastic, and biological properties of MC aqueous solution in a broad range of MC concentrations. It was evidenced by Differential Scanning Calorimetry (DSC) that crosslinking of MC is a reversible two-stage process, manifested by the appearance of two endothermic effects, related to the destruction of water cages around methoxy groups, followed by crosslinking via the formation of hydrophobic interactions between methoxy groups in the polymeric chains. The DSC results also allowed the determination of MC crosslinking kinetics. Complementary measurements of MC crosslinking kinetics performed by dynamic mechanical analysis (DMA) provided information on the final storage modulus, which was important from the perspective of tissue engineering applications. Cytotoxicity tests were performed using mouse fibroblasts and showed that MC at low concentration did not cause cytotoxicity. All these efforts allowed to assess MC hydrogel relevance for tissue engineering applications.

Keywords: methylcellulose; thermosensitive hydrogel; crosslinking kinetics; DSC; DMA; cellular tests

1. Introduction

Hydrogels are three dimensional polymeric structures, crosslinked by either chemical or physical interactions, forming a polymeric network. They are characterized by a wide range of processing possibilities in tailoring their biological and mechanical properties [1,2]. In this regard, the crosslinking method is essential, when determining the final properties of hydrogel including their stability in physiological conditions. Chemically crosslinked hydrogels consist of permanently formed junctions as a result of chemical reactions. Although the covalent crosslinking results in high stability and increased mechanical properties, the use of toxic crosslinking agents, usually, disqualify their application in tissue engineering. Physical crosslinking is a temporary effect of generation of the junctions, which are related to entanglements of polymeric chain, ionic bonds, hydrogen bonds, or hydrophobic interactions [2,3]. One of the interesting types of materials exhibiting physical interactions are the stimuli-responsive

hydrogels. Their crosslinking takes place under an external trigger. In this respect, magnetic (ferrogels), pH-stimuli-responsive or thermosensitive hydrogels are distinguished [4,5]. Especially, the last group has gained much attention in various fields of science [6]. An example of such an approach is methylcellulose (MC)—a polysaccharide, which is a derivative of cellulose. Contrary to pure cellulose, MC is water soluble. This is due to partial substitution of the hydroxyl groups (–OH), which are responsible for the formation of crystal fibers in pure cellulose, with the methoxy groups ($–OCH_3$), which prevents crystalline fibers formation [7].

Considering its effective support in cells regeneration [8] and having been approved by the Food and Drug Administration (USA), MC is an attractive material for tissue engineering or drug delivery systems [9]. Contrary to other natural hydrogels (e.g., alginate), MC constitutes a stable structure in physiological conditions, with mechanical properties similar to native tissues (e.g., meniscus, liver, or spinal cord) [10–14]. From the perspective of tissue engineering, the thermosensitive crosslinking of MC aqueous solution seems very promising, as it prevents the use of toxic crosslinking agents [15].

The physical crosslinking of MC is a consequence of the formation of hydrophobic domains. In MC aqueous solution, the crosslinking appears during heating near 40 °C [9]. The sol–gel transition is determined by the Lower Critical Solution Temperature (LCST), above which hydrophobic interactions start to prevail in the solution [8]. The LCST is known to depend on the methoxy group substitution degree, MC concentration as well as additives to the MC solution [1]. According to [16], the crosslinking process consists of two stages. At ambient conditions, polymer-solvent interactions between hydrophilic MC groups and water dominate. The "water cages" around the hydrophobic molecules of MC result in weak polymer–polymer interactions. This is a classic example of hydrophobic hydration, preventing crosslinking of MC at room temperature [16]. While the temperature increases near the physiological temperature, water cages are shattered and the hydrophobic regions of MC are exposed leading to stronger polymer–polymer interactions. Higher temperature amplifies the polymeric chains mobility and the methoxy groups get closer to each other and self-organize to form hydrophobic interactions. The partial polymeric chain rearrangement takes place and the primary hydrophobic interactions (non-cooperative) are formed. This step represents the first stage of crosslinking. While the hydrogel is still heating, hydrophobic domains and consequently three-dimensional networks are formed. The remaining bonded MC chains generate supplementary hydrophobic interactions, called cooperative, to increase the network cells' density. The higher temperature (above 60 °C) stimulates the network cells to uptake and retain water from the solution, which is an effect of osmotic forces. As a consequence, fully swelled, mechanically stable, and a crosslinked network is formed.

Considering the materials for tissue engineering applications, an appropriate kinetics of hydrogel crosslinking is extremely important. On one hand, it should take place slowly enough to allow for a complete injection and fill the injury, but on the other hand, it should be sufficiently fast to prevent it from moving away from the aimed location. The mechanical properties are important to provide an appropriate biomaterial adhesion to the tissue and to avoid pressure and the spreading of the injury among the tissues [17,18]. Crosslinking the kinetics of MC and its final stiffness depends on different parameters of the used product, such as the substitution degree or molecular weight, but it also might be adjusted using various concentrations and additives [19]. In this study, we used one particular type of MC with various concentrations, to determine the effect of the MC concentration on the crosslinking process.

Martin et al. [15] investigated the crosslinking rate of MC using the inverted test tube method. Briefly, the test tube was inverted and if the solution no longer flowed, it was considered to be a solid and the transition time was registered as the crosslinking time. It is worth noticing that this experiment was carried out in a simple manner, providing only the basic macroscopic information about the material. Another commonly used method for MC crosslinking kinetics determination involves rheological measurements (e.g., oscillatory shear measurements) [20,21] and DSC studies [22,23]. Despite the methods showing the dependencies between the MC network changes and the temperature, most of

the DSC measurements were just focused on the sol–gel transition temperature or their dependencies, while a certain salt was added to the MC solution.

The objective of our work was to systematically investigate the effect of MC concentration on the crosslinking kinetics of MC water solutions using two complementary methods—dynamic mechanical analysis (DMA) and DSC. DMA provides additional information on the viscoelastic properties of the final hydrogel. Both parameters—crosslinking kinetics and viscoelastic properties are crucial in the determination of the adequate MC concentrations for tissue engineering applications. Additionally, the biological properties of the MC aqueous solution was determined in order to evaluate its significance for tissue engineering application.

2. Materials and Methods

2.1. Preparation of MC Aqueous Solution

The MC (METHOCEL A15LV, Sigma Aldrich, St. Louis, MO, USA) solution was prepared in demineralized water at various weight concentrations (0.75–20 wt.%). The procedure was carried out using the "hot–cold" dispersion method, according to [24]. Briefly, the MC bulk was dispersed in three-fourth volume of demineralized water above 90 °C. Then, one-fourth of the volume of cold demineralized water was added and stirred for about 30 min. The final solution was stored at 4 °C, for 24 h, in order to ensure proper hydration of the polymer [24].

2.2. DSC

The measurements were carried out using a Pyris 1 DSC, Perkin Elmer (Waltham, MA, USA) differential scanning calorimeter in non-isothermal mode at constant heating and cooling rates of 2 K/min, in the temperature range –10–80 °C. In order to prevent water evaporation, dedicated stainless steel hermetic pans were used. As the heat flow of the thermal effects from MC was small and the hermetic pans have a low thermal conductivity, in order to increase the signal-to-noise ratio, the samples were of a higher weight, 70–75 mg, and they were measured with reference to a water sample of similar weight, which provided a similar heat capacity of sample and reference. At least three samples of each concentration were measured and, further, the most representative ones were measured during 10 heating–cooling cycles and the measurements were averaged. This further improved the signal. In order to reduce the artefacts from water reference, for the baseline, water versus water thermograms were recorded.

Detailed analysis of the DSC heating scans was performed, in order to provide information on the kinetics of the transitions. First, the thermal effects were obtained from the heating scans by subtraction of the polynomial of the fifth order. Further, deconvolution of the thermal effects was performed using the asymmetric double sigmoidal function. Thus, the obtained separated thermal effects were analyzed, providing information on the heat exchanged, ΔH, the temperature of the beginning of the effect, T_{onset}, and the transition rate, k. ΔH was obtained by integration of the thermal effect and the T_{onset} was determined at the cross-section of the tangent at the half-height of the DSC peak, with the horizontal baseline. The transition rate, k, was determined as the reciprocal of the time of the half transition with respect to its start time.

2.3. DMA

Several concentrations of aqueous MC solutions (1.75–10 wt.%) were analyzed using DMA, Anton Paar Physica MCR301 rheometer (Anton Paar Physica, Graz, Germany). The kinetics of MC crosslinking was investigated by measuring the viscoelastic properties (storage, G', and loss modulus, G'') of solutions at 37 °C in the oscillatory shear regime in a limited time range. Before the isothermal step, the samples were heated from 20 °C at a heating rate of 2 °C/min. The analysis was performed using cone-plate geometry (diameter—39.9 mm, angle 0.989°, and truncation 47 μm) and small-amplitude sinusoidal deformation (0.1% strain and 1 Hz frequency). A cone-plate geometry equipped with

a dedicated solvent trap that prevented water evaporation from the solution was used. In some publications a silicone oil was used to minimize this effect (e.g., [25]), however, in this study, the silicone oil interfered with the MC crosslinking process.

All concentrations were analyzed 3–4 times. The measured G' values were approximated with the biphasic dose-response function, belonging to the sinusoidal type of function, which was also used in the studies of progress of crosslinking by Maryanski and Dufresne [26,27]. Usually, this kind of function is used to show how an organism reacts to an applied drug dose, simulative agent, or stress. In our case, the use of this function allowed us to present how the various concentrations of MC influence their thermal crosslinking at a constant elevated temperature. Afterwards, the fitting curves were always extrapolated to the saturation plateau at a longer time (166 min) and then averaged. The kinetics of crosslinking was estimated from the time derivative of the averaged G', which allowed for the definition of the maximum rate of increase of G', taken as the maximum of the crosslinking rate of hydrogel. In order to estimate the hydrogel stiffness, dG'/dt were integrated, leading to the determination of the final storage modulus of hydrogel.

In order to compare the crosslinking kinetics from both methods (DMA and DSC), we determined the crosslinking rate, k, from the time of half transition, similar to the DSC case. We used the start of the crosslinking as the zero time-point, which differed from the procedure applied in the case of the time derivative of the G' method, for which the time was measured when the temperature reached about 37 °C. The start of the crosslinking, t_{onset}, was determined as the intersection of the tangent to the baseline before the start of the thermal effect and the tangent to the rising part of the thermal effect.

2.4. Biological Tests

2.4.1. Cellular Cultures

Biological tests were carried out using mouse fibroblasts L929 line (Sigma-Aldrich; Merck Millipore, Darmstadt, Germany). The cells were cultured in 75 cm^2 flasks in 89% High Glucose Dulbecco's Modified Eagle's Medium (DMEM), 10% fetal bovine serum (FBS), and 1% antibiotics, and were incubated at 37 °C in a 5% CO_2 environment. The culture medium was changed every three days. A culture flask with 70% of cell confluency was used in experiment. L929 cells were seeded as follows—the cells were harvested by washing with phosphate buffer saline (PBS), then 5 mL of 0.05% (0.25%, diluted five times with PBS) trypsin solution was added to the flask and placed for 3 min in the incubator. Following this step, the side of the flask was gently tapped in order to ensure the detachment of the cells from the bottom of the flask. A 10 mL of culture medium was added to the harvested cells and then centrifuged for 5 min at 100× g (times gravity, the unit of relative centrifugal force (RCF)) at room temperature. The collected pellet was resuspended within the culture medium, followed with dilution to the required cell density. L929 cells were seeded in a 48-well plate at a density of 5000 per well in 500 µL of growth medium and were left to attach to the plate in the incubator at 37 °C, in a 5% CO_2 environment.

2.4.2. MC Preparation

For these tests, the MC powder was added to the proper concentrations and was sterilized using UV light for 30 min (every 10 min, the powder was shaken to provide a homogenous sterilization). The MC aqueous solutions were prepared in water at concentrations of 1, 2.5, and 5 wt.%, respectively. The samples were added to the cells in a volume of 25, 50, and 100 µL. The obtained solutions of MC and the cells were incubated at 37 °C, overnight, to induce MC crosslinking. After crosslinking, 500 µL of the crosslinked MC with the appropriate cell amounts were added and incubated at 37 °C. The cells seeded on tissue culture plastic (TCP) served as a control.

2.4.3. Cytotoxicity Tests

Cytotoxicity of the MC aqueous solutions was evaluated in direct contact with the cells via the metabolic activity assay, using the PrestoBlue agent. In the PrestoBlue test, blue resazurin reagents are reduced to resorufin. As a result of these red fluorescent compound cells, viability might be measured quantitatively and visually (absorbance, by observing fluorescent outputs of reduced resorufin).

After three days of incubation, the culture medium was removed and the PrestoBlue–DMEM solution (1:10 *v*/*v*) was added. The plate was incubated for the next 90 min. As a final step, 100 µL of the solution from each well was transferred to a 96-well plate. Fluorescence was read with excitation/emission 530/620 nm filters, using the Fluoroscan Acent FL instrument (Thermo Fisher Scientific, Waltham, MA, USA). The obtained signals were compared with the fluorescence of PrestoBlue in wells without cells, which served as blank samples without any metabolic activity, and as wells of control (with 100% metabolic activity).

2.4.4. Cell Morphology

In order to evaluate how MC solutions affect the cells morphology in direct contact, scanning electron microscopy (SEM) and fluorescent images were taken. In both experiments, the samples were placed in a separate 48-well plate. L929 cells were seeded in cell density 3000 per well and were subjected to 5 days of long culture.

SEM images were obtained on the dried samples. Preparation for SEM assumed the following steps—the plate was taken out of the incubator, samples with cells were washed using PBS and treated with glutaraldehyde (GA) for 2 h. After that, they were washed with PBS three times, in order to remove the residues of GA. Then, the samples were dehydrated with a series of ethanol solutions (using increasing EtOH concentrations from 50 to 100 wt.%). After that, they were washed with EtOH:HDMS (hexamethydisilazane) solutions (1:2, 2:1 (*v*/*v*)) and 100% HDMS in which they were stored to dry. In each solution, the samples were left for 20 min. Finally, the dried samples were sputter-coated with 7 nm of gold. SEM imaging was carried out with a JEOL JSM-6390LV.

Fluorescent microscope (FM) imaging required fixing of the samples and staining of the cytoskeleton. Just before fixing and after the next steps, every sample was washed with PBS. In order to fix the samples, they were immersed in 3% formaldehyde for 20 min and then in 0.1% Triton X 100 for 5 min, to obtain permeable cell membranes. Then, they were put in a staining solution, ActinGreen (ThermoFisher Scientific, Waltham, MA, USA), for 30 min. The wet samples were placed on the standard glass plates and covered with a thin microscopic glass, in order to prevent drying of the sample. All images were taken using a Leica AM TIRF MC.

3. Results and Discussion

3.1. DSC

The DSC heating thermograms of MC solution showed quite complex thermal behavior and complex changes of the effects with varying MC concentration. For better understanding of the effect of the MC content on the thermal effects, all thermograms are presented in Figure 1a,b, as normalized to sample weight and normalized to MC weight, respectively. Except for the MC powder, all thermograms generally presented two endothermic effects. Both effects were more evident for low MC concentrations (0.5–8 wt.%). The low-temperature effect dominated over the high-temperature one, as far as the MC concentration decreased. It was seen that both endothermic peaks shifted to lower temperatures with increasing MC concentrations, (Figure 1) with the low-temperature peak becoming broader, which was particularly evident at MC concentrations of above 8 wt.%. (Figure 1a). MC in the powder form (~100 wt.%) only showed one broad endothermic peak (Figure 1a).

In Figure 1b, it could also be seen that, for the lowest MC concentrations, i.e., <wt.%, there appeared an additional effect, which was exothermic and preceded the low-temperature endothermic effect. The exothermic effect became stronger with a decrease in the MC concentration.

Based on the literature [16], we interpreted that the low-temperature endothermic effect was due to the destruction of the water cages and the high-temperature endothermic effect was due to the MC thermal crosslinking. For the exothermic effect observed in concentrations <2 wt.%, we interpreted it as due to the formation of water cages around methoxy groups. A more detailed explanation is given below.

The DSC cooling thermograms showed two exothermic effects (Figure 2), a high-temperature effect dominating over the low-temperature one. These effects gave evidence of the reverse processes, i.e., first decomposition of the three dimensional hydrogel network followed by water "incorporation" into the polymer structure. Both effects appeared in the temperature range of 30–55 °C. The most significant finding here was that the MC physical crosslinking was fully thermoreversible. Additionally, for MC concentrations <2 wt.%, the reverse effect of the destruction of water cages, which should be endothermic, was not observed, however, the occurrence of this process was evident from the repeating appearance of the exothermic peak upon a subsequent heating scan. Detailed analysis of the cooling scans would provide more insight into this question, however, the current study was devoted to the crosslinking kinetics and the cooling scans were not studied in detail. Additionally, it might be noted that, for the MC powder, the crosslinking was non-reversible as, upon cooling and subsequent heating scans, no thermal effect was observed (Figure 2).

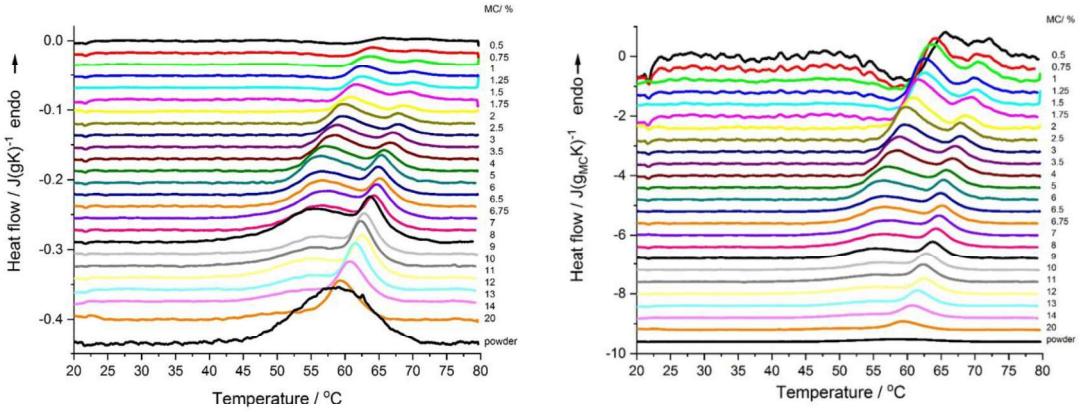

(**a**) (**b**)

Figure 1. DSC heating scans of MC solutions with various concentrations (indicated)—(**a**) heat flow normalized to the sample weight, and (**b**) heat flow normalized to the methylcellulose (MC) weight. Curves subtracted using polynomial. For comparison, the curves are shifted in *y*-axis.

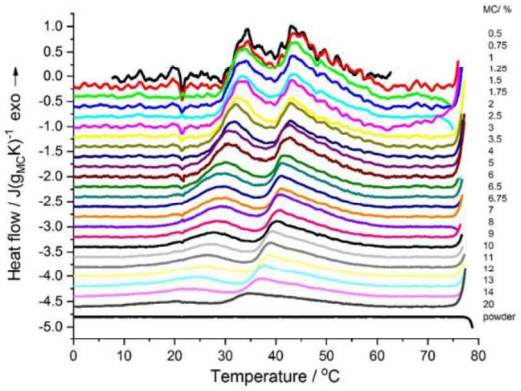

Figure 2. DSC cooling curves of the MC solutions with various concentrations (indicated) normalized to the MC weight. Curves subtracted using polynomial. For comparison, the curves are shifted in the *y*-axis.

Deconvolution of the thermal effects was performed using the asymmetric double sigmoidal function. The examples of the deconvolution of the heating scans with and without the exothermic effects are presented in Figure 3a,b, respectively.

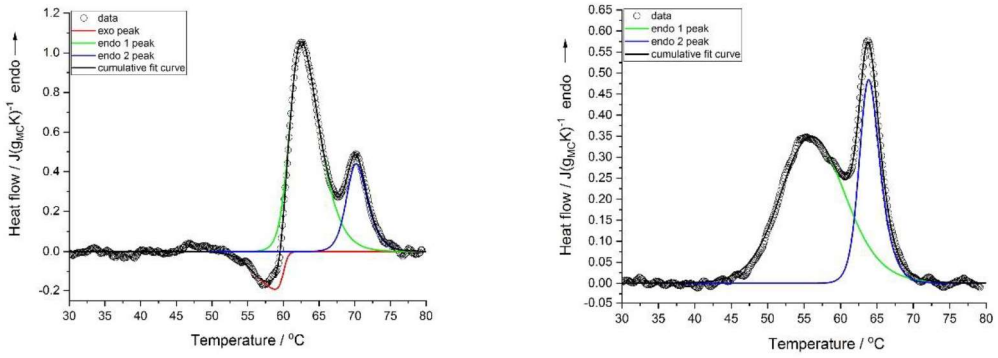

(**a**) (**b**)

Figure 3. Deconvolution of the thermal effects registered during heating for MC concentrations—(**a**) 1.5 wt.% and (**b**) 9 wt.%.

Detailed analysis of the deconvoluted peaks provided quantitative information on the effect of the MC concentration on the kinetics of the processes. The results are presented in Figures 4–6, showing the heat exchanged, ΔH, the temperatures at the start of the processes, T_{onset}, and their rates, k, respectively. In Figure 4, it can be seen that the maximum of the low-temperature endothermic effect (endo 1) was ca. 7 J/g_{MC}, whereas for the high-temperature endothermic effect (endo 2), the maximum heat was ca. 2 J/g_{MC}. In case the water cages were destructed (low-temperature endothermic effect), the highest heat levels were seen for the medium range of MC concentrations, i.e., 2–6 wt.%. In the case of the crosslinking process (high-temperature endothermic effect), the heat was constant up to 14 wt.% of the MC. At the highest MC concentrations, both heat levels dramatically decreased the low-temperature endothermic effect to 0 and the high-temperature endothermic effect to ca. 1 J/g_{MC}. In the left panel of Figure 4, in the low MC concentration range of <2 wt.%, the heat of the low-temperature endothermic effect decreased with decrease in the MC content. It was accompanied by the appearance of the exothermic effect, whose heat levels increased with a decrease in the MC content. Interestingly, the change in the exothermic heat showed two ranges of MC content dependence with a boundary at 1 wt.%.

There are some ideas to explain the genesis of the endothermic nature of the MC crosslinking during heating. Sekiguchi et al. [28] suggested that crosslinking might not only involve hydrophobic interactions. Other interactions might also be responsible for the double MC crosslinking process. Our explanation of the observed phenomena based on the DSC results during the heating of the MC solutions was the following. In the ambient conditions, MC was characterized by prevalence and dominance of hydrophilic interactions in the solution, such as water–water interaction and these same interactions between the hydrophilic parts of MC and the water molecules. Additionally, in the solution, the water molecules might have created ordered structures, i.e., water cages around the hydrophobic regions of MC, and intramolecular interactions between the polymeric chains were also formed. Formation of water cages around the methoxy groups was accompanied by heat release and entropy reduction, which was manifested by the exothermic effect preceding the endothermic effects for highly diluted MC solutions. The exothermic effect disappeared at higher MC concentrations. It is possible that in more densely packed polymeric networks, hydrophobic aggregates were previously created at lower temperatures than what was caused by the limited available space in the solution and the dominance of the polymeric phase over the solvent.

While heating, an appropriate amount of energy (heat) is delivered to the system, the water cages are destroyed, and the methoxy groups are released, and the number of ordered form of water molecules start to change. Heat was consumed to make the layer of the water cages thinner, increasing disordering and, thus, entropy ($\Delta S > 0$). This process was accompanied by the low-temperature endothermic effect.

Soon after the destruction of the water cages, the exposed methoxy groups in the MC chains underwent cross-linking due to intra- and intermolecular hydrophobic interactions. As we mentioned previously this step was considered to be the high-temperature endothermic effect.

The maximum effect of the heat on the water-cage destruction (low-temperature endothermic effect), at a particular range of MC concentration, in all probability could have been related to the presence of two limitations. In a dilute MC solution, the MC molecules might form micelles, providing a limited number of the methoxy groups to the solution and to the water cages around these molecules. On the other hand, at relatively high MC concentrations, the chains become densely packed, and their molecular mobility is limited, which also affects the mobility of the water molecules, and results in a reduction of the low-temperature endothermic effect. In the case of a high-temperature endothermic effect, the constant value of the heat at low and medium MC concentrations, might suggest similar employment of the methoxy groups, which at dilute MC solutions would create separated molecules that form micelles and at high-enough MC concentrations would form a hydrophobic network. Decrease in the heat of the high-temperature endothermic effect, at above 14 wt.% of MC was understood to be due to the aforementioned limited molecular mobility.

The dependence of the exothermic heat on the MC concentration in Figure 4, showed an abrupt change at 1 wt.% of the MC content. This behavior indicated the existence of some boundary, above which the exothermic heat weakly depended on the MC concentration and below which it depended strongly on the MC concentration. This might suggest the boundary between semi-dilute and dilute solution, respectively, however, this assumption needs further investigations.

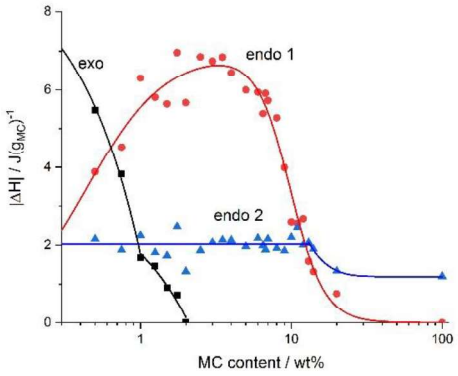

Figure 4. The absolute value of the heat exchanged upon heating during the exothermic, the low-temperature (endo 1) and the high-temperature (endo 2) endothermic effects versus the MC content.

Figure 5 presents the dependencies of T_{onset} and MC concentrations, which might serve as a phase diagram. It is rather clear that below the T_{onset} of the low-temperature endothermic effect, there existed a one-phase solution in the form of sol. Between the low-temperature and the high-temperature endothermic effect there was a sol–gel transition, while above the high-temperature endothermic effect there might have existed a cross-linked polymer (gel). According to [29], the MC gel remains stable up to 80 °C, where phase separation takes place. Additionally, Figure 4 shows the dependence of the T_{onset} of the exothermic effect, which showed a constant value. It suggests the existence of two sub-areas in dilute or semi-dilute sol, characterized by a lack of and formation of water cages below and above 52 °C, respectively.

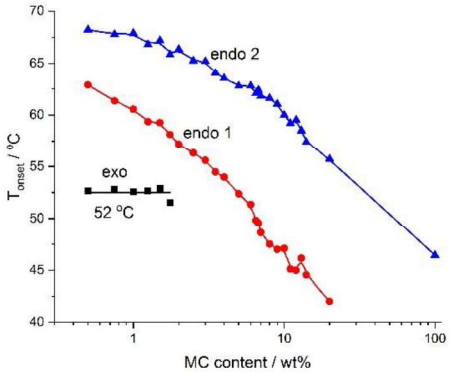

Figure 5. Phase diagram for various concentrations of MC constructed using the onset temperature.

The kinetics of the processes, described using rate, k, determined as the reciprocal of the half time of the process is presented in Figure 6. Figure 6 illustrates the effect of the MC concentration on the rates of the processes. From Figure 6a, it is evident that the low- and the high-temperature endothermic processes, as well as the exothermic one, differed in rates. The rate of destruction of the water cages (low-temperature endothermic effect) was seen to decrease with the MC concentration. This might have been due to a decrease in the MC molecular mobility. The rate of the formation of the water cages (exo) was seen to increase with MC concentration, confirming the reinforcing role of MC molecules in the creation of water cages. The rate of the crosslinking process (high-temperature endothermic effect) showed a reduction in the high MC concentration range. This was obviously due to a decrease in the molecular mobility. It was accompanied by a decrease in ΔH in Figure 4, indicating the formation of an imperfect crosslinked network of low density. At low and medium MC content, the crosslinking rate showed generally comparable values, however, it might be noted that, there existed two maxima at 2 wt.% and 9 wt.% of MC, separated by a local minimum at 4 wt.% of MC. As shown in Figure 4, up to 14 wt.% of MC, there was a constant value of ΔH, indicating the formation of highly dense crosslinking network. Thus, these kinetic features indicated the existence of two regimes in the MC crosslinking kinetics, which were expected to be controlled by different mechanisms. Due to these features, there were predicted differences in the structure of the crosslinked networks, however, further studies are necessary.

The kinetics was additionally affected by the temperature of the process. It can be seen in Figure 6b, that the processes occurring at higher temperatures were faster than those at lower temperatures. We anticipated that there was a similar effect of various molecular mobility, being dependent in this case on temperature. Interestingly, all rates showed similar values at the same temperature. Moreover, it might be noticed that the rates of crosslinking and destruction of the water cages showed a similar abrupt drop at 61 °C and in case of the former rate, it also showed two additional abrupt changes at 63 °C and 66 °C. This coincidence suggested that the two crosslinking mechanisms proposed above might have been temperature activated.

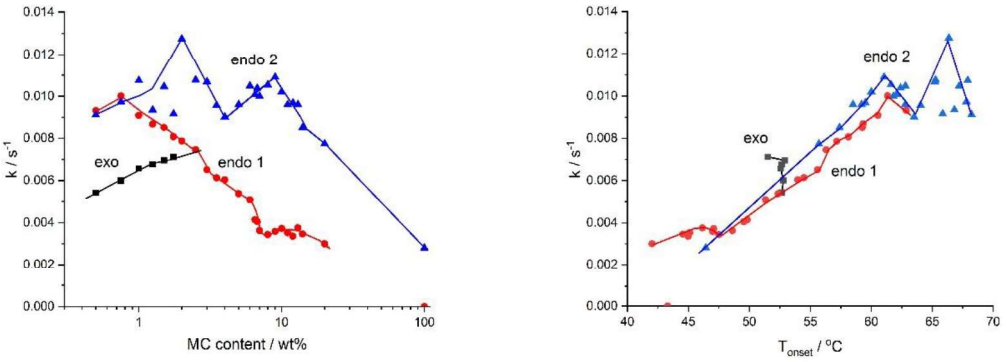

Figure 6. The rates, *k*, of water cages formation (exo), their destruction (endo 1), and of crosslinking (endo 2), as a function of—(**a**) the MC content and (**b**) the temperature, T_{onset}.

3.2. DMA

Analysis of the G′ and G″ as a function of time was used to determine the crosslinking kinetics of thermoresponsive materials. In most cases described in the literature, e.g., [29], the G′ and G″ curves intersected each other at a particular time with further domination of G′ over G″. While the G′ curve was below the G″ curve, the material presented viscous behavior characteristic for liquids. The intersection was the characteristic point, which was usually taken as the time (or temperature) of crosslinking [5]. The dominance of G′ over G″ indicated the elastic behavior of the material [29].

There is a specific group of materials in which the intersection of G′ and G′′ has not been detected. We observed such a situation for the isothermal measurements of the MC aqueous solutions. During every measurement, the G′ was higher than G″, showing the weak elastic character of MC aqueous solutions, even at ambient conditions. Consequently, in order to estimate the crosslinking kinetics, only G′ was analyzed as a function of time.

Results for small concentrations of MC ranging between 1 and 5 wt.% and the full range of MC concentrations 1–10 wt.% (shown in Figure 7a,b) indicated a sigmoidal growth of G′, which was non-ideal, particularly for lower concentrations. Different onset time of crosslinking among the various concentrations of MC was observed. The G′ of MC at the lowest concentration of 1 wt.% showed very different behavior, compared to the solutions with higher concentrations, with a very slow growth and the lowest final value. The final values of G′, for small MC concentrations (1–5 wt.%), increased with the MC concentration. An analysis of G′ at the full range of MC concentrations (Figure 6b) showed a smoother G′ increase for higher MC concentrations (6.75 and 10 wt.%), with a clearly marked stabilization at the end of the crosslinking. As expected, an increase in the G′ values with an increasing concentration for 5 and 10 wt.% of MC was also observed.

After heating up to 37 °C, for a long time, the MC aqueous solution showed a delayed thermal destruction of the water cages, resulting in an unstable increase of G′. The analysis of the G′ and *dG′/dt* curves clearly indicated that the crosslinking rate and the final G′ value depended on the temperature and polymer concentration. However, the heating time also played a key role here. As mentioned before, diluted MC aqueous solutions need prolonged heating to destroy water cages and initiate a polymeric chain rearrangement. Since the number of methoxy groups is partial and the distance between them is prominent, the greater amount of time that is needed to ensure a contact between them results in a hydrophobic bond formation. Solutions with the highest MC concentrations showed an instant G′ increase corresponding to the first step of crosslinking. In a denser polymeric network, there are partially formed hydrophobic interactions, and hence it results in less water cages breakage. As a result, G′ increase was more stable and needed less time to form fully crosslinked network. Another reason for the multiple effect of crosslinking for small concentration might be the temperature, which was not high enough to induce crosslinking. Since the hydrophilic solvent dominated in the

solution, it was difficult to destroy all of the water cages. Some of the methoxy groups were entrapped and could not form a fully formed hydrophobic network. Probably for such concentrations, a higher temperature was needed to induce crosslinking and increase the rate of the process. For the higher MC concentrations, the polymeric chains were closer to each other and it was feasible to form hydrophobic interactions. Denser packed MC chains tended to make bridges with water molecules [30]. In a partially cross-linked network, aggregation occurred at sufficiently high temperatures, when it was easier to break down water cages at higher concentrations.

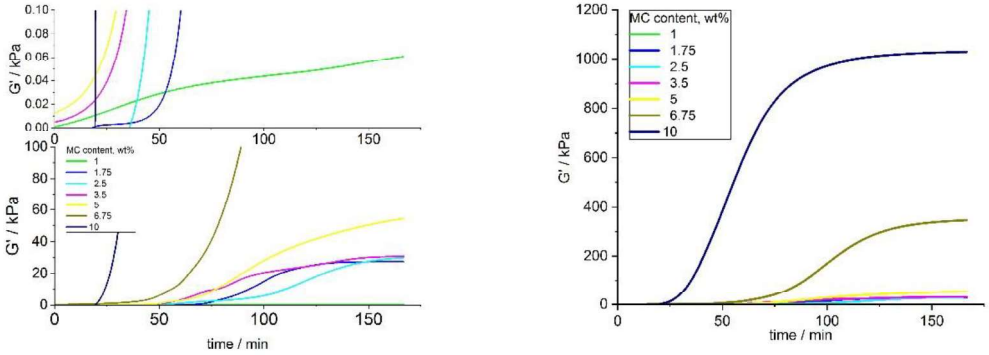

Figure 7. G′ versus time at 37 °C for several MC concentrations—(**a**) enlarged view of the low G′ range, and (**b**) the whole G′ range.

The time derivatives of G′ for low MC concentrations showed a complex multimodal character, which was a consequence of the non-ideal sigmoidal character of the G′ growth (Figure 8a,b). For every sample, the height of the first maximum was smaller than the second one, and appeared later than 50 min of the measurement. The height of the second maximum was always the highest and appeared in the time range of 80–120 min of the measurement. In some samples (1.75 and 3.5 wt.%), there was also a third smallest maximum, appearing at the latest stage of the process.

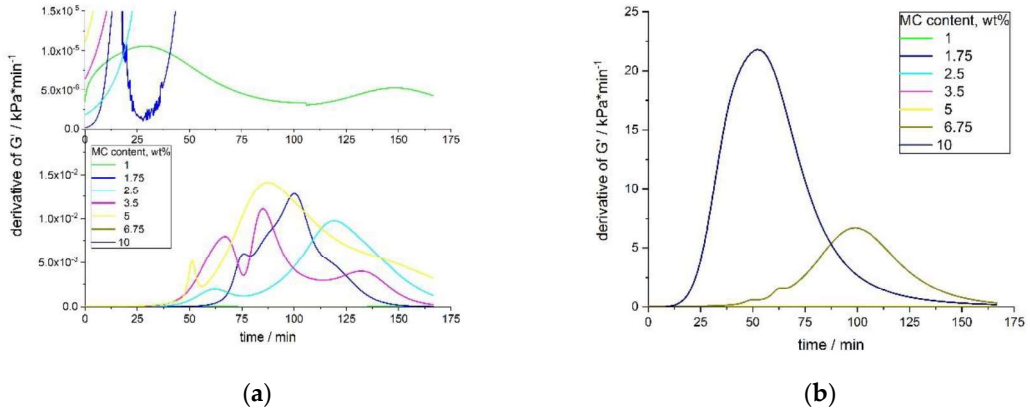

Figure 8. dG′/dt versus time for several MC solutions—(**a**) enlarged view of low MC concentrations, and (**b**) the whole dG′/dt range.

With an increasing MC concentration, the process became more homogenous and there might have been only one maximum in the time-derivative of the G′ curve. Moreover, the process became faster (according to the height of the peak and its time position) (Figure 8b). Although, MC at 6.75 wt.% still showed two maxima in the *dG′/dt*, the first maximum was practically negligible, as compared to the second large one. MC at 10 wt.% showed only one maximum at 52 min. The onset time of

the crosslinking differed for various concentrations, being shorter at higher concentrations. This was especially evident for the 6.75 and 10 wt.% of MC.

Figure 9 shows the crosslinking rate, as determined from the DMA results, as a function of the MC concentration. There were two maxima at ca. 3 wt.% and ca. 8 wt.% with the local minimum in between, which was qualitatively similar as obtained by the DSC for the crosslinking process, manifesting as the high-temperature endothermic effect (compared with the 'endo 2' in Figure 6a).

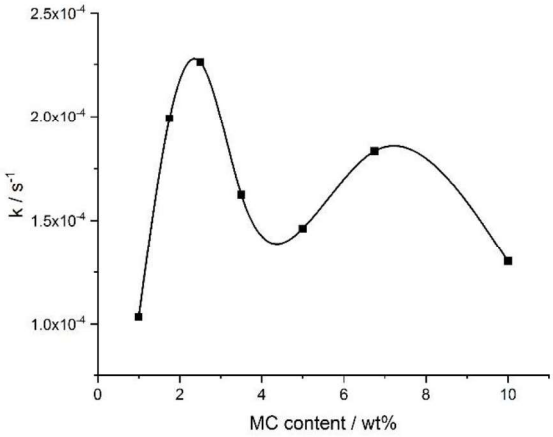

Figure 9. Crosslinking rate, *k*, determined by DMA, versus the MC content.

Table 1 shows the final maximum values of G′, which were determined as integrated extrapolated G′ derivatives. These values were analyzed and compared to the G′ of various human tissues (Table 2). G′ for the lowest MC concentration (1 wt.%) was significantly lower, as compared to others. MC of 1.75–3.5 wt.% showed similar values, and above these concentrations the G′ increased significantly.

The final G′ versus the MC concentration dependency was just as predicted. The higher concentration resulted in higher final hydrogel stiffness. The obtained results suggest that, with regards to the viscoelastic properties, the MC aqueous solution might be a suitable material used as a scaffold for tissue engineering. In order to definite a dedicated application of the studied MC concentrations, the obtained results were summarized and compared to the G′ of various human tissues (Tables 1 and 2). According to the tables, the stiffness of MC in concentrations of 1.75–3.5 wt.% might be used for spinal cord therapies as a scaffold or drug/cell delivery system. MC at the concentration of 6.75 wt.% presents similar mechanical properties (G′ value) to the human meniscus. MC at a concentrations of 10 wt.% shows high values, which according to Table 2, might be suitable for cartilage applications.

Table 1. Final storage modulus, G′, determined for several MC concentrations.

MC Concentration [wt.%]	Final G′ [kPa]	SD
1	0.06	0.004
1.75	27.4	0.53
2.5	29.9	1.56
3.5	30.7	1.44
5	54.4	7.57
6.75	346.2	10.92
10	1029.3	316.03

Table 2. G′ of various human tissues.

Tissue	G′ [kPa]	Ref.
Brain:		[31]
Cerebellum	1.77–2.03	
Cerebrum	2.34–2.64	
White matter	2.41–12.1	
Grey matter	2.34–6.6	
Skin (Human skin fibroblasts)	0.14–0.26	[32]
Meniscus:	280–330	[12]
Lateral Posterior	770	
Lateral Mid body	480	
Liver	37–340	[13]
Spinal cord *	5–42	[14]
Articular cartilage (hip and knee)	1000–1700	[33]

* Shear modulus of the human spinal cord.

3.3. Biological Tests

The cytotoxicity of the MC aqueous solutions was performed by the PrestoBlue assay after 3 days. Cells were directly exposed to 1, 2.5, and 5 wt.% of the MC aqueous solutions in volumes of 25, 50, and 100 µL. Biological tests including cytotoxicity and viability of the cells on MC hydrogels were carried out to assess its relevance in tissue engineering. For MC concentrations of 1 and 2.5 wt.%, the metabolic activity was about 90% of that of the untreated cells (Figure 10). For the lowest MC concentrations, each volume of added solution performed cell viability over 70%. MC of 5 wt.% achieved this cell viability in only one volume of 25 µL. Both of these values were ≥70%, which according to UNI ISO 10993-5 standard is considered to be non-toxic for cells. At higher MC concentrations, the metabolic viability was rather low (Figure 10).

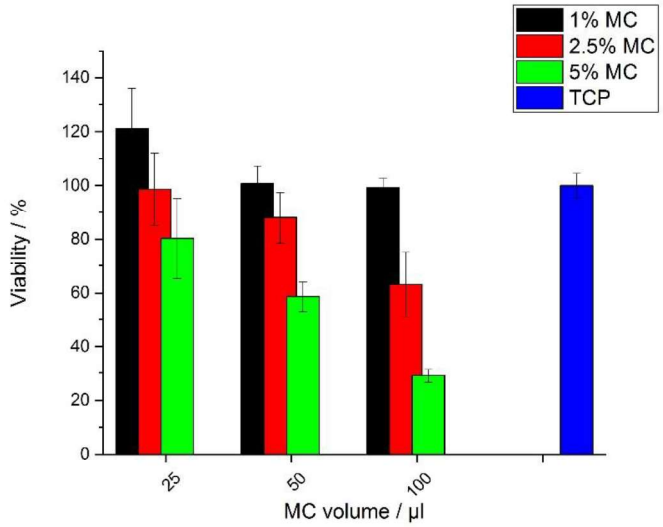

Figure 10. PrestoBlue cell proliferation results for the MC hydrogel for several MC concentrations (after 3 days).

SEM and fluorescence images (Figures 11 and 12) showed that the L929 fibroblasts penetrated the MC hydrogels to some extent. It was especially visible in fluorescent imaging that the density and viability of the cells were higher than that of the control. The varying FM cell image focus indicated different cell penetration depths into the hydrogel (Figure 12b). This effect was less visible on the SEM images (Figure 11b).

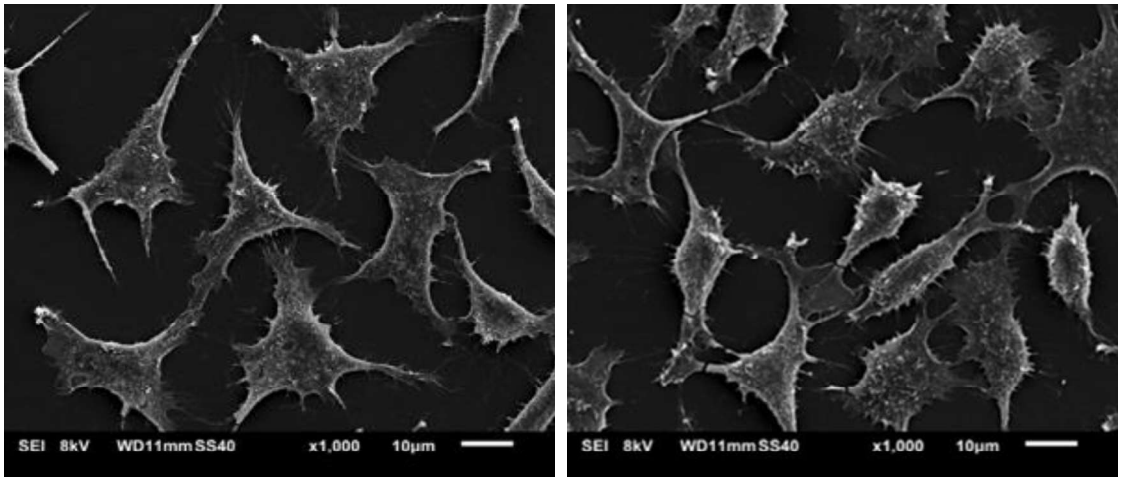

(**a**) (**b**)

Figure 11. SEM of L929 cells on (**a**) tissue culture plastic (TCP) (control) and (**b**) hydrogel containing 1 wt.% of MC (50 µL volume).

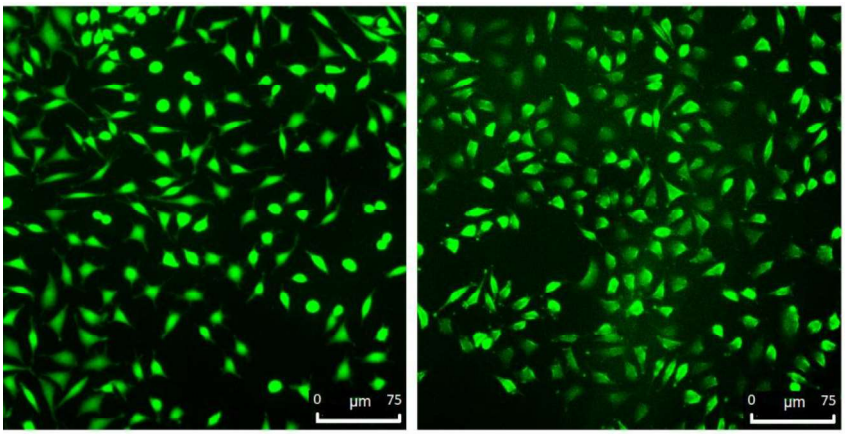

(**a**) (**b**)

Figure 12. Fluorescence microscopy of stained L929 cells on—(**a**) TCP (control) and (**b**) hydrogel containing 1 wt.% MC (50 µL volume).

Our results indicated that the L929 cells seeded on top of the gels remained viable with no indication of cell death throughout the culture duration. However, the different concentrations and added volumes of MC influenced the viability, metabolic activity, and morphology of this cell line. It was evident that MC with low MC concentrations (below 2.5 wt.%) did not cause cytotoxicity. At these concentrations an appropriate pH and availability of oxygen were ensured. However, at MC concentrations ≥5 wt.% the material seemed to be toxic for fibroblast. It was probably the effect of the acidic pH and a limited availability of oxygen. The limited availability of oxygen could have been a result of the high viscosity of the hydrogel. At these MC concentrations, the cells collapsed and did no longer had the possibility to conduct any metabolic activity. It was also observed that the amount of added hydrogel significantly influenced the cells viability. The more added hydrogel, the higher toxicity, especially, at higher MC concentrations. It was probably caused by the non-controlled pH in the MC aqueous solutions. However, in the future, we plan to study a mixture of MC with PBS, in order to control the pH of the solution, which is expected to increase cell viability on the investigated materials.

4. Conclusions

We systematically studied a broad range of MC concentrations in aqueous solutions, to explore in details, the crosslinking kinetics, thermal, viscoelastic, and biological properties. We have assessed the real value of MC as a material for tissue engineering, including its advantages and disadvantages. For this evaluation DSC, DMA measurements, and biological analyses were carried out. It was evidenced by DSC that the crosslinking of MC was a reversible two-stage process, manifested by the appearance of two endothermic effects related to the destruction of water cages around methoxy groups, followed by crosslinking via formation of hydrophobic interactions between methoxy groups in the polymeric chains. Moreover, at relatively small MC concentrations (below 2 wt.%), there appeared to be an additional exothermic process preceding the endothermic ones, which was most probably related to the formation of the water cages. Our DSC studies allowed us to construct the phase diagram for the studied MC aqueous solutions. The crosslinking kinetics of the MC solution, as determined by the DSC and DMA, was found to be quite complex, indicating three regimes. At MC higher than 13 wt.%, the crosslinking rate dramatically decreased with the MC concentrations, which was due to a reduced molecular mobility. At MC concentrations below 13 wt.%, there seemed to be two regimes evidenced by two maxima at 2 wt.% and 9 wt.%. In these regimes, the crosslinking mechanisms might differ and, moreover, the change of the mechanism might be temperature activated. These mechanisms need to be further investigated. Nevertheless, the obtained results allowed the selection of MC concentrations that might meet the tissue engineering expectations. Since MC at concentrations in the range of 1.7–3.5 wt.% and at ca. 9 wt.% showed the fastest crosslinking, these concentrations could be attractive for tissue engineering applications. Tissue engineering is rather demanding, it requires looking not only from the crosslinking rate perspective, but also from a mechanical and biological point of view. For lower MC concentrations, the final storage modulus (DMA) s comparable to native human tissues such as liver [13], spinal cord [14], or cartilage [33]. From biological tests, it was found that at low concentrations, MC provided a good cellular response and non-toxic environment. It was highly probable that it would be necessary in the future to modify MC solutions in order to improve their properties. Nevertheless, we are certain that, due to the minimally invasive manner through which these materials were introduced into the body, and because of the mechanical and the biological properties of MC, relatively small concentrations of this material can have a great potential as injectable scaffolds for tissue engineering.

Author Contributions: Conceptualization, B.N.-S., P.S., and A.G.; methodology, B.N.-S., A.G., D.K. and A.K.-M.; validation, B.N.-S., A.G., P.S., D.K., and A.K.-M.; writing—original draft preparation, P.S., A.G., B.N.-S., D.K., and A.K.-M.; visualization, B.N.-S., A.G., and P.S.; supervision, P.S. and A.G.; project administration P.S., A.G., and B.N.-S.; funding acquisition, B.N.-S.

Funding: This research was funded by the Narodowe Centrum Nauki (NCN), grant number 2018/29/N/ST8/00780. The Article Processing Charge (APC) was covered by the Project no. POWR.03.02.00-00-1028/17-00 implemented under the Operational Programme Knowledge Education Development 2014–2020, co-financed by the European Social Fund.

Acknowledgments: Anna Krzton-Maziopa acknowledges the partial financial support from the statutory budget of Faculty of Chemistry, Warsaw University of Technology.

Conflicts of Interest: The authors declare no conflict of interest.

References

1. Khaing, Z.Z.; Thomas, R.C.; Geissler, S.A.; Schmidt, C.E. Advanced biomaterials for repairing the nervous system: What can hydrogels do for the brain? *Mater. Today* **2014**, *17*, 332–340. [CrossRef]
2. Khaing, Z.Z.; Seidlits, S.K. Hyaluronic acid and neural stem cells: Implications for biomaterial design. *J. Mater. Chem. B* **2015**, *3*, 7850–7866. [CrossRef]
3. Aurand, E.R.; Lampe, K.J.; Bjugstad, K.B. Defining and designing polymers and hydrogels for neural tissue engineering. *Neurosci. Res.* **2012**, *72*, 199–213. [CrossRef] [PubMed]

4. Lopez-Lopez, M.T.; Rodriguez, I.A.; Rodriguez-Arco, L.; Carriel, V.; Bonhome-Espinosa, A.B.; Campos, F.; Duran, J.D.G. Synthesis, characterization and in vivo evaluation of biocompatible ferrogels. *J. Magn. Magn. Mater.* **2017**, *431*, 110–114. [CrossRef]
5. Koetting, M.C.; Peters, J.T.; Steichen, S.D.; Peppas, N.A. Stimulus-responsive hydrogels: Theory, modern advances, and applications. *Mater. Sci. Eng. R Rep.* **2015**, *93*, 1–49. [CrossRef]
6. Bain, M.K.; Bhowmick, B.; Maity, D.; Mondal, D.; Mollick, M.M.R.; Paul, B.K.; Chattopadhyay, D. Effect of PVA on the gel temperature of MC and release kinetics of KT from MC based ophthalmic formulations. *Int. J. Biol. Macromol.* **2012**, *50*, 565–572. [CrossRef]
7. Contessi, N.; Altomare, L.; Filipponi, A.; Farè, S. Thermo-responsive properties of methylcellulose hydrogels for cell sheet engineering. *Mater. Lett.* **2017**, *207*, 157–160. [CrossRef]
8. Nasatto, P.; Pignon, F.; Silveira, J.; Duarte, M.; Noseda, M.; Rinaudo, M. Methylcellulose, a cellulose derivative with original physical properties and extended applications. *Polymers* **2015**, *7*, 777–803. [CrossRef]
9. Ying, L.I.N.; Jiali, S.U.N.; Jiang, G.; Jia, Z.A.N.; Fuxin, D.I.N.G. In vitro evaluation of lysozyme-loaded microspheres in thermosensitive methylcellulose-based hydrogel. *Chin. J. Chem. Eng.* **2007**, *15*, 566–572.
10. Lee, K.Y.; Mooney, D.J. Alginate: Properties and biomedical applications. *Prog. Polym. Sci.* **2012**, *37*, 106–126. [CrossRef]
11. Gold, G.T.; Varma, D.M.; Taub, P.J.; Nicoll, S.B. Development of crosslinked methylcellulose hydrogels for soft tissue augmentation using an ammonium persulfate-ascorbic acid redox system. *Carbohydr. Polym.* **2015**, *134*, 497–507. [CrossRef] [PubMed]
12. Pereira, H.; Caridade, S.G.; Frias, A.M.; Silva-Correia, J.; Pereira, D.R.; Cengiz, I.F.; Reis, R.L. Biomechanical and cellular segmental characterization of human meniscus: Building the basis for tissue engineering therapies. *Osteoarthritis Cartilage* **2014**, *22*, 1271–1281. [CrossRef]
13. Ozcan, M.U.; Ocal, S.; Basdogan, C.; Dogusoy, G.; Tokat, Y. Characterization of frequency-dependent material properties of human liver and its pathologies using an impact hammer. *Med. Image Anal.* **2011**, *15*, 45–52. [CrossRef] [PubMed]
14. Bartlett, R.D.; Choi, D.; Phillips, J.B. Biomechanical properties of the spinal cord: Implications for tissue engineering and clinical translation. *Regen. Med.* **2016**, *11*, 659. [CrossRef] [PubMed]
15. Martin, B.C.; Minner, E.J.; Wiseman, S.L.; Klank, R.L.; Gilbert, R.J. Agarose and methylcellulose hydrogel blends for nerve regeneration applications. *J. Neural Eng.* **2008**, *5*, 221. [CrossRef]
16. Joshi, S.C.; Lam, Y.C. Modeling heat and degree of gelation for methyl cellulose hydrogels with NaCl additives. *J. Appl. Polym. Sci.* **2006**, *101*, 1620–1629. [CrossRef]
17. Lee, K.Y.; Bouhadir, K.H.; Mooney, D.J. Controlled degradation of hydrogels using multi-functional crosslinking molecules. *Biomaterials* **2004**, *25*, 2461–2466. [CrossRef]
18. Li, L.M.; Han, M.; Jiang, X.C.; Yin, X.Z.; Chen, F.; Zhang, T.Y.; Ou-Yang, H.W. Peptide-tethered hydrogel scaffold promotes recovery from spinal cord transection via synergism with mesenchymal stem cells. *ACS Appl. Mater. Interfaces* **2017**, *9*, 3330–3342. [CrossRef]
19. Kim, M.H.; Kim, B.S.; Park, H.; Lee, J.; Park, W.H. Injectable methylcellulose hydrogel containing calcium phosphate nanoparticles for bone regeneration. *Int. J. Biol. Macromol.* **2018**, *109*, 57–64. [CrossRef]
20. Sarkar, N. Kinetics of thermal gelation of methylcellulose and hydroxypropylmethylcellulose in aqueous solutions. *Carbohydr. Polym.* **1995**, *26*, 195–203. [CrossRef]
21. Fatimi, A.; Tassin, J.F.; Turczyn, R.; Axelos, M.A.; Weiss, P. Gelation studies of a cellulose-based biohydrogel: The influence of pH, temperature and sterilization. *Acta Biomater.* **2009**, *5*, 3423–3432. [CrossRef] [PubMed]
22. Chen, C.H.; Tsai, C.C.; Chen, W.; Mi, F.L.; Liang, H.F.; Chen, S.C.; Sung, H.W. Novel living cell sheet harvest system composed of thermoreversible methylcellulose hydrogels. *Biomacromolecules* **2006**, *7*, 736–743. [CrossRef] [PubMed]
23. Li, L. Thermal gelation of methylcellulose in water: Scaling and thermoreversibility. *Macromolecules* **2002**, *35*, 5990–5998. [CrossRef]
24. Chemistry of MetocelTM Cellulose Ethers—A Technical Review. Available online: http://msdssearch.dow.com/PublishedLiteratureDOWCOM/dh_08e5/0901b803808e5f58.pdf?filepath=dowwolff/pdfs/noreg/198-02289.pdf&fromPage=GetDoc (accessed on 1 October 2013).
25. Sandoval, M.L.; Camerucci, M.A. Rheological behavior of aqueous mullite-albumin-methylcellulose systems. *Ceram. Int.* **2017**, *43*, 7243–7252. [CrossRef]

26. Maryanski, M.J.; Audet, C.; Gore, J.C. Effects of crosslinking and temperature on the dose response of a BANG polymer gel dosimeter. *Phys. Med. Biol.* **1997**, *42*, 303. [CrossRef] [PubMed]
27. Dufresne, A.; Reche, L.; Marchessault, R.H.; Lacroix, M. Gamma-ray crosslinking of poly (3-hydroxyoctanoate-co-undecenoate). *Int. J. Biol. Macromol.* **2001**, *29*, 73–82. [CrossRef]
28. Sekiguchi, Y.; Sawatari, C.; Kondo, T. A gelation mechanism depending on hydrogen bond formation in regioselectively substituted O-methylcellulose. *Carbohydr. Polym.* **2003**, *53*, 145–153. [CrossRef]
29. Li, L.; Shan, H.; Yue, C.Y.; Lam, Y.C.; Tam, K.C.; Hu, X. Thermally induced association and dissociation of methylcellulose in aqueous solutions. *Langmuir* **2002**, *18*, 7291–7298. [CrossRef]
30. Dehabadi, L.; Udoetok, I.A.; Wilson, L.D. Macromolecular hydration phenomena. *J. Therm. Anal. Calorim.* **2016**, *126*, 1851–1866. [CrossRef]
31. Zhang, J.; Green, M.A.; Sinkus, R.; Bilston, L.E. Viscoelastic properties of human cerebellum using magnetic resonance elastography. *J. Biomech.* **2011**, *44*, 1909–1913. [CrossRef]
32. Schulze, C.; Wetzel, F.; Kueper, T.; Malsen, A.; Muhr, G.; Jaspers, S.; Käs, J.A. Stiffening of human skin fibroblasts with age. *Clin. Plast. Surg.* **2012**, *39*, 9–20. [CrossRef] [PubMed]
33. Lawless, B.M.; Sadeghi, H.; Temple, D.K.; Dhaliwal, H.; Espino, D.M.; Hukins, D.W. Viscoelasticity of articular cartilage: Analysing the effect of induced stress and the restraint of bone in a dynamic environment. *J. Mech. Behav. Biomed.* **2017**, *75*, 293–301. [CrossRef] [PubMed]

polymers

MDPI

Review

Hydrophilic Surface Functionalization of Electrospun Nanofibrous Scaffolds in Tissue Engineering

Beata Niemczyk-Soczynska *, Arkadiusz Gradys and Pawel Sajkiewicz

Institute of Fundamental Technological Research, Lab. Polymers & Biomaterials, Polish Academy of Sciences Pawinskiego 5b St., 02-106 Warsaw, Poland; argrad@ippt.pan.pl (A.G.); psajk@ippt.pan.pl (P.S.)

* Correspondence: bniem@ippt.pan.pl; Tel.: +48-6-2238-6179

Received: 21 October 2020; Accepted: 8 November 2020; Published: 10 November 2020

Abstract: Electrospun polymer nanofibers have received much attention in tissue engineering due to their valuable properties such as biocompatibility, biodegradation ability, appropriate mechanical properties, and, most importantly, fibrous structure, which resembles the morphology of extracellular matrix (ECM) proteins. However, they are usually hydrophobic and suffer from a lack of bioactive molecules, which provide good cell adhesion to the scaffold surface. Post-electrospinning surface functionalization allows overcoming these limitations through polar groups covalent incorporation to the fibers surface, with subsequent functionalization with biologically active molecules or direct deposition of the biomolecule solution. Hydrophilic surface functionalization methods are classified into chemical approaches, including wet chemical functionalization and covalent grafting, a physiochemical approach with the use of a plasma treatment, and a physical approach that might be divided into physical adsorption and layer-by-layer assembly. This review discusses the state-of-the-art of hydrophilic surface functionalization strategies of electrospun nanofibers for tissue engineering applications. We highlighted the major advantages and drawbacks of each method, at the same time, pointing out future perspectives and solutions in the hydrophilic functionalization strategies.

Keywords: surface functionalization; electrospinning; polymers; nanofiber; immobilization; tissue engineering

1. Introduction

Tissue engineering is an interdisciplinary field of science, in which polymeric scaffolds are crucial from the biomedical perspective [1]. In this field, various forms of scaffolds might be distinguished, among which the most important are: non-injectable and injectable hydrogels, sponges, 3D printed beams, and submicron- and nanofibers [2–5]. In recent decades, electrospun nanofibrous scaffolds have gained and enjoyed the great interest of tissue engineering applications [5] with the greatest importance of nanofibers composed of aliphatic polyesters, such as poly-L-lactide (PLLA), polycaprolactone (PCL), poly (lactic-co-glycolic acid) (PLGA), and poly (lactide-co-caprolactone) (PLCL) [6]. All of these polymers are biodegradable, biocompatible, easily processable, and have appropriate mechanical properties. It is easy to control their physical and mechanical properties by tuning the polymeric solution's concentration, using appropriate solvents and parameters of the process [7]. One of the most favorable properties of electrospun nanofibers is their morphology. It highly resembles collagen fibers in native ECM, making them attractive as scaffolds in tissue engineering, drug delivery systems, or wound dressings [8,9]. Besides aliphatic polyesters, semicrystalline fluoropolymers, especially polyvinylidene fluoride (PVDF), gained attention as smart piezoelectric scaffolds. While stress is applied to the PVDF scaffold, it generates and conducts electric signals, which induce cell regeneration [10]. This feature might be useful, especially in nervous system tissue engineering.

An appropriate scaffold formation should not only assume material morphological resemblance to the natural ECM, provide physical support for cells but mostly should contribute to cell–surface interactions [11]. Most of the electrospun polymers are rather hydrophobic, which is unfavorable from the point of view of tissue engineering. For instance, aliphatic polyesters such as PLLA or PCL show contact angles in the range of 116–135°, while for tissue engineering requirements, it ought to be below 100° [12,13]. Webb et al. [14] studied the highest level of cell attachment (NIH 3T3 fibroblasts) at hydrophilic surfaces, and the best results were observed for surfaces with contact angles in the range of 20–60°. In this regard, an appropriate hydrophilic functionalization that improves these features is thus necessary. A potential scaffold for medical applications also should have appropriate bulk properties and biological activity at the surface, but material rarely possesses both of these features simultaneously [15]. Synthetic materials have excellent bulk properties; however, their polymeric chains do not contain biologically active molecular motives. Integrin receptors bind cells with ECM, specifically, recognize Arg-Gly-Asp amino acid (RGD) sequences providing further cell adhesion to the surface. There are many natural materials, for instance, gelatin, fibronectin, laminin, or collagen, that might provide the ECM components with biological active sequences like RGD required for cell adhesion, accelerating cell growth, and providing a favorable environment for their proper functioning [13,16,17]. For this reason, it is clear that the presence of biomolecules plays a key role in promoting cell/biomaterial interactions [18].

Hydrophilic surface functionalization, followed by biomolecules attachment, can be realized by various strategies, which can be divided into three main groups: pre-electrospinning methods via bulk blending with another natural polymer [19,20], functionalization during electrospinning (e.g., coaxial electrospinning) or post-electrospinning methods such as wet chemical methods (aminolysis [6] or hydrolysis [21]), covalent grafting [22], plasma treatment [23], physical adsorption [24], or layer by layer (LBL) assembly [25]. Contrary to pre-electrospinning methods, most of the post-electrospinning methods alter fiber surface only, which is preferred from the perspective of scaffolds final properties [19].

This comprehensive review aims at an in-depth discussion on post-electrospinning hydrophilic surface functionalization strategies of polymeric nanofibers with an emphasis on their advantages and drawbacks, and the potential in further processing for tissue engineering applications. In this article, we present the electrospun nanofibers processing from both the materials science and the tissue engineering point of view.

2. Surface Functionalization Methods

2.1. Chemical Methods

Chemical surface functionalization leads to improved hydrophilicity on the fibers' surface through changing atoms or molecules as a consequence of chemical reactions. Contrary to physical treatment, this kind of method is permanent. Once modified, the surface should stay permanently changed, by forming stable covalent bonding between biomolecules and the polymer surface. This is the effect of exposing relevant functional groups on the surface of the nanofibers to the external chemical stimuli [26]. To attain covalent bonding with biomolecules, usually, two steps are needed. The first one provides exposing functional groups such as –OH, –COOH, and –NH2 needed for effective reactions. The next one is formation of covalent bonds between biomolecules and functional groups on the polymer surface [6].

An advantage of chemical functionalization is that it provides steady bioactive sites for further biomolecules immobilization, resulting in improved biological properties of the surface, on which the cells can attach and grow favorably.

On the other hand, there is a risk that in the preactivated state, an uncontrolled chemical functionalization might change the bulk properties of the polymeric scaffold [21]. Figure 1 presents

mechanisms of chemical surface modifications, while Table 1 summarizes the main pros and cons of the chemical surface functionalization methods applied to electrospun nanofibrous scaffolds.

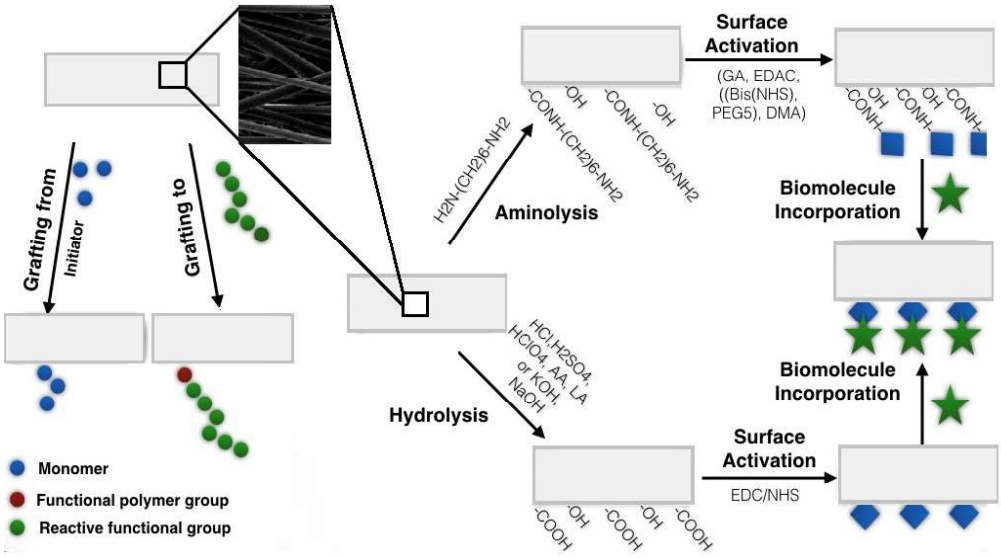

Figure 1. Chemical functionalization of electrospun nanofibers.

2.1.1. Wet Chemical Functionalization

Wet chemical functionalization of electrospun nanofibers is a chemical treatment under acid, or basic conditions, or with the presence of diamine, resulting in the polymer chains breaking at the sites of specific groups, like ester bonds in the case of polyesters.

Compared to the physical methods, wet chemical functionalization provides hydrophilic functionalization not only on the outer layer of the nanofiber surface, but also affects the deeper layer of the surface. The depth of reaction in wet chemical functionalization depends on the process/materials parameters like time reaction, and type and concentration of active substrates. Therefore, the reaction conditions must be precisely controlled [21,27] in order to minimize the changes of polymer bulk properties, which can ultimately lead to serious mechanical weakening or even destruction of polymer nanofibers [21,28]. It should be mentioned that wet chemistry usually uses harsh chemicals, making the method not ecologically friendly [29].

Depending on the method, –COOH, –OH, and $–NH_2$ groups appear onto the polymer surface as a result of wet functionalization. The most common methods of wet chemical functionalization, aminolysis and hydrolysis, are described in detail below.

Aminolysis

Aminolysis [30] is a surface functionalization method that incorporates free amine groups to the nanofibers surface, by the formation of covalent bonds between the amine from the other end of diamine used for functionalization and the specific polymer group. The most common diamines used for functionalization of various polyesters, both aromatic and aliphatic, are 1,6-hexanediamine, ethylenediamine, or N-aminoethyl-1,3-propanediamine [31]. After effective aminolysis reaction at carefully controlled conditions, e.g., diamines concentration, temperature, pH, and time, the hydroxyl, carboxyl, and amine groups remain as active groups on the modified surface, providing better wettability.

One of the advantages of the method is that the total time of the reaction is rather short: aminolysis can last from 2 up to 60 min [32,33]. The surface after the treatment is additionally characterized by higher roughness, favorable from the perspective of biomolecules immobilization and cells adhesion [21].

All of these features occur to be beneficial for both scenarios: when aminolysis is the ultimate treatment of surface functionalization ready for direct use, or while it serves as an intermediate step followed by immobilization of proteins such as collagen, fibronectin, and laminin, growth factors or bioactive groups. Adsorption of proteins on the aminolyzed surface can be performed via simple rinsing of the nanofibers for a certain period of time in the proteins solution [34,35].Although the whole procedure of physical adsorption of biological molecules seems to be relatively simple, there are some results indicating either insufficient concentration of –OH, –COOH, and $–NH_2$ groups on the modified surface or proteins conformation, which does not enhance cell adhesion. Zhao et al. reported that in the case of PCL, the aminolyzed surface showed only temporal improvement of cell adhesion for 4 h [34].

Aminolysis as the intermediate step seems to be more effective than as the ultimate step, and is more often used in protein immobilization [6,36,37]. The efficiency of protein immobilization can be increased by additional treatment with a particular coupling agent, for instant, glutaraldehyde (GA), 1-ethyl-3-(3-dimethylaminopropyl)-carbodiimide (EDAC), Bis-N-succinimidyl-(pentaethylene glycol) (Bis (NHS) PEG5), or dimethyl adipimidate (DMA) [31,36]. Such coupling agents provide better availability of the $–NH_2$ and –COOH on the surface, for covalent binding with biomolecules such as gelatin, chitosan, or collagen [28]. Depending on the choice of coupling agent, the functional group activation is carried out under specific pH, temperature, and time [31]. XPS, FTIR studies [31], and biological tests [34] have proved that such covalent binding between the surface and biomolecules significantly improves the morphology of the cells and promotes their proliferation. It indicates the importance of surface chemistry in cellular behavior on biomaterial substrates [34]. Aminolysis as the intermediate step is also widely used for growth factors immobilization. Haddad et al. have immobilized epidermal growth factors (EGF) to PLLA nanofibers through the coupling agent of (Bis (NHS)PEG5) [31]. Combining these treatments showed improved interactions between PLLA fibers and neural stem-like cells (NSLCs) after aminolysis in proliferation assay 2, 6, and 10 days [31].

Aminolysis might also be conjugated with other hydrophilic functionalization methods. Zhang et al. aminolyzed aligned PLLA fibers and then coated them with graphene oxide (GO) in the presence of the nerve growth factors (NGFs). Due to the phenol hydroxyl and epoxide groups on the basal plane and carboxylic groups at the edges, this treatment supposed to increase the hydrophilicity and growth and differentiation of various neural cell lines [37]. The water contact angle of the aligned PLLA decreased from 122.8 ± 1.5° to 96.8 ± 1.5° after aminolysis, and to 47.5 ± 2.2° after GO incorporation. The ultimate surface contact angle should be beneficial for cell growth accordingly to Webb's studies [15] MTT proliferation and differentiation tests on PC12 and Schwann cells proliferation assay confirmed that, in the presence of NGF and appropriate hydrophilicity, the aminolyzed aligned PLLA/GO fibers effectively promoted Schwann cell growth and induced differentiation of PC12 [37].

Despite many advantages, aminolysis has its limitations. Its efficiency depends on the crystallinity of functionalized polymers, particularly on the surface crystallinity, as shown by Jeznach et al. [6]. The method is challenging for polymers with high crystallinity and small ratios of ester/alkyl groups, as in the PCL case. Moreover, aminolysis is more effective for films than nanofibers, which is related to the surface crystallinity resulting from the difference in crystallization conditions [6]. Thus, highly crystalline nanofibers require harsher conditions and extended time of the aminolysis reaction. Another limitation of the method is the instability of the aminolyzed surface. Zhu et al. [38] reported that aminolyzed polymers might lose amine groups from the surface while being stored at 37 °C. To avoid this, it is necessary to keep materials at a temperature below the polymer Tg. Amine groups also disappear from the surface while kept in the phosphate buffer saline (PBS) due to a restructuring of the polymer membrane [38]. Briefly, at the surface, segments of the polymer chains rearrange to decrease surface energy resulting in amine groups' distancing from the surface. It constitutes a severe limitation for using of aminolyzed polymers in the industry or tissue engineering. Exceptionally, such scaffolds might be used very soon after fabrication or stored for a short time at very low temperatures.

Hydrolysis

The method is divided into alkaline and acid hydrolysis, which generally cleaves ester bonds to –COOH and –OH groups on the polyester's surface [21]. Depending on the conditions, acid or alkaline, there are different mechanisms of the hydrolysis reaction. Similarly to aminolysis, both acid and basic hydrolysis, require to be conducted under precisely controlled conditions such as temperature, pH. and time, and the reaction time varies from a few to dozens of minutes [39].

The acid hydrolysis has an electrophilic character, which means that high-speed protons easily penetrate into uncharged polymer chains and are restored by the reaction. Briefly, carbon radicals are formed from the polymeric backbone, whereupon unsteady –OOH groups bind with O_2 from H_2O, resulting in –OOH groups breakdown into various groups such as –OH, –COOH, –R–O–R', etc. [40]. Since –COOR groups are hardly available on the modified polymers' surface, strong acidic conditions, elevated temperature, and appropriate time are required [31]. In the acid hydrolysis, mineral acids such as H_2SO_4, $HClO_4$, and HCl and organic acids such as acetic acid (AA) or lactic acid (LA) are typically used [39,41,42]. Boland et al. chose 11.7 M HCl over NaOH for hydrolysis of PGA scaffolds to avoid a fiber diameter decrease. The hydrolysis of the –COO– exposed –COOH and –OH groups on the modified fiber surface, resulting in improved adhesion between surface and cells and their proliferation in the WST-1 proliferation assay on cardiac fibroblasts (FBs) after 4 days. However, in vivo studies on rat muscles were inconclusive and the whole functionalization procedure needs to be refined in the future. In other studies, Lee et al. used a mixture of $HClO_4/KClO_3$ in a saturated aqueous solution to modify PGA, PGLA, and PLLA scaffold surfaces. Although human chondrocytes and mouse NIH/3T3 fibroblasts showed an improved adhesion and proliferation after 2 days, this time might not be enough for further tissue engineering therapies [40]. An interesting phenomenon has been observed by Spinella et al. It is reported that in the case of some polymers such as cellulose nanocrystals, the use of H_2SO_4 for hydrolysis leads to a decrease in their thermal stability, leading to an uncontrolled release of H_2SO_4 from polymers during heating [43]. These features might limit the use of the acid hydrolysis in further studies on the surface functionalization of electrospun fibers for biomedical applications.

Due to the aforementioned limitations of the acid hydrolysis, for tissue engineering applications, the alkaline hydrolysis is more often chosen [43–45]. The alkaline hydrolysis has a nucleophilic character due to the presence of alkali metal hydroxides such as NaOH or KOH. The OH^- reacts with C=O, C–O, and C–O–C functional groups in the polymeric surface area, where there is the lowest electron density, and removes short segments of the polymeric chains. As a result, the hydrophilic groups such as –COOH and –OH are formed on the fibers' surface [44]. The higher concentration of the alkali metal hydroxide the deeper the modification, and additional oxidizing agents accelerate the reaction, which causes OH^- penetration deeper into the material. On the other hand, very fast and hence uncontrolled hydrolysis leads to a decrease in the nanofiber mat' mass and thickness [44]. Similarly to aminolysis, hydrolysis might also serve as an intermediate step before protein immobilization. Sadeghi et al. obtained PLGA scaffolds incorporated with collagen, applying hydrolysis as a 1st step followed by the 1-ethyl-3-(3-dimethylaminopropyl) carbodiimide/N-hydroxysuccinimide (EDC/NHS) crosslinking. The 1st step was carried out with the use of NaOH, in which fibers were hydrolyzed for 5 min at room temperature. Then, the fibers' surface was activated through immersing fibers in EDC/NHS at pH = 6 at 4 °C. It was found that the wettability of PLGA increased significantly after hydrolysis and collagen immobilization, while after aminolysis, water contact angle decreased from 132° to 98° and further to zero after collagen immobilization. Additionally, FTIR spectra confirmed the presence of immobilized collagen on PLGA fibrous scaffolds, proving the effectiveness of the functionalization method. Cell viability MTT tests on human dermal fibroblasts (HDFs) and the keratinocyte cell line (HaCaT) showed increased viability of the cells on the scaffolds with immobilized collagen after 14 days, proving that modified in this way scaffolds are appropriate for skin tissue engineering applications [45]. In the other publication, De Luca et al. report on hydrolytically modified PLLA nanofibers after using KOH and NaOH for 1 h at room temperature. FTIR spectra confirmed the effectiveness of this

method by showing the –COOH and –OH groups on the fibers' surface [46]. The presence of these groups also affected the hydrophilicity of the PCL fibers, improving their biocompatibility. The water contact angle decreased from 76.58 ± 1.25° to 54.13 ± 2.73° and 56.83 ± 2.88° after NaOH and KOH hydrolysis, respectively. MTS proliferation assay on Schwann cells demonstrated a substantial increase in cell attachment and proliferation after 1, 3, and 5 days on modified samples compared to untreated fibers [46].

2.1.2. Covalent Grafting

Covalent attachment or so-called "grafting" is generally carried out via chemical activation of appropriate reagents on the treated surface. Two major methods, "grafting to" and "grafting from", can be distinguished in this regard.

"Grafting to" uses a coupling reaction that modifies the end functional polymer group with the reactive functional groups resulting in a chemical change in the polymeric backbone. This type of grafting uses all kinds of polymerization, including atom-transfer radical-polymerization (ATRP), controlled free-radical polymerization (CFRP), or anionic polymerization [47,48]. Covalent grafting was used for hydrophilic surface functionalization on PCL, PLLA, or polysulfone (PSU) and many copolymers described below [49–52]. "Grafting to" is a method that might be used for a wide range of materials, for instance, various monomers, such as acrylonitrile [22], acrylate, acrylamide, and many others [47,48,53]. However, the polymerization time has to be precisely controlled; otherwise, fibers' morphology might be destroyed, and bulk properties of such material might be changed [54]. "Grafting to" might be combined with other methods of surface functionalization. Such a combination might bring not only hydrophilic surface functionalization but also provide additional features to the obtained fibers. Fu et al. combined technology of RAFT polymerization, ATRP, electrospinning, and "click chemistry" to obtain electrospun nanofibers made of poly (4-vinylbenzyl chloride) (PVBC), poly (glycidyl methacrylate) (PGMA), and poly-N-isopropylacrylamide (PNIPAM) to obtain fibers, which were solvent-resistant with the thermal-sensitive surface [48]. Contact angle measurements showed a significant change in PVBC74-b-PGMA46-g-PNIPAM7 fibers wettability depending on the ambient temperature. It was observed that the contact angle of hybrid fibers decreased from 140 to less than 30° after a temperature decrease from 45 to 20 °C [48].

In the field of hydrophilic surface functionalization even more popular than "grafting to" is "grafting from". In this method, the macromolecular backbone is modified with the purpose of introducing reactive functional groups on the surface. This method requires an initiator, which might be introduced to the surface through post-polymerization, copolymerization, or polycondensation [51,52]. For instance, "grafting from" might take place using an atmospheric pressure plasma jet (APPJ) with argon as processing gas and in open-air. Maffei et al. functionalized PCL fibers with human vitronectin adhesive cue (HVP peptide). In this respect, NH_2 groups were covalently grafted on the electrospun PCL mat by APPJ deposition of a coating using (3-aminopropyl) triethoxysilane (APTES) as a precursor. The fibers' morphology was found unchanged. The MTT viability assay confirmed that after functionalization adhesion and migration of 533 osteoblasts increased, however, only after 2 h of culture. Further cellular tests are expected [50].

The other methods assume copolymerization grafting, induced biomolecules grafting, grafting polymerization of acrylic acid (AAc) on polyesters surface followed by a chemical reaction with biomolecules, or thermal-induced graft polymerization. Such functionalization usually takes place on surfaces that were previously treated with plasma [55–57]. Ma et al. [55] used copolymerization grafting of methacrylic acid (MAA) initiated by Ce (IV) after an air plasma treatment of electrospun PSU fibers. The plasma treatment of exposed oxygen-containing groups on the polymer surfaces, among which –OH groups combined with Ce^{4+} formed a redox initiating system, which initiated the graft polymerization of MAA. The modified surface was activated with toluidine blue O (TBO) and stable –COO– groups were formed and served as binding sites between proteins and functionalized surface. After that, bovine serum albumin (BSA) was incorporated into the surface. The BSA served

as a substitute for the potential protein for further studies. BSA covalently immobilized on the PMAA grafted PSU fibers using the –COOH groups as coupling sites occurred to be successful. Obtained material served as a microfiltration membrane [55].

In the biomolecules grafting method, collagen type I (Col I), nanohydroxyapatite (nHA), fibrin, and chitosan are components that might be covalently incorporated into the polymer surface [56–61]. Chen et al. [62] treated PLLA nanofibers with oxygen plasma to expose –COOH groups on the surface and subsequently, by covalent grafting, cationized gelatin was incorporated into the fiber's surface using an appropriate coupling agent (carbodiimide). After combining these two methods, the hydrophilicity of the surface significantly improved with the contact angle decreasing from 135 to 15° after PLLA functionalization. Gelatin grafting to the PLLA fibers also slightly changed the fiber morphology; they became rougher because of gelatin adhesion to the fibers. This change in the scaffold morphology occurred to be beneficial for chondrocytes, which spread not only on the surface of the modified fibers but also attached to the inner areas of the material' structure. The MTS cell viability assay also confirmed that the modified surface created a more preferred environment for ECM production and chondrocytes proliferation even after 28 days [62]. Hesari et al. [51] incorporated plasma treatment with covalent grafting of gelatin to modify a PU scaffold. The surface was activated with oxygen plasma, and then gelatin macromolecules were incorporated into the surface. Combining these two methods did not significantly change the fibers' microstructure, but improved hydrophilicity, through an increase of $–NH_2$ and –COOH groups on the surface. Additionally, incorporated biomacromolecules influenced L929 fibroblasts' behavior in the MTT assay after 7 days. Functionalized surface increased cytocompatibility of the material, improved fibroblasts spreading, and their proliferation ratio. Generally, grafting of reagents, such as gelatin, changes the microstructure of the fiber mat and increases the average pore size, which might be good from the cells' perspective. On the other hand, it significantly impairs the mechanical properties of the material. Another thing is that gelatin increases the hydrolytic degradation rate, which might be favorable unless the process might be controlled [51]. On the other hand, surface graft polymerization usually requires plasma initiation to generate free radicals. Hence, conditions of the reaction have to be thoroughly controlled, otherwise undesirable side effects such as bulk properties deterioration, pore-blocking or collapsing, and fibers' degradation [28] may take place.

2.2. Physically/Chemically Functionalized Fibers

Plasma Treatment

Plasma treatment is a particular type of hydrophilic surface functionalization. It is usually categorized in the literature as a physical hydrophilic functionalization method [63,64]. However, plasma treatment results in significant chemical changes on the polymers surface such as chemical bonds breaking, leading to the introduction of various chemical groups like –OH, –COOH, CHO–, NH2–, –COO–, and reactive radicals, such as –COO (Figure 2) [65]. According to this, it could be classified as chemical functionalization [66]. Plasma treatment affects the surface energy of polymers and improves the wettability of the surface by changing their polarity. Type of the plasma source, time, and pressure are the main parameters controlling the functionalization process [23,26]. The method allows one to modify PGA, PLLA, PLGA, PCL, PEO, PVDF, PU, or polyaniline (PANI) electrospun mats, by forming appropriate functional groups such as –COOH on the modified surface as an effect of plasma glow discharge with O_2 and $C_3H_4O_2$ in the gaseous form [26,67–69]. Plasma (ionized gas) generates free radicals on the surface, which can behave similarly to polar groups [23]. Therefore, the following types of sources can be distinguished: argon, oxygen, methane [64–70], ammonia/helium, nitrogen, or air [19]. The plasma source might significantly influence the surface wettability, introducing different functional groups, which affect the immobilization of bioactive molecules on the treated surface. Asadian et al. [19] modified PCL fibers using various plasma sources such as oxygen, argon, ammonia/helium, or nitrogen showing a significant decrease in the contact angle from 135 before functionalization to 35° after

argon plasma, to 24° after nitrogen plasma, and to 13° after He/NH_2 plasma. The MTT assay on human foreskin fibroblasts (HFFs) revealed the significance of the discharged gas type on the cell viability. After 1 and 7 days of the cell culture, the number of viable cells was the highest for the argon plasma-treated samples and the lowest for the He/NH_3 plasma-treated samples. It was explained as a result of the presence of O_2-containing groups, which influenced more the cellular interaction than nitrogen functional groups after He/NH_3 plasma functionalization.

Table 1. Comparison of chemical methods of hydrophilic functionalization of electrospun nanofibers.

Chemical Method	Mechanism	Advantages	Disadvantages
Aminolysis	Splitting of polymer chains by reacting with-NH_2 groups and resulting introduction of active -NH_2 and -OH on the surface, which may further be explored in secondary reactions to incorporate other functional groups [6,31]	• short time of functionalization [6] • increased roughness of the surface [6] • non-toxicity of -NH_2 groups in direct contact with cells, resulting in increased cells adhesion [33,34]	• deep functionalization of the surface • requires precise control of the conditions of the reaction [31] • possible molecular degradation of polymer chains leading to mechanical weakness • high crystallinity of the polyester limits effective modification [6] • instability of amine groups on the surface at temperatures above Tg, especially when Tg is below physiological conditions [6] • use of harsh chemicals making this method not ecofriendly
Hydrolysis	Cleavage of chemical bonds in polymeric chains by water molecules resulting in OH and COOH formation on the modified surface	• a short time of functionalization • increased roughness of the surface	• deep and permanent functionalization of the surface • requires precise control of the conditions • possible molecular degradation of polymer chain leading to mechanical weakness • use of harsh chemicals making this method not ecofriendly
Covalent grafting	Chemical functionalization of the polymer backbone to introduce reactive functional groups on the surface [47,48]	• increase of average pore size resulting in better cell infiltration into the scaffold [51]	• increase of average pore size resulting in a decrease in mechanical properties [51] • requires precise control of functionalization time [28] • uncontrolled hydrolytic degradation after biomolecules grafting [51] • surface needs to be activated with plasma [51] • biomolecules grafting might change the fibers microstructure

Plasma treatment carries many advantages: it is ecofriendly and does not change bulk properties and hence mechanical properties of the fibers [71–73]. Compared to all chemical and physical hydrophilic functionalization methods, plasma treatment is the fastest method of surface functionalization and usually lasts from few seconds to few minutes [71]. Apart from all these advantages, plasma treatment effectively increases the hydrophilicity of hydrophobic polyesters modifying only the top of the fibers' surface without affecting the fiber layers beneath. In the case of PLLA nanofibers modification using O_2 plasma, Kooshki et al. [74] showed effective surface functionalization with –COOH and –OH groups resulting in a reduction of the contact angle from 135° to nearly zero [74]. Additionally, in vitro tests showed more significant mesenchymal stem cells (MSCs) attachment to the polymer surface and their enhanced proliferation in the MTT assay after 7 days.

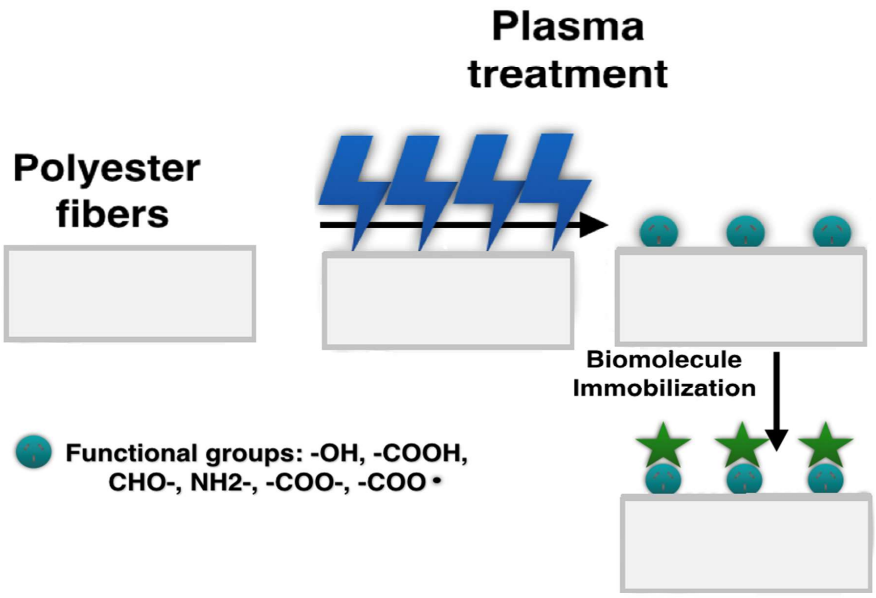

Figure 2. Plasma treatment of electrospun nanofibers.

Despite many advantages, plasma treatment has some disadvantages. Plasma does not affect the whole surface of the fibers, leaving some unmodified areas [28,31]. The method requires an appropriate plasma source and precise control of the modification time. Otherwise, the treatment might be ineffective or the morphology of fiber mats might be changed, even completely destroyed [75]. In some publications, it has been reported that plasma treatment might also worsen the mechanical properties of electrospun nanofibers [76]. Dolci et al., using atmospheric plasma for the PLLA nanofibrous scaffolds modification, observed the water contact angle reduction from 120 to 20°, and a drop in Young modulus from 86 ± 13 to 64 ± 8 MPa. Another limitation of this method is impermanence of the hydrophilic effect after functionalization, which fades away with time [77]. The reason is probably thermodynamic: a metastable system at a high free energy state proceeding towards a thermodynamically more stable state with lower free energy, which manifests in surface restructuring or so-called "surface aging" [78]. In effect, functional groups (polar groups) rearrange on the modified surface after being stored at room temperature. It was reported that storage conditions, type of polymer, and plasma treatment parameters significantly influence the stability of polar groups on the modified surface [79–82].

In order to prevent surface restructuring and extend the effect of plasma treatment, Wavhal et al. [83] recommend post-plasma grafting of acrylic acid (AA). This treatment allows for keeping hydrophilic groups on the polyethersulfone (PES) surface in an unchanged form for 2 months.

Undoubtedly, plasma treatment is a great method for surface activation; thereby, it is usually combined with other more permanent surface functionalization methods. Ghorbani et al. [69] activated the surface of PU-PANI scaffolds for bone regeneration with the use of oxygen plasma. The following step was PVA and PVA/3-glycidoxypropyltrimethoxysilane (GPTMS) immobilization to the activated surface. PVA immobilization allowed one to increase biocompatibility and amount of hydrophilic groups on the surface, while GPTMS provided better precipitation of hydroxyapatite and hence better osteoblasts adhesion to the modified surface. Atomic force microscopy (AFM) showed that after plasma treatment the degree of surface roughness increased from c.a. 97 to 144–429 nm. The waterdrop contact angle measurements showed a decrease from 116 for pure PU/PANI to 65° after plasma functionalization and to 62° after additional PVA/GPTMS immobilization, respectively. In vitro studies, using an MTT assay on MG-63 osteoblastoma cells, confirmed increased adhesion and proliferation of the cells on the functionalized surface after 7 days.

More examples of combining plasma treatment with other functionalization methods were described in the paragraph of covalent grafting and are discussed below.

2.3. *Physically Functionalized Fibers by Physical Adsorption*

Physical hydrophilic functionalization is an alternative to chemical methods and plasma surface functionalization (Figure 3). It allows overcoming some limitations of chemical methods. They do not change the bulk properties and therefore, mechanical properties, the process does not have to be precisely controlled: there are no risks of hydrolytic degradation, it does not require toxic solvents, which makes the method ecofriendly [84].

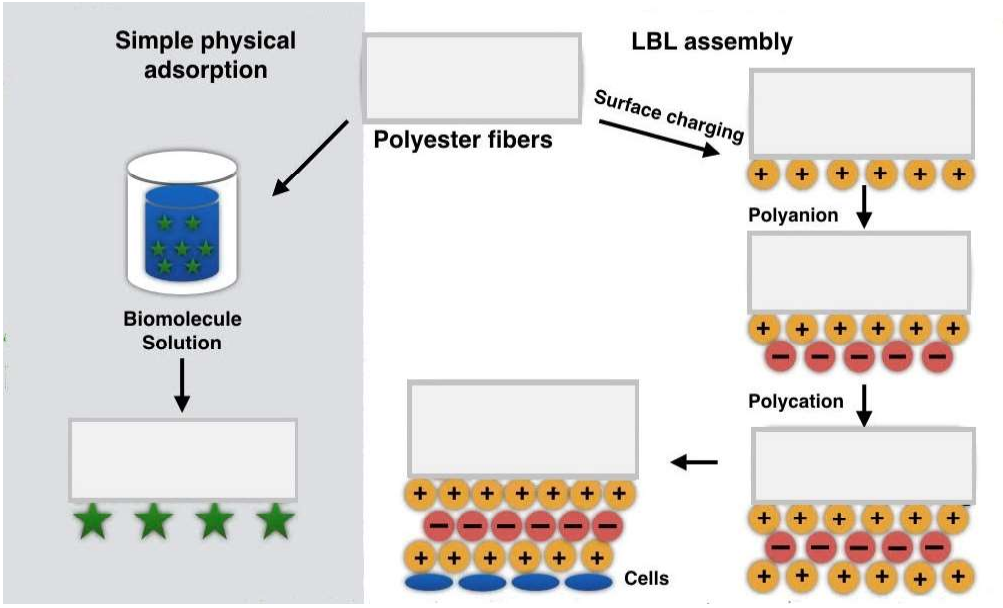

Figure 3. Physical functionalization of electrospun nanofibers.

On the other hand, hydrophilic functionalization is based on forming the whole spectrum of physical interactions such as hydrophobic or electrostatic interactions, which usually are unstable and impermanent [24]. Moreover, physical methods might adversely affect the fibers morphology [85].

The most popular physical methods of hydrophilic surface functionalization are discussed in the following sections. Table 2 summarizes the main advantages and drawbacks of the physical surface functionalization methods on electrospun nanofibers.

2.3.1. Simple Physical Adsorption

Physical adsorption is an uncomplicated method of hydrophilic and biological functionalization of electrospun nanofibers. The method assumes spraying or soaking of nanofibers in a biomolecules solution [24]. As a consequence of electrostatic, hydrogen, hydrophobic, and van der Waals interactions, biomolecules can adhere to the surface of the fibers [26,86]. Physical adsorption works for most nanofibrous polymers used in electrospinning such as PLGA, PEO, PLLA, poly (vinyl pyrrolidone)-iodine (PVPI), PCL, and PVA [87–90]. The most popular biomolecules adsorbed on the surface of the fibers are usually proteins, enzymes, polysaccharides, antibacterial agents, growth factors, or vitamins [24,26,91–93].

This kind of functionalization improves cell capability to recognize the surface receptors and increases their attachment to the modified surface without changing the bulk properties of the material scaffold [85]. Compared to chemical methods, or blending, physical adsorption protects biomolecules from denaturation in the presence of a harmful environment of organic solvents, high temperature,

or high voltage during the electrospinning process [94]. Moreover, physical adsorption seems to be a simple method providing fast immobilization of the biomolecules to the nanofibers' surface [89]. Nevertheless, some viscous bioactive agents such as hydrogels could change the fibers morphology significantly. Viscous solutions might fill most of the pores in the electrospun mats, blocking its availability for the cells. Esfahani et al. [85] modified polyamide-6 (PA6)/hydroxyapatite (HA) electrospun nanofibers with vitamin VD3 to enhance bone regeneration. Immersion in VD3 solution resulted in a dramatic increase in the fibers' thickness, changes in fibers' morphology, and blocking of pores after 1 h of immersion.

Another limitation of this kind of functionalization is impermanence since physical binding might be easily washed off the surface by polar solvents or the cell culture medium [24,95]. To extend the effectiveness of this method, resulting in enhanced cell affinity to the surface, it is necessary to combine two methods of surface functionalization. Yang et al. [24] conjugated plasma treatment and physical adsorption. PLLA samples were divided into modified with plasma and unmodified. Unmodified samples were directly soaked in collagen solution for 2 h, while modified samples were pretreated with ammonia plasma, followed by coating with collagen. The best effect has been seen while collagen adsorption was combined with plasma treatment. It increased the hydrophilicity of the fiber's surface through the increased amount of –OH, –COOH, and $–NH_2$ groups on the surface. It also facilitated collagen adsorption by forming of a strong polar interaction and hydrogen bonds between collagen and polar groups on the pretreated surface [24]. Conjugation of both functionalization methods increased affinity of 3T3 fibroblasts to the PDLA surface after 4 days, compared to the plasma-untreated fibers. In another paper, Jankowska et al. [96] modified poly (methyl methacrylate)/polyaniline PMMA/PANI with laccase enzyme by combining both adsorption and covalent binding methods to obtain potential membranes for separation processes or artificial scaffolds for medical applications. The first step of functionalization was the coupling reaction between 1-ethyl-3-[3-dimethylaminopropyl] carbodiimide hydrochloride/N-hydroxysuccinimide (EDC/NHS) and the PMMA/PANI surface. The second step was the physical adsorption of laccase. X-ray surface composition microanalysis confirmed that after combining covalent binding physical adsorption, the amount of oxygen, sulfur, chlorine, fluorine, and nitrogen increased significantly in comparison to the sample before surface functionalization. It was visible, especially in the content of sulfur and nitrogen, which increased almost twice after laccase binding.

2.3.2. LBL Assembly

The LBL technique is a specific type of physical adsorption, which works on the principle of adsorption of oppositely charged polymers. By alternate deposition of opposite charge layers, it is possible to create self-assembled coating and obtain the desired properties of the composite material [26]. LBL was used for hydrophilic functionalization of PLLA, polyacrylonitrile (PAN), PLGA, PNIPAM, PCL, or PCL/silk fibroins [97–103]. LBL usually allows creation of layers made of polyelectrolytes, mainly natural materials such as proteins or polysaccharides. The layers might be positively or negatively charged depending on the conditions in the solution, for instant, by choice of pH [101]. In studies conducted by Li et al. [25], heparin (Hep) and chitosan (Cs) were adsorbed on the PCL/silk fibroin (SF) nanofibers as scaffolds for treatment of cardiovascular diseases. The first layer was made of positively charged Cs. The second layer was made of Hep, in which charge was changed to negative by adjusting pH of the solution. Strong layers adhesion was a consequence of electrostatic binding between Cs and Hep. Cs provided antibacterial properties, while Hep improved protein activity and stimulated the release of anticoagulant and fibrinolytic substances from vascular endothelial cells. The Alamar blue test confirmed good biocompatibility and improved cell proliferation of modified PCL/SF scaffold. It was also demonstrated, that after LBL, human umbilical vein endothelial cells (HUVEC) showed improved adhesion and proliferation on the modified surface after 48 h. The antibacterial test showed that adsorbed layers reduced infectivity with *Escherichia coli* and *Staphylococcus aureus* up to 95% [25]. In another study, Zhang et al. [102] deposited two layers:

the self-assembling peptide (SAP) and RGD sequences on PCL nanofibers for neural tissue engineering applications. Adhesion between the first SAP layer and PCL surface was a consequence of strong hydrophobic interactions. Plasmid DNA (pDNA) complexes were used as a delivery system of the CRISPR/dCas9 gene expression control system and with positively charged SAP and negatively charged RGD was adsorbed as a consequence of electrostatic interactions. Deposited layers provided sustained release of pDNA, enhanced cell adhesion, and proliferation of human mesenchymal stem cells (hMSCs) and human neural progenitor cells (hNPCs) in Quant-iTPicoGreen dsDNA assay and Click-iTEdU cell proliferation assay after 7 days of culturing. Using this method for nanofibers functionalization also occurred to be a useful tool for non-viral genome editing.

LBL shows many advantages, one of them is that it does not change the bulk properties of nanofibers [103]. From the processing point of view, LBL is easy to conduct, universal for covering various even complex structures, and a wide range of charged substrates might be used in this technique [26]. Similarly to the physical adsorption, deposited biomolecules are protected from denaturation, avoiding the loss of provided functions [104].

The main limitation of this method is that both modified fibers surface and deposited layers always need to be charged. For this reason, before LBL functionalization, the surface has to be prepared by providing an appropriate charge. Chemical methods such as aminolysis, sulfonation of phenyl groups (if they are present in the polyester material), and alkaline hydrolysis are examples of methods providing an appropriate charge on the surface before LBL treatment [97,98,105]. Wang et al. [106] functionalized the surface of PCL aligned fibers through grafting amino groups with the use of polyethyleneimine (PEI) for 36 h. The next step was the LBL deposition of nanocoatings made of antibacterial drug poly-L-lysine (PLL) encapsulated in gelatin and heparin. According to FTIR analysis, deposited layers showed effective adhesion to the polymers surface as a consequence of electrostatic interactions, where the gelatin –COOH groups bound strongly with the PLL $–NH_3$ groups. Additionally, there were electrostatic interactions between the heparin –COOH groups and the PLL $–NH_3$ groups, and between heparin and gelatin. LBL coating, especially gelatin, was crosslinked with genipin (GNP), and at the end, MMP2 enzyme was adsorbed on the layers in order to induce the controlled release of PLL. SEM images showed that after GNP crosslinking, the fibers lost their morphology, and GNP presence most likely blocked the action of the enzyme through an uncoupling protein and reaction with free amino groups. Cell proliferation CCK-8 assay on HUVEC showed significant improvement in the cells amount on the scaffold after functionalization after 3 and 5 days. However, it was demonstrated that the layer of Gelatin/PLL had the greatest influence on the increased cell affinity to the surface. It was an effect of the presence of bioactive polypeptides of gelatin and positive charge of PLL, which promoted HUVECs increased attachment and proliferation [106].

Table 2. Comparison of electrospun nanofibers physical hydrophilic functionalization methods [24,26,85,93,97,98,104,106].

Physical Method	Mechanism	Advantages	Disadvantages
Simple physical adsorption	Weak physical interactions such as hydrophobic interactions, hydrogen bonds, van der Waals interactions [24,26]	• does not change bulk properties of the polymer [93] • protects biomolecules from challenging environment • simple, universal	• might change fibers morphology, for instance increases fibers thickness or clogs the pores [85] • impermanent [24]
LBL	Electrostatic interactions as an effect of alternate embedding of oppositely charged substances [26]	• does not change the bulk properties of polymer • protects biomolecules from a challenging environment [104] • simple, universal [26]	• only charged substances might be used [98,106] • modified surface needs to be charged, or previously pre-treated to deposit charge on the surface [97]

3. Tissue Engineering Applications of Functionalized Polymer Nanofibers

Electrospun nanofibrous scaffolds possess many interesting properties for tissue engineering applications, such as high surface area, and morphology, which fairly mimic ECM. Native ECM is responsible for the stimulation of cellular mobility and further migration. An appropriate interaction between fibrous ECM and the cellular cytoskeleton leads to improved cell mobility. Cells' ability to recreate their own ECM is crucial for effective tissue regeneration [107]. However, besides appropriate morphology, the perfect scaffold should also have appropriate biochemical cues, which might be obtained by surface chemistry modification. Electrospun nanofibers made of aliphatic polyesters show relatively poor hydrophilicity, and consequently, low biocompatibility [108]. Such materials without surface functionalization do not have functional groups, which might be recognized by cell-binding receptors increasing cell-scaffold adhesion.

An increase in hydrophilicity of electrospun membranes is the first step before immobilization of biomacromolecules such as proteins or growth factors, providing stable anchor points for the cells. The cells in contact with the scaffold need to feel materials surface biochemistry, which might promote cell-signaling pathways. One of the positive effects of biologically functionalized material is guiding the transcription factors responsible for the cell's fate and regulation of their differentiation [13]. Surface modification with a protein, such as gelatin, which is extensively involved in building of ECM, not only increases hydrophilicity but also mostly gives a cellular response. It is a result of the recognition of bioactive ligands of RGDsequences by integrins.

Another protein containing RGD sequences is silk fibroin [109]. Bhattacharjee et al. aminolyzed PCL nanofibers and activated the functional groups on the surface with GA, with subsequent silk fibroin immobilization. MTT viability assay and Alamar blue proliferation assay on osteoblast-like MG 63 cells showed not only increased cell growth and adhesion to the functionalized surface (Figure 4), but the cells were also able to create the native ECM, leading to bone tissue regeneration. Similarly to these studies, a different bioactive protein—collagen was immobilized to PCL fibers previously functionalized by aminolysis [110]. Biological tests on NIH 3T3 fibroblasts showed not only increased proliferation on functionalized scaffolds but also enhanced infiltration inside the scaffolds. An increase in cell proliferation was explained as a result of collagen presence, while enhanced infiltration most likely as a result of increased hydrophilicity, which influenced significantly cell–scaffold interactions.

The same method has been also proven in the case of scaffolds for neural regeneration. Amores et al. [111] used laminin and RGD-containing peptide GRGDSP as the immobilized biomolecules to the PCL scaffold. Proliferation tests using neural stem cells showed increased cells' density on the functionalized scaffolds due to good access of the cell integrin receptor to the laminin and RGD sequences on the scaffolds surface. Most importantly, neural stem cells were able to differentiate into neurons and astrocytes showing enhanced neurons alignment on the functionalized material. These examples have proven that proper scaffold morphology or mechanical properties alone are not sufficient for effective tissue regeneration. More challenging tissues, such as neural, seem to need a more sophisticated approach, such as hydrophilic functionalization followed by biological groups incorporation.

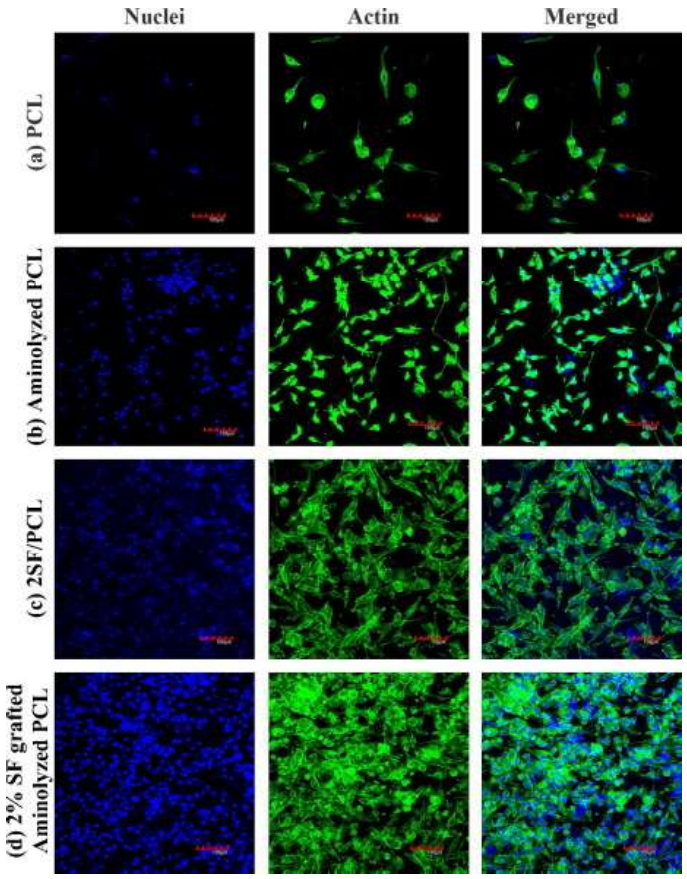

Figure 4. The cytoskeletal actin organization and distribution of MG-63 cells grown on (**a**) unmodified PCL nanofibers, (**b**) PCL after aminolysis, (**c**) PCL blended with silk fibroin (SF), and (**d**) aminolyzed PCL after subsequent SF immobilization at day-point 7. Reprinted from *Eur. Polym. J.* 2015, 71, 490–509 with permission from Elsevier [109].

4. Conclusions and Future Perspectives

The review discusses current methods used for hydrophilic surface functionalization of electrospun nanofibers targeting medical applications. Surfaces of nanofibrous mats can be functionalized with wet chemical methods, covalent grafting, plasma treatment, and physical methods based on physical adsorption. It may be concluded that a single hydrophilic functionalization method results in serious limitations, thus, an alternative approach is required. It may be expected that future strategies would be a combination of two or even more hydrophilic functionalization methods, at least one being chemical, for instance, covalent grafting, aminolysis, or oxygen plasma followed by physical LBL assembly. For instance, a combination of aminolysis, or hydrolysis with biomolecules immobilization, not only improves hydrophilicity of the surface but also significantly increases aliphatic polyester scaffolds biocompatibility. Both hydrophilicity and biomolecules incorporation are emerging important issues in tissue engineering applications. The most effective functionalization methods, ultimately, should provide sufficient surface biological activity, integrity, and mechanical properties of the scaffold. Future strategies might also include additional specific benefits for defined applications, for instance, electrical conductivity in scaffolds devoted to neural tissue engineering.

Future strategies combining more than one functionalization method are foreseen as highly important for further development of electrospun nanofibers for tissue engineering applications. We believe that combining and developing of hydrophilic functionalization methods will widely use functionalized electrospun nanofibers in clinical applications, and this is only a question of time.

Author Contributions: Conceptualization, B.N.-S.; validation, B.N.-S., A.G. and P.S.; writing—original draft preparation, B.N.-S.; writing, review and editing, B.N.-S., A.G. and P.S., visualization, B.N.-S., A.G. and P.S.; supervision, P.S. and A.G.; project administration P.S., A.G. and B.N.-S.; funding acquisition, B.N.-S. All authors have read and agreed to the published version of the manuscript.

Funding: This research was funded by the Narodowe Centrum Nauki (NCN), grant number 2018/29/N/ST8/00780. The Article Processing Charge (APC) was covered by the Project no. POWR.03.02.00-00-1028/17-00 implemented under the Operational Program Knowledge Education Development 2014–2020, cofinanced by the European Social Fund.

Conflicts of Interest: The authors declare no conflict of interest.

References

1. Carvalho, J.; Carvalho, P.; Gomes, D.; Goes, A. Chapter 11—Innovative Strategies for Tissue Engineering. In *Advances in Biomaterials Science and Biomedical Application*; Pignatello, R., Ed.; IntechOpen: London, UK, 2013; pp. 295–313.
2. Niemczyk, B.; Sajkiewicz, P.; Kołbuk, D. Injectable hydrogels as novel materials for central nervous system regeneration. *J. Neural Eng.* **2018**, *15*, 051002. [CrossRef] [PubMed]
3. Liu, J.; Chen, H.; Wang, Y.; Li, G.; Zheng, Z.; Kaplan, D.L.; Wang, X. Flexible Water-Absorbing Silk-Fibroin Biomaterial Sponges with Unique Pore Structure for Tissue Engineering. *ACS Biomater. Sci. Eng.* **2020**, *6*, 1641–1649. [CrossRef]
4. Kołbuk, D.; Heljak, M.; Choińska, E.; Urbanek, O. Novel 3D hybrid nanofiber scaffolds for bone regeneration. *Polymers* **2020**, *12*, 544. [CrossRef] [PubMed]
5. Kołbuk, D.; Urbanek, O.; Denis, P.; Choińska, E. Sonochemical coating as an effective method of polymeric nonwovens functionalization. *J. Biomed. Mater. Res. A* **2019**, *107*, 2447–2457. [CrossRef] [PubMed]
6. Jeznach, O.; Kołbuk, D.; Sajkiewicz, P. Aminolysis of various aliphatic polyesters in a form of nanofibers and films. *Polymers* **2019**, *11*, 1669. [CrossRef] [PubMed]
7. Arbade, G.K.; Srivastava, J.; Tripathi, V.; Lenka, N.; Patro, T.U. Enhancement of hydrophilicity, biocompatibility and biodegradability of poly(ε-caprolactone) electrospun nanofiber scaffolds using poly(ethylene glycol) and poly(L-lactide-co-ε-caprolactone-co-glycolide) as additives for soft tissue engineering. *J. Biomater. Sci.* **2020**, 1–17, just-accepted.
8. Wang, D.; Xu, Y.; Li, Q.; Turng, L.-S. Artificial Small-Diameter Blood Vessels: Materials, Fabrication, Surface Modification, Mechanical Properties, and Bioactive Functionalities. *J. Mater. Chem. B.* **2020**, *8*, 1801–1822. [CrossRef]
9. Cegielska, O.; Sajkiewicz, P. Targeted drug delivery systems for the treatment of glaucoma: Most advanced systems review. *Polymers* **2019**, *11*, 1742. [CrossRef]
10. Zaszczynska, A.; Sajkiewicz, P.; Gradys, A. Piezoelectric Scaffolds as Smart Materials for Neural Tissue Engineering. *Polymers* **2020**, *12*, 161. [CrossRef]
11. Denis, P.; Wrzecionek, M.; Gadomska-Gajadhur, A.; Sajkiewicz, P. Poly(glycerol sebacate)–poly(l-lactide) nonwovens. Towards attractive electrospun material for tissue engineering. *Polymers* **2019**, *11*, 2113. [CrossRef]
12. Guo, X.; Xia, B.; Lu, X.B.; Zhang, Z.J.; Li, Z.; Li, W.L.; Huang, Y.C. Grafting of mesenchymal stem cell-seeded small intestinal submucosa to repair the deep partial-thickness burns. *Connect. Tissue Res.* **2016**, *57*, 388–397. [CrossRef] [PubMed]
13. Dulnik, J.; Denis, P.; Sajkiewicz, P.; Kołbuk, D.; Choińska, E. Biodegradation of bicomponent PCL/gelatin and PCL/collagen nanofibers electrospun from alternative solvent system. *Polym. Degrad. Stab.* **2016**, *130*, 10–21. [CrossRef]
14. Wei, Z.; Gu, J.; Ye, Y.; Fang, M.; Lang, J.; Yang, D.; Pan, Z. Biodegradable poly (butylene succinate) nanofibrous membrane treated with oxygen plasma for superhydrophilicity. *Surf. Coat. Technol.* **2020**, *381*, 125147. [CrossRef]
15. Webb, K.; Hlady, V.; Tresco, P.A. Relative importance of surface wettability and charged functional groups on NIH 3T3 fibroblast attachment, spreading, and cytoskeletal organization. *J. Biomed. Mater. Res.* **1998**, *41*, 422–430. [CrossRef]
16. Ikada, Y. Surface modification of polymers for medical applications. *Biomaterials* **1994**, *15*, 725–736. [CrossRef]

17. Ruoslahti, E. RGD and other recognition sequences for integrins. *Annu. Rev. Cell Dev. Biol.* **1996**, *12*, 697–771. [CrossRef] [PubMed]
18. Bellis, S.L. Advantages of RGD peptides for directing cell association with biomaterials. *Biomaterials* **2011**, *32*, 4205–4210. [CrossRef]
19. Asadian, M.; Dhaenens, M.; Onyshchenko, I.; De Waele, S.; Declercq, H.; Cools, P.; De Geyter, N. Plasma functionalization of PCL nanofibers changes protein interactions with cells resulting in increased cell viability. *ACS Appl. Mater. Interfaces* **2018**, *10*, 41962–41977. [CrossRef]
20. Dulnik, J.; Kołbuk, D.; Denis, P.; Sajkiewicz, P. The effect of a solvent on cellular response to PCL/gelatin and PCL/collagen electrospun nanofibres. *Eur. Polym. J.* **2018**, *104*, 147–156. [CrossRef]
21. Zhu, Y.; Gao, C.; Liu, X.; Shen, J. Surface modification of polycaprolactone membrane via aminolysis and biomacromolecule immobilization for promoting cytocompatibility of human endothelial cells. *Biomacromolecules* **2002**, *3*, 1312–1319. [CrossRef]
22. You, X.; Piao, C.; Chen, L. Preparation of a magnetic molecularly imprinted polymer by atom-transfer radical polymerization for the extraction of parabens from fruit juices. *J. Sep. Sci.* **2016**, *39*, 2831–2838. [CrossRef] [PubMed]
23. Alves, P.; Pinto, S.; de Sousa, H.C.; Gil, M.H. Surface modification of a thermoplastic polyurethane by low-pressure plasma treatment to improve hydrophilicity. *J. Appl. Polym. Sci.* **2011**, *122*, 2302–2308. [CrossRef]
24. Yang, J.; Bei, J.; Wang, S. Enhanced cell affinity of poly (d,l-lactide) by combining plasma treatment with collagen anchorage. *Biomaterials* **2002**, *23*, 2607–2614. [CrossRef]
25. Li, L.; Wang, X.; Li, D.; Qin, J.; Zhang, M.; Wang, K.; Zhao, J.; Zhang, L. LBL deposition of chitosan/heparin bilayers for improving biological ability and reducing infection of nanofibers. *Int. J. Biol. Macromol.* **2020**, *154*, 999–1006. [CrossRef]
26. Yoo, H.S.; Kim, T.G.; Park, T.G. Surface-functionalized electrospun nanofibers for tissue engineering and drug delivery. *Adv. Drug Deliv. Rev.* **2009**, *61*, 1033–1042. [CrossRef]
27. Holmes, C.; Tabrizian, M. Surface functionalization of biomaterials. In *Stem Cell Biology and Tissue Engineering in Dental Sciences*; Vishwakarma, A., Sharpe, P., Shi, S., Ramalingam, M., Eds.; Elsevier BV: Amsterdam, The Netherlands, 2015; pp. 187–206.
28. Huang, L.; Arena, J.T.; McCutcheon, J.R. Surface modified PVDF nanofiber supported thin film composite membranes for forward osmosis. *J. Membr. Sci.* **2016**, *499*, 352–360. [CrossRef]
29. Upadhyay, R.K.; Waghmare, P.R. Eco-friendly preparation of superhydrophobic copper surfaces for oil/water separation. *Environ. Chem. Lett.* **2020**, *18*, 505–510. [CrossRef]
30. Haddad, T.; Noel, S.; Liberelle, B.; El Ayoubi, R.; Ajji, A.; De Crescenzo, G. Fabrication and surface modification of poly lactic acid (PLA) scaffolds with epidermal growth factor for neural tissue engineering. *Biomatter* **2016**, *6*, e1231276. [CrossRef]
31. Croll, T.I.; O'Connor, A.J.; Stevens, G.W.; Cooper-White, J.J. Controllable Surface Modification of Poly(lactic-co-glycolic acid) (PLGA) by Hydrolysis or Aminolysis I: Physical, Chemical, and Theoretical Aspects. *Biomacromolecules* **2004**, *5*, 463–473. [CrossRef]
32. Morillo, M.D.; Magdi, A.M.; Rodríguez, M.; García, M.; Faccini, M. Aminated Polyethylene Terephthalate (PET) Nanofibers for the Selective Removal of Pb(II) from Polluted Water. *Materials* **2017**, *10*, 1352. [CrossRef]
33. Zhu, Y.; Leong, M.; Ong, W.; Chanpark, M.; Chian, K. Esophageal epithelium regeneration on fibronectin grafted poly(l-lactide-co-caprolactone) (PLLC) nanofiber scaffold. *Biomaterials* **2007**, *28*, 861–868. [CrossRef] [PubMed]
34. Zhao, Y.; Tan, K.; Zhou, Y.; Ye, Z.; Tan, W.-S. A combinatorial variation in surface chemistry and pore size of three-dimensional porous poly(ε-caprolactone) scaffolds modulates the behaviors of mesenchymal stem cells. *Mater. Sci. Eng. C* **2016**, *59*, 193–202. [CrossRef] [PubMed]
35. Chastain, S.R.; Kundu, A.K.; Dhar, S.; Calvert, J.W.; Putnam, A.J. Adhesion of mesenchymal stem cells to polymer scaffolds occurs via distinct ECM ligands and controls their osteogenic differentiation. *J. Biomed. Mater. Res. A* **2006**, *78*, 73–85. [CrossRef] [PubMed]
36. Zhu, Y.; Gao, C.; Liu, X.; He, T.; Shen, J. Immobilization of biomacromolecules onto aminolyzed poly (L-lactic acid) toward acceleration of endothelium regeneration. *Tissue Eng.* **2004**, *10*, 53–61. [CrossRef] [PubMed]
37. Zhang, K.; Zheng, H.; Liang, S.; Gao, C. Aligned PLLA nanofibrous scaffolds coated with graphene oxide for promoting neural cell growth. *Acta Biomater.* **2016**, *37*, 131–142. [CrossRef] [PubMed]

38. Zhu, Y.; Mao, Z.; Gao, C. Aminolysis-based surface modification of polyesters for biomedical applications. *RSC Adv.* **2013**, *3*, 2509–2519. [CrossRef]
39. Boland, E.D.; Telemeco, T.A.; Simpson, D.G.; Wnek, G.E.; Bowlin, G.L. Utilizing acid pretreatment and electrospinning to improve biocompatibility of poly (glycolic acid) for tissue engineering. *J. Biomed. Mater. Res. B Biomater.* **2004**, *71*, 144–152. [CrossRef]
40. Lee, S.J.; Khang, G.; Lee, Y.M.; Lee, H.B. Interaction of human chondrocytes and NIH/3T3 fibroblasts on chloric acid-treated biodegradable polymer surfaces. *J. Biomater. Sci.* **2002**, *13*, 197–212. [CrossRef]
41. Kongdee, A.; Okubayashi, S.; Tabata, I.; Hori, T. Impregnation of silk sericin into polyester fibers using supercritical carbon dioxide. *J. Appl. Polym. Sci.* **2007**, *105*, 2091–2097. [CrossRef]
42. Spinella, S.; Re, G.L.; Liu, B.; Dorgan, J.; Habibi, Y.; Leclere, P.; Raquez, J.M.; Dubois, P.; Gross, R.A. Polylactide/cellulose nanocrystal nanocomposites: Efficient routes for nanofiber modification and effects of nanofiber chemistry on PLA reinforcement. *Polymer* **2015**, *65*, 9–17. [CrossRef]
43. Wang, Y.Q.; Cai, J.Y. Enhanced cell affinity of poly (L-lactic acid) modified by base hydrolysis: Wettability and surface roughness at nanometer scale. *Curr. Appl. Phy.* **2007**, *7*, e108–e111. [CrossRef]
44. Getnet, M.; Chavan, R. Catalyzation of alkaline hydrolysis of polyester by oxidizing agents for surface modification. *Int. J. Sci. Basic Appl. Res.* **2015**, *22*, 232.
45. Sadeghi, A.R.; Nokhasteh, S.; Molavi, A.M.; Khorsand-Ghayeni, M.; Naderi-Meshkin, H.; Mahdizadeh, A. Surface modification of electrospun PLGA scaffold with collagen for bioengineered skin substitutes. *Mater. Sci. Eng.* **2016**, *66*, 130–137. [CrossRef] [PubMed]
46. De Luca, A.C.; Terenghi, G.; Downes, S. Chemical surface modification of poly-ε-caprolactone improves Schwann cell proliferation for peripheral nerve repair. *J. Tissue Eng. Regen. M* **2012**, *8*, 153–163. [CrossRef] [PubMed]
47. Fu, G.D.; Lei, J.Y.; Yao, C.; Li, X.S.; Yao, F.; Nie, S.Z.; Kang, T.; Neoh, K.G. Core–Sheath Nanofibers from Combined Atom Transfer Radical Polymerization and Electrospinning. *Macromolecules* **2008**, *41*, 6854–6858. [CrossRef]
48. Fu, G.D.; Xu, L.Q.; Yao, F.; Zhang, K.; Wang, X.F.; Zhu, M.F.; Nie, S.Z. Smart Nanofibers from Combined Living Radical Polymerization, "Click Chemistry", and Electrospinning. *ACS Appl. Mater. Interfaces* **2009**, *1*, 239–243. [CrossRef]
49. Maffei, A.; Michieli, N.; Brun, P.; Zamuner, A.; Zaggia, A.; Roso, M.; Kalinic, B.; Falzacappa, E.; Scopece, P.; Gross, S.; et al. An atmospheric pressure plasma jet to tune the bioactive peptide coupling to polycaprolactone electrospun layers. *Appl. Surf. Sci.* **2020**, *507*, 144713. [CrossRef]
50. Minko, S. Grafting on Solid Surfaces: "Grafting to" and "Grafting from" Methods. In *Polymer Surfaces and Interfaces*; Springer: Berlin/Heidelberg, Germany, 2008; pp. 215–234.
51. Hesari, S.M.; Ghorbani, F.; Ghorbani, F.; Zamanian, A.; Khavandi, A. Plasma surface modification technique–induced gelatin grafting on bio-originated polyurethane porous matrix: Physicochemical and in vitro study. *Polym. Compos.* **2020**, *20*, 1–12. [CrossRef]
52. Sun, Y.; Du, H.; Deng, Y.; Lan, Y.; Feng, C. Preparation of polyacrylamide via surface-initiated electrochemical-mediated atom transfer radical polymerization (SI-eATRP) for Pb^{2+} sensing. *J. Solid State Electr.* **2016**, *20*, 105–113. [CrossRef]
53. Mushtaq, M.; Jindani, R.; Farooq, A.; Li, X.; Saba, H.; Wasim, M.; Siddiqui, Q. Characterization of electrospun polylactide nanofibers modified via atom transfer radical polymerization. *J. Ind. Text.* **2020**, 1–11. [CrossRef]
54. Matyjaszewski, K.; Tsarevsky, N.V. Macromolecular engineering by atom transfer radical polymerization. *J. Am. Chem. Soc.* **2014**, *136*, 6513–6533. [CrossRef]
55. Ma, Z.; Kotaki, M.; Ramakrishna, S. Surface modified nonwoven polysulphone (PSU) fiber mesh by electrospinning: A novel affinity membrane. *J. Membr. Sci.* **2006**, *272*, 179–187. [CrossRef]
56. Chen, J.P.; Chiang, Y.P. Surface modification of non-woven fabric by DC pulsed plasma treatment and graft polymerization with acrylic acid. *J. Membr. Sci.* **2006**, *270*, 212–220. [CrossRef]
57. Ding, Z. Immobilization of chitosan onto poly-?-lactic acid film surface by plasma graft polymerization to control the morphology of fibroblast and liver cells. *Biomaterials* **2004**, *25*, 1059–1067. [CrossRef]
58. Sadeghzade, N.; Nouri, M.; Nateri, A.S. Evaluating Osteogenic Differentiation of Mesenchymal Stem Cells on Poly (caprolactone) Electrospun Scaffolds by Image Processing Techniques. *Bionanoscience* **2020**, *10*, 381–388. [CrossRef]

59. Toledo, A.L.M.M.; Ramalho, B.S.; Picciani, P.H.S.; Baptista, L.S.; Martinez, A.M.B.; Dias, M.L. Effect of three different amines on the surface properties of electrospun polycaprolactone mats. *Int. J. Polym. Mater.* **2020**, 1–13. [CrossRef]
60. Wu, C.A. Comparison of the Structure, Thermal Properties, and Biodegradability of Polycaprolactone/Chitosan and Acrylic Acid Grafted Polycaprolactone/Chitosan. *Polymer* **2005**, *46*, 147–155. [CrossRef]
61. Chen, J.-P.; Li, S.-F.; Chiang, Y.-P. Bioactive Collagen-Grafted Poly-L-Lactic Acid Nanofibrous Membrane for Cartilage Tissue Engineering. *J. Nanosci. Nanotechnol.* **2010**, *10*, 5393–5398. [CrossRef]
62. Chen, J.P.; Su, C.H. Surface modification of electrospun PLLA nanofibers by plasma treatment and cationized gelatin immobilization for cartilage tissue engineering. *Acta Biomater.* **2011**, *20117*, 234–243. [CrossRef]
63. Singh, M.; Vajpayee, M.; Ledwani, L. Eco-friendly Surface Modification and Nanofinishing of Textile Polymers to Enhance Functionalisation. In *Nanotechnology for Energy and Environmental Engineering*; Ledwani, L., Sangwai, J., Eds.; Springer: Cham, Switzerland, 2020; pp. 529–559.
64. Pashkuleva, I.; Marques, A.P.; Vaz, F.; Reis, R.L. Surface modification of starch based biomaterials by oxygen plasma or UV-irradiation. *J. Mater. Sci. Mater. Med.* **2010**, *21*, 21–32. [CrossRef]
65. Dorai, R.; Kushner, M.J. A model for plasma modification of polypropylene using atmospheric pressure discharges. *J. Phys. D Appl. Phys.* **2003**, *36*, 666. [CrossRef]
66. Yang, F.; Wolke, J.G.C.; Jansen, J.A. Biomimetic calcium phosphate coating on electrospun poly(ε-caprolactone) scaffolds for bone tissue engineering. *Chem. Eng. J.* **2008**, *137*, 154–161. [CrossRef]
67. Fasano, V.; Laurita, R.; Moffa, M.; Gualandi, C.; Colombo, V.; Gherardi, M.; Focarete, M.L. Enhanced electrospinning of active organic fibers by plasma treatment on conjugated polymer solutions. *ACS Appl. Mater. Interfaces* **2020**, *12*, 26320–26329. [CrossRef] [PubMed]
68. Kupka, V.; Dvořáková, E.; Manakhov, A.; Michlíček, M.; Petruš, J.; Vojtová, L.; Zajíčková, L. Well-blended PCL/PEO electrospun nanofibers with functional properties enhanced by plasma processing. *Polymers* **2020**, *12*, 1403. [CrossRef] [PubMed]
69. Ghorbani, F.; Zamanian, A.; Aidun, A. Conductive electrospun polyurethane-polyaniline scaffolds coated with poly (vinyl alcohol)-GPTMS under oxygen plasma surface modification. *Mater. Today Commun.* **2020**, *22*, 100752. [CrossRef]
70. Min, B.M.; Jeong, L.; Yeo, I.S.; Kim, H.N.; Yoon, Y.I.; Jang, D.H.; Park, W.H. Plasma-treated silk fibroin nanofibers for skin regeneration. *Int. J. Biol. Macromol.* **2009**, *44*, 222–228.
71. Occhiello, E.; Morra, M.; Morini, G.; Garbassi, F.; Humphrey, P. Oxygen-plasma-treated polypropylene interfaces with air, water, and epoxy resins: Part I. Air and water. *J. Appl. Polym. Sci.* **1991**, *42*, 551–559. [CrossRef]
72. Park, K.; Ju, Y.M.; Son, J.S.; Ahn, K.D.; Han, D.K. Surface modification of biodegradable electrospun nanofiber scaffolds and their interaction with fibroblasts. *J. Biomater. Sci.* **2007**, *18*, 369–382. [CrossRef]
73. Nisticò, R.; Magnacca, G.; Faga, M.G.; Gautier, G.; D'Angelo, D.; Ciancio, E.; Martorana, S. Effect of atmospheric oxidative plasma treatments on polypropylenic fibers surface: Characterization and reaction mechanisms. *Appl. Surf. Sci.* **2013**, *279*, 285–292. [CrossRef]
74. Kooshki, H.; Ghollasi, M.; Halabian, R.; Kazemi, N.M. Osteogenic differentiation of preconditioned bone marrow mesenchymal stem cells with lipopolysaccharide on modified poly-l -lactic-acid nanofibers. *J. Cell. Physiol.* **2018**, *234*, 5343–5353. [CrossRef]
75. Cheng, Q.; Lee, B.L.-P.; Komvopoulos, K.; Yan, Z.; Li, S. Plasma surface chemical treatment of electrospun poly (l -lactide) microfibrous scaffolds for enhanced cell adhesion, growth, and infiltration. *Tissue Eng. Part. A* **2013**, *19*, 1188–1198. [CrossRef] [PubMed]
76. Park, H.; Lee, K.Y.; Lee, S.J.; Park, K.E.; Park, W.H. Plasma-treated poly (lactic-co-glycolic acid) nanofibers for tissue engineering. *Macromol. Res.* **2007**, *15*, 238–243. [CrossRef]
77. Dolci, L.S.; Quiroga, S.D.; Gherardi, M.; Laurita, R.; Liguori, A.; Sanibondi, P.; Focarete, M.L. Carboxyl Surface Functionalization of Poly (l-lactic acid) Electrospun Nanofibers through Atmospheric Non-T hermal Plasma Affects Fibroblast Morphology. *Plasma Process. Polym.* **2014**, *11*, 203–213. [CrossRef]
78. Morra, M.; Occhiello, E.; Garbassi, F. Contact angle hysteresis on oxygen plasma treated polypropylene surfaces. *J. Colloid Interface Sci.* **1989**, *132*, 504–508. [CrossRef]
79. De Geyter, N.; Morent, R.; Leys, C. Influence of ambient conditions on the ageing behaviour of plasma-treated PET surfaces. *Nucl. Instrum. Methods Phys. Res. B Beam Interact. Mater. At.* **2008**, *266*, 3086–3090. [CrossRef]

80. Mrad, O.; Saunier, J.; Aymes-Chodur, C.; Mazel, V.; Rosilio, V.; Agnely, F.; Yagoubi, N. Aging of a medical device surface following cold plasma treatment: Influence of low molecular weight compounds on surface recovery. *Eur. Polym. J.* **2011**, *47*, 2403–2413. [CrossRef]
81. Pascual, M.; Balart, R.; Sanchez, L.; Fenollar, O.; Calvo, O. Study of the aging process of corona discharge plasma effects on low density polyethylene film surface. *J. Mater. Sci.* **2008**, *43*, 4901–4909. [CrossRef]
82. Vandenbossche, M.; Hegemann, D. Recent approaches to reduce aging phenomena in oxygen-and nitrogen-containing plasma polymer films: An overview. *Curr. Opin. Solid State Mater. Sci.* **2018**, *22*, 26–38. [CrossRef]
83. Wavhal, D.S.; Fisher, E.R. Hydrophilic modification of polyethersulfone membranes by low temperature plasma-induced graft polymerization. *J. Membr. Sci.* **2002**, *209*, 255–269. [CrossRef]
84. Garbassi, F.; Morra, M.; Occhiello, E. Chemical modifications. In *Polymer Surfaces from Physics to Technology*; Garbassi, F., Morra, M., Occhiello, E., Eds.; Willey: Chichester, UK, 1994; pp. 242–274.
85. Esfahani, H.; Ghiyasi, Y. Effect of HA Nanoparticles on Adsorption of Vitamin D3 on Super-Hydrophobic PA6 Nanofibrous Scaffold. *Matéria* **2020**, *25*. [CrossRef]
86. Yoshida, M.; Langer, R.; Lendlein, A.; Lahann, J. From advanced biomedical coatings to multi-functionalized biomaterials. *J. Macromol. Sci. Polym. Rev.* **2006**, *46*, 347–375. [CrossRef]
87. Casper, C.L.; Yamaguchi, N.; Kiick, K.L.; Rabolt, J.F. Functionalizing electrospun fibers with biologically relevant macromolecules. *Biomacromolecules* **2005**, *6*, 1998–2007. [CrossRef]
88. Patel, S.; Kurpinski, K.; Quigley, R.; Gao, H.; Hsiao, B.S.; Poo, M.M.; Li, S. Bioactive nanofibers: Synergistic effects of nanotopography and chemical signaling on cell guidance. *Nano Lett.* **2007**, *7*, 2122–2128. [CrossRef] [PubMed]
89. Shitole, A.A.; Raut, P.; Giram, P.; Rade, P.; Khandwekar, A.; Garnaik, B.; Sharma, N. Poly (vinylpyrrolidone)-iodine engineered poly (ε-caprolactone) nanofibers as potential wound dressing materials. *Mater. Sci. Eng. C* **2020**, *110*, 110731. [CrossRef] [PubMed]
90. Gao, D.; Mi, Y.; Gao, Z. Green approaches for the fabrication of electrospun poly (vinyl alcohol) nanofibers loaded epidermal growth factor derivative. *Mater. Lett.* **2020**, *276*, 128237. [CrossRef]
91. Shelke, N.B.; James, R.; Laurencin, C.T.; Kumbar, S.G. Polysaccharide biomaterials for drug delivery and regenerative engineering. *Polym. Adv. Technol.* **2014**, *25*, 448–460. [CrossRef]
92. Sakai, S.; Liu, Y.; Yamaguchi, T.; Watanabe, R.; Kawabe, M.; Kawakami, K. Immobilization of Pseudomonas cepacia lipase onto electrospun polyacrylonitrile fibers through physical adsorption and application to transesterification in nonaqueous solvent. *Biotechnol. Lett.* **2010**, *32*, 1059–1062. [CrossRef]
93. Kowalczyk, T. Functional Micro-and Nanofibers Obtained by Nonwoven Post-Modification. *Polymers* **2020**, *12*, 1087. [CrossRef]
94. Rao, G.K.; Kurakula, M.; Yadav, K.S. Application of Electrospun Materials in Gene Delivery. In *Electrospun Materials and Their Allied Applications*; Inamuddin, R.B., Mohd, I.A., Abdullah, M.A., Eds.; Scrivener publishing: Austin, TX, USA, 2020; pp. 265–306.
95. Bu, Y.; Ma, J.; Bei, J.; Wang, S. Surface modification of aliphatic polyester to enhance biocompatibility. *Front. Bioeng. Biotechnol.* **2019**, *7*, 98. [CrossRef]
96. Jankowska, K.; Zdarta, J.; Grzywaczyk, A.; Kijeńska-Gawrońska, E.; Biadasz, A.; Jesionowski, T. Electrospun poly (methyl methacrylate)/polyaniline fibres as a support for laccase immobilisation and use in dye decolourisation. *Environ. Res.* **2020**, *184*, 109332. [CrossRef]
97. Müller, K.J.F.; Quinn, A.P.R.; Johnston, M.; Becker, A.; Greiner, F. Caruso Polyelectrolyte functionalization of electrospunfibers. *Chem. Mater.* **2006**, *18*, 2397–2403. [CrossRef]
98. Truong, Y.B.; Glattauer, V.; Briggs, K.L.; Zappe, S.; Ramshaw, J.A. Collagen-based layer-by-layer coating on electrospun polymer scaffolds. *Biomaterials* **2012**, *33*, 9198–9204. [CrossRef] [PubMed]
99. Huang, S.J.; Soenen, E.; van Gulck, J.; Rejman, G.; Vanham, B.; Lucas, B.; Geers, K.; Braeckmans, V.; Shahin, P.; Spanoghe, J.; et al. Electrospun polystyrene fibers for HIV entrapment. *Polym. Adv. Technol.* **2014**, *25*, 827–834. [CrossRef]
100. Chunder, A.; Sarkar, S.; Yu, Y.; Zhai, L. Fabrication of ultrathin polyelectrolyte fibers and their controlled release properties. *Colloids Surf. B* **2007**, *58*, 172–179. [CrossRef]
101. Wu, Z.R.; Ma, J.; Liu, B.F.; Xu, Q.Y.; Cui, F.Z. Layer-by-layer assembly of polyelectrolyte films improving cytocompatibility to neural cells. *J. Biomed. Mater. Res. Part. A* **2007**, *81*, 355–362. [CrossRef]
102. Zhang, K.; Chooi, W.H.; Liu, S.; Chin, J.S.; Murray, A.; Nizetic, D.; Chew, S.Y. Localized delivery of CRISPR/dCas9 via layer-by-layer self-assembling peptide coating on nanofibers for neural tissue engineering. *Biomaterials* **2020**, *256*, 120225. [CrossRef]

103. He, L.; Shi, Y.; Han, Q.; Zuo, Q.; Ramakrishna, S.; Xue, W.; Zhou, L. Surface modification of electrospun nanofibrous scaffolds via polysaccharide–protein assembly multilayer for neurite outgrowth. *J. Mater. Chem.* **2012**, *22*, 13187–13196. [CrossRef]
104. Sánchez, L.D.; Brack, N.; Postma, A.; Pigram, P.J.; Meagher, L. Surface modification of electrospunfibres for biomedical applications: A focus on radical polymerization methods. *Biomaterials* **2016**, *106*, 24–45. [CrossRef]
105. Teo, W.E.; Ramakrishna, S. Electrospun nanofibers as a platform for multifunctional, hierarchically organized nanocomposite. *Compos. Sci. Technol.* **2009**, *69*, 1804–1817. [CrossRef]
106. Wang, D.; Wang, X.; Li, X.; Jiang, L.; Chang, Z.; Li, Q. Biologically responsive, long-term release nanocoating on an electrospun scaffold for vascular endothelialization and anticoagulation. *Mater. Sci. Eng. C* **2020**, *107*, 110212. [CrossRef]
107. Ghobeira, R.; De Geyter, N.; Morent, R. Plasma surface functionalization of biodegradable electrospun scaffolds for tissue engineering applications. In *Biodegradable Polymers: Recent Developments and New Perspectives*; Geraldine, R.C., Ed.; IAPC Publishing: Zagreb, Croatia, 2017; pp. 191–236.
108. Dufay, M.; Jimenez, M.; Degoutin, S. Effect of cold plasma treatment on electrospun nanofibers properties: A review. *ACS Appl. Bio. Mater.* **2020**, *3*, 4696–4716. [CrossRef]
109. Bhattacharjee, P.; Naskar, D.; Kim, H.-W.; Maiti, T.K.; Bhattacharya, D.; Kundu, S.C. Non-mulberry silk fibroin grafted PCL nanofibrous scaffold: Promising ECM for bone tissue engineering. *Eur. Polym. J.* **2015**, *71*, 490–509. [CrossRef]
110. Krithica, N.; Natarajan, V.; Madhan, B.; Sehgal, P.K.; Mandal, A.B. Type I collagen immobilized poly (caprolactone) nanofibers: Characterization of surface modification and growth of fibroblasts. *Adv. Eng. Mater.* **2012**, *14*, B149–B154. [CrossRef]
111. de Sousa, A.M.C.; Rodrigues, C.A.; Ferreira, I.A.; Diogo, M.M.; Linhardt, R.J.; Cabral, J.; Ferreira, F.C. Functionalization of Electrospun Nanofibers and Fiber Alignment Enhance Neural Stem Cell Proliferation and Neuronal Differentiation. *Front. Bioeng. Biotechnol.* **2020**, *8*, 1215.

Micron 145 (2021) 103066

Contents lists available at ScienceDirect

Micron

journal homepage: www.elsevier.com/locate/micron

Shortening of electrospun PLLA fibers by ultrasonication

Beata Niemczyk-Soczynska, Judyta Dulnik, Oliwia Jeznach, Dorota Kolbuk, Pawel Sajkiewicz *

Institute of Fundamental Technological Research, Lab. Polymers & Biomaterials, Polish Academy of Sciences, Pawinskiego 5b St., 02-106, Warsaw, Poland

ARTICLE INFO

Keywords:
Electrospinning
Ultrasonication
Short fibers
Polymers

ABSTRACT

This research work is aimed at studying the effect of ultrasounds on the effectiveness of fiber fragmentation by taking into account the type of sonication medium, processing time, and various PLLA molecular weights. Fragmentation was followed by an appropriate filtration in order to decrease fibers length distribution. It was evidenced by fiber length determination using SEM that the fibers are shortened after ultrasonic treatment, and the effectiveness of shortening depends on the two out of three investigated parameters, mostly on the sonication medium, and processing time. The gel permeation chromatography (GPC) confirmed that such ultrasonic treatment does not change the polymers' molecular weight.

Our results allowed to optimize the ultrasonic fragmentation procedure of electrospun fibers while preliminary viscosity measurements of fibers loaded into hydrogel confirmed their potential in further use as fillers for injectable hydrogels for regenerative medicine applications.

1. Introduction

Therapies dedicated to cardiac, cartilage, muscle, and nerve regeneration require advanced, well-designed approaches. An ideal scaffold should provide a 3-dimensional structure, with adequate biocompatibility, biodegradability, offering mechanical support for cells, but primarily mimicking native extracellular matrix (ECM) (Lis et al., 2013). In other words, such a scaffold should provide an appropriate environment supporting cell proliferation, regeneration and encouraging the formation of healthy and functional living tissue.

There are plenty of methods allowing scaffold fabrication such as 3-D printing (Gorecka et al., 2020), self-assembly (Zhu et al., 2010), phase separation (Liu and Ma, 2009), solution blowing (Cui et al., 2020), or electrospinning that has been commonly used for many years. Electrospinning is a cheap and uncomplicated method that allows to use a wide spectrum of polymeric materials (Jeznach et al., 2019; Dulnik et al., 2018). Electrospun nanofibers topography might be controlled through material, process and ambient parameters, providing optimal structure/properties. In reality electrospun mats are, however, more 2- than 3-dimensional and have small pores from the perspective of living cell requirement. Since there is only one way to implement electrospun fibers inside the body, by surgery, it also limits their application in some fields of tissue engineering (Niemczyk et al., 2018). In contrast to electrospun mats, hydrogels are 3-dimensional structures which, depending on the used material, might be injected in targeted injury, perfectly filling the lesion. There are two serious limitations of hydrogels. One of them is their poor mechanical properties that cause cells to collapse during culturing. Another one is the lack of fibrous structure mimicking collagen, fibronectin, or laminin fibers of native ECM. Nowadays, using only one type of method for scaffold fabrication seems to be insufficient for the high requirements of tissue engineering. Combination of two or more scaffold fabrication methods gives more possibilities; therefore, such an approach is currently getting ever-growing attention. Compared to electrospun mats, short fibers could provide dispersion in the liquid media. For instance, combination of injectable hydrogels with short electrospun nanofibers allows obtaining a material with a unique fibrous structure and properties attractive for tissue engineering. Such conjugation may improve the mimicry of ECM, providing an appropriate environment for neural cell regeneration, strengthen the hydrogel mechanically, and provide additional support for cell growth. Besides aforementioned advantages, short fibers are able to keep the injection ability of the whole hydrogel/short fibers on the acceptable level. In order to achieve the latter condition it is necessary to shorten long electrospun fibers to avoid an excessive growth of viscosity during solution injection. According to Wasupalli et al. (Wasupalli and Verma, 2020) ~100 μm length of short electrospun fibers added to the hydrogel are considered to be injectable.

In the literature, there are several effective methods of electrospun fibers shortening. To the most important ones are fiber fragmentation during electrospinning, i.e., by tuning parameters of electrospinning

* Corresponding author.
E-mail address: psajk@ippt.pan.pl (P. Sajkiewicz).

https://doi.org/10.1016/j.micron.2021.103066
Received 15 February 2021; Received in revised form 29 March 2021; Accepted 29 March 2021
Available online 1 April 2021

(Regev et al., 2013; Greenfeld and Zussman, 2013), core-shell electrospinning by leaching of the shell from the core-shell fibers (Ravichandran et al., 2012), electric spark (Fathona and Yabuki, 2013), or post-electrospinning methods, which might be subsequently divided into chemical and physical (mechanical) methods. One of the post-electrospinning chemical methods is aminolysis, which provides nanofibers fragmentation through the chemical cutting of polymeric chains with the use of a particular diamine (Jeznach et al., 2019). By adjusting the reaction conditions such as temperature, diamine concentration, and reaction time, stacked crystalline lamellae are formed in the non-crystalline polymer fibers, which degrade into smaller segments due to amorphous phase breakdown (Kim and Park, 2008). To strengthen the effect of fragmentation, additional mechanical supportive methods are used. In many studies Castro et al., 2016, Petre et al., 2019, ultrasonication is used to destroy more of amorphous parts between lamellae in aminolysed nanofibers and prevent fibers aggregation (Heo et al., 2017). Although aminolysis seems to be effective, it has to be precisely controlled otherwise polymers might losing their output characteristics such as mechanical properties (Huang et al., 2016).

An alternative to the chemical methods is mechanical (physical) ones. In this field, motor-driven blade cutting under liquid nitrogen (Thieme et al., 2011; Jiang et al., 2013), cryo-micro cutting (Liao et al., 2020), UV cutting with the presence of masks with a defined size of slits (Stoiljkovic and Agarwal, 2008), laser cutting (Creighton et al., 2020) and ultrasonication (Sawawi et al., 2013; Mulky et al., 2014) might be distinguished. Ultrasonication is one of the methods used, among others, for electrospun fibrous scaffold disintegration and their pore size expansion. Additional use involves short electrospun fibers fabrication. The fibers fragmentation mechanism assumes bubble cavitation and implosion, followed with releasing energy and subsequent fibers fracture and fragmentation (Sawawi et al., 2013). It allows obtaining short fibers from brittle materials in a very fast and simple manner (Sawawi et al., 2013). However, similarly to most of the mechanical methods, it results in broad nanofibers' length distribution, consequently limiting the scope of their applications (Liao et al., 2020). To overcome this problem, an additional step narrowing fiber length distribution is needed.

This publication aim was to investigate the effect of some ultrasonication and material parameters - sonication medium, processing time, polymer molecular weight, on the effectiveness of PLLA electrospun fibers fragmentation. Since PLLA is a biocompatible, and its glass transition temperature (Tg) is above room temperature, the polymer characterizes relative brittleness, which enables effective fragmentation by ultrasonication (Zaszczynska et al., 2020; Kolbuk et al., 2020).

Additionally, post-fragmentation of short fibers was carried out to narrow down the nanofibers length distribution.

This work allowed to optimize the procedure of ultrasonic fibers fragmentation and provided information of the material that might be used as a component of the injectable composite hydrogels system for tissue engineering application.

2. Experimental

2.1. Electrospinning

Poly(l-lactide) acid (PLLA) with different molecular weights has been used - Purasorb PL 18 (M_w ~ 217−225 kDa Purac, Netherlands), Purasorb PL 24 (M_w ~ 260 kDa, Purac, Netherlands), and Purasorb PL 49 (M_w ~ 330 kDa, determined from the gel permeation chromatography described below in this work, Purac, Netherlands) (Nyanhongo et al., 2013; Kasuga et al., 2012). All of the PLLA samples were dissolved in 1,1,1,3,3,3, -hexafluoro-2-propanol (HFIP, Iris Biotech GmbH, Germany) at room temperature and subsequently left to stir overnight. For electrospinning 10 wt. % of PLLA PL 18, 8 wt. % of PLLA PL 24 as well as 5 wt. % of PLLA PL 49 were prepared. All of the PLLA solutions were loaded into a 5-ml syringe and placed into a Bioinicia horizontal setup (Valencia, Spain) used for the electrospinning process. The solutions flowed through 23-gauge stainless steel needles with an inner diameter of 0.337 mm with the flow rate in the range of 1−2 ml/h. The distance between the needle and the collector was 15 cm. The fibers were collected on a rotating drum collector (5 cm radius and 7 cm length) rotating at 1000 rpm to obtain oriented fibers. The linear velocity was 5.24 m/s. The process was carried out at the temperature range of 22−25 °C and humidity range of 29–45 %. The positive voltage applied to the needle was in the range of 12−14 kV. The collector always maintained an electric potential of −2 kV. After electrospinning, all materials were placed under a fume hood in order to evaporate the solvents residuals.

2.2. Fragmentation

The electrospun mats were cut into c.a. 1-mm square pieces using a scalpel and subsequently placed in a 50 mL falcon containing 8 mL of sonication medium being a mixture of demineralized water with ethanol, or isopropanol. Ultrasonic fragmentation was carried out using UP200Ht (Hielscher, Germany) ultrasonic homogenizer with a S26d2 type 12-cm-diameter titanium sonotrode, working at 26 kHz. The amplitude of 90–98 % with a sonication interval of 1 s/1 s ON/OFF, with the total running time varied from 30 to 60 min. The sonication medium used for this study was kept in the ice bath in order to avoid excessive temperature increase during the process that may cause sonotrode destruction. According to Sawawi et al. (2013), the process temperature does not influence the fibers fragmentation and fibers final length.

After fragmentation, a sonication medium containing short fibers was directly poured onto a foil under the fume hood to evaporate the medium or filtered through 40 μm cell strainers to provide narrower fibers length distribution. Then short fibers were dried overnight before further characterization.

2.3. Characterization

The electrospun nanofibers morphology was investigated using a Scanning Electron Microscope (SEM) (JEOL JSM-6390LV, Japan). Prior to imaging, all of the samples were sputtered with 8 nm of gold. The acceleration voltage was 7 kV. To evaluate fiber orientation, diameters and lengths, the ImageJ software was applied. The fiber diameter and length distributions were calculated by means of 100 fibers measurements for each sample and subsequently approximated with Gaussian and Biphasic dose-response functions. The fiber orientation was determined with the use of ImageJ software supplemented with the Fiji directions plugin. This plugin generated a histogram presenting the number of fibers in a given direction, which was created due to periodic repeats in intensity in the analysed SEM image using the Fourier image analysis method (Clemons et al., 2018). Obtained histograms were approximated with Gauss function, of which a half-width was designated.

2.4. Wide-angle x-ray scattering (WAXS)

The WAXS was used to investigate the degree of crystallinity of electrospun PLLA PL 18, PLLA PL 24 and PLLA PL 49. The WAXS scans were registered with the use of D8 Discover diffractometer, Bruker, Germany. To record the radial profiles, CuK_α radiation at a voltage of 40 kV and a current of 20 mA, $\lambda = 1.5418$ Å in coupled theta, 2Theta mode was used. For measurements, a reflection mode with the Goebel optics was used for beam formation with a 1 mm slit and Soller collimator. Lynx Eye 1-D silicon eye with high sensitivity was used as a detector. A diffraction angle of 2 Theta was in the range of 6–30 °, while data collection time at the angular point was 1 s. The WAXS results were prepared for further analysis by subtraction of a background scan (scan without the sample) using Bruker evaluation software. After that, WAXS scans were numerically analysed using PeakFit software by

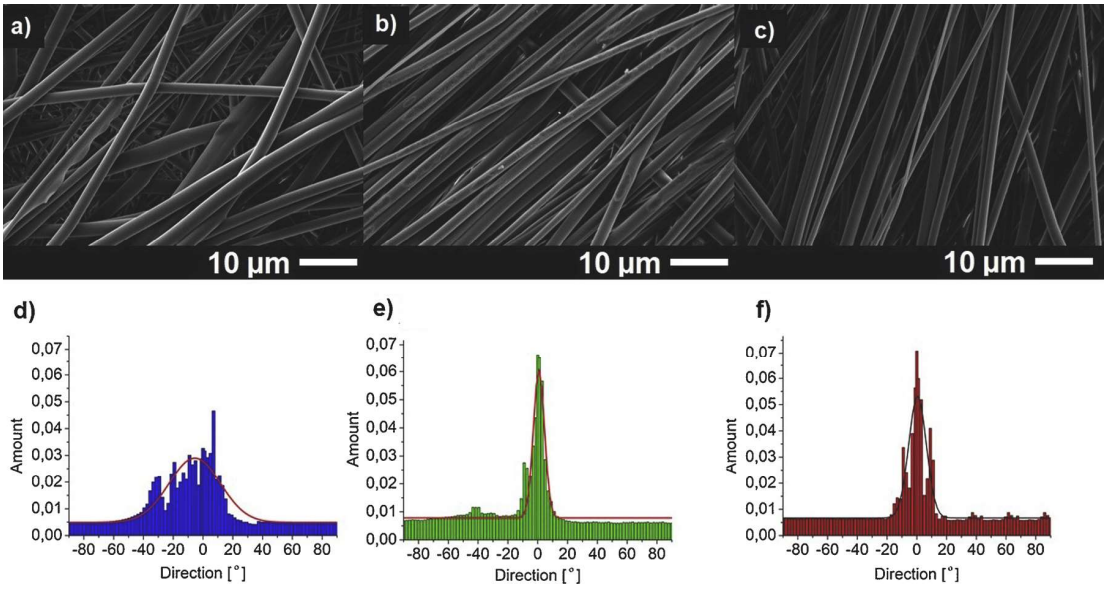

Fig. 1. SEM images of electrospun nanofibers and fiber orientation distribution (with numerical approximation) for: a), d) 5 wt. % PLLA PL 49; b), e) 8 wt. % PLLA PL 24; c), f) 10 wt. % PLLA PL 18.

deconvolution with the Gauss functions for amorphous scattering and Pearson VIII for crystal scattering diffraction. Finally, the crystallinity degree was assigned as a ratio of crystalline diffraction peaks area and the overall area in the investigated scattering range.

2.5. Gel permeation chromatography (GPC)

In order to check if ultrasonic treatment decreases PLLA molecular weight, as reported by Chen et al. (2018a), GPC measurements have been carried out. The analysed PLLA samples were dissolved in chloroform ($CHCl_3$) at 2.0 mg/mL. Solutions were then filtered using 0.22 µm syringe filters (Biosens). Number average (M_n) and weight average (M_w) molecular weights of the PLLA samples were determined using Shimadzu LC-2030C Plus 3D Prominence-i instrument, with a refractive index detector, RID-20 calibrated with polystyrene standards and a Phenogel ™ 5um 10E5 Å column (Phenomenex). The tetrahydrofuran (THF) was used as the eluent, at 40 °C. THF flow rate was 1 mL/min. A universal calibration was used for the evaluation of the Mn and Mw, using Mark–Houwink constants for PLA (a = 0.65, K = 0.001 dl/g) and polystyrene (PS) (α = 0.7, K = 0.00014 dl/g), which was used as a standard (Nuuttila, 2018).

Based on GPC results, the determination of the molecular weight distribution was obtained by a numerical deconvolution. It was necessary because of incomplete solubility of PLLA in chloroform with a most probable tendency of molecular aggregation.

Deconvolution was carried out with the log-normal function using Origin software to determine lower molecular weight component, which corresponds to the part of the polymer that is actually molecularly dissolved in the solvent. For this component, the subsequent number average molecular weight (M_n) and weight average molecular weight (M_w) were determined using the following equations:

$$\overline{M}_n = \frac{\Sigma_i N_i M_i}{\Sigma_i N_i} \quad (1)$$

$$\overline{M}_w = \frac{\Sigma_i N_i M_i^2}{\Sigma i N_i M_i} \quad (2)$$

where N_i is the number of polymer molecules, while M_i is their molecular weight.

2.6. Viscosity of hydrogel

The hydrogel system was made of 2 wt. % Methylcellulose (METHOCEL A15 LV, Sigma Aldrich) and 2 wt. % Agarose (SeaprepR, Lonza) mixed in the wt. ratio of 1:1. This solution served for preliminary studies for formation of injectable hydrogel loaded with fibers. The viscosities of hydrogel without fibers, hydrogel loaded with 1 mg/ml and 2 mg/ml of PLLA PL 49 short fibers were investigated.

HADV-III Ultra fitted with cone/plate geometry, at a constant temperature of 22 °C and a constant shear rate 500 s^{-1}. The chosen shear rate was the highest possible achieved by the viscometer with an available cone of CP-52 (cone angle 3°). It is as close as possible to the shear rates estimated for the real systems used for hydrogel injection in medical practice. The applied shear rate, $\gamma = 500\ s^{-1}$, results in volumetric flow rate of solution, Q = 2 µL/s, at the inner diameter of the needle, R =0.36 mm (23 gauge needle), during injection as can be determined using the following equation (Pakravan et al., 2012):

$$\gamma = \frac{4Q}{\pi R^3} \quad (3)$$

All of the measurements were carried out four times for each sample after 1 s and after 5 min.

2.7. Statistics

A difference between fragmented fibers length depending on used sonication solution as well as ultrasonication time was analysed using one-way ANOVA method between groups ANOVA and analysis of variance tests (ANOVA). All statistical analyses were performed for $p < 0.05$.

3. Results and discussion

3.1. Electrospinning and fragmentation

The applied electrospinning conditions lead to formation of fibers with preferred orientation (Fig.1). The choice of such morphology for further fragmentation was motivated by the literature reports. According to Sawawi et al. (2013), fragmentation of oriented electrospun nanofibers is less challenging since the degree of fiber entanglement is

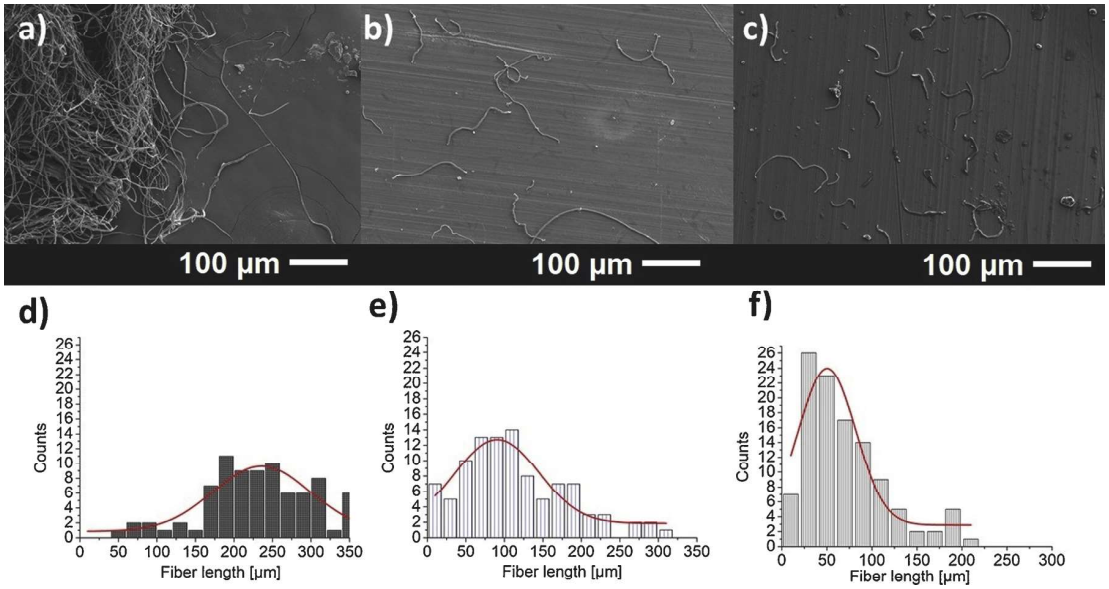

Fig. 2. SEM images and histograms of fiber length distribution of 10 wt. % PLLA PL 18 electrospun nanofibers fragmented in: a), d) water, b), e) ethanol, c), f) isopropanol for 60 min.

much lower compared to randomly oriented polymer fibers. It was also reported that higher degree of fiber alignment in the original web led to obtaining shorter fibers upon fragmentation (Castro et al., 2016; Sawawi et al. (2013)). Fig.1 presents SEM images of electrospun samples together with their directionality histograms. Degree of fiber orientation was characterized as inversely proportional to the half-width of directionality distribution, being the highest for 8 wt. % PLLA PL 24 and the lowest for 5 wt. % PLLA PL 49 (Fig. 1).

10 wt. % PLLA PL 18 fibrous mats were subjected to ultrasonic fragmentations in various sonication media - water, ethanol, and isopropanol. Fig. 2 illustrates the morphology of fragmented fibers together with corresponding fiber length distributions for solutions used during sonication. Since the PLLA fibers were mostly tangled after ultrasonication in water, and their average fibers length was 237 ± 6.7 μm, it is evident that water is not effective as a sonication medium. Ethanol and isopropanol were more effective as sonication solutions with statistically significant differences in the average values of the fiber length and variances at the 0.05 level, for both solutions. The average PLLA fibers length fragmented in ethanol was 91 ± 6.9 μm, while these fragmented in isopropanol were almost 2-fold lower (50 ± 4.9 μm) (Fig.2 d, e).

This phenomenon can be explained by different molecular interactions between polymer and sonication solutions in both cases (Sawawi et al., 2013). To evaluate the interactions between polymer and solvent, Hansen solubility parameters can be used (Hansen, 2007; Bordes et al., 2010). According to this methodology, the interactions are divided into a dispersing part (δd), polar part (δh), and hydrogen part (δh).

$$\delta = (\delta_d^2 + \delta_p^2 + \delta_h^2)^{\frac{1}{2}} \quad (4)$$

These parameters create a 3-D solubility space called "Hansen space", where solvent meets polymers molecules. When the

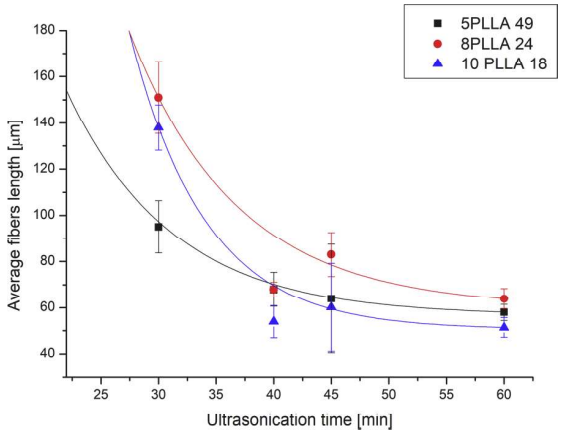

Fig. 3. Average fiber length vs. time of ultrasonication in isopropanol. Approximation with exponential function.

aforementioned polymer and solvent parameters, considered as points in Hansen space, are nearby, the probability that the solvent dissolves the polymer is high. To determine the distance between solubility parameters of solvent and solute, the following equation is used:

$$R_a^2 = 4(\delta_{d2} - \delta_{d1})^2 + (\delta_{p2} - \delta_{p1})^2 + (\delta_{h2} - \delta_{h1})^2 \quad (5)$$

While R_a is an interaction radius, δ_{d1}, δ_{p1}, δ_{h1} are parameters of solute, while δ_{d2}, δ_{p2}, δ_{h2} are parameters of solvent.

By comparing R_a with the solubility radius of polymer, R_0, it is possible to evaluate the solubility of a particular polymer in various solvents. The ratio of R_a and R_0 is called relative energy difference

Table 1
Literature Hansen solubility parameters for PLLA, water, ethanol and isopropanol (Agrawal et al., 2004; Abbott and Hansen, 2008), and calculated RED.

	δd [MPa$^{0.5}$]	δp [MPa$^{0.5}$]	δh [MPa$^{0.5}$]	R0 [MPa$^{0.5}$]	Ra [MPa$^{0.5}$]	RED
PLLA	16.85	9.00	4.05	9.71	–	–
Water	15.5	16.00	42.3	–	24.35	4.01
Ethanol	15.8	8.8	19.4	–	15.36	1.59
Isopropanol	15.80	6.1	16.4	–	24.77	1.33

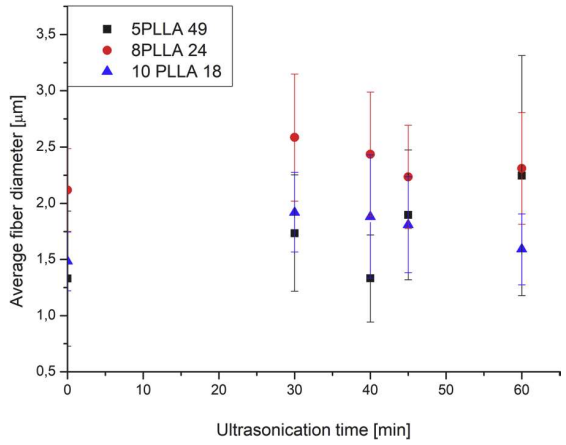

Fig. 4. Average fiber diameter vs. time of ultrasonication in isopropanol.

(RED). The relative energy density 0 means there is no energy difference, RED less than 1 indicate high affinity and RED greater than 1 indicate progressively lower affinity between polymer and a solvent (Hansen, 2007; Barton, 1991).

Based on the eq. (5) we investigated the PLLA solubility in water, ethanol and isopropanol (Agrawal et al., 2004; Abbott and Hansen, 2008). The results show (Table 1) that all of the solvents are considered to be poor which is expected from the ultrasonication medium. The solvents used as a sonication medium are supposed to help fibers shortening during sonication. It is evident from Table 1 that the calculated RED is the lowest for isopropanol indicating the strongest molecular interactions with PLLA. This fact is consistent with our macroscopic observations clearly indicating that isopropanol is a most effective medium for PLLA ultrasonication. The isopropanol was consequently chosen for further studies.

The next investigated parameter that influenced the effectiveness of ultrasonic fragmentation was PLLA molecular weight. Fibers of PLLA PL 49, PLLA PL 24 and PLLA PL 18 had at the longest sonication time the average values of 58 ± 3.5 µm, 64 ± 4.4 µm and 51 ± 4.2 µm, respectively (Fig. 3). The results shown in Fig. 3 clearly indicate that there is no dependence between efficiency of ultrasonic fragmentation and the polymers molecular weight after long time of fragmentation in the investigated range of molecular weights.

The parameter that was also considered to be crucial for the efficiency of fiber fragmentation was the ultrasonication time. Figs. 3, 4 present fibers length and diameter vs. ultrasonication time for PLLA samples with different molecular weights. Independent of the molecular weight, fiber length decreased exponentially with the ultrasonication time. The stable fiber length was practically approached after 40 min of ultrasonication at the range of 58 −70 µm. The shortest fibers were obtained for 10 wt. % PLLA PL 18.

The analysis of fiber diameter vs. ultrasonication time indicates no statistically significant effect of ultrasonication time on fiber diameter (Fig.4).

The subsequent step was filtration through 40 µm cell strainers of fibers previously ultrasonically fragmented for 60 min. Analysis of SEM images (Fig. 5), corresponding histograms (Fig. 6) and the resulting fiber lengths (Table 2) indicates that filtration reduced the fraction of relatively long fibers leading to slight reduction of the average fiber length. These results indicated the reduction of the average fiber length 1.2−1.7-fold after filtration. The shortest fibers after filtration were obtained for 10 wt. % PLLA PL 18 and 5 wt. % PLLA PL 49 (Table 2).

Additional parameter used by us for comparison of fiber length

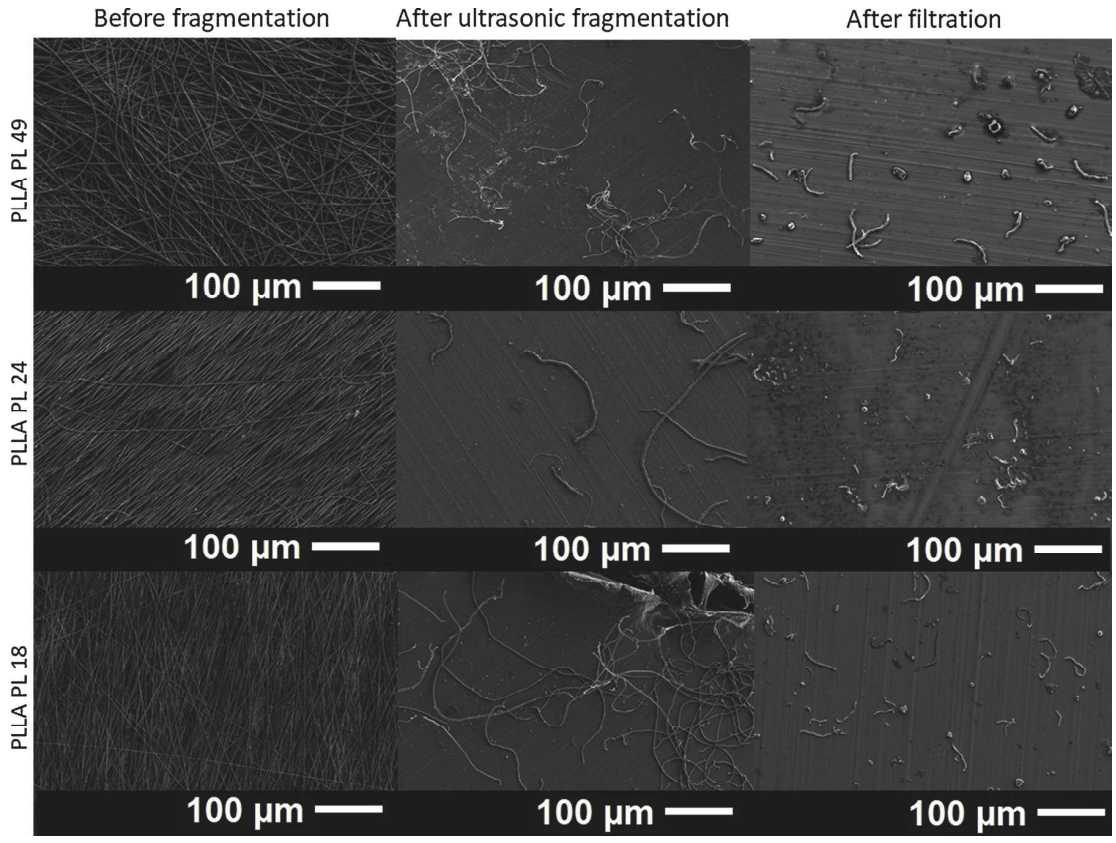

Fig. 5. SEM images of electrospun nanofibers.

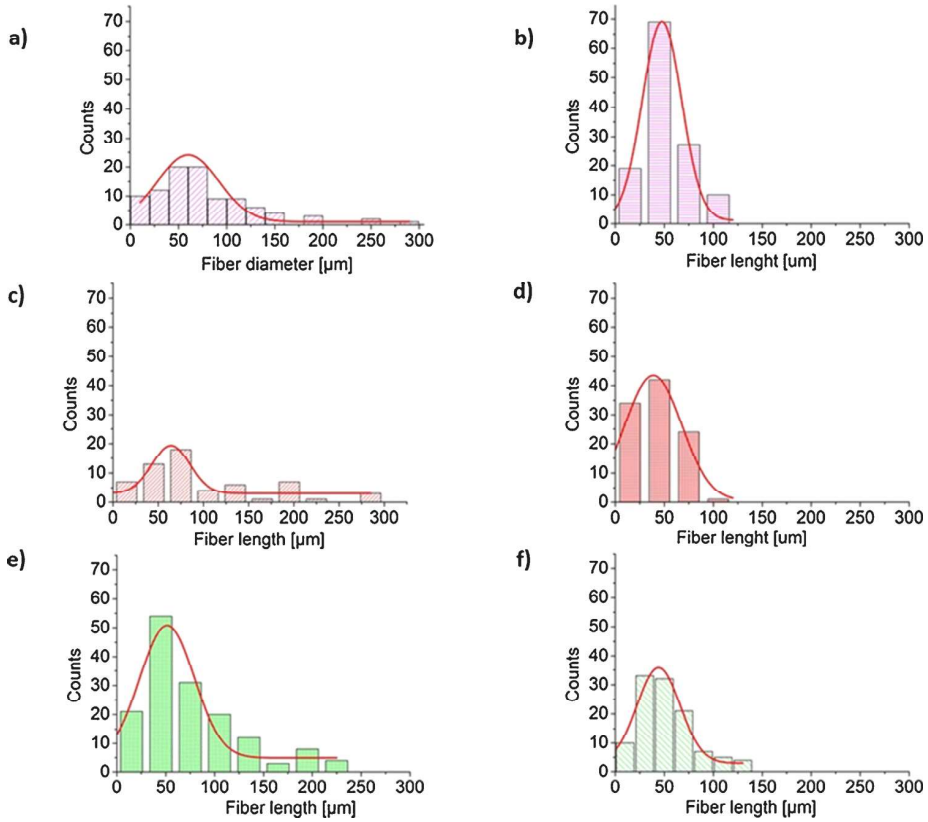

Fig. 6. Histograms of fiber length distribution for: a) 5 wt. % PLLA 49 after 60 min of fragmentation, b) 5 wt. % PLLA 49 after subsequent filtration c) 8 wt. % PLLA PL 24 after fragmentation and d) 8 wt. % PLLA PL 24 after subsequent filtration, e) 10 wt. % PLLA PL 18 after fragmentation, f) 10 wt. % PLLA PL 18 after subsequent filtration.

Table 2
Comparison of the average fibers diameter before and after filtration.

Material	fiber length before filtration [μm]	fiber length after filtration [μm]
PLLA PL 49	58 ± 3.5	42 ± 2
PLLA PL 24	64 ± 4.4	46 ± 3.4
PLLA PL 18	51 ± 4.2	44 ± 2

before and after filtration was the coefficient of variation (CV) defined as a ratio of the standard deviation (SD) to the mean fiber length. The PLLA fibers exhibited quite wide fiber length distribution after 60 min of fragmentation. For PLLA PL 49, PLLA PL 24, and PLLA PL18 CV before filtration CV was 6, 6.9, and 8.2 % while after filtration was 4.7, 7.4 and 4.5 %, respectively.

Our results indicate that as expected there are no changes of fiber diameter after filtration.

3.2. WAXS

Fig. 7 and Table 3 present the WAXS profiles of electrospun PLLA PL 49, PLLA PL 24, and PLLA PL 18. All of the profiles consist of a broad scattering approximated using two Gauss functions with a maximum at 2Theta = 14.9°, 21.2° and several peaks coming from the diffraction on crystal planes. Amorphous components arise from two characteristic inter-chain spacings (Monnier et al., 2015; Chen et al., 2018b). In the case of electrospun fibers, crystallinity was extremely low, increasing slightly with the decrease of polymers molecular weight. For electrospun PLLA PL 49 sample there is no crystallinity, while the PLLA PL 24 sample and PLLA PL 18 sample showed only one low intensity peak from (110/200) planes from the mesomorphic form at 2Theta = 16.5°. Mesophase is developed from the strain-oriented amorphous chains (Jeznach et al., 2019). After ultrasonic fragmentation all of the samples showed a dramatic increase of crystallinity evidencing by relatively strong crystalline peaks at 2Theta of 15.11°, 16.5°, 18.9° and 22.3° corresponding to (010), (110/200), (203) and (015) crystallographic planes, respectively (Jeznach et al., 2019). We anticipated that the observed increase in crystallinity after ultrasonic fragmentation is mostly due to increased molecular mobility, favouring crystallization as a result of temperature increase during the ultrasonication process. The ice bath keeps the appropriate temperature for a while, but after 60 min of fragmentation, the sonication solution with fibers is heated by ultrasounds up to 42 °C, which is close to the glass transition the temperature of PLLA.

3.3. Gel permeation chromatography (GPC)

Fig. 8 and Table 4 show the changes in the molecular weight distribution of PLLA before, after electrospinning, and after subsequent fibers fragmentation. The GPC results indicate that the molecular weight distribution of PLLA is not affected by both electrospinning and subsequent fragmentation. Similarly to the Lees report (Lee et al., 2011), the position and intensity of GPC peaks were similar before and after polymers processing.

Contrary to the chemical and physical fragmentation methods such as UV treatment (Abbott and Hansen, 2008), the ultrasonication method does not cause PLLA molecular degradation. It is essential in scaffold designing to avoid mechanical weakening during post-electrospinning functionalization (Alves et al., 2011).

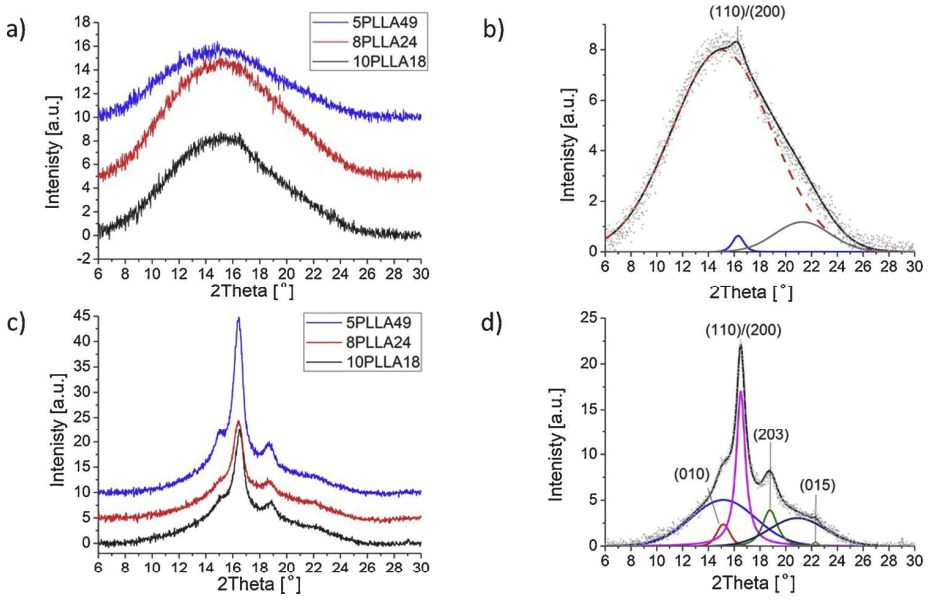

Fig. 7. WAXS profiles of PLLA PL 49, PLLA PL 24, and PLLA PL 18. Experimental curves: a) after electrospinning, c) after subsequent fragmentation. Example of numerical fitting with Gauss (amorphous) and Pearson VII (crystals) functions: b) after electrospinning, d) after subsequent fragmentation.

Table 3
The crystallinity degree of PLLA PL 49, PLLA PL 24 and PLLA PL 18.

Material	Crystallinity degree of electrospun fibers [%]	Crystallinity degree of fragmented fibers [%]
PLLA PL 49	0.35	52.06
PLLA PL 24	0.78	41.43
PLLA PL 18	0.98	40.17

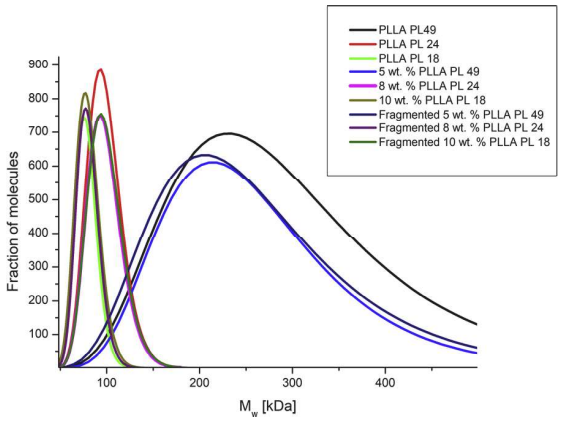

Fig. 8. Lower molecular weight component for PLLA samples from GPC analysis before, and after polymers processing.

3.4. Viscosity of hydrogel

The change of viscosities for each sample after 1 s and 5 min were within the error range. Such behaviour demonstrates the hydrogel stability before and after fibers addition. From the results it is evident that viscosity of the solutions increased with the fibers concentration (Table 5). The viscosity increase is directly proportional to the amount of added fibers, and obtained hydrogels loaded with fibers are still considered to be injectable. According to Jezek et al. (2011) the viscosity that limits liquid injectability is 10 mPa ˙s through a 22 gauge needle.

Table 4
The average molecular weight calculated from Lognormal fit and Mark-Houwink parameters for PLLA ($\alpha = 0.65$, K = 1 E-3 dl/g) and PS ($\alpha = 0.7$, K = 1.41 E-4 dl/g).

Material	$\overline{M}_n$ [kDa]	$\overline{M}_w$[kDa]
PLLA PL 49 pellets	230	327
5 wt. % PLLA PL49	268	335
Fragmented 5 wt. % PLLA PL49	266	337
PLLA PL 24 pellets	95	98
8 wt. % PLLA PL 24	95	99
Fragmented 8 wt. % PLLA PL 24	78	88
PLLA PL 18 pellets	76	78
10 wt. % PLLA PL 18	78	80
Fragmented 10 wt. % PLLA PL 18	76	78

The estimated SD was as follows: for PLLA pellets 21–38 %; for electrospun fibers 11–19 %; for fragmented fibers 13–18 %.

Table 5
Viscosity measurements of hydrogel before and after addition of short fibers.

Material	Viscosity [Pa ˙s]
2 wt. % Methylcellulose/2 wt. % Agarose after 1 s	131.4 ± 5.2
2 wt. % Methylcellulose/2 wt. % Agarose after 5 min	128.6 ± 6.3
2 wt. % Methylcellulose/2 wt. % Agarose loaded with 1 mg/ml of PLLA PL 49 fibers after 1 s	137.9 ± 2.8
2 wt. % Methylcellulose/2 wt. % Agarose loaded with 1 mg/ml of PLLA PL 49 fibers after 5 min	137.9 ± 3
2 wt. % Methylcellulose/2 wt. % Agarose loaded with 2 mg/ml of PLLA PL 49 fibers after 1 s	147.8 ± 15
2 wt. % Methylcellulose/2 wt. % Agarose loaded with 2 mg/ml of PLLA PL 49 fibers after 5 min	148.8 ± 14

4. Conclusions

We showed that among investigated ultrasonication parameters, sonication medium, and the duration of the process are essential for the efficiency of fibers fragmentation. We successfully optimized the

ultrasonic fragmentation process, by choosing isopropanol as a sonication medium and relevant fragmentation time of 60 min. The post-fragmentation filtration through 40 um filters additionally reduced fiber length distribution and coefficient of variation by removing the fraction of long fibers.

These studies show that such classic and simple physical methods as ultrasonication effectively shorten PLLA oriented electrospun fibers. Although the method does not change the molecular weight of the polymer, it affects crystallinity of PLLA fibers.

Considering many possibilities offered by electrospun nanofibers, production of short nanofibers increases the range of their potential use. They might find new applications as coatings or smart composites, showing that electrospinning has still a lot to offer as a method.

The preliminary viscosity studies confirmed good dispersion of the short electrospun nanofibers in the liquid media, injectability of hydrogel/short fibers system, and demonstrates the great potential of such an approach in many fields of science. In the future, more characteristics of a hydrogel loaded with short fibers will be investigated in terms of controlled injectability, mechanical and biological properties mimicking ECM. These features will provide an essential cognitive step toward designing composite scaffolds for tissue engineering applications.

Declaration of Competing Interest

The authors declare no conflict of interest.

Acknowledgements

The authors acknowledge the funding provided by the Narodowe Centrum Nauki (NCN), grant number 2018/29/N/ST8/00780.

References

Abbott, S., Hansen, C.M., 2008. Hansen solubility parameters in practice. Hansen-Solubility.com.
Agrawal, A., Saran, A.D., Rath, S.S., Khanna, A., 2004. Polymer 45 (25), 8603–8612.
Alves, P., Pinto, S., de Sousa, H.C., Gil, M.H., 2011. J. Appl. Polym. Sci. 122, 2302–2308.
Barton, A.F., 1991. CRC Handbook of Solubility Parameters and Other Cohesion Parameters, 2nd ed.
Bordes, C., Freville, V., Ruffin, E., Marote, P., Gauvrit, J.Y., Briançon, S., Lanteri, P., 2010. Int. J. Pharm. 383 (1–2), 236–243.
Castro, A.G.B., Lo Giudice, M.C., Vermonden, T., Leeuwenburgh, S.C.G., Jansen, J.A., van den Beucken, J.J.J.P., Yang, F., 2016. ACS Biomater. Sci. Eng. 2 (11), 2099–2107.
Chen, S., Li, R., Li, X., Xie, J., 2018a. Adv. Drug Deliv. Rev. 132, 188–213.
Chen, Y., Han, L., Ju, D., Liu, T., Dong, L., 2018b. Polymer 140, 47–55.
Clemons, T.D., Bradshaw, M., Toshniwal, P., Chaudhari, N., Stevenson, A.W., Lynch, J., Iyer, K.S., 2018. RSC Adv. 8 (18), 9661–9669.
Creighton, R.L., Phan, J., Woodrow, K.A., 2020. Sci. Rep. 10, 7949.
Cui, T., Yu, J., Li, Q., Wang, C.F., Chen, S., Li, W., Wang, G., 2020. Adv. Mater. 32 (32), 2000982.
Dulnik, J., Kolbuk, D., Denis, P., Sajkiewicz, P., 2018. Eur. Polym. J. 104, 147–156.
Fathona, I.W., Yabuki, A., 2013. J. Mater. Process. Technol. 213 (11), 1894–1899.
Gorecka, Z., Idaszek, J., Kolbuk, D., Choinska, E., Chlanda, A., Swieszkowski, W., 2020. Mat. Sci. Eng. C-Mater 114 pp.111072-1-11.
Greenfeld, I., Zussman, E., 2013. J. Polym. Sci. Part B: Polym. Phys. 51 (18), 1377–1391.
Hansen, C.M., 2007. Hansensolubility parameters: a user's handbook. CRC press.
Heo, M., Lee, S.J., Lee, D., Heo, D.N., Lee, J.S., Youn, Y.H., Kwon, I.K., 2017. Fiber Polym 18 (11), 2248–2254.
Huang, L., Arena, J.T., McCutcheon, J.R., 2016. J. Membr. Sci. 499, 352–360.
Jezek, J., Rides, M., Derham, B., Moore, J., Cerasoli, E., Simler, R., Perez-Ramirez, B., 2011. Adv. Drug Deliv. Rev. 63 (13), 1107–1117.
Jeznach, O., Kolbuk, D., Sajkiewicz, P., 2019. Polymers 11 (10) pp.1669-1-16.
Jiang, S., Duan, G., Schöbel, J., Agarwal, S., 2013. A. Greiner Compos. Sci. Technol 88, 57–61.
Kasuga, T., Obata, A., Maeda, H., Ota, Y., Yao, X., Oribe, K., 2012. J. Mater. Sci. Mater. Med. 23 (10), 2349–2357.
Kim, T.G., Park, T.G., 2008. Macromol. Rapid Commun. 29 (14), 1231–1236.
Kolbuk, D., Jeznach, O., Wrzecionek, M., Gadomska-Gajadhur, A., 2020. Polymers 12 (8) pp.1731-1-17.
Lee, J.B., Jeong, S.I., Bae, M.S., Yang, D.H., Heo, D.N., Kim, C.H., Kwon, I.K., 2011. Tissue Eng. Part A 17 (21-22), 2695–2702.
Liao, X., Hu, P., Agarwal, S., Greiner, A., 2020. Macromol. Mater. Eng. 305 (2), 1900629.
Lis, A., Szarek, D., Laska, J., 2013. Polim. Med. 43, 302–312.
Liu, X., Ma, P.X., 2009. Biomaterials 30, 4094–4103.
Monnier, X., Delpouve, N., Basson, N., Guinault, A., Domenek, S., Saiter, A., Dargent, E., 2015. Polymer 73, 68–78.
Mulky, E., Yazgan, G., Maniura-Weber, K., Luginbuehl, R., Fortunato, G., Bühlmann-Popa, A.M., 2014. Mater. Sci. Eng. C 45, 277–286.
Niemczyk, B., Sajkiewicz, P., Kolbuk, D., 2018. J. Neural Eng. 15 (5) pp.051002-1-15.
Nuuttila, M., 2018. Gel Permeation Chromatography Methods in the Analysis of Lactide-based Polymers.
Nyanhongo, G.S., Rodríguez, R.D., Prasetyo, E.N., Caparrós, C., Ribeiro, C., Sencadas, V., Guebitz, G.M., 2013. React. Funct. Polym. 73 (10), 1399–1404.
Pakravan, M., Heuzey, M.-C., Ajji, A., 2012. Biomacromolecules 13 (2), 412–421.
Petre, D.G., Kucko, N.W., Abbadessa, A., Vermonden, T., Polini, A., Leeuwenburgh, S.C., 2019. J. Mech. Behav. Biomed. Mater. 90, 472–483.
Ravichandran, R., Venugopal, J.R., Sundarrajan, S., Mukherjee, S., Sridhar, R., Ramakrishna, S., 2012. Nanotechnology 23 (38), 385102.
Regev, O., Reddy, C.S., Nseir, N., Zussman, E., 2013. Macromol. Mater. Eng. 298 (3), 283–291.
Sawawi, M., Wang, T.Y., Nisbet, D.R., Simon, G.P., 2013. Polymer 54 (16), 4237–4252.
Stoiljkovic, A., Agarwal, S., 2008. Macromol. Mater. Eng. 293 (11), 895–899.
Thieme, M., Agarwal, S., Wendorff, J.H., Greiner, A., 2011. Polym. Adv. Technol. 22 (9), 1335–1344.
Wasupalli, G.K., Verma, D., 2020. Mater. Sci. Eng. C 107, 110343.
Zaszczynska, A., Gradys, A., Sajkiewicz, P., 2020. Polymers 12 (11), pp. 2754-1-19.
Zhu, A., Lu, Y., Pan, Y., Dai, S., Wu, H., 2010. Colloids Surf. B Biointerfaces 76, 221–225.

polymers

MDPI

Article

Toward a Better Understanding of the Gelation Mechanism of Methylcellulose via Systematic DSC Studies

Beata Niemczyk-Soczynska, Pawel Sajkiewicz and Arkadiusz Gradys *

Institute of Fundamental Technological Research, Polish Academy of Sciences, Pawinskiego 5b St., 02-106 Warsaw, Poland; bniem@ippt.pan.pl (B.N.-S.); psajk@ippt.pan.pl (P.S.)
* Correspondence: argrad@ippt.pan.pl

Abstract: A methylcellulose (MC) is one of the materials representatives performing unique thermal-responsive properties. While reaching a critical temperature upon heating MC undergoes a physical sol-gel transition and consequently becomes a gel. The MC has been studied for many years and researchers agree that the MC gelation is related to the lower critical solution temperature (LCST). Nevertheless, a precise description of the MC gelation mechanism remains under discussion. In this study, we explained the MC gelation mechanism through examination of a wide range of MC concentrations via differential scanning calorimetry (DSC). The results evidenced that MC gelation is a multistep thermoreversible process, manifested by three and two endotherms depending on MC concentration. The occurrence of the three endotherms for low MC concentrations during heating has not been reported in the literature before. We justify this phenomenon by manifestation of three various transitions. The first one manifests water–water interactions, i.e., spanning water network breakdown into small water clusters. It is clearly evidenced by additional normalization to the water content. The second effect corresponds to polymer–water interactions, i.e., breakdown of water cages surrounded methoxy groups of MC. The last one is related to the polymer–polymer interactions, i.e., fibril hydrophobic domain formation. Not only did these results clarify the MC crosslinking mechanism, but also in the future will help to assess MC relevance for various potential application fields.

Keywords: methylcellulose; thermosensitive hydrogel; crosslinking; DSC

Citation: Niemczyk-Soczynska, B.; Sajkiewicz, P.; Gradys, A. Toward a Better Understanding of the Gelation Mechanism of Methylcellulose via Systematic DSC Studies. *Polymers* **2022**, *14*, 1810. https://doi.org/10.3390/polym14091810

Academic Editor: Hai-Feng (Frank) Ji

Received: 13 April 2022
Accepted: 26 April 2022
Published: 28 April 2022

1. Introduction

Smart or so-called stimuli-responsive materials are up-and-coming to a wide range of scientific and industrial fields such as textiles, the food industry, sensors, or materials for biomedical applications [1–6]. Excellent examples of such materials are piezoelectric electrospun nanofibers [7], self-repairing films [8], or hydrogels [9]. The latter represents a unique behavior by changes in swelling, degradation, or gelation as a response to external stimuli in a specified and adjustable manner. In this respect, these materials might respond to pH, electric and magnetic field, light, or temperature [10–12]. Among many stimuli-responsive hydrogel materials, methylcellulose (MC) displays a thermal responsive character and deserves special attention due to its interesting physical crosslinking nature [13]. MC belongs to the simplest cellulose derivative, where hydroxyl groups (-OH), initially present in cellulose, are partially substituted with methoxy groups (-OCH_3). Such modification makes cellulose amphiphilic, water-soluble, and exhibit thermally reversible crosslinking behavior near the physiological temperature, which is particularly interesting from the point of view of biopolymeric materials development [14,15].

MC aqueous solutions demonstrate physical crosslinking due to weak physical interactions which appear under particular temperature conditions. The lower critical solution temperature (LCST) defines the MC sol-gel transition. Depending on such parameters as substitution degree (DS), i.e., the average number of -OH groups substituted with -OCH_3

in glucose units; the heating rate; the presence of additives; and molecular mass (MW), LCST might appear in the range of 30–80 °C [16]. Below LCST, MC aqueous solution is in a sol state, where solvent–solvent and polymer–solvent interactions dominate in the solution. Above LCST, polymer–polymer interactions start to prevail resulting in the formation of 3D hydrogel structure. In many literature reports, e.g., [17,18], describing LCST crosslinking behavior, it is stated that MC crosslinking occurs through several stages in low- as well as high-concentrated MC solutions. Nevertheless, the nature of MC crosslinking mechanisms is still under debate. According to Chevillard et al. [17], the MC multistep crosslinking mechanism, derived from rheological measurements, is explained by the existence of three gels in the phase diagram. The first one is a low-temperature low concentration gel which forms through weak hydrophobic domains, the second one was found at high concentration and forms through appearance of crystallites, while the third one forms during phase separation [19]. More current studies [18,20] tend to accept new MC crosslinking mechanisms based on fibril formation. This theory assumes primary nucleation followed by coalescence of associated chains with further crystallization. For many years, the MC crosslinking mechanism was related to destruction of "water-cages" surrounding -OCH_3 groups and simultaneously interacting with -OH through hydrogen bonds followed by the formation of associated hydrophobic domains [21–24]. Other current studies of MC crosslinking mechanisms conducted by Yang et al. [25] confirmed this theory, but also showed that formation of associated hydrophobic domains of MC chains resembles fibril structures. The studies were confirmed with rheological measurements, accompanied with all-atom molecular dynamic simulations. Especially the latter method, as opposed to most of the experimental methods, allowed to detect and qualify the actual molecular interactions between MC chains and water molecules.

The MC crosslinking mechanism still remains unclear because providing adequate experimental conditions is usually challenging. MC shows reversible sol-gel transition, and the thermally crosslinked hydrogel is expected to return to the sol form upon cooling to the temperature below LCST. Nevertheless, upon the temperature change, the sol-gel reversible transition kinetics might vary and be unrepeatable [11]. Those differences depend on heating/cooling rate, thus, on the time allowed for assembly of the hydrogel network or its decomposition. The sol-gel transition of MC has been characterized using various methods, e.g., rheological measurements such as dynamic mechanical analysis [26], the inversion tube [27], or DSC [19,28].

Rheological measurements might give clear information about materials' crosslinking point when intersection of the storage modulus (G′) and the loss modulus (G″) curves results in clear dominance of G′ over G″ [29]. But there exist types of polymers, where crosslinking does not show any or clear enough the G′ and G″ intersection point. Some commercially available materials belong to this group including MC aqueous solutions. In such a case, depending on the measurement conditions: isothermal or in heating/cooling mode, detailed information on the maximum of crosslinking rate or crosslinking temperature might be determined from the time or temperature derivative of the G′ curve. Another difficulty in MC crosslinking measurements is ensuring hermetic conditions to avoid water evaporation resulting in unreliable results. Since rheological studies dedicated to hydrogels are based on plate or cone geometry, there are few methods to avoid water evaporation from the solution. One of them is using a solvent trap, e.g., silicone oil [30]. Nevertheless, in our previous studies [26], we observed that silicone oil partially reacted with MC hindering its crosslinking effect. Another method of avoiding water evaporation uses additional covering plates. Nevertheless, long measurements of MC crosslinking at higher temperatures results in partial drying out of MC solutions. In this regard, extra covering plates seem insufficient and although keeping the same parameters during measurements, obtained results might be biased.

Using the inversion tube method which ensures hermetic conditions, it is possible to indicate the sol-gel transition macroscopically determining mobility of crosslinked hydrogel after inverting the vial filled with the sample. When hydrogel does not flow after

a particular time, e.g., 10 s, it is considered to be crosslinked [31]. However, that method is not able to provide fundamental information about hydrogels structure after crosslinking time, i.e., if the hydrogel crosslinked partially or formed a fully crosslinked polymeric network. The method also cannot provide any details of the crosslinking mechanism.

DSC seems to overcome all of the above-mentioned limitations connected with alternative sol-gel transition characterization methods. The hermetic environment preventing water evaporation might be easily ensured by using special hermetic pans, while registered thermograms may show the thermal effects accompanying the structural changes that take place in MC solution in an isothermal or heating/cooling mode. With this method, it could be clearly answered if MC crosslinking mechanism resembles more crystallites formation or hydrophobic associations, the first of which is exo- and the second- endothermic effect.

Therefore, our studies are aimed at clarification of the MC thermal crosslinking mechanism by thorough and systematical analysis of DSC thermograms for a wide range of MC concentrations. Our results show several endotherms appearing during heating as well as cooling, which have never been noticed and discussed before. The dependencies of thermal effects on MC concentration were used for the interpretation of molecular mechanisms during heating and compared with the experiments and interpretations described in the literature. These results allowed us to assess MC relevance for such applications as in situ crosslinking scaffolds for tissue regeneration, cell, growth factor, or drug delivery systems.

2. Materials and Methods

2.1. Materials

MC (METHOCEL A15LV, Sigma Aldrich, St. Louis, MO, USA, viscosity of 10–25 mPa*s, 2% in H_2O (20 °C)) was used for hydrogel formation. A wide range of concentrations, i.e., 0.5–14 wt% was prepared according to the procedure reported in our previous publication [26].

2.2. DSC

Thermograms were registered using a power-compensation differential scanning calorimeter Pyris 1 DSC (Perkin-Elmer, Waltham, MA, USA). The scans were registered at non-isothermal conditions, at a constant heating/cooling rate of 2 K/min, in the temperature range from −5 to 100 °C, equilibrated isothermally for 5 min. The samples were loaded into dedicated stainless steel hermetically sealed pans that ensured no sample mass exchange with the environment, which was assured by checking the stability of sample mass. Preliminary measurements revealed a very low heat flow signal of the transitions; thus, special approaches were implemented. The pans were top filled resulting in the sample's mass in the range of 63–78 mg. Instead of the standard approach of the measurements against an empty reference pan, in order to improve the heat flow signal from the thermal effects, the samples were measured against a reference pan filled with demineralized water of comparable mass c.a. 70 mg. This provided comparable heat capacities of the sample and reference. Additionally, the heating/cooling cycle was repeated ten times and averaged to increase the heat flow-to-noise signal ratio, which further improved the quality of measurements. The same procedures were used previously in [26], however, in slightly narrower temperature range, i.e., −10–80 °C and less MC concentration points have been studied. The choice to increase the low temperature limit from −10 to −5 °C enabled to avoid unwanted occasionally occurring crystallization of water in the reference pan. The choice to increase the high temperature limit from 80 °C to 100 °C substantially improved analysis of the thermal effects. In current studies we also decided to increase the number of MC concentration points to reveal and better understand the effect of the MC concentration on the crosslinking mechanism.

DSC heating/cooling scans registered at a constant rate were subjected to the analysis of the MC content impact on the thermal effects, i.e., on each of several over-imposed peaks. It was essential to separate individual peaks reflecting their asymmetric shape. Much effort was put into the peaks' deconvolution (NLSF with tolerance 1×10^{-9}, standard Leveberg Marquardt iteration algorithm, the confidence level for parameters 95%), which

was realized using the asymmetric double sigmoid (ADS) function and the nonlinear least squares fitting method. Individual peaks were characterized by the parameters determined from ADS fitting and analysis as the peak area, representing the transition latent heat, ΔH, peak's maximum temperature position, T_p, and peak's full width at half maximum, FWHM, reflecting the transition rate (all of the ADS function parameters are included in the Supplementary Data). Before peak deconvolution, the scans were subtracted with a baseline approximated with 5th order polynomial. All the data were analyzed using Origin software.

3. Results

Figure 1 shows the heating and cooling scans for all used MC concentrations after baseline subtraction and normalization to MC mass. Several thermal effects might be observed: all endothermic during heating and all exothermic during cooling. In the heating mode, there are, generally, two maxima; however, for the lower MC content (below 9 wt%) there is discernible a low temperature (LT) shoulder, which evidences its maximum only at MC 1 wt% (Figure 2). Although this shoulder was registered by Nishinary et al. [32], it was not analyzed. The MC 1 wt% curve after peak deconvolution showing evident three maxima is presented in Figure 2a and an example of a heating scan with the LT shoulder is provided for the MC 3 wt% in Figure 2b. In Figure 1a it may be observed that increasing the MC content leads to shifting of the peaks toward lower temperatures and to a decrease of the LT shoulder. It was found that above 9 wt% of MC, high quality of fitting was approached using only two peaks corresponding to the medium-temperature (MT) and the high-temperature (HT) transitions without taking into account the LT peak (Figure 2c). In our previous studies [26], for the low MC concentration range, instead of the LT, we reported a low temperature exothermic effect followed by two endothermic effects, i.e., MT and HT. This conclusion resulted from much lower the high temperature limit (80 °C), which affected the baseline subtraction. Thus, current results provide also an update of these previously published in [26].

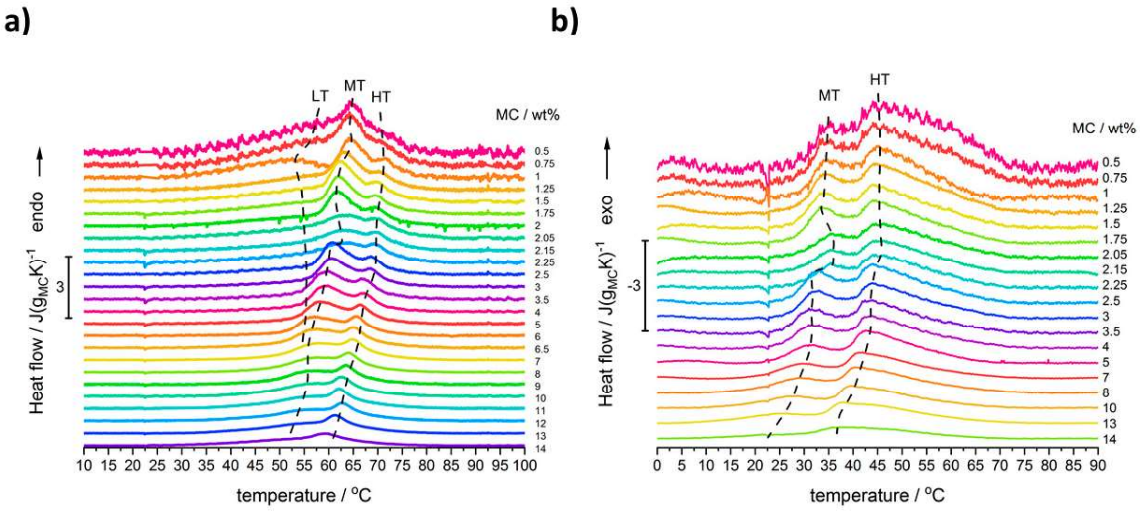

Figure 1. DSC scans registered during: (**a**) heating and (**b**) cooling for solutions of MC at mass content as indicated, normalized to MC mass. Curves shifted in Y-axis for clearness.

Moreover, in the MC content range (2–2.5 wt%), a peculiarity was found, which is seen as a deviation in the thermal effects from the general trend. In order to confirm this behavior, several samples were investigated using new solutions prepared with additional MC concentrations between 2 and 2.5 wt%. In Figure 1a,b, there are these additional three curves with lower intensities, indicated as 2.05, 2.15, and 2.25 wt%, confirming a shift in

peaks' position, when compared to the general trend. The details of this peculiarity will be discussed further.

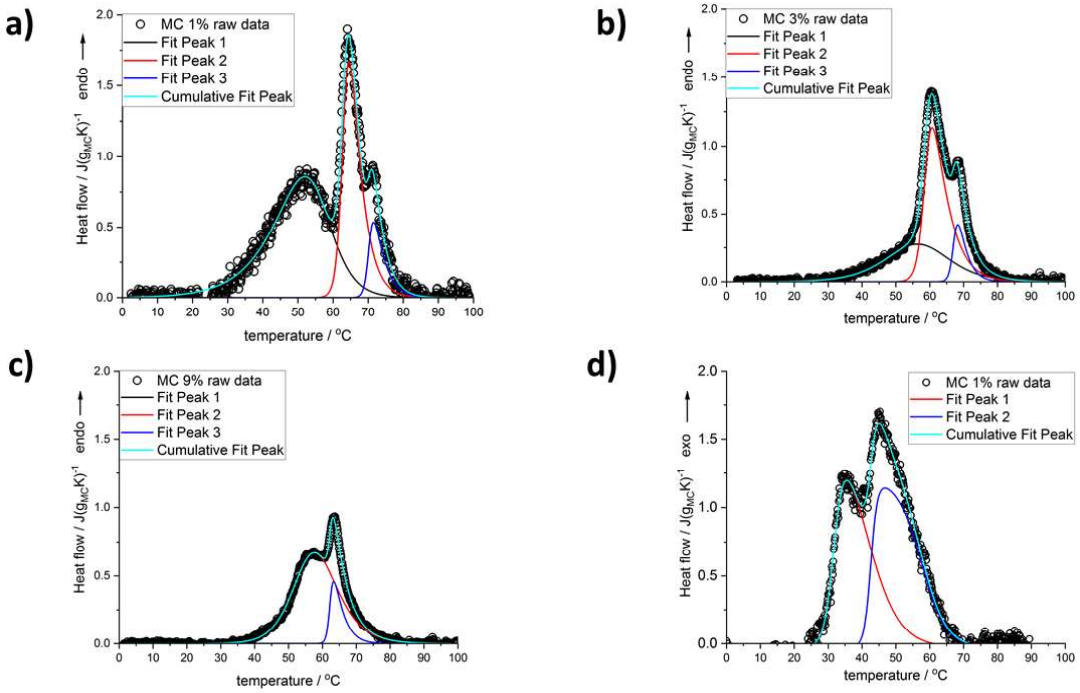

Figure 2. Deconvolution of the peaks seen on the scans registered for MC content: (**a**) 1 wt%, (**b**) 3 wt%, (**c**) 9 wt% during heating, and (**d**) 1 wt% during cooling.

In the case of the cooling mode, in the whole MC content range, the exothermic effects always showed two maxima, and the use of two peaks in the peak deconvolution approach was found sufficient. An example of the peak deconvolution of the MC 1 wt% cooling curve is presented in Figure 2d. Regarding the difference in the number of the peaks observed during heating and cooling, the question, if one of the peaks is hidden or excluded from the cooling measurement, may be explained by comparing the total heat measured during both modes. In Figure 3, the total heats are presented as normalized to the sample mass (Figure 3a) and to the MC content mass (Figure 3b). It may be seen that both heats are very similar in value and trend; however, the heat upon cooling is higher by 14 wt% than the heat upon heating. It is generally encountered that the latent heat of transition (ΔH, enthalpy change) increases with temperature. Thus, when upon heating, the transition takes place at a higher temperature than upon cooling, the heat upon heating would be expected higher. The reason behind the higher cooling heat value is not clear at the moment; however, from similar values and trends it may be rather expected that the heat of the LT peak, as observed during heating, is present but hidden in the thermal effects observed during cooling.

Moreover, in Figure 3a it is seen that the ΔH normalized to the sample mass, depends on MC content quite linearly. For cooling mode, there is a higher slope (0.16 J/g_{MC}) than for heating mode (0.12 J/g_{MC}); however, both dependencies do not extrapolate to zero at zero MC content but lead to similar ordinates, c.a. 0.213 J/g. It suggests that some of the heat may come from another source than MC, most probably from water. Another indication of this observation comes from Figure 3b presenting the transition heat normalized to the MC mass. It may be seen that in the lower MC content range, the values are very high reaching 45 and 50 J/g_{MC} and the heats decrease strongly before reaching plateaus at c.a.

15 and 18 J/g_{MC} for heating and cooling, respectively, which start from c.a. 7 wt% of MC. This constant transition heat indicates its dependence on MC only.

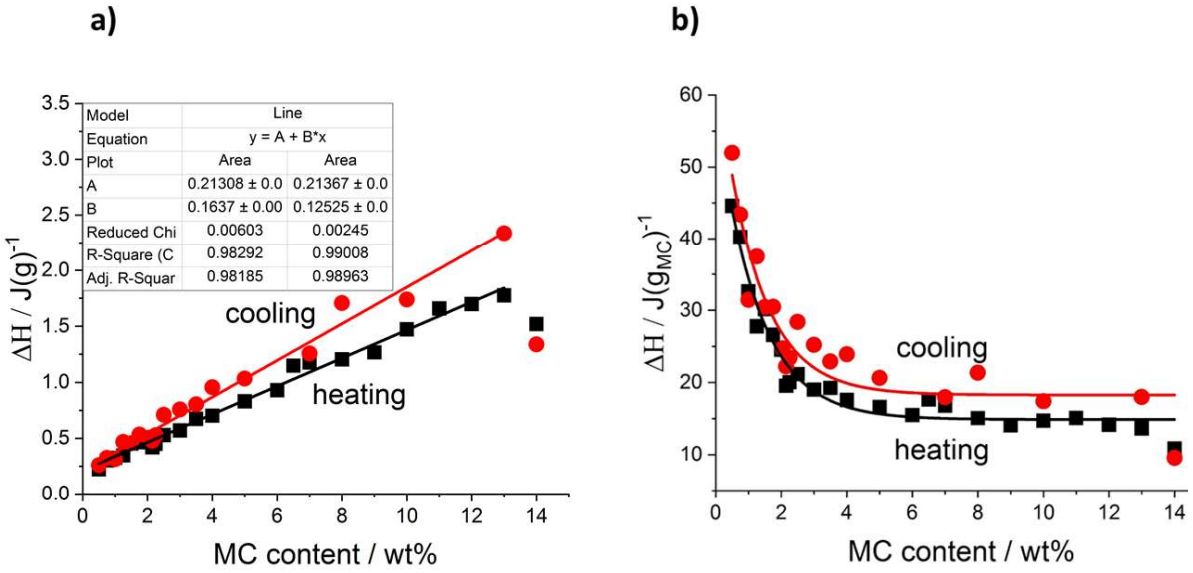

Figure 3. Total transition heat determined during heating and cooling: (**a**) normalized to the sample mass, (**b**) normalized to the MC content mass.

Further detailed analysis of the thermal effects relies on results obtained using the peak deconvolution approach. The results are presented as a function of MC content providing the peak parameters such as the temperature peak position (T_p), the ΔH, and the peak full width at half maximum (FWHM) in Figure 4 for heating and Figure 5 for cooling. With the increase of MC content, all the peaks' positions, generally, shift to a lower temperature (Figures 4a and 5a); however, the LT peak position in heating mode (Figure 4a) is the least affected. In Figure 4b, presenting the peaks' heat normalized to the sample mass, the heat of the MT and HT peaks generally increases dynamically with the MC content, while the LT peak heat shows a slow decrease. These observations indicate that the MT and HT peaks relate to the transitions involving MC molecules, while the LT peak relates to a transition involving water molecules only. This conclusion is supported by the domination of the LT peak over the MT and HT peaks in the lower MC concentration range. The LT peak heat being c.a. 0.22 J/g is similar to the value obtained with a linear approximation of the total heat in Figure 3a, decreases slowly to c.a. 0.15 J/g in the MC content range 6–8 wt% and above 8 wt% the peak is not detectable.

Another parameter analyzed is the peak's width, FWHM, describing the temperature range of the transition, which might be related to the transition rate. Thus, a higher transition rate could be expected for a narrow peak. It is shown in Figure 4c that the strongest changes with MC content are seen for the MT peak showing a four-fold increase. The widths of the LT and HT peaks were found the highest and lowest, respectively, and weakly dependent on MC content, except for a decrease at the lowest MC content in the case of the LT peak and a small increase at the highest MC content in the case of the HT peak.

Clear evidence that the LT peak's heat is probably related to water molecules only, and the heats of the MT and HT peaks are related to MC molecules, comes from the comparison of the heats using two different normalizations—to water and MC content (Figure 4d). It is seen that the LT peak's heat increases with the increase of water content (decrease of MC content) approaching the extrapolated value at zero MC content, which is practically the same irrespective of the type of normalization (Figures 3a and 4b,d).

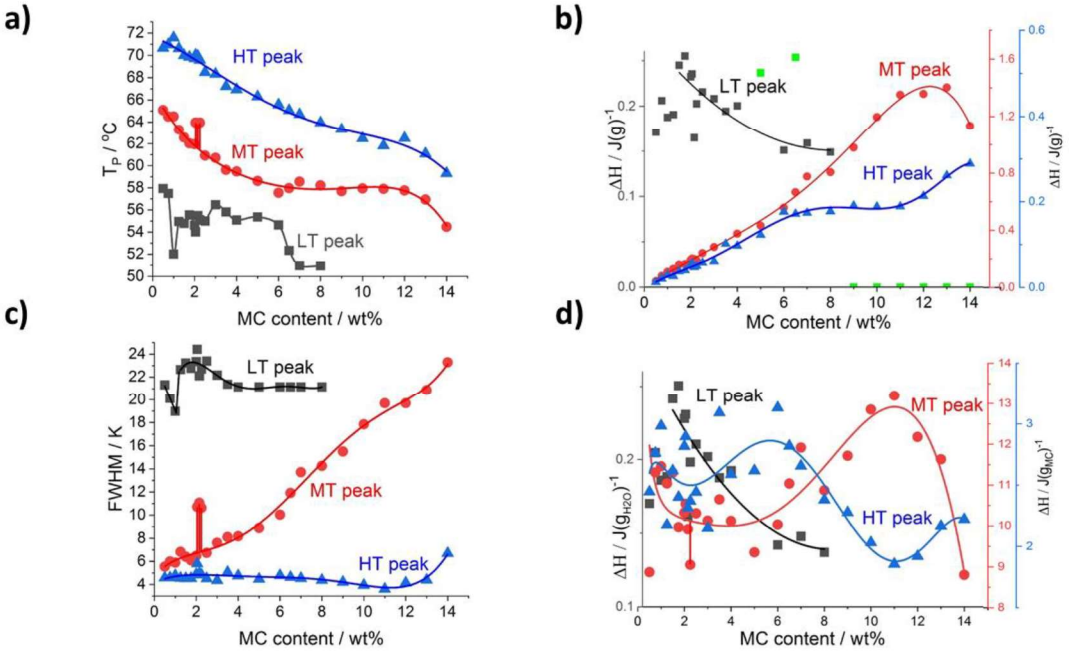

Figure 4. Deconvolution results for heating scans as a function of MC content: (**a**) peaks' temperature position and (**b**) peak's transition heat normalized to sample mass (**c**) peaks' width FWHM, (**d**) peak's heat normalized to H_2O (LT peak) and MC content (MT and HT peaks). Green points in (**b**) are LT peak area values excluded from the trend analysis due to high deviation.

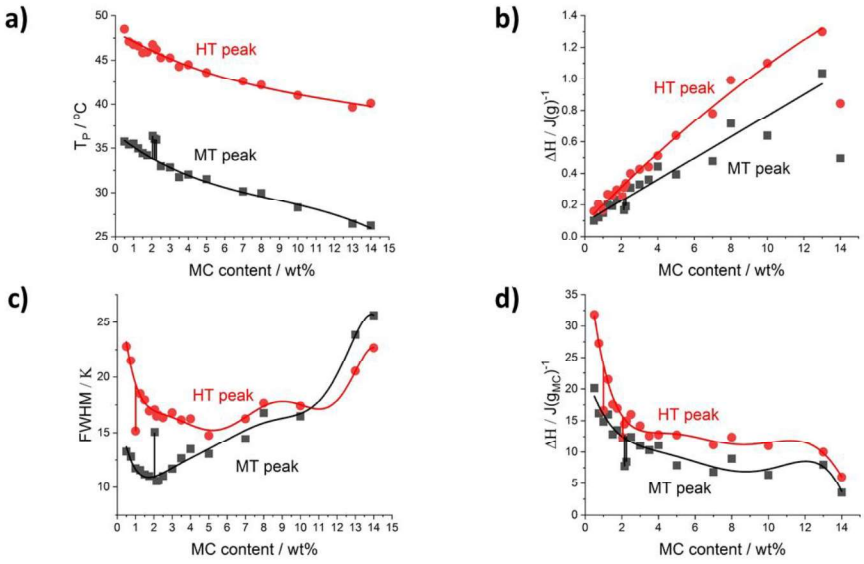

Figure 5. Deconvolution results for cooling scans as a function of MC content: (**a**) peaks' temperature position, (**b**) peak's transition heat normalized to sample mass, (**c**) peaks' full with at half maximum, (**d**) peak's heat normalized to MC mass.

In the case of MT and HT heats in J/g_{MC} (Figure 4d), there is a relatively large deviation in the lower MC content range, up to 7 wt%, making the analysis more difficult. In this

MC content range, the heat dependencies for both MT and HT peaks can be treated as more or less independent on MC content with c.a. 10 J/g_{MC} and 2.6 J/g_{MC} for the MT and HT peak, respectively. In the higher MC content range, above 7 wt%, both peaks show opposite behavior characterized by local extrema at 11 wt%. The heat of the MT peak reaches 13.4 J/g_{MC} at the maximum, and the heat of the HT peak decreases to 1.9 J/g_{MC} at the minimum.

In the cooling mode (Figure 5a), the temperature positions of the two peaks, MT and HT, follow similarly decreasing trends as in the heating mode (Figure 4a). The heats of both peaks normalized to sample mass increase with MC concentration, except for the last point (Figure 5b). Moreover, both heats extrapolated to zero MC content result in the same heat, c.a. 0.1 J/g (Figure 5b). In the case of the heats normalized to MC content (Figure 5d), in the lowest MC content range, both dependencies decrease steeply with MC content. These behaviors indicate that the LT peak as observed upon heating is included in the heat registered upon cooling. Furthermore, upon cooling there is an opposite and much different relation of the two heats than observed upon heating for the heats of the MT and HT peaks. First, upon cooling the HT peak, heat dominates over LT by 5 wt% (Figure 5b), while upon heating the MT peak, heat is four to seven times higher than the HT peak heat (Figure 4b). This indicates that comparing the two modes, the transitions rather proceed using different routes and mechanisms. Thus, the LT peak hidden under the cooling peaks treated as the MT and HT peaks makes the analysis not clear.

Regarding the peak width, FWHM, in cooling mode (Figure 5c), its dependence on MC content is more complex than that observed for heating mode (Figure 4c). The MT peak dependence increases strongly with the MC content, while the HT peak dependence is much flatter.

The peculiarity in the MC content range (between 2 and 2.5 wt%), was found related to changes in the MT peak. It clearly manifests as an increase in temperature position, T_p, an increase in the peak's width, FWHM, and a decrease in the transition heat, ΔH, observed in both the heating and cooling modes (indicated by vertical sticks in Figures 4 and 5). The peculiarity is most probably related to the slowing down of the MT transition rate. A deeper explanation of this phenomenon needs further investigation.

4. Discussion

A molecular interpretation of the phenomena during gelling of MC solutions based on the DSC results is given below. First, the endotherms visible on DSC scans might be an effect of polydispersity of MC molecular weight, heterogeneity of the MC substitution degree (SD) or inhomogeneous position of the -OCH_3, and multistep mechanism of MC crosslinking [32]. According to many literature reports, e.g., [18,20,25,33–38] we will discuss the last reason for the appearance of multiple effects of MC gelation.

The lack of exothermic effects during heating does not support the mechanism of the primary nucleation and subsequent crystals growth as proposed by Coughlin or Schmidt [18,20]. Since crystals formation is accompanied by exothermic effects, that are not revealed in our current studies, we dismiss this theory.

On the contrary, in line with our DSC results is the interpretation of the MC crosslinking mechanism based on the water cages' destruction and association of the fibril hydrophobic domains. Our interpretation is that the first transition manifested by the LT endotherm at c.a. 50 °C, is an effect of water–water interactions close to polymer chains, while the second-MT endotherm at c.a. 55–70 °C, and the third-HT one at c.a. 65–72 °C, correspond to the polymer–water and polymer–polymer interactions, respectively. The LT endotherm can be explained by the so-called thermal breaking of the hydration shell described widely in the literature [33–36]. Briefly, two different states of hydration water can coexist simultaneously at lower temperatures, i.e., shells of water formed around amphiphilic polymers. It is recalled that the amphiphilic character of MC results from the presence of both the hydrophilic -OH and the hydrophobic -OCH_3 groups in its molecular chain. One state of water is characteristic for low-concentrated solutions, where large water

aggregates surrounding polymer molecules appear using hydrogen bonds. According to Brovchenko et al. [33], in this state, called the spanning water network, hydrated structures are more ordered than that of bulk water. It was explained by molecular dynamics simulations [37] that the water dipole moment becomes oriented with polymer structure due to its much slower relaxation process. The second state of hydration water is characteristic for higher concentrated solutions, where small water clusters surround polar and nonpolar polymer groups. The transition from one state to the other takes place during heating and has been described as the thermal breaking of the hydration shell [36]. In detail, the process takes place, when the dominating spanning water network breaks down to form more disordered small clusters, which is a result of decreasing number of hydrogen bonds broken by temperature increase. This phenomenon is observed at c.a. 50 °C, which corresponds to the first endotherm observed in Figure 2a. From the literature, we know the H-bond rupture processes only, in which energy according to molecular simulation ranges from 0.2 to 4.2 kcal/mol [36]. According to our results, thermal breaking of the hydration shell might cease from c.a. 9 wt% (Figure 2c), meaning only small water clusters exist in the solution. The MT endotherm is interpreted as coming from polymer–water interactions and is an effect of dehydration of water from water cages that surround -OCH_3 groups and destruction of hydrogen bonds between water molecules and -OH groups in MC [38]. The confirmation of the described above theory found an additional confirmation in studies conducted by Yang et al. [25], where it was shown that the number of hydrogen bonds between MC chains and water molecules significantly decreases with increasing temperature.

After these processes, which correspond to the first stage of MC crosslinking, the MC chains start to reorganize forming intra- and intermolecular MC–MC hydrogen bonds and MC–MC hydrophobic interactions. Yang et al.'s analysis [25] of hydrophobic and hydrophilic solvent-accessible surface area (SASA) showed that at higher temperatures the contribution of hydrophobic interactions prevails over hydrogen bonding in the solution, resulting in MC chains aggregation. Bodvik et al. [39] explain that MC chains are arranged in fibril structures, to minimize the energy of the hydrogel system by a maximum decrease of the contact between -OCH_3 groups with water molecules. This process is observed as the HT endothermic peak.

Reproducibility of the thermal effects during several repetitive heating and cooling cycles proves reversible character of MC crosslinking process (Figure 2d). The HT exotherm observed during cooling may correspond to massive dissociation of fibril hydrophobic aggregates with simultaneous rearranging of water molecules into more ordered structures. As a result, the fibril network is gradually weakened [29]. Since the two processes occur together, more heat is exchanged resulting in the dominance of HT exotherm over MT [40] (Figure 5b,d). According to Li et al. [29], the LT exotherm occurs at the critical temperature, at which the hydrogel network has been completely interrupted. The LT exotherm is related to the formation of water molecules around nonpolar regions of MC polymeric chains also known as water cages and continues the formation of water–MC and water–water hydrogen bonds. These processes might occur simultaneously, since they are visible as one exothermic peak.

According to the current report of Bonetti et al. [11], but also the previous ones [41–43], an increase in MC concentration in the solution leads to a decrease in LCST. The higher MC concentration leads to an increase in the density of the polymer network in the solution leading to enhanced polymer–polymer interactions at lower temperatures [11,43,44]. It is the result of the decreased contribution of interaction between water–water over water–polymer and polymer–polymer interactions with the increased MC concentration (Figure 4a). The fact that for low MC concentrations, the LT and MT consume more heat than HT during heating (Figure 4b) may be explained by a large amount of energy needed to destroy strong hydrogen bonds between water molecules. This process is observed as LT. A lot of energy is also used to break the water cages surrounding -OCH_3 groups, resulting in a prevailing endothermic effect (MT). Li et al. [29] reported during heating most of the heat is used to destroy hydrogen bonds between water molecules and water cages. The

remaining heat is used for hydrophobic aggregation which is registered as HT. Li et al. showed that the heat needed for the formation of hydrophobic aggregates (observed as HT effect) is always lower than that needed for water cages breakdown (observed as LT effect), which is also observed in Figure 4b.

While heats are normalized to H_2O and MC mass, similarly to the normalization to the sample's mass, the LT effect decreases to 0 with MC contribution. The polymer phase contribution prevails over the solvent and there are diminished amounts of hydrogen bonds between water molecules.

The decrease of MT and HT exotherm heats during cooling with increasing MC concentration (Figure 5d) might be explained as follows. During cooling, the hydrophobic fibril network is decomposed and simultaneously water molecules start to form ordered structures. These two processes are visible as one HT exotherm. More heat is released during water molecules organization (formation of strong hydrogen bonds between water molecules) than by dissociation of weak hydrophobic interactions. While the increase of MC concentration leads to formation of fewer hydrogen bonds between water molecules, resulting in a significant decrease of released heat. The MT exotherm corresponds to water cages formation and further hydrogen bonds formation. The decrease of MT transition heat with MC increasing concentration has a similar reason as in the case of HT where fewer hydrogen bonds are formed at lower amounts of water molecules.

5. Conclusions

In our research, we justified the gelation mechanism of MC through systematic investigations of a wide range of MC concentrations using DSC measurements. The results prove the MC gelation is a multistep reversible process dictated by the LCST character. The gelation occurring during heating is manifested by three or two endotherms, depending on more or less diluted MC solutions, respectively. An additional first endothermic effect observed for lower concentrated MC solutions has not been described so far. It was evidenced by our results that this low-temperature effect corresponds to the interactions between water molecules, i.e., destruction of the spanning water network formed by hydrogen bonding into small water clusters. The other further two effects are related to polymer–water, which is destruction of "water cages" around -OCH_3 groups, and polymer–polymer interactions that is the formation of fibril-like hydrophobic domains.

We believe that our results allow a comprehensive understanding of the MC gelation mechanism and will be useful for further studies related to MC characteristics and designing MC-based hydrogel systems for a wide range of potential applications such as tissue engineering, drug-, cell-, growth factors delivery, and diagnostics.

Supplementary Materials: The following supporting information can be downloaded at: https://www.mdpi.com/article/10.3390/polym14091810/s1. Supplementary data present the dependencies of the pa-rameters of the asymmetric double sigmoid (ADS) functions, which were used for deconvolution of the peaks seen as the thermal effects during heating and cooling. Figure S1: The ADS functions parameters of the peaks determined for the heating mode. Figure S2: The ADS functions parameters of the peaks determined for the cooling mode.

Author Contributions: Conceptualization, B.N.-S., P.S. and A.G.; methodology, B.N.-S. and A.G.; validation, B.N.-S., A.G. and P.S.; writing—original draft preparation, B.N.-S., P.S. and A.G.; visualization, B.N.-S., A.G. and P.S.; supervision, P.S. and A.G.; project administration, B.N.-S., P.S. and A.G.; funding acquisition, B.N.-S. All authors have read and agreed to the published version of the manuscript.

Funding: This research was funded by the Narodowe Centrum Nauki (NCN), grant number 2018/29/N/ST8/00780. The article processing charge (APC) was covered by the Project no. POWR.03.02.00-00-1028/17-00 implemented under the Operational Programme Knowledge Education Development 2014–2020, co-financed by the European Social Fund.

Institutional Review Board Statement: Not applicable.

Informed Consent Statement: Not applicable.

Data Availability Statement: The data used in this article can be retrieved by private corresponding author request.

Conflicts of Interest: The authors declare no conflict of interest.

References

1. Niemczyk-Soczynska, B.; Dulnik, J.; Jeznach, O.; Kolbuk, D.; Sajkiewicz, P. Shortening of electrospun PLLA fibers by ultrasonication. *Micron* **2021**, *145*, 103066. [CrossRef] [PubMed]
2. Galaev, I.Y.; Mattiasson, B. 'Smart'polymers and what they could do in biotechnology and medicine. *Trends Biotechnol.* **1999**, *17*, 335. [CrossRef]
3. Qiu, Y.; Park, K. Environment-sensitive hydrogels for drug delivery. *Adv. Drug Deliv. Rev.* **2001**, *53*, 321. [CrossRef]
4. Hu, J.; Meng, H.; Li, G.; Ibekwe, S.I. A review of stimuli-responsive polymers for smart textile applications. *Smart Mater. Struct.* **2012**, *21*, 053001. [CrossRef]
5. Whitcombe, M.J.; Alexander, C.; Vulfson, E.N. Smart Polymers for the Food Industry. *Trends Food Sci. Technol.* **1997**, *8*, 140. [CrossRef]
6. Dias, Y.J.; Robles, J.R.; Sinha-Ray, S.; Abiade, J.; Pourdeyhimi, B.; Niemczyk-Soczynska, B.; Kołbuk, D.; Sajkiewicz, P.; Yarin, A.L. Solution-blown poly(hydroxybutyrate) and ε-poly-l-lysine submicro- and microfiber-based sustainable nonwovens with antimicrobial activity for single-use applications. *ACS Biomater. Sci. Eng.* **2021**, *7*, 3980–3992. [CrossRef]
7. Zaszczynska, A.; Sajkiewicz, P.; Gradys, A.; Tymkiewicz, R.; Urbanek, O.; Kolbuk, D. Influence of process-material conditions on the structure and biological properties of electrospun polyvinylidene fluoride fibers. *Bull. Pol. Acad. Sci. Tech. Sci.* **2020**, *68*, 627–633.
8. Guo, M.; Chen, L.; Fang, T.; Wang, R.; Nuraje, N.; Brodelius, P.E. Synthesis, properties and applications of self-repairing carbohydrates as smart materials via thermally reversible DA bonds. *Polym. Adv. Technol.* **2021**, *32*, 1026–1037. [CrossRef]
9. Niemczyk, B.; Sajkiewicz, P.; Kolbuk, D. Injectable hydrogels as novel materials for central nervous system regeneration. *J. Neural Eng.* **2018**, *15*, 051002. [CrossRef]
10. Niemczyk-Soczynska, B.; Zaszczynska, A.; Zabielski, K.; Sajkiewicz, P. Hydrogel, electrospun and composite materials for bone/cartilage and neural tissue engineering. *Materials* **2021**, *14*, 6899. [CrossRef]
11. Bonetti, L.; De Nardo, L.; Farè, S. Thermo-responsive methylcellulose hydrogels: From design to applications as smart biomaterials. *Tissue Eng. Part B Rev.* **2021**, *27*, 486–513. [CrossRef] [PubMed]
12. Schmaljohann, D. Thermo-and pH-responsive polymers in drug delivery. *Adv. Drug Deliv. Rev.* **2006**, *58*, 1655. [CrossRef] [PubMed]
13. Qiu, X.; Hu, S. "Smart" materials based on cellulose: A review of the preparations, properties, and applications. *Materials* **2013**, *6*, 738–781. [CrossRef] [PubMed]
14. Nishida, K.; Morita, H.; Katayama, Y.; Inoue, R.; Kanaya, T.; Sadakane, K.; Seto, H. Salting-out and salting-in effects of amphiphilic salt on cloud point of aqueous methylcellulose. *Process Biochem.* **2017**, *59*, 52–57. [CrossRef]
15. Doelker, E. Cellulose derivatives. In *Biopolymers I. Advances in Polymer Science*; Langer, R.S., Peppas, N.A., Eds.; Springer: Berlin/Heidelberg, Germany, 2007; Volume 3, pp. 154–196.
16. Wu, D.; Cheng, J.; Su, X.; Feng, Y. Hydrophilic modification of methylcellulose to obtain thermoviscosifying polymers without macro-phase separation. *Carbohydr. Polym.* **2021**, *260*, 117792. [CrossRef] [PubMed]
17. Chevillard, C.; Axelos, M.A.V. Phase separation of aqueous solution of methylcellulose. *Colloid Polym. Sci.* **1997**, *275*, 537–545. [CrossRef]
18. Coughlin, M.L.; Liberman, L.; Ertem, S.P.; Edmund, J.; Bates, F.S.; Lodge, T.P. Methyl cellulose solutions and gels: Fibril formation and gelation properties. *Prog. Polym. Sci.* **2021**, *112*, 101324. [CrossRef]
19. Takahashi, M.; Shimazaki, M.; Yamamoto, J. Thermoreversible gelation and phase separation in aqueous methyl cellulose solutions. *J. Polym. Sci. B Polym. Phys.* **2001**, *39*, 91–100. [CrossRef]
20. Schmidt, P.W.; Morozova, S.; Owens, P.M.; Adden, R.; Li, Y.; Bates, F.S.; Lodge, T.P. Molecular weight dependence of methylcellulose fibrillar networks. *Macromolecules* **2018**, *51*, 7767–7775. [CrossRef]
21. Joshi, S.C.; Lam, Y.C. Modeling heat and degree of gelation for methyl cellulose hydrogels with NaCl additives. *J. Appl. Polym. Sci.* **2006**, *101*, 1620–1629. [CrossRef]
22. Haque, A.; Morris, E.R.; Richardson, R.K. Polysaccharide substitutes for gluten in non-wheat bread. *Carbohydr. Polym.* **1994**, *25*, 337–344. [CrossRef]
23. Li, L.; Thangamathesvaran, P.M.; Yue, C.Y.; Tam, K.C.; Hu, X.; Lam, Y.C. Gel Network Structure of Methylcellulose in Water. *Langmuir* **2001**, *17*, 8062–8068. [CrossRef]
24. Kobayashi, K.; Huang, C.I.; Lodge, T.P. Thermoreversible gelation of aqueous methylcellulose solutions. *Macromolecules* **1999**, *32*, 7070–7077. [CrossRef]
25. Yang, Y.; Wu, W.; Liu, H.; Xu, H.; Zhong, Y.; Zhang, L.; Mao, Z. Aggregation behaviors of thermo-responsive methylcellulose in water: A molecular dynamics simulation study. *J. Mol. Graph.* **2020**, *97*, 107554. [CrossRef]

26. Niemczyk-Soczynska, B.; Gradys, A.; Kolbuk, D.; Krzton-Maziopa, A.; Sajkiewicz, P. Crosslinking kinetics of methylcellulose queous solution and its potential as a scaffold for tissue engineering. *Polymers* **2019**, *11*, 1772. [CrossRef]
27. Martin, B.C.; Minner, E.J.; Wiseman, S.L.; Klank, R.L.; Gilbert, R.J. Agarose and methylcellulose hydrogel blends for nerve regeneration applications. *J. Neural Eng.* **2008**, *5*, 221. [CrossRef]
28. Fahad, M.; Khan, M.A.; Gilbert, M. Investigation of Thermal Gel Formation of Methylcellulose in Glycols Using DSC and XRD. *Gels* **2021**, *7*, 205. [CrossRef]
29. Li, L.; Shan, H.; Yue, C.Y.; Lam, Y.C.; Tam, K.C.; Hu, X. Thermally induced association and dissociation of methylcellulose in aqueous solutions. *Langmuir* **2002**, *18*, 7291–7298. [CrossRef]
30. Sandoval, M.L.; Camerucci, M.A. Rheological behavior of aqueous mullite-albumin-methylcellulose systems. *Ceram. Int.* **2017**, *43*, 7243–7252. [CrossRef]
31. Braim, S.A.; Shakesheff, K.M.; Saunders, B.R.; Alexander, C. Thermoresponsive magnetic colloidal gels via surface-initiated polymerisation from functional microparticles. *J. Mater. Chem. B* **2016**, *4*, 962–972. [CrossRef]
32. Nishinari, K.; Hofmann, K.E.; Moritaka, H.; Kohyama, K.; Nishinari, N. Gel-sol transition of methylcellulose. *Macromol. Chem. Phys.* **1997**, *198*, 1217–1226. [CrossRef]
33. Brovchenko, I.; Oleinikova, A. Which properties of a spanning network of hydration water enable biological functions? *Chem. Phys. Chem.* **2008**, *9*, 2695–2702. [CrossRef] [PubMed]
34. Xu, H.; Dill, K.A. Water's hydrogen bonds in the hydrophobic effect: A simple model. *J. Phys. Chem.* **2005**, *109*, 23611–23617. [CrossRef] [PubMed]
35. Oleinikova, A.; Brovchenko, I.; Smolin, N.; Krukau, A.; Geiger, A.; Winter, R. Percolation transition of hydration water: From planar hydrophilic surfaces to proteins. *Phys. Rev. Lett.* **2005**, *95*, 247802. [CrossRef]
36. Brovchenko, I.; Krukau, A.; Smolin, N.; Oleinikova, A.; Geiger, A.; Winter, R. Thermal breaking of spanning water networks in the hydration shell of proteins. *J. Chem. Phys.* **2005**, *123*, 224905. [CrossRef] [PubMed]
37. Sheu, S.Y.; Liu, Y.C.; Zhou, J.K.; Schlag, E.W.; Yang, D.Y. Surface topography effects of globular biomolecules on hydration water. *J. Phys. Chem.* **2019**, *123*, 6917–6932. [CrossRef]
38. Bonetti, L.; De Nardo, L.; Variola, F.; Fare, S. In-situ Raman spectroscopy: An effective technique for the quantification of LCST transition of methylcellulose hydrogels. *Mater. Lett.* **2020**, *274*, 128011. [CrossRef]
39. Bodvik, R.; Dedinaite, A.; Karlson, L.; Bergstrom, M.; Baverback, P.; Pedersen, J.S.; Edwards, K.; Karlsson, G.; Varga, I.; Claesson, P.M. Aggregation and network formation of aque-ous methylcellulose and hydroxypropulmethylcellulose solutions. *Colloids Surf.* **2010**, *354*, 162–171. [CrossRef]
40. Lv, R.; Luan, T.; Yu, F.; Zhang, H. Rheological and micro-DSC studies on the aqueous mixtures of methylcellulose and ammonium poly (3-thiophene acetic acid). *Carbohydr. Polym.* **2011**, *85*, 862–868. [CrossRef]
41. Sarkar, N. Thermal gelation properties of methyl and hydroxypropyl methylcellulose. *J. Appl. Polym. Sci.* **1979**, *24*, 1073–1087. [CrossRef]
42. Sanz, T.; Fernandez, M.A.; Salvador, A.; Munoz, J.; Fiszman, S.M. Thermogelation properties of methylcellulose (MC) and their effect on a batter formula. *Food Hydrocoll.* **2005**, *19*, 141–147. [CrossRef]
43. Chen, C.H.; Tsai, C.C.; Chen, W.; Mi, F.L.; Liang, H.F.; Chen, S.C.; Sung, H.W. Novel living cell sheet harvest system composed of thermoreversible methylcellulose hydrogels. *Biomacromolecules* **2006**, *7*, 736–743. [CrossRef] [PubMed]
44. Nishinari, K. Sol-gel transition of biopolymer dispersions. *Macromol. Symp.* **2000**, *159*, 205–214. [CrossRef]

RSC Advances

PAPER

View Article Online
View Journal | View Issue

Cite this: *RSC Adv.*, 2022, **12**, 26882

A methylcellulose/agarose hydrogel as an innovative scaffold for tissue engineering

Beata Niemczyk-Soczynska, *[a] Arkadiusz Gradys, [a] Dorota Kolbuk, [a] Anna Krzton-Maziopa, [b] Piotr Rogujski, [c] Luiza Stanaszek, [c] Barbara Lukomska [c] and Pawel Sajkiewicz [a]

In situ crosslinked materials are the main interests of both scientific and industrial research. Methylcellulose (MC) aqueous solution is one of the representatives that belongs to this family of thermosensitive materials. At room temperature, MC is a liquid whereupon during temperature increase up to 37 °C, it crosslinks physically and turns into a hydrogel. This feature makes it unique, especially for tissue engineering applications. However, the crosslinking rate of MC alone is relatively slow considering tissue engineering expectations. According to these expectations, the crosslinking should take place slowly enough to allow for complete injection and fill the injury avoiding clogging in the needle, and simultanously, it should be sufficiently fast to prevent it from relocation from the lesion. One of the methods to overcome this problem is MC blending with another substance that increases the crosslinking rate of MC. In these studies, we used agarose (AGR). These studies aim to investigate the effect of different AGR amounts on MC crosslinking kinetics, and thermal, viscoelastic, and biological properties. Differential Scanning Calorimetry (DSC) and dynamic mechanical analysis (DMA) measurements proved that AGR addition accelerates the beginning of MC crosslinking. This phenomenon resulted from AGR's greater affinity to water, which is crucial in this particular crosslinking part. *In vitro* tests, carried out using the L929 fibroblast line and mesenchymal stem cells (MSCs), confirmed that most of the hydrogel samples were non-cytotoxic in contact with extracts and directly with cells. Not only does this type of thermosensitive hydrogel system provide excellent mechanical and biological cues but also its stimuli-responsive character provides more novel functionalities for designing innovative scaffold/cell delivery systems for tissue engineering applications.

Received 3rd August 2022
Accepted 15th September 2022

DOI: 10.1039/d2ra04841h

rsc.li/rsc-advances

1 Introduction

Stimuli-responsive materials have gained attention in many fields of science.[1] Under appropriate external stimulation, these smart materials might present changes in wettability, swelling behavior, electrical conductivity or show reversible sol–gel transition.[2–5] Such features have been used in smart hydrogel development, and at the same time, have met the criteria of tissue engineering requirements. Hydrogels are a group of polymers that absorb a large amount of water under particular stimulation in an aqueous environment. They are very attractive from a tissue engineering perspective due to the 3-dimensionality of the hydrogel network and physical resemblance to living tissues.[1] The application of ultraviolet (UV) radiation, pH, and temperature change are the most common examples of factors inducing crosslinking of stimuli-responsive hydrogels. For instance, UV light might stimulate *in situ* crosslinking of gelatin methacryloyl (GelMA), which serves as a scaffold in many tissue engineering fields. Although UV light can repidly and easily crosslink hydrogels, there is a risk of generating free radicals, resulting in cell mutations and the occurrence of damage in cell DNA.[6] Another example of stimuli-responsive hydrogels with an application as a scaffold in tissue engineering is sodium alginate, which can be stimulated by pH. Despite its natural origin, good biocompatibility, ease of chemical modification, and attractive release profile of tissue growth factors, it has also shown poor mechanical properties resulting in instability in the physiological environment.[7,8] Interesting stimuli-responsive materials are natural-based injectable thermosensitive hydrogels, in which crosslinking is stimulated with the change of temperature. Such materials are solutions in ambient conditions, but when temperature increases or decreases, the hydrogel is formed as an effect of physical interactions.[9] Temperature-responsive systems which crosslink during heating are of particular interest because they

[a]*Institute of Fundamental Technological Research, Polish Academy of Sciences, Pawinskiego 5b St., 02-106 Warsaw, Poland. E-mail: bniem@ippt.pan.pl*
[b]*Faculty of Chemistry, Warsaw University of Technology, Noakowskiego 3 St., 00-664 Warsaw, Poland*
[c]*NeuroRepair Department, Mossakowski Medical Research Institute, Polish Academy of Sciences, 5 Pawinskiego St., 02-106 Warsaw, Poland*

might be injected through a syringe to the targeted tissue, where it undergoes *in situ* crosslinking.[10,11] The following natural-based hydrogels have been used in tissue engineering: Xyloglucan, Chitosan as well as Hyaluronic acid (HA) derivatives. Xyloglucan mixed with poly-D-lysine was used as a scaffold for Central Nervous System (CNS) regeneration and showed good axon response in direct contact.[12] However, it crosslinks at *ca.* 20 °C, so there is a risk of clogging inside the needle during injection. Chitosan and HA alone are not thermosensitive; therefore, they need to be mixed with other thermosensitive materials. For instance, chitosan/glycerophosphate (GP) composite provides thermal sensitivity and a fast crosslinking rate. Nevertheless, in the end, this system occurred to be cytotoxic.[13] Whereas, HA was mixed with Pluronic, showing appropriate biocompatibility, release profile, and crosslinking rate as drug delivery systems.[14] Despite the better functionality of such a blend, it was reported that HA might degrade rapidly in physiological conditions and its mechanical properties might be not sufficient from the perspective of tissue engineering requirements.[15] Additionally, HA's synthesis is very complicated and expensive, making the material unattractive from an economic point of view.[16]

Obviously, tissue engineering needs a material, which crosslinks at the physiological temperature, is biocompatible, non-toxic for cells, stable under physiological conditions, and displays adequate mechanical properties. High quality and favorable prices of such an approach would also be beneficial. In this respect, an interesting material seems to be methylcellulose aqueous solution (MC), which alone demonstrates thermosensitive behavior. The MC is methylated cellulose, in which some of the hydroxyl groups (–OH) are replaced with the methoxy groups ($-OCH_3$). The presence of methoxy groups prevents crystallization, making MC water-soluble.[17] There were plenty of proposed MC crosslinking mechanisms such as micelle formation,[18] phase separation,[19] nucleation and crystallization,[20,21] or hydrophobic fibril-like domains formation.[22,23] The last one said that MC undergoes thermal reversible crosslinking throughout temperature increase, resulting in hydrophobic interactions formation. The temperature of crosslinking depends on the degree of substitution with the desired value near 37 °C.[24] The two-step crosslinking mechanism of MC involves two distinct stages. Briefly, the 1st stage assumes destruction of "water cages" located in the vicinity of nonpolar functional groups. In this instance, nonpolar groups $-OCH_3$ are considered.[25] Generally, this phenomenon is a specific type of "dehydration" leading to $-OCH_3$ groups exposure as well as their self-organization, which is terminated with the formation of hydrophobic interactions. The 2nd stage assumes creation of a hydrophobic 3-dimensional network. Recently a new MC crosslinking mechanism regarding fibril formation has been discovered.[20,26] While temperature increases, MC chains spontaneously self-aggregate and form hydrophobic fibrils. Detailed mechanism of hydrophobic fibril formation has been clarified by Bodvik *et al.*[27] who indicated that such arrangement of MC chains decreases the energy of the hydrogel system by the highest possible level of minimization of the $-OCH_3$ and water interactions.

MC offers many advantages, *i.e.*, it is non-toxic for cells, stable in physiological environments, and cell culture media. MC's mechanical properties might be easily tailored, by adjusting its concentration, to make it suitable for various native tissues.[28] Contrary to HA, MC is also attractive from an economic point of view. All these features make MC an attractive candidate for tissue engineering applications.[9] On the other hand, a pure MC solution has some limitations: the first one is a crosslinking rate which is not fast enough for tissue engineering and drug delivery system requirements. The second one is its non-cell-adhesive nature.[18]

To overcome those limitations, MC might be blended with other materials that can act as an MC "crosslinking initiator." In this instance, the "crosslinking initiation" relies on faster dehydration of water surrounding $-OCH_3$ groups. To overcome the issue of MC's poor cell adhesivity, MC might be blended with bioactive proteins (*e.g.*, laminin) or with polymers increasing cell adhesion, *e.g.*, agarose (AGR).[29,30]

The authors' idea is to fabricate such a composite consisting of MC and AGR aqueous solutions. AGR is a purified linear galactan hydrocolloid derived from marine algae that consist of repeating agarobiose disaccharide units.[30] This polymer also belongs to the thermosensitive hydrogels group, but its crosslinking occurs during cooling below room temperature by the aggregation mechanism, similar to gelatin. The melting point occurs near the physiological temperature; hence it is complicated to use its pure form as an *in situ* crosslinking scaffold for tissue engineering. On the other hand, AGR is a great candidate to obtain thermosensitive blends. According to,[30] AGR accelerates MC crosslinking by its additional dehydration, leading to improvement of hydrophobic interactions between the polymeric chains that considerably enhances MC's mechanical properties. An additional part of the MC crosslinking mechanism in the MC/AGR system might concern interactions between AGR and MC three-dimensional network.[31] Since the blending of MC and AGR solutions has been reported in only a few publications,[30] the cross-linking mechanism of the MC/AGR system is not yet fully known.

Consequently, our studies aimed to investigate and clarify the effect of AGR addition on MC crosslinking's mechanism and kinetics, the mechanical properties of the final hydrogel, and the biological properties at *in vitro* conditions.

2 Experimental

2.1 Preparation of MC aqueous solution

Methylcellulose (MC, METHOCEL A15LV, Sigma Aldrich) and agarose (SeaPrepR, Lonza) solutions were prepared at various weight concentrations and proportions. At first 1, 2.5, 3, and 5 wt% (w/w) of MC water solutions were prepared and stirred overnight. The final solutions were stored at 4 °C overnight to ensure proper hydration of the polymer.[32] AGR powder was dispersed in hot water at 80 °C according to,[30] after which the solution was added to the MC solution in the appropriate ratio. The 1, 2.5, and 5 wt% of MC solutions were mixed with AGR

solutions at the wt. ratio of 1 : 0.3; 1 : 0.7 and 1 : 1. The 3 wt% MC was mixed with AGR at the wt. the ratio of 1 : 1.

For purposes of DSC studies, it was necessary to prepare more MC/AGR concentrations, where MC and AGR were mixed in a wt ratio of 1 : 1, at the following concentrations: 1, 1.25, 1.5, 1.75, 2, 2.05, 2.15, 2.25, 2.5, 3, 4, 5 wt%.

2.2 DSC

Differential scanning calorimetry measurements were conducted using the Pyris 1 DSC PerkinElmer (USA, Waltham) calorimeter. The measurements were conducted at the same conditions as in our previous studies,[23] *i.e.*, non-isothermally, in the temperature range of −5–100 °C, and at the constant heating–cooling rate of 2 K min^{-1}. Each sample was placed into a dedicated hermetic pan to avoid water evaporation. In order to improve the heat flow signal to noise ratio, the sample mass was high (in the range of *ca.* 60–80 mg), the measurements were carried out against a reference water sample of a comparable mass, and the scans were run for 10 cycles and averaged.

The MC thermal effects were normalized to MC mass and subjected to a deconvolution procedure using Nonlinear Least Squares Fitting with an Asymmetric Double Sigmoid Function (ADS) in order to distinguish each peak that comes from a particular crosslinking stage. For fitting Origin2021b software was used.

2.3 Rheology

The viscoelastic properties, including storage modulus (G') and loss modulus (G''), were derived from the MC/AGR water solutions. For this purpose, DMA, MCR 301 rheometer (Anton Paar Physica, Germany) was used. Kinetics of crosslinking was studied based on G' measurements of solutions at 37 °C under an oscillatory shear regime. All measurements were carried out in a limited time range. Prior to measurement, the MC/AGR solutions were heated in the DMA setup from 20 °C to 37 °C, at the heating rate of 2 K min^{-1}. A cone-plate geometry with a diameter of 39.9 mm, an angle of 0.989°, and truncation of 47 μm was used in every measurement. The geometry was equipped with an extra solvent trap, preventing water evaporation from the solution. A small-amplitude sinusoidal deformation (0.1% strain and 1 Hz frequency) was applied. For the sake of statistics, measurements for each MC/AGR concentration were repeated 3–4 times. The obtained G' values were approximated using the sinusoidal type of function, including Logistic and Biphasic Dose-response functions. Subsequently, the fitting functions were extrapolated to achieve the saturation plateau at a longer time range and then averaged. Two methods have determined the crosslinking kinetics: from the time derivative of the averaged G' and the crosslinking rate, k. The first method allowed defining the maximum rate of G' growth, as the hydrogel's maximum crosslinking rate. The dG'/dt integration allowed to determine the final storage modulus. The second one assumed crosslinking rate k determination from the half transition time, at 50% of crosslinking and the beginning of crosslinking, (t_{onset}). The t_{onset}, was determined as the tangent intersection to the baseline before starting the thermal effect and the tangent to the rising part of the thermal effect at 37 °C. The transition rate, k, was determined as the reciprocal of the time of the half transition with respect to its t_{onset}.

2.4 Biocompatibility analysis

2.4.1 Sample preparation. Before making solutions, MC bulk and AGR bulk were sterilized with ultraviolet light (UV). The UV sterilization took place for 30 min, and during that time, the bulk was slightly shaken every 10 min to assure equal sterilization. Both MC and AGR solutions were prepared in PBS, to avoid hyperosmotic stress, at the same concentrations, described in subsection 2. Additionally, two MC/AGR concentrations, *i.e.*, 3/3 wt% and 5/1.5 wt% were dissolved in DMEM for additional comparison. Before cell seeding, hydrogels were kept for 72 h in the incubator at 37 °C to induce entire crosslinking of the MC/AGR solution.

2.4.2 Fibroblasts culture. *In vitro* tests were carried out with the use of the L929 line of fibroblasts (Sigma Aldrich). Cells were cultivated in 75 cm^2 flasks containing a medium prepared of High Glucose Dulbecco's Modified Eagle's Medium (DMEM), 10% fetal bovine serum (FBS), and 1% antibiotics. Cells were incubated in a 5% CO_2 environment at a constant temperature of 37 °C. Harvesting of the cells took place in 70–80% confluent flasks. In the first step cells in phosphate buffer saline (PBS). After that step, 5 ml of 0.05% of trypsin solution was added to the cells and placed in the incubator for a few minutes. Then the flask was tapped delicately in order to detach the cells. After obtaining harvested cells, 10 ml of culture medium was added and centrifuged. The centrifugation was carried out at ambient temperature conditions, at 100 × g, for 5 min. To obtain the required cell density, the pellet was resuspended with a culture medium and then diluted.

2.5 Fibroblasts evaluation

2.5.1 Presto blue cytotoxicity tests on extracts. In order to obtain extracts for the cytotoxicity test, 5 samples of each hydrogels type were placed in a 48-well plate. They were immersed in 500 μL of culture medium per well, kept at 37 °C, and gently stirred for 24 h. For reference, along with wells with samples, 5 wells without hydrogel were filled with the medium as well. At the same time L929 cell suspension was seeded into another 48-well plate in the same amount of wells as sample extracts plus control with density 1×10^4 cells per well and put in an incubator for 24 h. The wells filled with DMEM only served as reference. After that time the culture medium from cell-seeded wells was replaced with material extracts and the plate was placed in the incubator for another 24 h.

Presto blue assay assumed reduction of resazurin reagents to a resorufin which was the main cell viability compound. The result of this reduction was changing colour from blue to fluorescent red. This assay allowed for quantitative and visual analysis through absorbance and optical evaluation of fluorescent results of resorufin reduction. After 1 and 3 days of cultivation, DMEM was removed and each well was filled with 180 μL of PBS and 20 μL of Presto blue reagent and then the plate was

returned to the incubator for 60 min. This step was completed, and 100 μL from each well was transferred to the 96-well plate. The fluorescence read with excitation/emission 530/620 nm filters was measured with the use of 530/620 nm excitation/emission wavelength by Fluoroscan Ace bnt FL Thermo Fisher Scientific. The results were compared with the Presto Blue fluorescence of blank samples, which did not show metabolic activity, and the control (Tissue Culture Plate TCP), which showed 100% of metabolic activity.

Cellular number was evaluated in studies on extracts. Briefly, the calibration curve was prepared after 1, 2 and 3 days of cell cultivation on TCP based on the known number of cells (TC20 automated cell counter Bio-Rad) and relative fluorescence unit determined (RFU) from Presto Blue for this known number of cells. On day 1 and 3, the cell number of all analyzed hydrogels was evaluated in comparison to TCP.

2.5.2 Fibroblasts morphology. For microscopy analysis cells were seeded on crosslinked hydrogels with the density of 5×10^4 per well in 250 μL of the medium in a 24-well plate. Before analysis, seeded cells were stained with the CellTrace™ Yellow Cell Proliferation Kit (Thermo Fisher Scientific). Briefly, 3 μg of CellTrace dye labelled 10^6 cells, and the staining was carried out for 20 min. After 1 and 3 days, samples were observed under fluorescence microscopy (Leica AM TIRF MC). Additionally, *Z*-stack images were made to obtain the 3D view of fibroblasts distribution and viability on the hydrogel.

2.6 MSCs evaluation

2.6.1 3D culture of hBM-MSCs in MC/AGR hydrogels. Prior to cell seeding 150 μL (single 48-well is covered (6.59 mm^2) and the height of hydrogel is about 2.36 mm) of each MC/AGR hydrogel blend was inserted into a 24-well Nunc™ Cell-Culture Treated Multidish (Cat. No. 142485; Thermo Fisher Scientific, Waltham, MA, USA) at room temperature (RT), and incubated for 72 hours in a humidified atmosphere at 37 °C and 5% CO_2 to polymerize. Human Bone-Marrow Derived Mesenchymal Stem/Stromal Cells (hBM-MSCs) were isolated as previously described.[33] The isolation protocol was approved by the ethical review board of the Medical University of Warsaw, and all samples were processed after informed written consent. 1×10^4 hBM-MSCs in the third passage were seeded per well (V = 1.9 cm^2) with each MC/AGR hydrogel blend, and cultured in RoosterNourish-MSC-XF medium, composed of RoosterBasal™-MSC (Cat. No. SU-005) supplemented with RoosterBooster™-MSC-XF (Cat. No. SU-016) from RoosterBio, Inc., Frederick, MD, USA, in a humidified atmosphere at 37 °C and 5% CO_2. Cells seeded in empty wells and cultured in parallel were treated as controls. All experiments were performed in duplicates and repeated at least three times.

2.6.2 Cell viability assessment of hBM-MSCs. LIVE/DEAD™ Viability/Cytotoxicity Kit for Mammalian Cells (Cat. No. L3224; Thermo Fisher Scientific, Waltham, MA, USA) was used to distinguish between live and dead hBM-MSCs, as previously described.[34] Briefly, 0.5 μL of calcein AM and 2 μL of ethidium homodimer-1 were suspended in 1 ml of sterile PBS, and 200 μL of the solution was added per well, followed by a 20 min incubation at 37 °C in the dark. Stained cells were visualized using a fluorescence microscope Cell Observer SD (Carl Zeiss, Jena, Germany) in *Z*-stack mode, performed in the Laboratory of Advanced Microscopy Techniques, Mossakowski Medical Research Institute, Polish Academy of Sciences.

2.6.3. Morphological analysis of hBM-MSCs. CellTrace™ Yellow Cell Proliferation Kit (Cat. No. C34573; Thermo Fisher Scientific, Waltham, MA, USA) was used to assess the morphology of hBM-MCSs cultured in MC/AGR hydrogel blends. Briefly, 1×10^6 hBM-MSCs in the third passage were labelled with CellTrace™ yellow reagent as per Manufacturer's protocol, and seeded as described in paragraph 2.5.2. Labelled cells were visualized using Leica AM TIRF MC fluorescent microscope (Leica Microsystems, Wetzlar, Germany) in *Z*-stack mode.

2.7 Statistical analysis

One-way ANOVA method was used to determine statistical significance between various concentrations of MC/AGR in DMA tests and biological studies. The Tukey test of all pairs determined the statistical significance between individual groups. All statistical analyzes were performed for $p < 0.05$. The statistical analysis was performed using GraphPad Prism 9.4.1 Software. A p value of less than 0.05 was considered statistically significant; p values are expressed as follows: $0.05 > p > 0.01$ as*; $0.01 > p > 0.001$ as**; $p < 0.001$ as***; $p < 0.0001$ as****.

The DMA results and biological studies are presented as the mean value ± SD.

3 Results and discussion

3.1 DSC

The heating scans of MC/AGR concentrations normalized to MC weight after baseline subtraction are presented in Fig. 1. There might be observed several complex over-imposed endothermic effects that come from MC gelation. For all samples, a clear shoulder at low temperatures (LT) and two sharp maxima at medium and high temperatures (MT and HT) are observed. This phenomenon was described in detail in our previous studies.[23] Briefly, the low-temperature shoulder corresponds to changes in water–water interactions close to polymer chains, due to the water network destruction into smaller clusters. The medium-temperature endotherm (MT) and high-temperature endotherm (HT) correspond directly to the MC crosslinking mechanism, *i.e.*, breaking of "water cages" and subsequent fibril hydrophobic domains formation.[23]

In Fig. 1, it may be clearly seen practically for all investigated compositions except for the lowest MC 1 wt%, that addition of agarose increases the heat of thermal effects, especially at low temperature side. To reveal the effect of AGR addition on the individual thermal effects, peak deconvolution analysis using asymmetric double sigmoid function was performed, of which examples are presented in Fig. 1 and the deconvolution results are presented in Fig. 2 as the individual peak's temperature position, TP, and heat, ΔH.

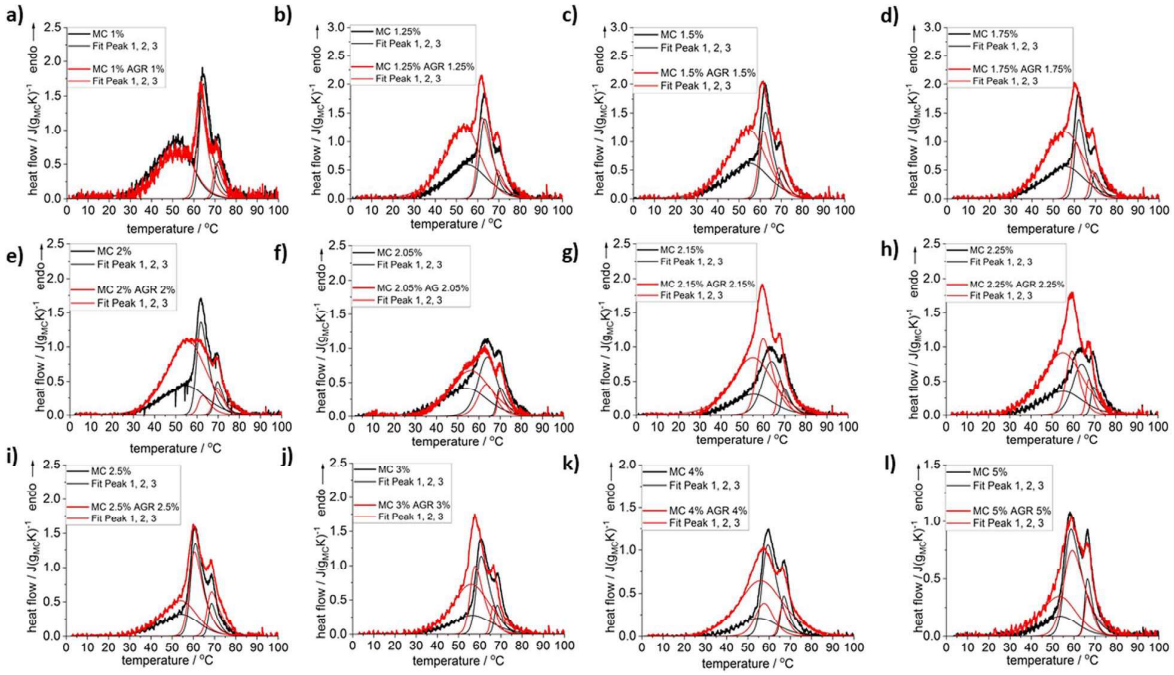

Fig. 1 DSC heating scans registered for selected compositions of MC without and with the addition of AGR plus example results of the peak deconvolution. Normalization to MC weight.

From Fig. 2 it may be seen that AGR addition generally strongly increases the heat of the LT peak, corresponding to water–water interactions, while the heats of the MT and HT peaks change variously without clear dependence on MC concentration. A clear shift of the MT and HT peaks to lower temperature is observed, especially, at lower MC concentrations being evidence of crosslinking acceleration after the addition of AGR.

The increase of LT endotherm corresponding to the water molecules interactions, *i.e.*, destruction of the spanning water

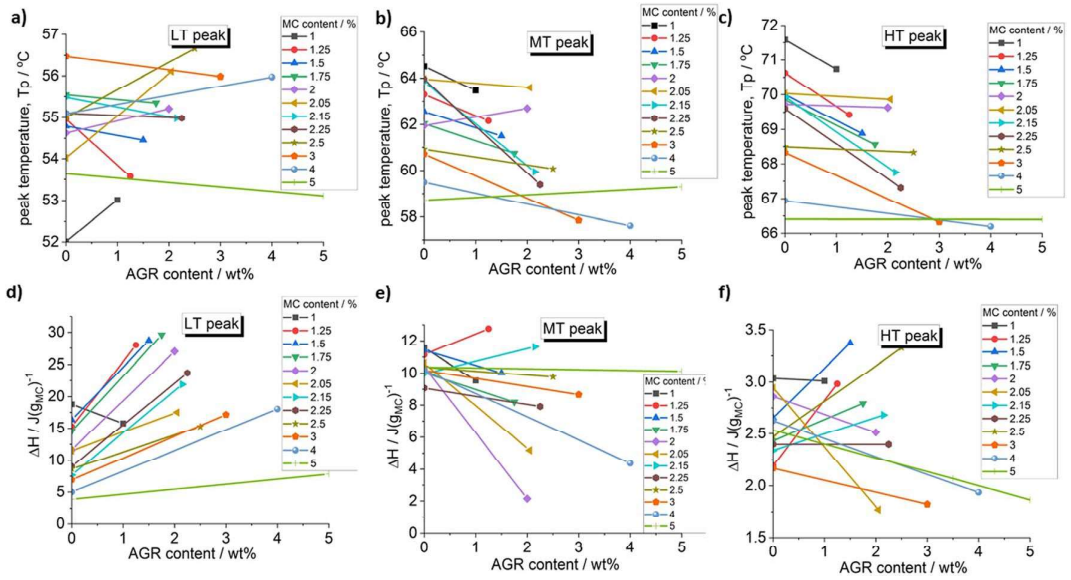

Fig. 2 Effect of agarose addition on the peak temperature and the peak heat of the deconvoluted peaks: (a) and (d) LT peak, (b) and (e) MT peak and (c) and (f) HT peak.

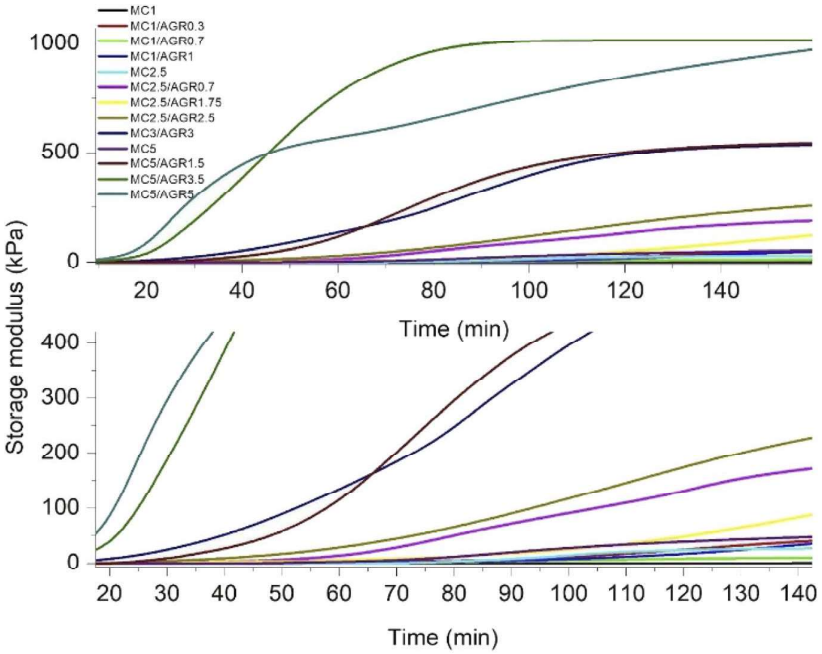

Fig. 3 Average G' as a function of time for various concentrations of MC and MC/AGR.

network into small water clusters,[23] could be explained by AGRs higher affinity to water.[30] Since AGR molecules strongly interacts with water molecules, spanning water network destruction is more efficient, which is visible as increase of the LT peak in MC/AGR blends.[30]

The inconclusive trend of MT and HT height after AGR addition could be the result of complex interactions between MC and AGR. Most likely, interactions between AGR and MC chains prevail over MC hydrophobic interactios, decreasing the molecular mobility and resulting MC crosslinking.[28]

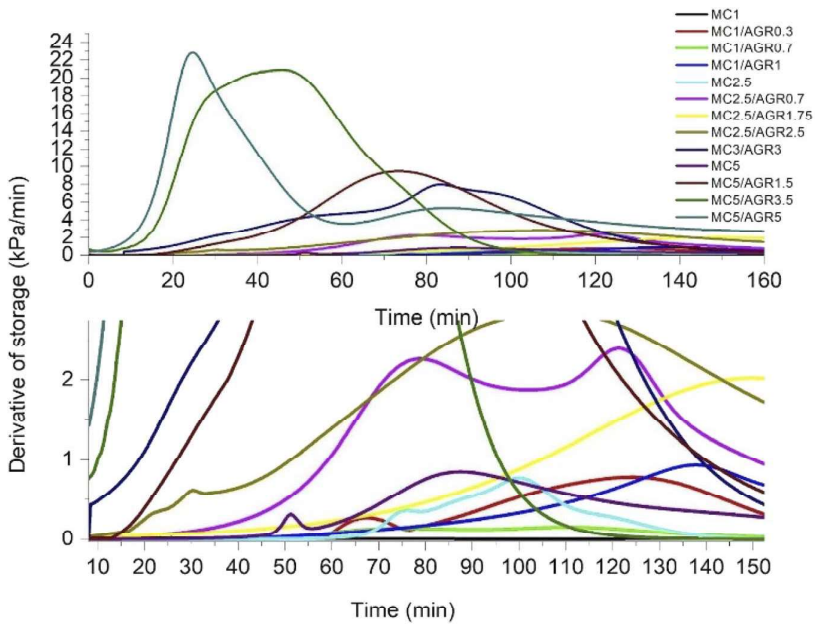

Fig. 4 The time derivative of G' for various MC and MC/AGR concentrations.

3.2 Rheology

Since G' and G'' curves did not cross, showing the characteristic crosslinking point at a certain time or temperature, as reported by Li *et al.*,[35] we estimated a crosslinking rate directly by analyzing G' as a time function. All the G' curves of MC and MC/AGR showed a sigmoidal character (Fig. 3). As we presumed, the beginning of crosslinking occurred at a different time among various concentrations, and it was connected with the hydrogel concentration and the amount of AGR in the solution. It is evident from Fig. 3 that irrespective of the MC concentration, the addition of AGR leads to an earlier start and a faster rate of crosslinking which is in line with DSC results. However, in any solution, AGR addition did not accelerate reaching the plateau of G'.

The G' time derivative analysis clearly indicates that there are at least two local maxima of the crosslinking rate, as it was visible for pure MC (Fig. 4). After mixing 0.7 wt% of AGR with 1 wt% of MC, the 1st maximum of crosslinking rate was observed after 70 minutes. Addition of 1 wt% of AGR to 1 wt% of MC, resulted in a very small maximum after shorter time (*c.a.* 25 min). At this MC concentration, AGR addition significantly affects the beginning of crosslinking (t_{onset}). The same trend of the first maximum crosslinking rate acceleration is observed at 2.5 wt% MC – mixed with 1.75 wt% of AGR provided the first very small maximum at 30 min while in the case of 2.5 wt% AGR the first crosslinking rate maximum took place after a few minutes. An interesting phenomenon has been observed for 5 wt% of MC, which showed the first maximum of crosslinking rate at 50 min. While after adding 5 wt% AGR, the first maximum was after 90 min, but its intensity was at least 10 fold higher than the first maximum in pure MC. In all cases, the second and further maxima of crosslinking were larger and shifted to the higher time range after AGR addition. Usually, these maxima were stretched in the time range.

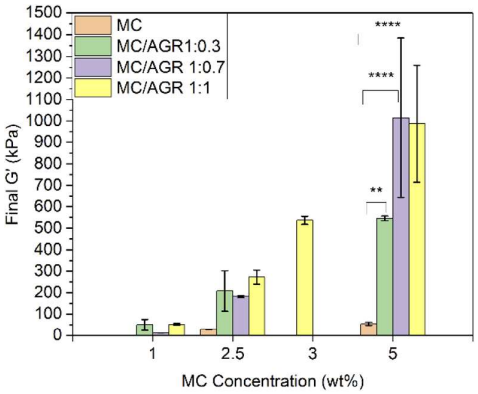

Fig. 6 Final G' for various MC and MC/AGR concentrations. Statistical significance $^{**}p < 0.001$, $^{****}p < 0.0001$.

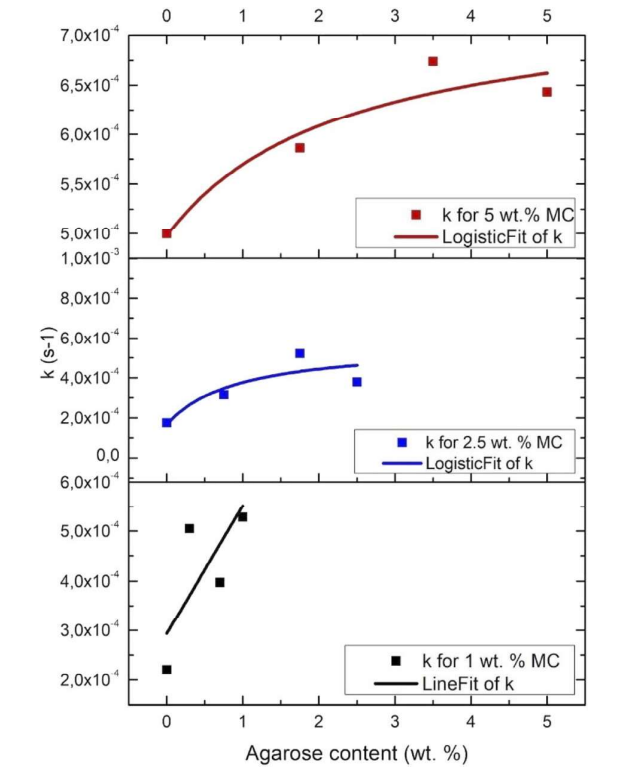

Fig. 5 Crosslinking rate (k) determined from DMA results, *vs.* the MC/AGR content.

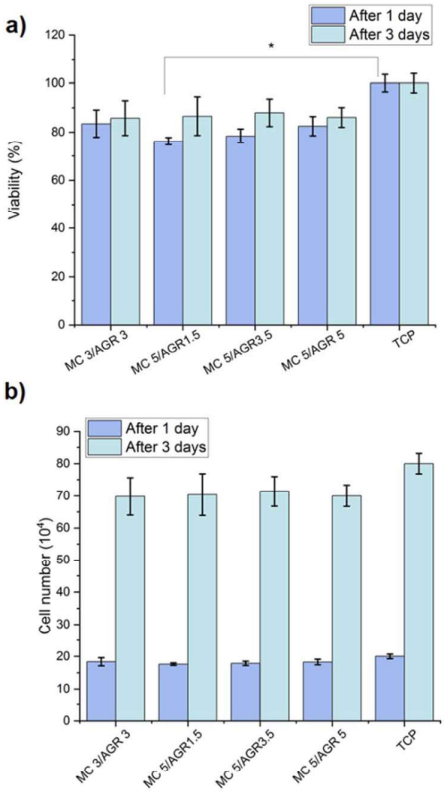

Fig. 7 The L929 (a) viability and (b) cell number, determined on MC/AGR hydrogels after 1 and 3 days. Statistical significance: $^{*}p < 0.05$.

Thermal physical crosslinking of MC/AGR is an interesting feature while designing smart *in situ* gelling injectable hydrogels. One of the most important advantages of such an approach is avoiding of chemical modifications and using of toxic crosslinking agents.[36]

DMA results clearly showed that thermal MC crosslinking initiation is strongly dependent on AGR contribution in the MC/AGR solution. The higher the contribution of AGR, the faster the beginning of crosslinking (t_{onset}) (Fig. 4). As we predicted, AGR plays role of an initiator of MC crosslinking, decreasing t_{onset} of crosslinking from dozens to a few minutes. In contrast, AGR did not accelerate the formation of the hydrophobic fibril MC aggregates, resulting in reaching a plateau of G'. This means AGR aqueous solution only accelerates the first step of MC crosslinking. The mechanism of MC/AGR crosslinking might be explained in the following manner. At ambient conditions, MC polymeric chains interpenetrate AGR chains, preventing AGR crosslinking. At this temperature, the solution is a sol. The heating of the solution causes MC water cages' destruction, in other words, dehydration. Since AGR has a greater affinity to water, dehydration takes place faster than in pure MC. Martin *et al.*[30] reported that another reason for faster MC/AGR crosslinking might be the effect of MC and AGR chain interactions. The results of such interactions are forming fibrils through stronger hydrophobic bonds and considerably enhanced mechanical properties of MC.

On the other hand, the second step of MC crosslinking seemed to be prolonged after AGR addition. The reason can be related to the strong interactions between MC and AGR chains resulting in decreased molecular mobility as an effect of the partially crosslinked network formation which slows further hydrophobic interaction formation.[28,37] However, we should consider that during crosslinking, G' reaches a much higher value in a shorter time after AGR addition (Fig. 3). It could be the effect of additional interactions between MC and AGR polymeric chains.[30,31] The higher the G' value, the higher the degree of crosslinking, making the whole hydrogel system more stable and provides higher mechanical properties.[38] Despite the slow changing of G' in time, there is a decreased risk of hydrogel decomposition and displacement from dedicated tissue.

Fig. 5 presents the crosslinking rate, k, as derived from the DMA results, as a function of the AGR content. The crosslinking rate increases with the increase of AGR contribution.The final value of G' as a function of all the measured sample concentrations was determined and shown in Fig. 6. The final G' increased with MC concentration and was always higher after AGR addition.

From DMA studies it is evident that small concentrations of these hydrogel systems (1–2.5 wt%) showed, statistically insignificant changes in viscoelastic properties after AGR addition. The values in this range of concentrations correspond to the native human spinal cord. The G' of MC 1/AGR 0.7 is similar to the G' of the human spinal cord which is in the range of 5–42 kPa.[39] This hydrogel composition might be interesting for CNS tissue engineering considering the perspective of hydrogels' mechanical properties. Above 5 wt% there are visible statistically significant differences in viscoelastic properties after AGR addition, which contribution in the solution increased the final G'.

The G' of higher MC/AGR concentrations, *i.e.*, MC 5/AGR 3.5 or MC 5/AGR 5 corresponds to the G' of human articular cartilage.[40]

3.3 Biological tests

Small concentrations ~1 and 2.5 wt% of MC/AGR showed relatively low strength and viscosity after crosslinking, resulting in immediate cells collapsing into the bottom of the well in our preliminary studies. Thus they showed susceptibility to insufficient gelation.[28] Thus, these concentrations were disregarded in biological tests.

3.3.1 Biocompatibility test. Viability using Presto Blue assay was evaluated on hydrogel extracts of MC 3/AGR 3, MC 5/AGR 1.5, MC 5/AGR 3.5, and MC 5/AGR 5 after 1 and 3 days. Tests were carried out to investigate MC/AGR solutions' relevance in tissue engineering applications.

The viability results (Fig. 7a) showed the non-toxic character of the MC/AGR hydrogel. There was slightly lower viability for

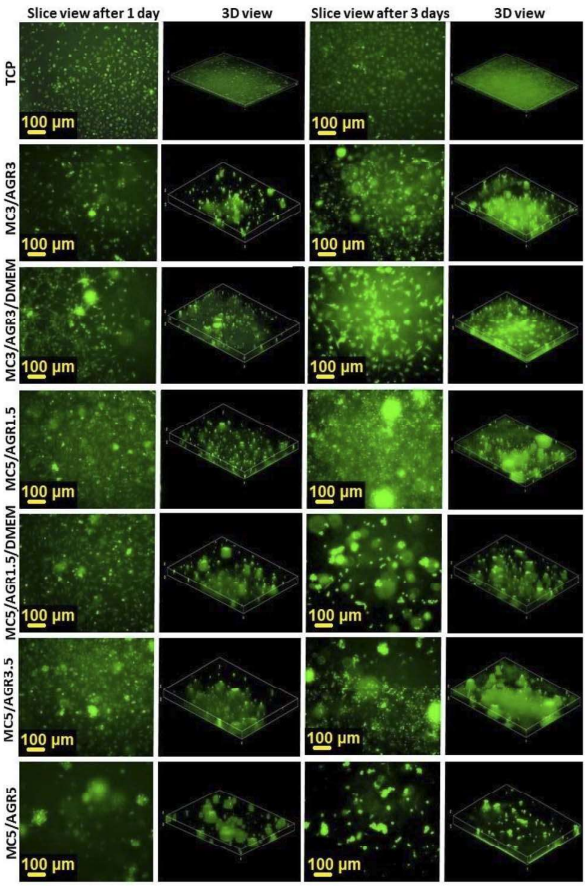

Fig. 8 Fibroblasts distribution in 3D cultures by an FM after 1 and 3 days. The slice views (the bottom of the well) and 3D views show various distributions in 3D culture depending on MC/AGR concentration.

hydrogel samples in comparison to the control (TCP). Yet all of these samples accomplished values ≥70%, which is considered non-toxic to the living cells according to the standard of ISO 10993-5. Most likely the cells could be covered with thick layer of diluted hydrogel. Szot *et al.* reported increased hydrogels layer thickness could provide hypoxia and limited nutrient diffusion.[41] According to this, the balance between the migration of cellular waste products and the supply of fresh supplements/proteins from the medium was not maintained, resulting in a reduced viability value after 1 day. However, cellular viability increased after 3 days of cultivation due to fresh media additives.

Additionally, cell number after 1 and 3 days during *in vitro* study on extracts was estimated based on calibration curve for known number of cells (determined by flow cytometry Bio-Rad) and relative fluorescence unit (determined from Presto Blue) (Fig. 7b). The results showed the differences of cell number

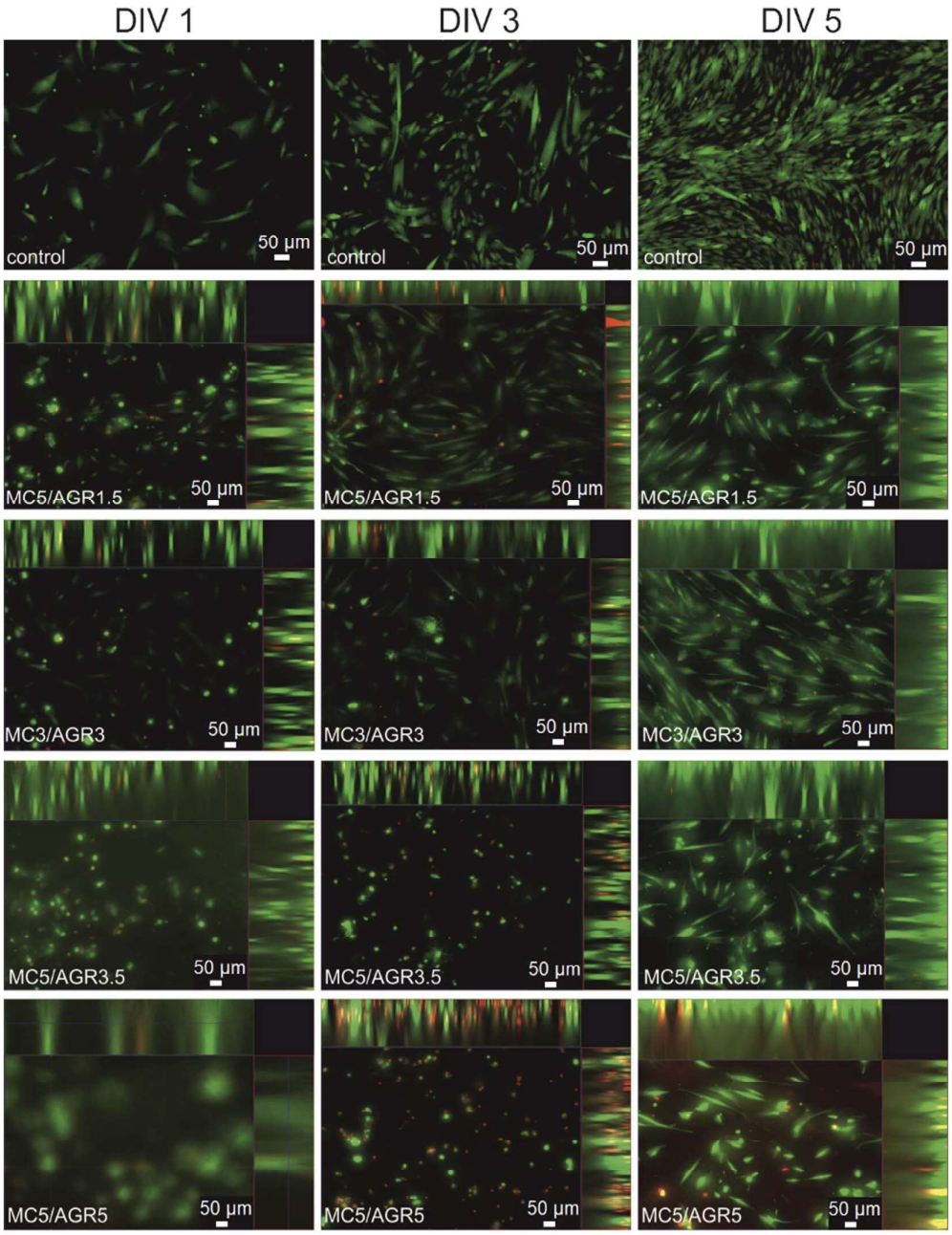

Fig. 9 Representative pictures, rendered by maximum intensity projection (MIP) in orthogonal projection, of hBM-MSCs seeded and cultured for 5 days on the following hydrogel combinations: MC5/AGR1.5, MC3/AGR3, MC5/AGR3.5, and MC5/AGR5.

between studied MC/AGR concentrations were statistically insignificant.

3.3.2 Fibroblasts morphological observation. Fig. 8 represents fluorescence microscope imaging (FM) of the cells on MC/AGR hydrogels with various MC and AGR ratios. The images presented fibroblasts' distribution in the volume of hydrogel in relation to the control in 2D hydrogel-surface culture and 3D culture. The 3D view not only allows precise observation of cell penetration into the volume of hydrogel but also mimics *in vivo* cell growth. To evaluate exact cell distribution and investigate whether cells infiltrated the entire hydrogel volume, 3D views based on *Z*-stack images of hydrogels have been prepared (Fig. 8). The 3 D views were compared with images taken from the bottom (one slice). All of the tested hydrogels showed good viability and cells were distributed in hydrogel rather homogeneously. However, for other samples, there were visible some cellular aggregates which had round shapes. It is especially visible for MC5/AGR1.5/DMEM and MC 5/AGR5. This is most likely an effect of insufficient oxygen availability in those parts of hydrogel resulting in cell death or uneven crosslinking rate in these particular samples.

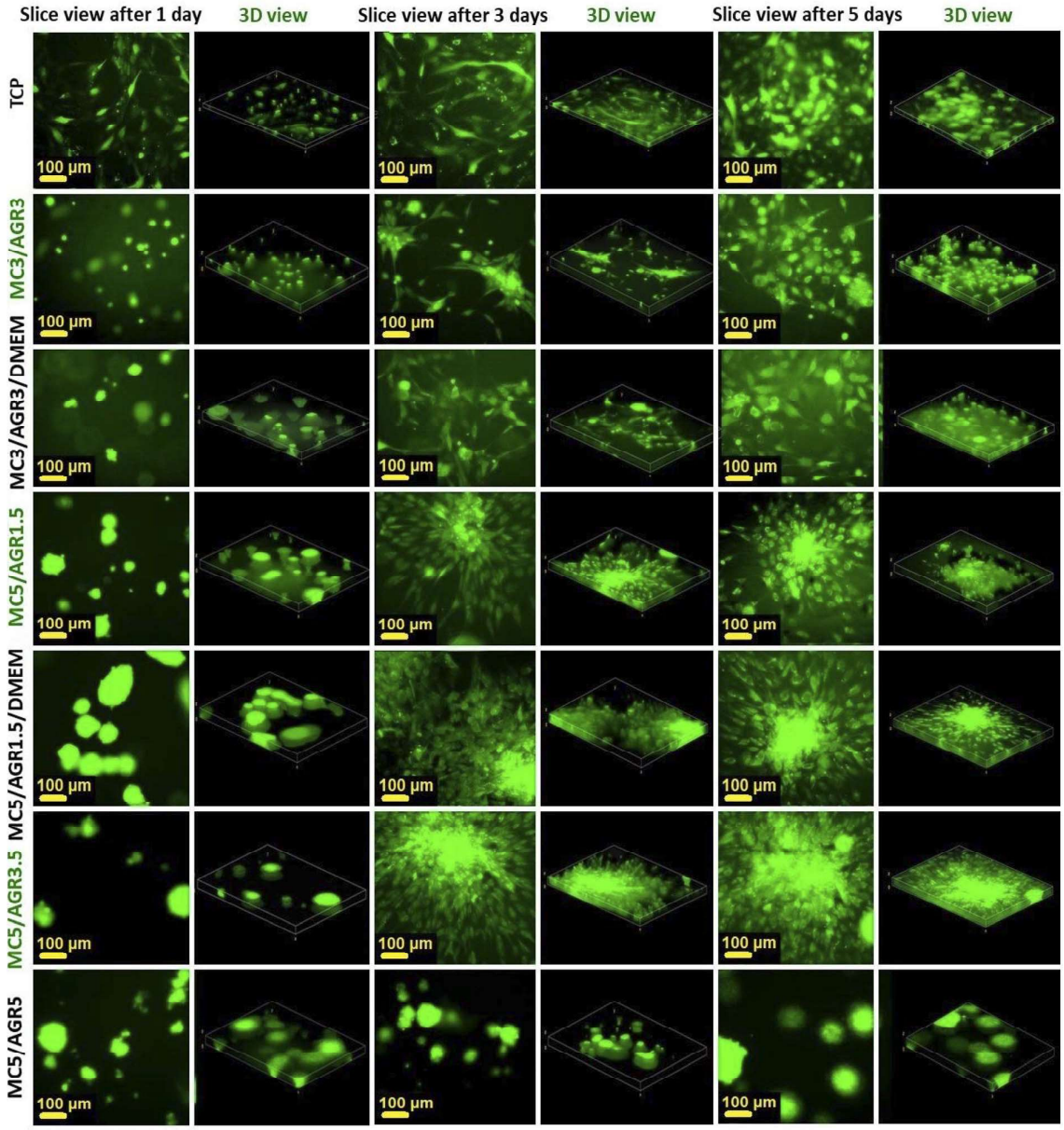

Fig. 10 Cell distribution in 3D cultures by an FM after 1, 3, and 5 days. The slice views and 3-D views show cell distributions in 3D culture depending on MC/AGR concentration.

The best fibroblasts distribution in the hydrogel was observed for MC3/AGR3/DMEM, MC5/AGR1.5, and MC5/AGR3.5. These three samples also showed the significant density and viability of the cells in comparison to the control.

3.3.3 Viability of hBM-MSCs cultured in methylcellulose/agarose hydrogels. To assess the viability of hBM-MSCs cultured in methylcellulose/agarose hydrogels cells were stained with calcein AM and ethidium homodimer-1 (EthD-1). In living cells, calcein AM is converted into green-fluorescent calcein, whereas in dead cells EthD-1 binds to DNA and emits red fluorescence. Stainings and microscopic analyses were performed at three-time points: one, three, and five days after seeding cells in MC/AGR hydrogels which polymerized for 72 hours. All compositions of hydrogels were non-toxic for hBM-MSCs (Fig. 9). The cells encapsulated in hydrogels remained alive throughout the whole time of culture. The highest number of dead cells was visible in the MC5/AGR5 combination suggesting its negative influence on cell viability. It might be related to relatively high viscosity of hydrogel and decreased gas and/or nutrient exchange. In the case of MC5/AGR1.5 and MC3/AGR3 combinations, some of the cells migrated to the bottom of the cells already after the 1st day of culture probably due to appropriate viscosity of the hydrogel. On the other hand in the MC5/AGR3.5 and MC5/AGR5 time of migration throughout the hydrogel was longer – most of the cells migrated after 5 days of culture. Therefore, depending on the therapeutic approach one could achieve appropriate conditions for the cell migration by manipulation of hydrogel composition.

3.3.4 MSCs morphological observations. Morphological MSCs distribution and their penetration into the hydrogel volume are illustrated in Fig. 10, where 2D and 3D views obtained *via* FM are shown. It is visible that cells were suspended in all volumes of the hydrogel after one day. However, the FM images of MC5/AGR5 were different from other samples. It showed a small number of cells formed in aggregates that have round shapes in comparison to the control.

For other samples, after 3 and 5 days cells adhered and proliferated on the bottom of the wells, showing adequate morphology and distribution in comparison to TCP control. The adequate MSCs distribution in the hydrogel was observed for most of the samples. The shape of the cell depends on its origin, environment and time of cultivation.[42] According to the image of viability evaluated by live dead test (Fig. 9), after 5 days most of the MSC probably migrated to the bottom of the well which is more stiff than hydrogel. That is the reason why cells were more spread/elongated and less spherical. This effect was not observed for L929 which indicates lower cellular volume and probably does not reach well bottom (Fig. 8).[42] Additionally, interactions between the cell and hydrogel depend on mechanical properties of the hydrogel. According to literature, the difference in the stiffness of hydrogels determine cellular area.[43] Authors present that the area of cells seeded on stiffer hydrogel was statistically significantly higher than on soft hydrogel.

The cell migration through the volume of the hydrogel might be beneficial from the perspective of cell delivery systems. It seems that investigated hydrogels (except for MC5/AGR5) can provide a supportive environment, mechanically protecting the cells during the transplantation procedure. Additionally, the structure of the hydrogel allows for cell migration within the scaffold and thus enables the settlement of transplanted cells in the host tissue. It is especially visible after one day of cell culturing (Fig. 10) where cells embedded in hydrogel showed spherical morphology. According to Kim *et al.*[38] this morphology is beneficial for embedding cells in hydrogel matrix approaching as a potential injectable cell delivery system. Thus, most of the MC/AGR concentrations could be used as MSCs delivery systems that provide faster regeneration of injured tissues.

4 Conclusions

Since MC crosslinking, especially its first step, is mostly dependent on water cages forming/breaking mechanism, the addition of agarose is essential here. AGR has greater affinity to water and effectively uptakes water molecules from MC solution, resulting in faster MC crosslinking.

Our DSC and DMA results that are mutually consistent, clearly demonstrate the addition of AGR promotes MC crosslinking by effective uptaking of water molecules from MC solution, resulting in an easier hydrophobic interaction formation.

In the case of DSC this promotion of MC crosslinking is visible for the low temperature effect as an increase in the LT peak area and a shift of the MT and HT effects towards lower temperatures (times).

Isothermal measurements of time dependence of G' indicated that t_{onset} of crosslinking is faster with the increase of AGR contribution in the solution. The AGR has a significant influence on MC crosslinking initiation, but at the same time, does not play a role in further steps of MC crosslinking. Additionally, the presence of AGR in the system resulted in improved mechanical properties, *i.e.*, the final G' value of the MC hydrogel systems which was most prominent for small concentrations. On the one hand, the final value of G' small MC/AGR concentrations implies that they might be useful as scaffolds for CNS tissue engineering from the mechanical point of view. But on the other hand, *in vitro* tests verified that small MC/AGR concentrations do not provide adequate support for cells as scaffolds or cell delivery systems. Therefore they do not meet the expectations of tissue engineering.

The appropriate AGR contribution in the MC/AGR hydrogel systems of higher concentration, not only did provide adequate crosslinking rate and enhanced mechanical properties, but also influenced good cellular response *in vitro* and showed non-toxic character. However, the desired mechanical properties from the perspective of certain native tissues do not guarantee expected *in vitro* results. For instance, Bonetti *et al.*,[44] crosslinked chemically MC to increase its stiffness and cellular response but *in vitro* tests did not show significant differences in adhesion and proliferation of L929 fibroblasts seeded on chemically crosslinked and non-crosslinked MC. In our studies, MC5/AGR5 is supposed to be a perfect biomaterial, especially for cellular support from the mechanical perspective. However, the sample

was too viscous, which resulted in disturbing the balance between oxygen/nutrients delivery and draining of cellular metabolites.

On the other hand, the two hydrogel systems of MC3/AGR3 and MC5/AGR3.5 have decent mechanical and biological properties showing the best potential as a smart injectable scaffold/cell delivery system for tissue engineering. Therefore, the comprehensive understanding of MC/AGR properties, *i.e.*, MC gelation and its kinetic after AGR addition, mechanical and biological properties, is essential to materials' proper design for future *in vivo* studies.

Author contributions

B·N·S., D. K. and P. S. conceived the project. B. N. S. optimized and developed the hydrogels. B. N. S. and A. K. K. performed and analysed the DMA experiments. B. N. S. and A. G. performed DSC experiments. A. G. analysed DSC experiments. D. K. performed *in vitro* tests on fibroblasts. B. N. S. and D. K. analysed and performed morphological observations of fibroblasts and mesenchymal stem cells. P. R., L. S. and B. L. performed *in vitro* tests on and mesenchymal stem cells, analyzed and performed morphological observations. B. N. S, A. G., D. K., A. K·K., P. R., L. S., B. L. and P. S. wrote the manuscript. B. N. S. provided financial support.

Conflicts of interest

There are no conflicts to declare.

Acknowledgements

Beata Niemczyk-Soczynska acknowledges National Science Centre (NCN), grant number 2018/29/N/ST8/00780. Beata Niemczyk-Soczynska and Piotr Rogujski acknowledge the European Social Fund (POWR.03.02.00-00-I028/17-00). Anna Krzton-Maziopa acknowledges the support from statutory budget of Faculty of Chemistry, WUT. Dorota Kolbuk acknowledges the Norway Grants 2014-2021, the National Centre for Research and Development: NOR/SGS/BioLigaMed/0272/2020 BioLigaMed.

References

1 R. Esmaeely Neisiany, M. S. Enayati, P. Sajkiewicz, Z. Pahlevanneshan and S. Ramakrishna, *Front. Mater.*, 2020, **7**, 25.
2 H. Ge, Y. Hou, T. Sun, L. Chen, G. Zhang and L. Jiang, *Adv. Mater.*, 2007, **19**, 2520.
3 J. Kopecek and Y. Yang, *Polym. Int.*, 2007, **56**, 1078.
4 A. Zaszczynska, P. Sajkiewicz and A. Gradys, *Polymers*, 2020, **12**, 161.
5 J. F. Mano, *Adv. Eng. Mater.*, 2008, **10**(6), 515–527.
6 I. Noshadi, S. Hong, K. E. Sullivan, E. Shirzaei Sani, R. Portillo-Lara, A. Tamayol and N. Annabi, *Biomater. Sci.*, 2017, **5**(10), 2093–2105.
7 K. Y. Lee and D. J. Mooney, *Prog. Polym. Sci.*, 2012, **37**(1), 106–126.
8 A. M. Araszkiewicz, E. P. Oliveira, T. Svendsen, K. Drela, P. Rogujski, I. Malysz-Cymborska, M. Fiedorowicz, R. L. Reis, J. M. Oliveira, P. Walczak, M. Janowski, B. Lukomska and L. Stanaszek, *Int. J. Mol. Sci.*, 2022, **23**(5), 2465.
9 P. Nasatto, F. Pignon, J. Silveira, M. Duarte, M. Noseda and M. Rinaudo, *Polymers*, 2015, **7**, 777–803.
10 M. S. Kim, S. J. Park, H. J. Chun and C. H Kim, *Tissue Eng. Regener. Med.*, 2011, **8**, 117–123.
11 Y. Xu, Z. Li, X. Li, Z. Fan, Z. Liu, X. Xie and J. Guan, *Acta Biomater.*, 2015, **26**, 23–33.
12 D. R. Nisbet, A. E. Rodda, M. K. Horne, J. S. Forsythe and D. I. Finkelstein, *Tissue Eng., Part A*, 2010, **16**, 2833.
13 G. Molinaro, J. C. Leroux, J. Damas and A. Adam, *Biomaterials*, 2002, **23**, 2717–2722.
14 Y. Lee, H. J. Chung, S. Yeo, C. H. Ahn, H. Lee, P. B. Messersmith and T. G. Park, *Soft Matter*, 2010, **6**(5), 977–983.
15 B. F. Chong, L. M. Blank, R. Mclaughlin and L. K. Nielsen, *Appl. Microbiol. Biotechnol.*, 2005, **66**, 341–351.
16 Y. Lei, S. Gojgini, J. Lam and T. Segura, *Biomaterials*, 2011, **32**, 39–47.
17 N. Contessi, L. Altomare, A. Filipponi and S. Fare, *Mater. Lett.*, 2017, **207**, 157–160.
18 L. Bonetti, L. De Nardo and S. Fare, *Tissue Eng., Part B*, 2021, **27**(5), 486–513.
19 M. Takahashi, M. Shimazaki and J. Yamamoto, *J. Polym. Sci., Part B: Polym. Phys.*, 2001, **39**(1), 91–100.
20 M. L. Coughlin, L. Liberman, S. P. Ertem, J. Edmund, F. S. Bates and T. P. Lodge, *Prog. Polym. Sci.*, 2020, **112**, 101324.
21 P. W. Schmidt, S. Morozova, P. M. Owens, R. Adden, Y. Li, F. S. Bates and T. P. Lodge, *Macromolecules*, 2018, **51**(19), 7767–7775.
22 Y. Yang, W. Wu, H. Liu, H. Xu, Y. Zhong, L. Zhang and Z. Mao, *J. Mol. Graphics*, 2020, **97**, 107554.
23 B. Niemczyk-Soczynska, P. Sajkiewicz and A. Gradys, *Polymers*, 2022, **14**, 1810.
24 D. Wu, J. Cheng, X. Su and Y. Feng, *Carbohydr. Polym.*, 2021, **260**, 117792.
25 M. S. Jhon and J. D. Andrade, *J. Biomed. Mater. Res.*, 1973, **7**(6), 509–522.
26 S. Morozova, *Polym. Int.*, 2020, **69**(2), 125–130.
27 R. Bodvik, A. Dedinaite, L. Karlson, M. Bergstrom, P. Baverback, J. S. Pedersen, K. Edwards, G. Karlsson, I. Varga and P. M. Claesson, *Colloids Surf., A*, 2010, **354**, 162–171.
28 B. Niemczyk-Soczynska, A. Gradys, D. Kolbuk, A. Krzton-Maziopa and P. Sajkiewicz, *Polymers*, 2019, **11**, 1772.
29 S. E. Stabenfeldt, A. J. Garcia and M. C. LaPlaca, *J. Biomed. Mater. Res., Part A*, 2006, **77**(4), 718–725.
30 B. C. Martin, E. J. Minner, S. L. Wiseman, R. L. Klank and R. J. Gilbert, *J. Neural Eng.*, 2008, **5**, 221.
31 C. J. Rivet, K. Zhou, R. J. Gilbert, D. I. Finkelstein and J. S. Forsythe, *Biomatter*, 2015, **5**, e1005527.

32 https://www.stobec.com/DATA/PRODUIT/1688~v~data_8733.pdf.
33 K. Drela, L. Stanaszek, K. Snioch, Z. Kuczynska, M. Wrobel, S. Sarzynska, P. Legosz, P. Maldyk and B. Lukomska, *Stem Cell Res. Ther.*, 2020, **11**, 262.
34 S. Vieira, P. Strymecka, L. Stanaszek, J. Silva-Correia, K. Drela, M. Fiedorowicz, I. Malysz-Cymborska, P. Rogujski, M. Janowski, R. L. Reis, B. Lukomska, P. Walczak and J. M. Oliveira, *J. Mater. Chem. B*, 2020, **8**(27), 5928–5937.
35 L. Li, H. Shan, C. Y. Yue, Y. C. Lam, K. C. Tam and X. Hu, *Langmuir*, 2002, **18**(20), 7291–7298.
36 C. Li and A. Strachan, *Polymer*, 2010, **51**(25), 6058–6070.
37 J. Y. Shin, Y. H. Yeo, J. E. Jeong, S. A. Park and W. H. Park, *Carbohydr. Polym.*, 2020, **238**, 116192.
38 E. J. Kim, J. S. Choi, J. S. Kim, Y. C. Choi and Y. W. Cho, *Biomacromolecules*, 2015, **17**(1), 4–11.
39 R. D. Bartlett, D. Choi and J. B. Phillips, *Regener. Med.*, 2016, **11**, 659.
40 B. M. Lawless, H. Sadeghi, D. K. Temple, H. Dhaliwal, D. M. Espino and D. W. Hukins, *J. Mech. Behav. Biomed. Mater.*, 2017, **75**, 293–301.
41 C. S. Szot, C. F. Buchanan, J. W. Freeman and M. N. Rylander, *Biomaterials*, 20112011, **32**(31), 7905–7912.
42 N. Perez Gonzalez, J. Tao, N. D. Rochman, D. Vig, E. Chiu, D. Wirtz and S. X. Sun, *Mol. Biol. Cell*, 2018, **29**(21), 2509–2601.
43 Z. Zhuang, Y. Zhang, S. Sun, Q. Li, K. Chen, C. An and H. Wang, *ACS Biomater. Sci. Eng.*, 2020, **6**(5), 3091–3102.
44 L. Bonetti, L. De Nardo and S. Fare, *Gels*, 2021, **7**(3), 141.

RSC Advances

PAPER

Cite this: *RSC Adv.*, 2023, **13**, 11889

Methylcellulose/agarose hydrogel loaded with short electrospun PLLA/laminin fibers as an injectable scaffold for tissue engineering/3D cell culture model for tumour therapies†

Beata Niemczyk-Soczynska,[a] Dorota Kolbuk,[a] Grzegorz Mikulowski,[a] Iwona A. Ciechomska[b] and Pawel Sajkiewicz *[a]

Received 8th February 2023
Accepted 10th April 2023

DOI: 10.1039/d3ra00851g

rsc.li/rsc-advances

This research aimed at designing and fabricating a smart thermosensitive injectable methylcellulose/agarose hydrogel system loaded with short electrospun bioactive PLLA/laminin fibers as a scaffold for tissue engineering applications or 3D cell culture models. Considering ECM-mimicking morphology and chemical composition, such a scaffold is capable of ensuring a hospitable environment for cell adhesion, proliferation, and differentiation. Its viscoelastic properties are beneficial from the practical perspective of minimally invasive materials that are introduced to the body *via* injection. Viscosity studies showed the shear-thinning character of MC/AGR hydrogels enabling the potential injection ability of highly viscous materials. Injectability tests showed that by tuning the injection rate, even a high amount of short fibers loaded inside of hydrogel could be efficiently injected into the tissue. Biological studies showed the non-toxic character of composite material with excellent viability, attachment, spreading, and proliferation of fibroblasts and glioma cells. These findings indicate that MC/AGR hydrogel loaded with short PLLA/laminin fibers is a promising biomaterial for both tissue engineering applications and 3D tumor culture models.

1. Introduction

Diseases and accidents leading to the injury of the central nervous system (CNS), *i.e.*, the brain and spinal cord, are extremely challenging from the perspective of medicine and tissue engineering. The reason for that is progressive, irreversible neuron degeneration, and lack of particular targeted therapy.[1,2] Injuries and diseases of the CNS have always been a serious global socioeconomic problem. According to global statistics, spinal cord injury (SCI) affects over 500 000 people every year according to Global incidence data,[3] while traumatic brain injury is experienced by 27 000 000 people every year.[4] In 2016, there were 330 000 CNS cancer cases, particularly brain tumors.[5] Since currently brain tumors lead to 190 000 deaths per year,[6] there is huge demand to find therapies that allow a better understanding of tumour cell behavior and, subsequently, implementation of targeted therapy.

Current clinical TBI strategies focus on therapeutic agents (such as drugs, cells or growth factors) delivery, scaffold implantation, or combining both of those approaches.[7] Although therapeutic agent delivery alone seems to be the perfect strategy, only their low concentrations actually reach the injured area of the CNS. In addition, growth factors might rapidly degrade after being introduced into the body, while cell transplantation shows the possibility of cell migration to the other CNS areas resulting in abnormal growth of the tissue or performing poor viability due to an unfavorable environment for cell growth.[7,8] Increasing doses of therapeutic agents to trigger the desired therapeutic effect could lead to systemic toxicity.[9] To overcome this problem, invasive therapeutics delivery is widely used. Such a method allows the delivery of high doses of therapeutics into injured areas and avoids exposure of the surrounding tissues to the applied drug. However, such treatment also disrupts the blood–brain barrier (BBB) and is conducted *via* complex surgeries.[10] This is especially common for brain tumor therapies, where chemotherapeutics are delivered directly to the tumor and at the same time, do not enter the systemic circulation. However, complex brain or spinal cord surgeries carry a huge danger of after-surgery complications such as subsequent neuronal damage or inflammations.[7]

Most of the current clinical approaches focus on drug/cell delivery only, but not on providing ECM-mimicking nontoxic microenvironment restoring neurons' main functions. Consequently, the currently available clinical therapies, including

[a]*Institute of Fundamental Technological Research, Polish Academy of Sciences, Pawinskiego 5b St., 02-106 Warsaw, Poland. E-mail: psajk@ippt.pan.pl*

[b]*Nencki Institute of Experimental Biology PAS, 3 Pasteur Street, 02-093 Warsaw, Poland*

† Electronic supplementary information (ESI) available. See DOI: https://doi.org/10.1039/d3ra00851g

surgeries and less invasive treatments, focus mostly on post-trauma relief but do not provide real prolonged therapeutic effects or effective regeneration of injured CNS.[3] These limitations could be overcome by implementing the scaffold in the injured areas that mimic the natural ECM of CNS providing excellent conditions for cell regeneration.[11] Additionally, CNS mimicking microenvironment could be useful as a 3D cell culture model to investigate and understand brain tumors, *i.e.*, cellular morphology, phenotype, gene expression pattern, mechanism of spreading, tumor-immune cell interactions, and drug resistance.[12]

A new approach of natural minimally invasive and "smart" biomaterials such as injectable hydrogels loaded with nanoparticles or nanofibers (*e.g.*, ref. 13 and 14) are in the area of recent interest in tissue engineering. In this field, injectable *in situ* crosslinked hydrogels offer many advantages such as good biocompatibility and processability. The injectability of such materials determines their non-invasive and fast introduction into the lesion, which allows for avoiding long and complex surgeries.[15] Hydrogels form 3D structures that characterize large amounts of water in a polymeric network mimicking the brain extracellular matrix (ECM), which stimulates stem cell adhesion, proliferation, and differentiation for neural tissue engineering. Such mimicry makes hydrogels an important supporting factor that provides better cell integrity with the material.[16,17] In some stimuli-responsive types of hydrogel, external stimulation, like pH, or temperature change provoke its crosslinking. Nevertheless, hydrogels usually perform poor mechanical properties and lack fibrous structure providing adequate support for cell activity.[18,19] For instance, Thonhoff *et al.*[20] tested commercially available hydrogels of Matrigel and PuraMatrix with fetal human neural stem cells (hNSCs) regarding cytotoxicity and stem cell support ability and differentiation. The studies showed that tested hydrogels supported cells insufficiently resulting in reduced survival of hNSCs and poor migration capabilities within the injured cavity.

According to Ucar *et al.*[7] combination of appropriate natural and synthetic biomaterials might overcome all of these problems by providing a hospitable environment that mimics native ECM, for tissue regeneration. Such an environment should provide biocompatibility, adequate support for cells, and, consequently adequate mechanical properties, *i.e.*, 1–10 kPa for the brain,[21] and 0.52–1.88 MPa for the spinal cord.[22] Besides those properties, a perfect material should mimic ECM biochemically, to provide good cell-material (*i.e.*, cell-ECM proteins/proteoglycans interactions) and cell–cell interactions. This has been shown to play a crucial role in cell fate.[23,24] In this respect, the incorporation of native ECM components such as peptide sequences that interact with cell membrane integrins Ile-Lys-Val-Ala-Val (IKVAV) or growth factors (neurotrophic growth factors (NGFs)).[25,26]

Most of the current research dedicated to neural tissue engineering focuses on hydrogels loaded with nanoparticles, which are considered safe and effective in delivering cells or drugs into the injured area.[27] One example is thermoreversible gelation polymer (TGP) loaded with poly(lactic-*co*-glycolic acid) (PLGA) microspheres for rats' glioma treatment.[28] However, similarly to drug delivery systems, too few nanoparticles can be absorbed by macrophages immediately after injection into the body;[27] thus, most of these approaches seem not applicable as a supportive structure for neural cells.

Currently, cellulose-based materials and hydrogels strengthened with short nanofibers are becoming increasingly popular in tissue engineering, and medicine but also 3D cell culture models, *i.e.*, a well-defined platform that maintains cell viability and replicates native cellular environments similar to those found in tissues. This technology provides mechanical, biochemical, morphological, and physiological guidance on the properties of tumor cells in a 3D environment. One of the examples of using cellulose-based materials is hydrogel consisting of collagen/nanocellulose nanofibers as a 3D model for developing a therapy against pancreatic ductal adenocarcinoma (PDAC).[29]

In this work, we propose a thermosensitive injectable hydrogel system loaded with short electrospun biologically active fibers that have been studied as a potential scaffold for the central nervous system (CNS) tissue engineering or 3D glioblastoma culture model. The base component of the proposed hydrogel systems is the cellulose derivative of methylcellulose (MC) approved by the Food and Drug Administration (FDA). The MC alone undergoes thermal reversible crosslinking as an effect of the temperature increase near 37 °C. The crosslinking mechanism of MC is a result of a unique type of dehydration based on "water cages" destruction, and subsequent 3D fibril network formation, which was thoroughly discussed in our previous studies.[30–32] Another hydrogel component is agarose (AGR), which strengthens the hydrogel mechanically and fulfils an important function of the MC crosslinking rate accelerator by faster dehydration of water cages of MC.[32] The MC/AGR hydrogel properties were additionally enriched by introducing the short electrospun fibers. Short electrospun fibers are especially valuable while designing hydrogel composite systems. Similarly to the fibrous mats such fibers strengthen and improve hydrogel mechanically, and after proper biological functionalization also biochemically. Contrary to fibrous mat, short fibers could be easily dispersed in the liquid media, *e.g.* hydrogel solution. Additionally, short fibers provide ECM mimicry and injection ability of whole composite material, which in the case of tissue engineering allows avoiding long-term complex surgeries. The such minimally invasive solution increases potential patients' comfort and faster convalescence.[33,34]

Electrospun-oriented PLLA fibers are widely used as scaffolds for neural tissue regeneration, mainly due to their biocompatibility, controlled degradation, and mechanical properties similar to neural tissue. The fibrous structure effectively supports the regeneration of neurons in both *in vitro* and *in vivo* conditions.[35,36] PLLA was also selected due to its appropriate stiffness and brittleness necessary for further fragmentation using ultrasonication. Nevertheless, most synthetic electrospun fibers are biochemically inert and hydrophobic, which also concerns PLLA fibers. Consequently, electrospun PLLA fibers needed adequate modifications. The first one, described in detail in our previous studies,[33] is fragmentation using ultrasonication which is to ensure the appropriate size of fibers to maintain the possibility of hydrogel injection. The second one, described in this article, was PLLA fiber modification by protein immobilization using the physical

adsorption method; such an approach overcame fibers' biological inertia. Considering CNS tissue engineering requirements and our goal to provide an appropriate microenvironment by our hydrogel system, laminin was the protein that was chosen. Laminin is one of the key ECM components that provides an effective site of IKVAV for neuronal cell adhesion and increased hydrophilicity of the short PLLA fibers. This protein is essential, especially for nerve regeneration – it effectively binds Schwann cells, and regeneration of axons takes place only in the laminin presence.[35,37]

Although MC/AGR/PLLA/fibronectin hydrogel system for brain therapy was studied previously by Rivet *et al.*,[18] we present new chemical composition of MC/AGR/PLLA/laminin that was not previously described in the literature. Additionally different materials characteristic was conducted in our studies than this described in ref. 18, which could provide new insight in designing similar approaches.

The objective of these studies was to design and fabricate a thermosensitive injectable hydrogel system that provides a hospitable environment for cell regeneration. Such an approach might serve as scaffold cell regeneration as well as a 3D cell culture model that mimics the spatial organization of neural tumors to develop new anti-cancer therapies. In this respect, MC/AGR hydrogel loaded with short electrospun PLLA/laminin fibers was designed and investigated in terms of viscosity, injectability, morphology, and the biological properties studied in direct contact with L929 fibroblasts as well as LN18 and WG4 glioma cells. Such characteristics allowed us to evaluate the potential and significance of the hydrogel system for neural tissue engineering applications and as a 3D tumor cell culture model.

2. Experimental

2.1. Preparation of MC/AGR solution

The MC and AGR powder were sterilized *via* UV for 30 min. In order to provide equal sterilization the powders were gently shaken every 10 min. The 3 and 5 wt% MC (METHOCEL A15LV, Sigma Aldrich) was added to the 3 and 3.5 wt% AGR (SeaPrepR, Lonza) aqueous solutions respectively. The powder MC and AGR were dissolved in phosphate-buffered saline (PBS, Life Technologies) separately and stirred overnight. Then, the AGR solution was mixed with the MC solution and left to stir overnight to provide a homogeneous mixture of both solutions.

The thermal physical crosslinking of MC/AGR took place under temperature increase at *ca.* 37 °C as described in our previous publications.[31,32]

2.2. MC/AGR degradation

The 3MC/3AGR and 5MC/3.5AGR hydrogel samples for degradation tests were soaked in PBS at 37 °C to mimic the physiological environment for 3 weeks. The specific procedure was conducted as follows:

(1) Each 2 ml micro-centrifuge tube was weighed before and after addition of 500 μl of hydrogels (21 samples for each group, w2-w1 was assigned as wet weight ww). The hydrogels were stored overnight at 37 °C in incubator to provide thermal physical gelation.

(2) 500 μl of PBS previously stored at 37 °C was added to the tube with hydrogel samples. The addition of heated PBS was in order to avoid hydrogel degelation.

(3) All of the samples were marked and put into an incubator at 37 °C.

(4) The PBS was changed every 3 days.

(5) At 1, 2, 4, 6, 8,12, 18 day (t), three samples of each group were taken out, the PBS was removed, and samples were dried in a vacuum dryer (MEMMERT VO) at 50 mBar for 24 h at room temperature. Dry weight (wd(t)) of each sample was weighed.

In respect to the samples weight from the 1st day, dry to wet weight ratio of 3MC/3AGR and 5MC/3.5AGR were calculated (wd(1)/ww(1)). According to this the theoretical initial dry weight at t day was calculated according the following equation:

$$\mathrm{wd}(t)^* = \mathrm{ww}(t) \times \mathrm{wd}(1)/\mathrm{ww}(1)$$

Degradation at t day was determined from the following equation:

$$\text{Degradation } (t) = \frac{\mathrm{wd}(t)^* - \mathrm{wd}(t)}{\mathrm{wd}(t)^*} \times 100\%$$

2.3. Preparation of short PLLA/laminin electrospun fibers

PLLA fibers with oriented morphology (PURASORB PL 49, Purac, Netherlands) were electrospun and subsequently fragmented using ultrasonication as previously described.[33] Their average length after ultrasonication was in the range of 40–60 μm. The PLLA mats and short fibers were sterilized using a UV light for 30 min, and then with 70% ethanol and left overnight to evaporate the residuals of ethanol. The SEM images of PLLA fibers before and after ethanol treatment were included in ESI (Fig. A†). Ethanol caused slight fibers relaxation, but the fiber morphology changes were not significant. After that, laminin was immobilized to the PLLA mats and short fibers by physical adsorption. Fiber samples without immobilized protein served as a reference. The 1 mg of laminin from Engelbreth–Holm–Swarm murine sarcoma basement membrane (Sigma Aldrich) was dissolved in PBS to obtain the protein concentration of 41 μg ml^{-1}. The solution was vortexed delicately for 2 h. The PLLA fiber mat and short fibers were immersed in laminin solutions for 24 h at 4 °C. All of the samples were washed 3 times with demineralized water for 8 h to remove non-adherent proteins.

2.4. Preparation of short fibers/hydrogel system

The PLLA and PLLA/laminin short fibers were added to the MC/AGR hydrogels at 2.5 mg ml^{-1} and 5 mg ml^{-1} and stirred on a magnetic stirrer overnight.

2.5. Fiber characterization

2.5.1 Water contact angle (WCA). The WCA measurements of electrospun mats were carried out to evaluate the changes in

the PLLA fiber's surface wettability before and after the physical adsorption of laminin. Additionally, some PLLA samples were selected and treated with 70% ethanol to decrease the surface tension of fibers and increase the amount of immobilized protein.[38] After ethanol evaporation, PLLA fibers were modified with laminin.

All of the measurements were conducted with the use of Data Physics OCA 15EC (Germany) using the sessile drop method. A 2 μl water drop was dispensed onto the surface of the fibers. The surface contact angles were measured at 1 and 3 s.

2.5.2 Bicinchoninic acid assay (BCA) assay. Total protein adsorption was assigned by using the BCA assay (Sigma Aldrich). BCA protocol assumes the formation of purple-coloured products obtained in the chelation reaction of two bicinchoninic acid molecules with Cu^{+}. The BCA working reagent preparation assumed mixing 50 parts of BCA reagent A, 50 parts of BCA reagent B, and 1 part of BCA C. Protein adsorption was determined for the previously ethanol-treated, rinsed with water, and dried PLLA electrospun mats and short fibers. The laminin solutions at concentrations of 0, 0.5, 5, 10, 15, 20, 25, and 30 μg ml^{-1} served as a standard curve.

After being weighed, mats and short fibers were placed in a 24-well plate, soaked in 200 μl of PBS, and incubated at 37 °C for 2 h. After that, 200 ml of BCA solution was added to each fibrous sample, and laminin dilutions for a standard curve, and were gently shaken at 37 °C for 2 h.

The absorbance at 562 nm was determined by a microplate spectrophotometer (Fluoroskan Ascent, Thermo Scientific). From obtained absorbance, the average absorbance values of blank samples were subtracted, and subsequently, normalized values were plotted as a function of mass concentration (g L^{-1}).

2.6. Hydrogel system/short fibers characterization

2.6.1 Viscosity. The viscosities of 3MC/3AGR and 5MC/3.5AGR hydrogel without fibers and filled with 2.5 mg ml^{-1} and 5 mg ml^{-1} of PLLA PL 49 short fibers were measured *via* HADV-III Ultra viscometer equipped with a cone/plate geometry (CP-52 (cone angle 3°)). The measurements were carried out at a constant temperature of 22 °C and 37 °C, and various constant shear rates of 50, 100, 200, 300, 400, 500, and 500 s^{-1}. Very low and high viscosities beyond the measurement possibilities were extrapolated numerically using the Carreau regression model which fit well with the experimental results.[39]

2.6.2 Injectability test. Evaluation of MC/AGR and MC/AGR/PLLA injectability was carried out *via* a servo hydraulic loading actuator (MTS Systems GmbH). The system was electronically controlled based on a displacement LVDT sensor in order to perform an accurate expansion velocity. The stand was interchangeably equipped with two various Interface load cells of 1500ASK-1000N and 1500ASK-125N of two measuring ranges: max. 1000 N and max. 125 N (Interface, Inc., Scottsdale, Arizona, USA). The 1 ml of each solution was loaded into the 1 ml glass syringe (FORTUNA OPTIMA Ganzglasspritze, Poulten Graf GmbH, Germany) coupled with a 23 gauge needle ($d = 0.34$ mm). The syringe was placed in a special holder, where the tip of the piston was in contact with the dynamometer, and the syringe was pointing downwards. The solutions were injected into previously heated and thermally crosslinked 2.5 wt% MC hydrogel, having a shear modulus that corresponds to the native human spinal cord.[31] To keep 2.5 wt% MC in crosslinked form as well as provide conditions that fairly mimic the *in vivo* conditions, the hydrogel solution was heated to 37 °C during all injectability tests.

The 1 ml of solutions were injected with two different flow rates of 1 ml min^{-1} and 0.125 ml min^{-1}. During an experiment of hydrogel injection, the injection force was registered. According to many literature reports, *i.e.* Kim *et al.*[40] the force of 50 N is considered to be the maximum value above which a manual injection is impossible. To evaluate the maximum force needed to perform the injection, the highest registered values were taken, averaged from the three measurements, and subsequently determined as the average maximum injectability force for each sample. The measurements were acquired *via* an individually prepared electronic code that was based on the MTS Systems testing environment.

2.6.3 Hydrogel system/short fibers morphology. The morphology of hydrogel loaded with short electrospun nanofibers was investigated using a Scanning Electron Microscope (SEM) (JEOL JSM-6390LV, Japan). Before imaging samples were placed into the freezer at −70 °C overnight. Then frozen samples were freeze-dried in a vacuum freeze dryer to remove water residuals. All of the freeze-dried samples were sputtered with 8 nm of gold. The acceleration voltage was 7 kV.

2.6.4 Biological tests. Based on the results of our previous studies, *i.e.*,[32] a hydrogel system of 5MC/3.5AGR was selected due to its good mechanical and biological properties. For biological studies, the following samples were studied: a pure 5MC/3.5AGR hydrogel, 5MC/3.5AGR with the addition of laminin (5MC/3.5AGR/L), 5MC/3.5AGR modified with 2.5 mg ml^{-1} short PLLA fibers (5MC/3.5AGR/F), 5MC/3.5AGR with the addition of laminin and modified with 2.5 mg ml^{-1} short PLLA fibers (5MC/3.5AGR/L/F) and 5MC/3.5AGR with the addition of laminin and modified with 2.5 mg ml^{-1} short PLLA/laminin fibers (5MC/3.5AGR/L/F/L).

Samples preparation: MC and AGR powder were sterilized with UV light for 30 min. While sterilizing, the powder was gently shaken every 10 min to provide homogenous sterilization. After that, MC and AGR powder was dissolved in sterile PBS. The choice of PBS as a solvent prevents hyperosmotic stress. For 3MC/3AGR/L, 5MC/3.5AGR/L, 3MC/3AGR/L/F/L, and 5MC/3.5AGR/L/F/L samples additionally 1mg of laminin was added to the solution.

Simultaneously, short electrospun fibers were sterilized with UV light for 30 min, then sterilized with 70 wt% ethanol and left under the hood for ethanol evaporation. After that sterile laminin was introduced to the fibers as reported in Section 2.4.2.

Then sterile hydrogel solutions and fibers were mixed and left overnight for stirring. The homogenous hydrogel solutions were stored for 72 h in the incubator at 37 °C to provide thermal crosslinking of the MC/AGR system as was previously reported.[32]

2.6.4.1 Evaluation of biocompatibility on mouse fibroblasts. Fibroblasts culture: biocompatibility tests were carried out with the use of the L929 line of fibroblasts (Sigma Aldrich). Cells were

cultured in 75 cm^2 flasks containing a medium prepared of High Glucose Dulbecco's Modified Eagle's Medium (DMEM), 10% fetal bovine serum (FBS), and 1% antibiotics. Cells were incubated in a 5% CO_2 environment at a constant temperature of 37 °C. Harvesting of the cells took place in 70–80% confluent flasks. In the first step cells in PBS. After that step, 5 ml of 0.05% of trypsin solution was added to the cells and placed in the incubator for a few minutes. Then the flask was tapped delicately in order to detach the cells. After obtaining harvested cells, 10 ml of culture medium was added and centrifuged. The centrifugation was carried out at an ambient temperature. The pellet was resuspended with a culture medium to obtain the required cell density.

Biocompatibility evaluation: to determine the cellular response to the prepared set of hydrogels loaded with short fibers, a series of different studies were performed including cytotoxicity on hydrogel extracts as well as cellular morphology evaluation in direct contact.

Extracts for *in vitro* tests were determined from 5 samples of each hydrogel type (100 μl) placed in a 48-well plate according procedure reported before.[41] Briefly, samples were immersed in 300 μl of culture medium per well, kept at 37 °C, and gently stirred for 24 h. For reference, along wells with samples, 5 wells without hydrogel were filled with the medium as well. At the same time L929 cell suspension was seeded into another 48-well plate in the same amount of wells as sample extracts plus control with density 2×10^4 cells per well and put in an incubator for 24 h. After that time the culture medium from cell-seeded wells was replaced with material extracts and the plate was placed in the incubator for another 24 h contact with materials.

In the next step, extracts were removed, and each well was filled with 180 ml of PBS and 20 ml of Presto Blue reagent. After this step, the plate was returned to the incubator for 60 min. This step was completed, and 100 ml from each well was transferred to the 96-well plate. The fluorescence read with excitation/emission 530/620 nm filters was measured with the use of 530/620 nm excitation/emission wavelength by Fluorescent Accent FL Thermo Fisher Scientific. The results were compared with the Presto Blue fluorescence of blank samples, which did not show metabolic activity, and the control (Tissue Culture Plate TCP), which showed 100% of metabolic activity.

Fibroblast morphology in contact with hydrogels was analyzed with microscopy. L929 cells were seeded on crosslinked hydrogels with the density of 5×10^4 per well in 250 ml of the medium in a 24-well plate. Before analysis, seeded cells were stained with the CellTrace™ Yellow Cell Proliferation Kit (Thermo Fisher Scientific). Briefly, 3 mg of CellTrace dye-labelled 1×10^6 cells, and the staining was carried out for 20 min. After 3 days, samples were observed under fluorescence microscopy (Leica AM TIRF MC).

2.6.4.2 Evaluation of morphology of glioma cells. Glioma cells culture. Human malignant LN18 glioma cells were obtained from American type culture collection and were cultured in Dulbecco's-modified Eagles' medium (DMEM) supplemented with 10% fetal bovine serum (FBS; Gibco, Invitrogen) and antibiotics: 100 ml^{-1} penicillin and 100 μg ml^{-1} streptomycin (Gibco, Invitrogen) in a humidified atmosphere of CO_2/air (5%/95%) at 37 °C (Heraeus, Hanau). Cell lines were authenticated using multiplex cell authentication by Multiplexion in Heidelberg, Germany.

Patient-derived glioma cell culture WG4 (GBM WHO grade 4) was developed as previously described.[42] Cells were cultured in DMEM/Nutrient Mixture F-12, GlutaMAX™ medium (DMEM/F-12, GlutaMAX™) supplemented with 10% FBS (Gibco, Invitrogen) and antibiotics (100 U per ml penicillin, 100 μg ml^{-1} streptomycin) in a humidified atmosphere of CO_2/air (5%/95%) at 37 °C (Heraeus, Hanau).

For morphological analysis of glioma cells, LN18 or WG4 cells were seeded (5×10^4 or 3×10^4 per well, respectively) onto crosslinked hydrogels-coated 24-well plates in 300 ml of appropriate medium. Before seeding, glioma cells were stained with 5 μM CellTrace™ Yellow dye for 20 min according to the manufacturer's instructions (CellTrace TM Cell Proliferation Kit, Thermo Fisher Scientific). The changes in cell morphology were monitored at various times by fluorescence microscopy (OLYMPUS IX70) using excitation at 530–550 nm.

WG4 cell morphology in contact with hydrogels in higher magnification was analyzed with fluorescence microscopy. Similar to the above-described methodology, WG4 cells were stained with the CellTrace™ Yellow Cell Proliferation Kit (Thermo Fisher Scientific) and seeded on crosslinked hydrogels. After 1 and 3 days, samples were observed under fluorescence microscopy (Leica AM TIRF MC) in transmitted light axis brightfield mode (TL-BF) and fluorescence mode to show cellular-substrates integration.

2.6.4.3 Statistics. The one-way ANOVA method was used to evaluate the statistical significance between the wettability of unmodified PLLA fibers, PLLA modified with laminin, PLLA modified with EtOH, and subsequently with laminin; the amount of immobilized laminin to the electrospun, fragmented, and EtOH-modified PLLA fibers. Additionally, the same statistic was used to evaluate the statistical significance between the forces needed to inject hydrogel systems and hydrogel systems loaded with nanofibers; and biological studies. A Tukey's test of all groups evaluated the statistical significance between individuals. The statistical analyses were conducted for $p < 0.05$ using GraphPad Prism 9.4.1 Software. The p below 0.05 was considered to be significant statistically, where $0.05 > p > 0.01$ is assigned as "*", $0.01 > p > 0.001$ is assigned as "**", $p < 0.001$ is assigned as "***", while $p < 0.0001$ is assigned as "****".

The WCA, BCA, viscosity, injectability, and cytotoxicity data are shown as mean ± SD ($n = 3$).

3. Results

3.1. MC/AGR degradation

The degradation rate of MC/AGR showed sustained degradation of both 3MC/3AGR and 5MC/3.5AGR over 12 days. The full materials' degradation occurred after 18 days. The 5MC/3.5AGR resulted in slightly slower degradation than 3MC/3AGR during 12 days of degradation studies (Fig. 1).

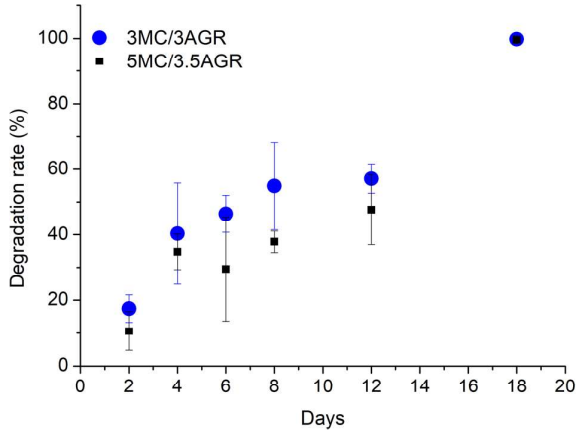

Fig. 1 Degradation of 3MC/3AGR and 5MC/3.5MC for 3 weeks at 37 °C.

3.2. Fiber characterization

3.2.1 WCA. The results of WCA measurements before and after laminin incorporation into the fibers are shown in Fig. 2. Additionally, some of the PLLA/laminin samples were previously treated with EtOH to decrease the surface tension of the fiber mat. The contact angles for all samples were in the range of 98–125 °. As predicted, the short fiber samples modified with laminin and previously modified with EtOH and laminin showed a slight decrease in contact angle compared to the non-treated samples (Fig. 2).

3.2.2 BCA. Surface modification with proteins *via* physical adsorption involves such interactions as electrostatic, hydrogen, hydrophobic, and van der Waals, which allows good biomolecule adhesion to the fibers surface.[43,44] Laminin was selected to determine its adhesion ability to electrospun mats as well as short fibers made of PLLA. Since there are many reports of qualitative studies of laminin-PLLA relations using X-ray photoelectron spectrometry (XPS) (*e.g.* ref. 35, 45 and 46), our studies were focused on quantification of laminin coupled onto fibers *via* BCA assay (Fig. 3). The two parameters that were considered to improve laminin adsorption were taken into account. One of them was a higher area of short fibers, while another was the additional treatment of PLLA fibers with EtOH before they were adsorbed with laminin.

The BCA assay indicated that both factors – fibers fragmentation and EtOH treatment lead to an increase in the amount of adsorbed laminin on the fibers surface, resulting in the highest adsorption for short fibers treated with EtOH (Fig. 3).

3.3. Short fibers/hydrogel system characterization

3.3.1 Viscosity. The viscosity was determined for 3MC/3AGR and 5MC/3.5AGR at different shear rates at room and physiological temperatures. The viscosity measurements as a function of shear rates indicate non-Newtonian shear-thinning characters of investigated hydrogels (Fig. 4). The Carreau model, commonly used to describe shear-thinning fluids [*e.g.* ref. 48], was well fitted to our experimental data, with R^2 >

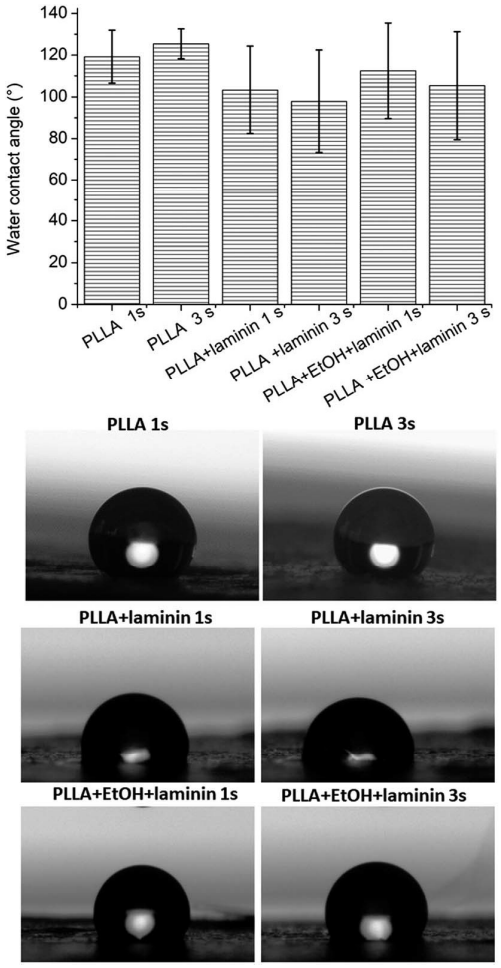

Fig. 2 WCA measurements of PLLA before laminin functionalization, after EtOH treatment, and after laminin functionalization.

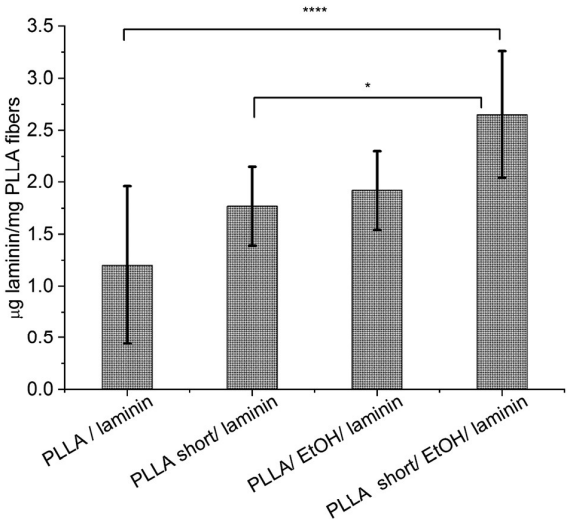

Fig. 3 Quantitative determination of laminin on PLLA fibers *via* BCA assay. Statistical significance: *p < 0.05, ****p < 0.0001.

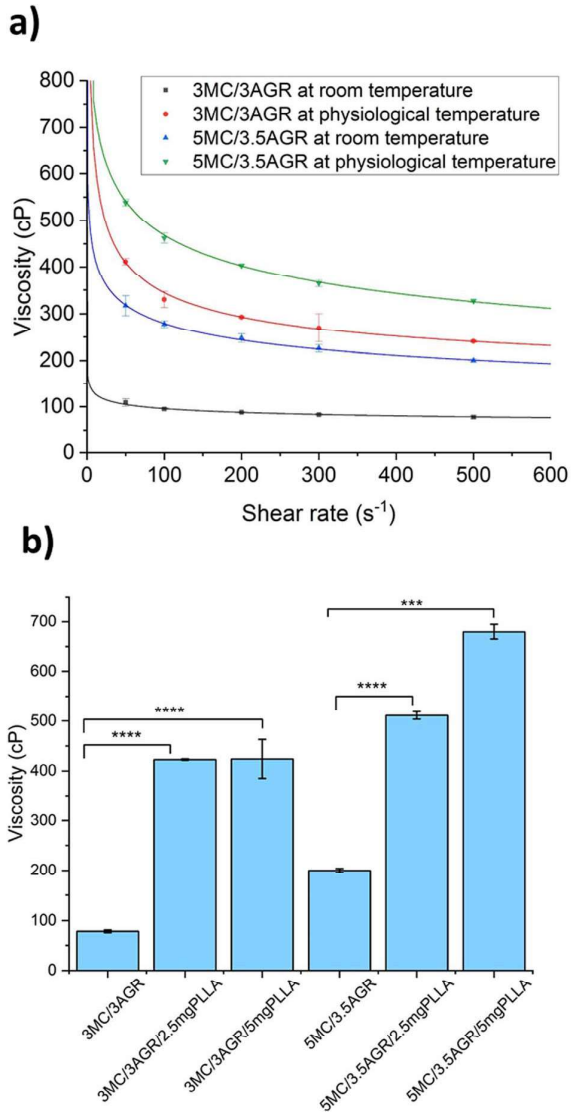

Fig. 4 (a) 3MC/3AGR and 5MC/3.5AGR viscosities *vs.* shear rate fitted with Carreau-model, (b) viscosity of 3MC/3AGR and 5MC/3.5AGR before and after short fibers addition at $\gamma = 500\ s^{-1}$ at room temperature. Statistical significance: ***$p < 0.001$, ****$p < 0.0001$.

0.94. Irrespective of the temperature, MC/AGR showed the shear-thinning effect, being most pronounced for higher temperature and polymer concentration. The effect of temperature on shear thinning phenomena is well pronounced at lower polymer concentrations (3MC/3AGR) (Fig. 4a).

Another observation is an increase in the viscosity of hydrogel systems with the MC and AGR concentration and the addition of short fibers. The addition of short fibers statistically significantly increased the viscosity of the hydrogel system (Fig. 4b).

3.3.2 Injectability tests. In these studies, injectability measurements are defined as the easiness of hydrogel extrusion represented as the injection force. According to the literature reports[47,48] there are three components of injection force that were observed during force measurements (Fig. 5b). The first one is a plunger-stopper break-loose force (PBF), which is the force initiating the displacement of the plunger. In our studies, PBF was not analyzed due to using of a special glass syringe with a precisely adjusted plunger, which enables its easy slide resulting in minimization of gliding force under steady conditions, allowing neglecting PBF.[49] The second one is a dynamic glide force (DGF), that provides approximately sustained movement of the hydrogel out of the syringe (Fig. 5b).[50] The last one is a maximum force (F_{max}), the highest force that is needed to move the plunger during the injection (Fig. 5b). Usually, the F_{max} and the PBF are the same values.[51] In our studies, F_{max} results from the materials' nature, *i.e.*, when hydrogel aggregates or accumulation of short fibers reaches the syringe, the force increases rapidly for a moment and then returns to the steady state.

Fig. 6 shows the average forces, *i.e.*, DGF, and F_{max}. The measurements were conducted for a volumetric flow rate of 1ml min^{-1} (Fig. 6a) and 0.125 ml min^{-1} (Fig. 6b). According to the literature reports, injection ability depends on needle size and geometry, injection rate, *i.e.*, volumetric flow rate, and the viscosity of the hydrogel.[47] In our studies, we used one needle size of 23G as commonly used for manual injection, as it limits invasiveness and increases patients' comfort.[51]

For the applied flow rate of 1 ml min^{-1}, it was observed a statistically significant increase in DGF with hydrogel systems concentrations, and the content of short fibers in the solution (Fig. 6a). Despite the visible trend of increase in F_{max} with increasing viscosity of hydrogel systems, the statistically significant value was observed only between the smallest MC/AGR concentration without PLLA fibers and the highest MC/AGR concentration with the largest amounts of PLLA fibers.

For a flow rate of 0.125 ml min^{-1} (Fig. 6b), the forces were practically independent of the samples' viscosity, and the differences between them were statistically insignificant. For this flow rate, the DGF and F_{max} forces were lower in comparison to 1 ml ml^{-1}.

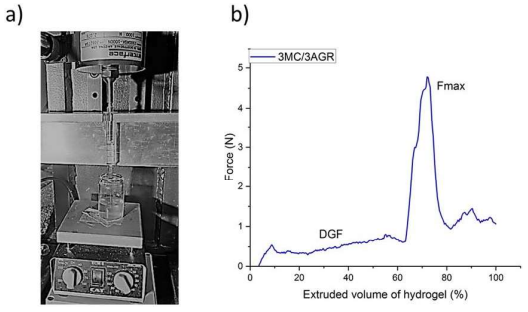

Fig. 5 Injectability test of MC/AGR hydrogels and MC/AGR short PLLA fibers hydrogel systems: (a) digital image of injectability test. The hydrogel system injection into the hydrogel, which simulates storage modulus (G') of the spinal cord, *i.e.* 5–42 kPa,[52] (b) representative example of the force measurement as a function of extruded volume (%) of 3MC/3AGR hydrogel at flow rate 0.125 ml min^{-1}.

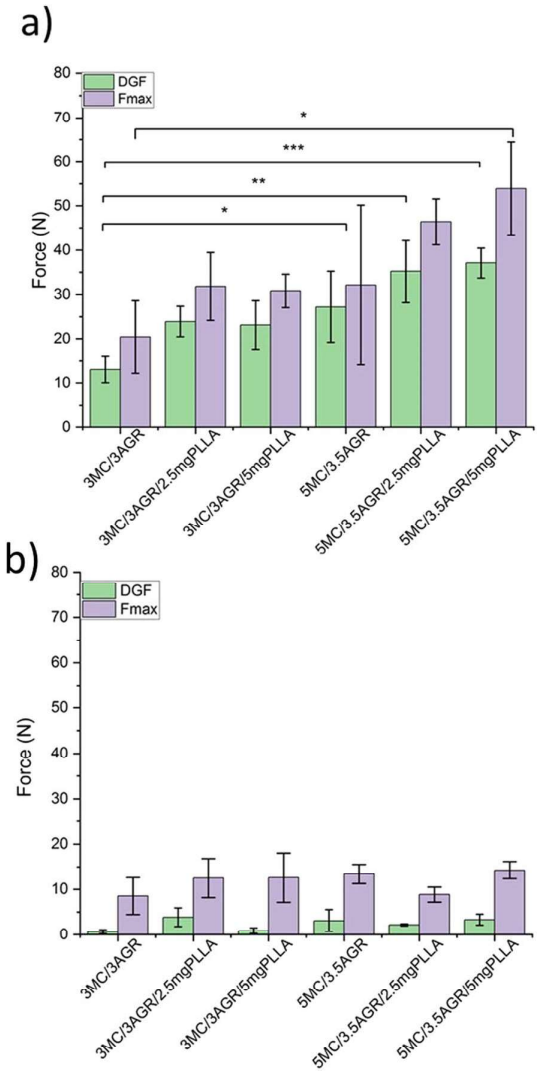

Fig. 6 Average forces, *i.e.*, DGF, and F_{max}, needed to make an injection of hydrogel through a 23G needle for various MC/AGR concentrations and PLLA fibers contents. The applied flow rates of (a) 1 ml min^{-1}, (b) 0.125 ml min^{-1}. Statistical significance: *$p < 0.05$, **$p < 0.01$, ***$p < 0.001$.

Additionally, for both flow rates, it was observed that short PLA fibers addition increased the F_{max} needed for hydrogel system injection. However, no significant differences in forces with the amounts of added fibers were observed.

3.3.3 SEM. The SEM images presented in Fig. 7 compare the hydrogel of 3MC/3AGR and 5MC/3.5AGR before and after PLLA short fibers addition. The images show the presence of short PLLA fibers inside the hydrogel structure. The morphology of both 3MC/3AGR and 5MC/3.5AGR filled with 2.5 and 5 mg of PLLA short fibers showed complex, 3D characteristic structures.

3.3.4 Biological tests

3.3.4.1 Evaluation of biocompatibility. Viability tests were conducted using Presto Blue assay on the above 5MC/3.5AGR

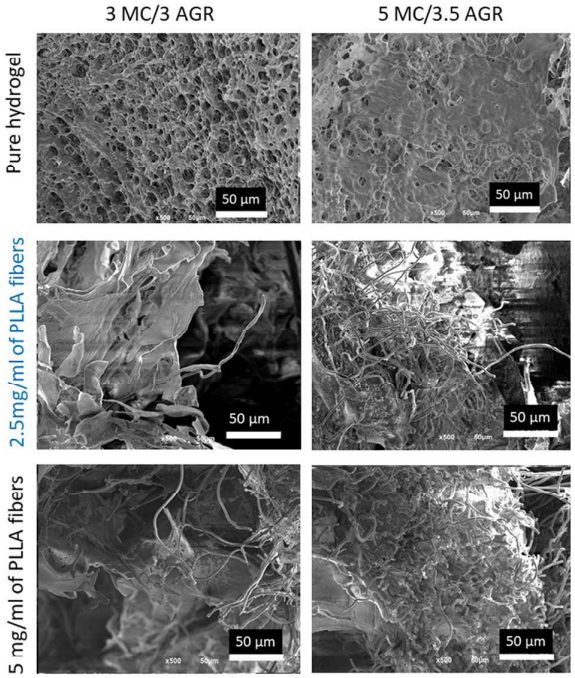

Fig. 7 SEM images of pure 3MC/3AGR and 5MC/3.5AGR hydrogel and after subsequent PLLA short fibers addition.

hydrogel systems extracts after one and three days. Conducting such studies allowed us to assess the materials' relevance for tissue engineering applications.

The results indicated the cell viability was at a similar level as the control (tissue culture plastic (TCP)) and did not show values below 70%. A value of ≥70% under ISO 10993-5 standard is considered to be the limit of nontoxicity. The cell viability of most of the samples was comparable to the control. The exception was the 5MC/3.5AGR_L/F/L sample, where cell

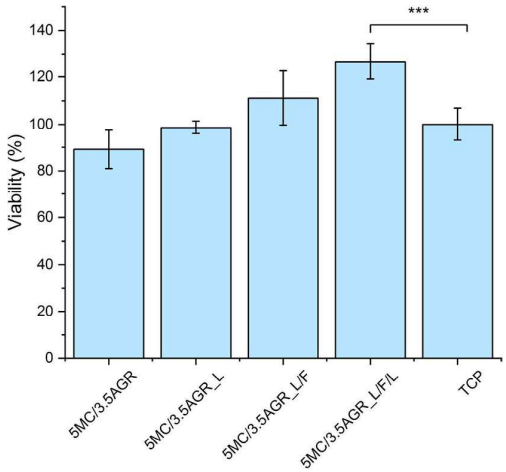

Fig. 8 Fibroblasts viability tests on extracts. Statistical significance ***$p < 0.001$.

viability was statistically significantly higher in comparison to the control (Fig. 8).

3.3.4.2 Morphology of fibroblasts seeded on hydrogel systems and hydrogel systems loaded with short fibers. The L929 fibroblasts morphology on 5MC/3.5AGR hydrogel, 5MC/3.5AGR_L (hydrogel with added laminin), 5MC/3.5AGR_L/F (hydrogel with added laminin and modified with short PLLA fibers), and 5MC/3.5AGR_L/F/L (hydrogel with added laminin and modified with short PLLA/laminin fibers) using FM are shown in Fig. 9. In comparison to the control TCP (tissue culture plastic) the materials show increased amounts of fibroblasts, their homogeneous distribution on the hydrogel surface. Cellular spreading and extended morphology of cells seeded on hydrogels are characteristic of proper L929 growth and indicator of good material–cell interactions. Such morphology was observed for 5MC/3.5AGR_L and 5MC/3.5AGR_L/F in comparison to the TCP. The 5MC/3.5AGR_L/F/L showed a different distribution than other samples and the control. It could be the effect of cell aggregates and multilayering formation, where cells overgrow on each other forming many layers of variously oriented cells due to a laminin-rich substrate.[53]

A fibroblast morphology is bipolar with parallel orientation to the substrate,[54] such orientation is especially visible on Fig. 9 for hydrogel 5MC/3.5AGR. Cells seeded on 5MC/3.5AGR_L and 5MC/3.5AGR_L/F hydrogels indicated spindle-like morphology characteristic of polar substrates and good cellular interaction. The fibroblast amount on most hydrogels was similar to the control which corresponds with cellular viability (Fig. 8).

3.3.4.3 Morphology of glioma cells seeded on hydrogel systems and hydrogel systems loaded with short fibers. LN18 and WG4 glioma cells cultured on 3D hydrogels substrates: 5MC/3.5AGR, 5MC/3.5AGR_L, 5MC/3.5AGR_L/F, and 5MC/3.5AGR_L/F/L were compared with 2D monolayer culture (TCP). The 2D monolayer culture was characterized by flat cell morphology for both glioma cell lines. The presence of protruded serval broad lamellipodium on 2D monolayer culture was especially visible for both lines after 3 days of culturing (Fig. 10 and 11). The 3D cell culture hydrogels exhibited aggregate formation and related round-shape morphology for LN18 cells after one and three days of cell culture.

Contrary to LN18, the WG4 cells seeded on 3D hydrogels showed spindle morphology with clear polarity after one and three days (Fig. 11).

All hydrogels were noncytotoxic for glioma cell growth and proliferation. The glioma cell from both lines was in various hydrogel heights providing their infiltration in hydrogel volumes.

Images from fluorescence microscopy of WG4 cells cultured on 3D hydrogels substrates were taken in transmitted light axis brightfield mode (TL-BF) and fluorescence mode after 1 and 3 days of culturing. Images in transmission show hydrogels morphology and short fibers occurrence (ESI Fig. B and C,† left column). Cellular skeleton was illustrated in fluorescence mode (ESI Fig. B and C,† middle column). Images from both modes were merged to highlight cellular-hydrogel integration (Fig. Band C,† right column). After 3 days of culturing, WG4

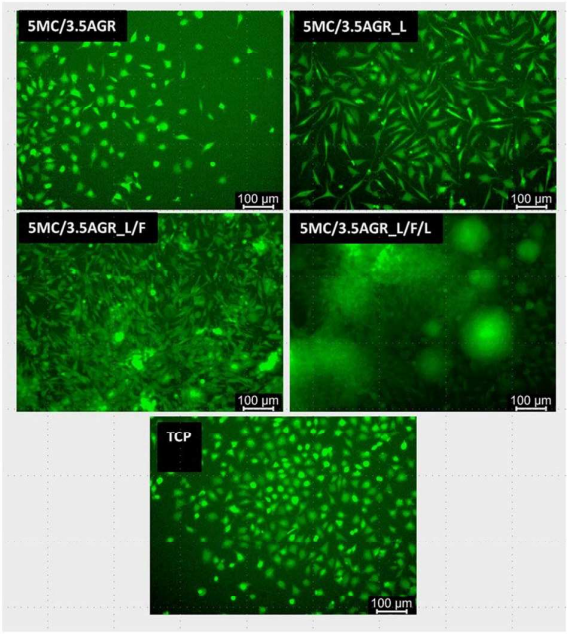

Fig. 9 FM images of L929 fibroblast morphology while seeded on various variants of MC/AGR hydrogel systems after 3 days of culturing.

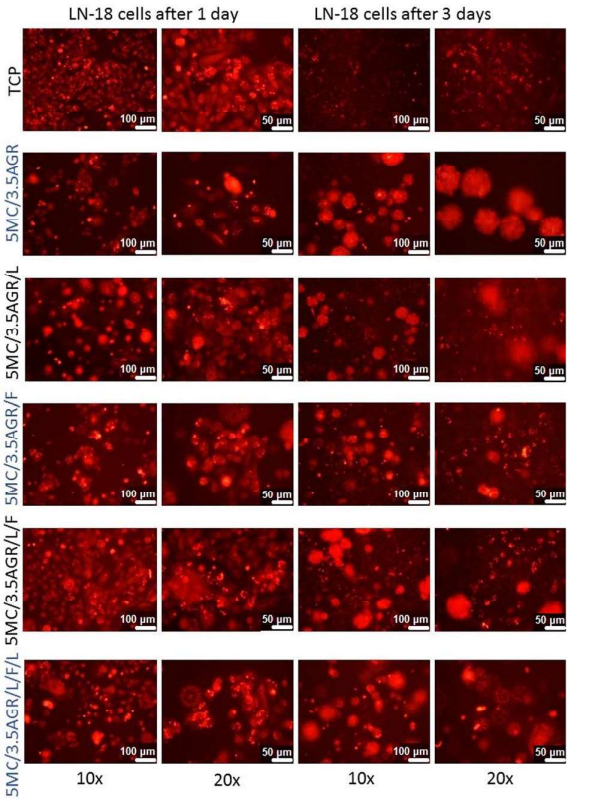

Fig. 10 LN18 glioma cell morphology by FM after 1 and 3 days of culturing.

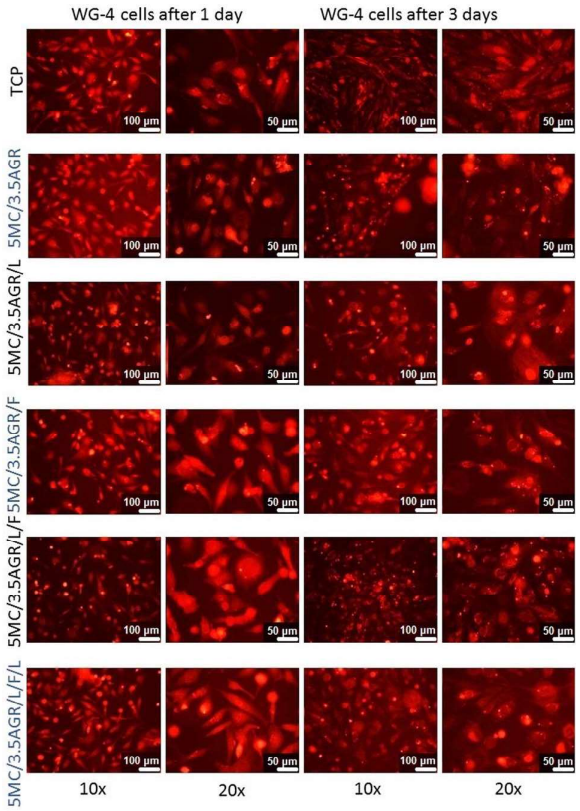

Fig. 11 WG4 glioma cell morphology by FM after 1 and 3 days of culturing.

cells seeded on 5MC/3.5AGR_L/F/L showed the best connection between the cells and show well-developed lamellipodia with filopodia in comparison to other samples and the control.

4. Discussion

In this paper, a thermosensitive injectable MC/AGR hydrogel system loaded with short electrospun bioactive PLLA/laminin fibers as a smart scaffold for tissue engineering or a 3D cell culture model has been studied.

The degradation rate of hydrogel plays an important role in scaffolds implanting and cell-material response. Proper scaffold degradation should provide tissues outgrowth and vascularization at lesion. For instance, scaffolds dedicated bone tissue engineering should not degrade for two weeks, while for central nervous system tissue engineering biomaterial should be stable for *ca.* 1–2 months.[55] In our results, both materials degraded after 18 days indicating, in the future degradation rate should be improved by incorporation of some additives or increasing the concentrations of both hydrogel components. According to the Zhuo et al.,[55] adding polyethylene glycol (PEG) to MC could extend the degradation to ca. 50% after 21 days, and a higher MC contribution in the solution could decrease the degradation rate in hyaluronic acid/MC hydrogel due to its stable chemical structure at physiological conditions.

Still, during our biological studies, both hydrogels weight loss was in the range of 10–17% after 2 days of cell culturing, which according to the literature, *e.g.*, ref. 56 is irrelevant to the 3 day studied cell response.

Laminin, used by us as for modification of short fibers, is ECM native protein that is synthesized after nerve damage and supplies surface cues essential to neurite outgrowth and regeneration.[57] Aliphatic polyesters such as PLLA are biochemically inert, decreasing cell attachment to the material. To overcome this limitation, various chemical (*e.g.* aminolysis, hydrolysis, chemical grafting) and physical (*e.g.* physical adsorption, layer-by-layer assembly) functionalization methods and protein immobilization are used. In comparison to chemical fiber modification methods, the physical adsorption of laminin into PLLA fiber's surface allowed to keep the bulk properties of the polymer and mechanical properties,[43] and simultaneously increase hydrophilicity and provide bioactive surface cues enhancing cell–materials attachment. The studies dedicated to short PLLA fibers modification with laminin and previously treated with EtOH showed the most satisfactory increase of hydrophilicity and laminin attachment. This is most likely the effect of a high surface area of short electrospun fibers, increased surface roughness,[58] and lower surface tension for EtOH-treated mats.[59,60] All of these parameters are favorable from the cellular perspective.

The MC/AGR hydrogel system loaded with short electrospun bioactive PLLA/laminin fibers was characterized in terms of viscosity, injectability, morphology, and biological properties.

The observed increase of viscosity measured at 37 °C is a consequence of the thermal gelation of MC. Regardless of the temperature, the hydrogel system characterized the shear-thinning effect, which is a consequence of molecular disentanglement and chain alignment toward applied forces. It leads to a reduction of molecular interactions and a larger amount of free space, resulting in viscosity reduction. This effect is naturally better manifested in higher molecular weight polymers or in physically crosslinked polymers like our MC/AGR hydrogel at 37 °C, being highly entangled systems. In the case of a relatively low concentration system, for instance, 3MC/3AGR, at room temperature, the entanglement density is expected to be low at rest, so there is no large shear thinning effect. An increase of shear thinning effect for such low concentrated systems is evident at higher temperature at which a physical crosslinking occurs, increasing effective chain entanglements at rest.

Additionally, all of the obtained viscosities of hydrogels and short fibers/hydrogel systems are below 1000 cP (Fig. 4). According to Bradshaw *et al.*,[61] this value is considered to be a limit of injection ability through a 23 gauge needle. To confirm these reports, additional studies of injectability tests on hydrogels and short fibers/hydrogel systems were carried out.

The injectability tests were conducted to study materials from a practical clinical perspective. Depending on applied injection rates, DGF and F_{max} were different, the higher injection rate resulted in higher DGF and F_{max}. The results were consistent with the literature reports, *i.e.* ref. 50, showing that the slower injection rate could overcome difficulties caused by

large aggregates during hydrogel extrusion, resulting in reduction of injection force.

Our results clearly documented an increase of the F_{max} after short PLLA fibers addition. The lack of any statistically significant differences in forces as a function of added fibers content could be explained by a weak dependence of PLLA fiber orientation along the applied shear on the fibers concentration, at least in this range of concentrations, resulting in insignificant effect on the ultimate viscosity at a particular shear rate.

According to the literature reports *e.g.* Kim *et al.*[40] 30 N is the F_{max}, which is reasonable to make an injection by humans. Above 30 N injection by humans remains difficult or even impossible. From Fig. 6a it is evident that when the flow rate of 1 ml min^{-1} is applied, only 3MC/3AGR, 3MC/3AGR loaded with PLLA fibers, and 5MC/3.5AGR pure hydrogel are within the F_{max} limit. While the flow rate is decreased (Fig. 6b), all of the measured samples showed a F_{max} below 20 N. Thus, similarly to ref. 50, by decreasing the volumetric flow rate, all of the hydrogels could be easily injected through a 23G needle by humans.

The importance of ECM-mimicking morphology provides topographical cues for cellular adhesion and allows nutrients and gas transportation, which is also justified in the literature.[62,63] The morphology of both hydrogel system variants showed unique 3D fibrous structures that, according to literature reports, are similar to native ECM in rat spinal cord.[64,65] Additionally, hydrogel systems functionalized with short PLLA fibers also showed a clear resemblance to porcine native cartilage ECM as shown by Chen *et al.*[66] According to Narkar *et al.*,[67] designed biomaterials for tissue engineering applications should not only mimic native ECM in such biological stimuli as adhesive proteins and provide adequate mechanical properties but also should provide morphology that various cells could respond to.

In vivo increased cell proliferation rates evoked by a favorable environment enhance tissue regeneration faster.[68] Additionally, the laminin-rich scaffolds are especially decent from the perspective of nerve regeneration, where they provide guidance cues to ensuing axons that are capable of migrating from the proximal to distal ends. Such material's functionalization increases their functionalities range: laminin-rich scaffolds not only would enhance nerve regeneration but also, with the use of modern processing methods, could increase bone regeneration capabilities.[69] The presence of a high amount of ECM protein contact guidance cues in the hydrogel system, consistent with literature reports, resulted in increased cell viability.[70]

Another important factor determining scaffold relevance for tissue engineering applications is the morphology of cells subcultured onto the scaffold. Cell morphology is strongly involved in overall physiology and could point out such processes as apoptosis or growth inhibition.[71] Also, cell distribution could provide decent information on whether cells are well attached to the material. The homogenous cell distribution indicates high cell adhesion to the scaffold, while the formation of cellular agglomerated clusters indicates the multilayering formation as a result of laminin-rich substrate. Most of the studied hydrogels substrates showed higher amounts of flattened and extended cells distributed homogeneously on the surface of the whole material compared to the control. This observation confirmed good physiology and cellular interaction with hydrogels. An unusual morphology of 5MC/3.5AGR_L/F/L (Fig. 9) could be the effect of cellular aggregation or cell multilayering formation, where cells overgrow on each other forming many layers of cells. Since this variant of the hydrogel system had the highest amounts of laminin, the multilayering effect of the cells could be the consequence of intensive ECM production by cells in such an environment and higher proliferation rate, which is clearly visible in Fig. 9. We observed increased viability and proliferation of cells seeded on hydrogels with laminin additive (Fig. 8 and 9), similarly to the literature reports.[72,73]

Glioma cell morphology and motility highly depend on three-dimensional architecture *in vivo*, substrate stiffness, and biochemical signalization.[74,75] It is challenging to provide all of these factors in classic 2D culture. Application of 3D hydrogel model *in vitro* to study glioma cell motility, the morphology, proliferation and function of the cells therein is more adequate to the actual *in vivo* conditions than 2D cultures.

The glioma cell morphology could provide crucial information about their migration pattern, which is a prerequisite for tumor invasiveness and metastasizing ability but also their physiology. A round glioma cell morphology indicates the smallest adherent area with little actin-rich protrusions. Such morphology demonstrates no interactions between the substrate and the cells. Elongated morphology with well-developed filopodia and lamellipodia demonstrates higher migration rates and increased adhesion to the substrate. Additionally, LN18 cells are spindle-shaped and WG4 are more star-shaped cells. Due to the change of the media from standard medium (which contains serums) to stem cell culture medium (without serum, but with growth factors EGF, FGF and supplement B27), both LN18 and WG4 form spheres.[76] Therefore, the spherical shape of the cell seeded on hydrogels may be a sign of the lack of access of cells to the serum in the hydrogel.

Substrate stiffness also is an important parameter in glioma cell proliferation. Pogoda *et al.* reported, glioma cells do not spread on lower stiffness of hydrogel substrates showing round morphology.[75] In other studies, Ulrich *et al.*[77] reported glioma cells seeded on stiffer hydrogel substrates significantly influence motility and increase cellular proliferation in comparison to substrates with mechanical properties similar to native tissues. Glioma cell migration depends on contractile forces generated by actomyosin and relies on the regulation of dynamic spaces between the cellular cytoskeleton and ECM. Stiffer surfaces increase the expression and activity of contractile proteins in glioma cells. Additionally, for glioma cells seeded on the stiffer substrate, the confluency was faster and this phenomenon is most likely the effect of the changed cell cycle upon the change of mechanochemical feedback during mitosis.[77] LN18 cells have a smaller volume than WG4, therefore their interaction with the hydrogel results from the difference in stiffness. We may also cell behavior on our hydrogels according to the Johnson–Kendall–Roberts (JKR) theory which predicts the form of contacts between soft, adhesive surfaces by balancing

adhesion energy, favoring contact, against elastic energy and opposes deformation.[78] When the contact radius of the cell with hydrogel is much larger than solid surface tension/substrate stiffnesses (Ysv/E), the contact is described by the JKR theory, which balances adhesion and elastic stresses. The surface tension contribution is negligible. We presume this to be the case with WG4 on fiber hydrogels. However, when the contact radius is much smaller than Ysv/E, surface tension governs contact mechanics and adhesion mimics adsorption on a fluid interface. The undeformed solid surface hits the particle at a fixed contact angle given by the generalized Young's law. Elastic forces are negligible. This behavior is observed for LN18 cells on hydrogels with lower Young's modulus. It corresponds also with previous observation, that LN18 which are smaller than WG4, seeded collapse in hydrogels with lower Young modulus as spheres. The retention of the spherical shape is additionally caused by lower access to the serum in media.[76]

Additionally, biochemical cues play a crucial role in glioma cells' stimulation or inhibition. According to the literature,[79] laminin stimulates human glioma cell migration *in vitro*. Thus, in our studies, the WG4 cell showed the spindle-like morphology and the best-developed lamellipodia with filopodia, accompanied cellular migration, while seeded on the sample with the highest amounts of laminin. Future studies could use such a 3D laminin-rich hydrogel platform loaded with fibers to investigate the characteristic features of glioma cells and could be an essential part of the complex dependencies of growth factors, integrins, and extracellular matrix during glioma cell invasion.

Conclusions

The conducted research was focused on designing modern and smart kinds of material – injectable thermosensitive hydrogel loaded with short bioactive electrospun nanofibers. Although hydrogels and electrospun fibers separately are commonly used in tissue engineering, combination of short electrospun PLLA/laminin fibers with MC/AGR hydrogel is a novelty in the context of currently published literature reports. The obtained results provide fundamental knowledge of composite material which could be valuable for both materials science and tissue engineering. Our results show that laminin incorporation *via* physical adsorption to the PLLA short fibers with previous EtOH treatment efficiently decreased the water contact angle. The properties of PLLA short fibers, *i.e.*, a large surface area, and roughness, as well as adequate sample preparation using EtOH reducing surface tension, lead to the incorporation of the largest amount of protein. The introduction of modified short fibers into hydrogel allows the system to mimic the native ECM morphology, providing good cellular response, *i.e.*, cell–material interactions and increased fibroblasts and WG4 cell proliferation.

Despite the fact that addition of short fibers lead to increase of hydrogel system viscosity, injectability tests have shown that, depending on the injection rate used, hydrogels loaded with short fibers could be extruded with a force considered reasonable for a human.

In the future studies, thermosensitive hydrogels loaded with short fibers could be additionally modified with some additives such as PEG to improve the hydrogels degradation rate, and studied more thoroughly in terms of neural cell response. On the other hand, considering increased stiffness of material, its injection ability and lack of effective therapies for cartilage defects, cartilage tissue engineering could be also the right direction.

On the other hand, considering good glioma cells response, such approaches should serve as a 3D cell culturing platform for studying, understanding and manipulating glioma cell physiology. An interesting study for the future assumes hydrogel systems that could be integrated with microfluidic devices to study static and dynamic glioma cell growth conditions as more sophisticated model for the study of glioma cells behavior in a controlled microenvironment generated by fluidic conditions in an ECM-biomimetic hydrogel matrix.

Author contributions

B. N. S., D. K. and P. S. conceived the project. B. N. S. optimized and developed the hydrogel systems loaded with short bioactive fibers. B. N. S. performed WCA, BCA, viscosity measurements and analysed the results, B. N. S. and G. M. performed injectability tests. D. K. performed *in vitro* tests on fibroblasts. B. N. S. and D. K. analysed *in vitro* studies and performed morphological observations of fibroblasts, I. A. C. performed *in vitro* tests on glioma cells, analysed and performed morphological observations. B. N. S, D. K., G. M., I. A. C. and P. S. wrote the manuscript. B. N. S. providedfinancial support.

Conflicts of interest

There are no conflicts to declare.

Acknowledgements

This research was funded by the Narodowe Centrum Nauki (NCN), grant number 2018/29/N/ST8/00780.

References

1 Y. Zhao, H. Mu, Y. Huang, S. Li, Y. Wang, R. A. Stetler and Y. Shi, *J. Neuroinflammation*, 2022, **19**(1), 1–19.
2 A. Movahedpour, O. Vakili, M. Khalifeh, P. Mousavi, A. Mahmoodzadeh, M. Taheri-Anganeh and S. H. Khatami, *Cell Biochem. Funct.*, 2022, **40**(3), 232–247.
3 V. Strøm, G. Månum, M. Arora, C. Joseph, A. Kyriakides, M. Le Fort and J. Middleton, *J. Rehabil. Med.*, 2022, **54**, jrm00302.
4 D. Clark, J. B. Cheserem, I. D. Bhagavatula, A. Figaji and P. Hutchinson, *Neurosurgery and Global Health*, Springer, Cham, 2022, pp. 19–32.
5 A. P. Patel, J. L Fisher, E. Nichols, F. Abd-Allah, J. Abdela, A. Abdelalim and C. Fitzmaurice, *Lancet Neurol.*, 2019, **18**(4), 376–393.
6 O. Rominiyi and S. J. Collis, *Mol. Oncol.*, 2022, **16**(1), 11–41.

7 B. Ucar, *Neurochem. Int.*, 2021, **146**, 105033.
8 D. Silva, R. A. Sousa and A. J. Salgado, *Mater. Today Bio*, 2021, **9**, 100093.
9 C. T. Lu, Y. Z. Zhao, H. L. Wong, J. Cai, L. Peng and X. Q. Tian, *Int. J. Nanomed.*, 2014, **9**, 2241.
10 Q. Li, X. Shao, X. Dai, Q. Guo, B. Yuan, Y. Liu and W. Jiang, *NPG Asia Mater.*, 2022, **14**(1), 1–14.
11 M. Jury, I. Matthiesen, F. Rasti Boroojeni, S. L. Ludwig, L. Civitelli, T. E. Winkler and D. Aili, *Adv. Healthcare Mater.*, 2022, **11**(11), 2102097.
12 N. Shah, P. M. Hallur, R. A. Ganesh, P. Sonpatki, D. Naik, K. P. Chandrachari and A. Chaubey, *Sci. Rep.*, 2021, **11**(1), 1–18.
13 E. Ansorena, P. De Berdt, B. Ucakar, T. Simón-Yarza, D. Jacobs, O. Schakman and A. des Rieux, *Int. J. Pharm.*, 2013, **455**(1–2), 148–158.
14 A. Hsieh, T. Zahir, Y. Lapitsky, B. Amsden, W. Wan and M. S. Shoichet, *Soft Matter*, 2010, **6**, 2227–2237.
15 D. Wu, E. S. Pak, C. J. Wingard and A. K. Murashov, *Neurosci. Lett.*, 2012, **507**(1), 72–77.
16 A. Lis, D. Szarek and J. Laska, *Polim. Med.*, 2013, **43**(4), 302–312.
17 F. Guilak, D. M. Cohen, B. T. Estes, J. M. Gimble and W. Liedtke, *Cell Stem Cell*, 2009, **5**(1), 17–26.
18 C. J. Rivet, K. Zhou, R. J. Gilbert, D. I. Finkelstein and J. S. Forsythe, *Biomatter*, 2015, **5**(1), e1005527.
19 K. S. Anseth, C. N. Bowman and L. Brannon-Peppas, *Biomaterials*, 1996, **17**(17), 1647–1657.
20 J. R. Thonhoff, D. I. Lou, P. M. Jordan, X. Zhao and P. Wu, *Brain Res.*, 2008, **1187**, 42–51.
21 J. George, C. C. Hsu, L. T. B. Nguyen, H. Ye and Z. Cui, *Biotechnol. Adv.*, 2020, **42**, 107370.
22 Y. A. Miroshnikova, J. K. Mouw, J. M. Barnes, M. W. Pickup, J. N. Lakins, Y. Kim and V. M. Weaver, *Nat. Cell Biol.*, 2016, **18**(12), 1336–1345.
23 B. Niemczyk-Soczynska, A. Zaszczynska, K. Zabielski and P. Sajkiewicz, *Materials*, 2021, **14**(22), 6899.
24 L. Buzanska, M. Zychowicz, A. Sarnowska and K. Domanska-Janik, *Postepy Biochem.*, 2013, **59**(2), 175–186.
25 Y. T. Wei, W. M. Tian, X. Yu, F. Z. Cui, S. P. Hou, Q. Y. Xu and I. S. Lee, *Biomed. Mater.*, 2007, **2**(3), S142.
26 N. Comolli, B. Neuhuber, I. Fischer and A. Lowman, *Acta Biomater.*, 2009, **5**(4), 1046–1055.
27 F. Ordikhani, S. Sheth and S. P. Zustiak, *Int. J. Pharm.*, 2017, **516**(1–2), 71–81.
28 T. Ozeki, D. Kaneko, K. Hashizawa, Y. Imai, T. Tagami and H. Okada, *Int. J. Pharm.*, 2012, **427**(2), 299–304.
29 R. Curvello, V. Kast, M. H. Abuwarwar, A. L. Fletcher, G. Garnier and D. Loessner, *Front. digit. health*, 2021, **3**, 704584.
30 B. Niemczyk-Soczynska, P. Sajkiewicz and A. Gradys, *Polymers*, 2022, **14**(9), 1810.
31 B. Niemczyk-Soczynska, A. Gradys, D. Kolbuk, A. Krzton-Maziopa and P. Sajkiewicz, *Polymers*, 2019, **11**(11), 1772.
32 B. Niemczyk-Soczynska, A. Gradys, D. Kolbuk, A. Krzton-Maziopa, P. Rogujski, L. Stanaszek, B. Lukomska and P. Sajkiewicz, *RSC Adv.*, 2022, **12**(41), 26882–26894.
33 B. Niemczyk-Soczynska, J. Dulnik, O. Jeznach, D. Kolbuk and P. Sajkiewicz, *Micron*, 2021, **145**, 103066.
34 M. Wang, J. Du, M. Li, F. Pierini, X. Li, J. Yu and B. Ding, *Biomater. Sci.*, 2023, 1–12.
35 K. Zhang, H. Zheng, S. Liang and C. Gao, *Acta Biomater.*, 2016, **37**, 131–142.
36 H. S. Koh, T. Yong, C. K. Chan and S. Ramakrishna, *Biomaterials*, 2008, **29**(26), 3574–3582.
37 R. Milner, M. Wilby, S. Nishimura, K. Boylen, G. Edwards, J. Fawcett and R. Pytela, *Dev. Biol.*, 1997, **185**(2), 215–228.
38 E. J. Falde, J. Wang and M. W. Grinstaff, *RSC Adv.*, 2017, **7**(78), 49795–49798.
39 T. Bodnar, A. Sequeira and M. Prosi, *Appl. Math. Comput.*, 2011, **217**(11), 5055–5067.
40 M. H. Kim, B. S. Kim, H. Park, J. Lee and W. H. Park, *Int. J. Biol. Macromol.*, 2018, **109**, 57–64.
41 J. Dulnik, D. Kolbuk, P. Denis and P. Sajkiewicz, *Eur. Polym. J.*, 2018, **104**, 147–156.
42 I. A. Ciechomska, P. Przanowski, J. Jackl, B. Wojtas and B. Kaminska, *Sci. Rep.*, 2016, **6**(1), 1–15.
43 B. Niemczyk-Soczynska, A. Gradys and P. Sajkiewicz, *Polymers*, 2020, **12**(11), 2636.
44 D. Kolbuk, M. Ciechomska, O. Jeznach and P. Sajkiewicz, *RSC Adv.*, 2022, **12**(7), 4016–4028.
45 L. He, S. Tang, M. P. Prabhakaran, S. Liao, L. Tian, Y. Zhang and S. Ramakrishna, *Macromol. Biosci.*, 2013, **13**(11), 1601–1609.
46 S. Kakinoki and T. Yamaoka, *J. Mater. Chem. B*, 2014, **2**(31), 5061–5067.
47 F. Cilurzo, F. Selmin, P. Minghetti, M. Adami, E. Bertoni, S. Lauria and L. Montanari, *AAPS PharmSciTech*, 2016, **17**(6), 1508.
48 Q. Zhang, M. A. Fassihi and R. Fassihi, *AAPS PharmSciTech*, 2018, **19**(4), 1520–1528.
49 K. Yoshino, K. Nakamura, A. Yamashita, Y. Abe, K. Iwasaki, Y. Kanazawa and S. Suzuki, *J. Pharmaceut. Sci.*, 2014, **103**(5), 1520–1528.
50 A. Ryl and P. Owczarz, *Polymers*, 2020, **12**(10), 2260.
51 A. Shavandi, A. E. D. A. Bekhit, Z. Sun and M. A. Ali, *J. Sol. Gel Sci. Technol.*, 2016, **77**(3), 675–687.
52 R. D. Bartlett, D. Choi and J. B. Phillips, *Regen. Med.*, 2016, **11**(7), 659–673.
53 T. Boontheekul, H. J. Kong and D. J. Mooney, *Biomaterials*, 2005, **26**(15), 2455–2465.
54 N. Lakshman, A. Kim and W. M. Petroll, *Exp. Eye Res.*, 2010, **90**, 350–359.
55 F. Zhuo, X. Liu, Q. Gao, Y. Wang, K. Hu and Q. Cai, *Mater. Sci. Eng. C*, 2017, **81**, 1–7.
56 Y. Wu, Z. Yang, J. B. K. Law, A. Y. He, A. A. Abbas, V. Denslin and E. H. Lee, *Tissue Eng.*, 2017, **23**(1–2), 43–54.
57 D. McDonald, C. Cheng, Y. Chen and D. Zochodne, *Neuron Glia Biol.*, 2006, **2**, 139.
58 Y. Ren, S. Wang, R. Liu, J. Dai, X. Liu and J. Yu, *RSC Adv.*, 2016, **6**(36), 30139–30147.
59 M. Gryta, *Chem. Pap.*, 2013, **67**(9), 1201–1209.
60 C. Zhang, X. Yuan, L. Wu, Y. Han and J. Sheng, *Eur. Polym. J.*, 2005, **41**(3), 423–432.

61 J. Bradshaw and S. White, *ONdrugDelivery*, 2018, **91**, 16–21.
62 G. S. Hussey, J. L. Dziki and S. F. Badylak, *Nat. Rev. Mater.*, 2018, **3**(7), 159–173.
63 R. T. Miller, *Matrix Biol.*, 2017, **57**, 366–373.
64 A. Padhi and A. S. Nain, *Ann. Biomed. Eng.*, 2020, **48**(3), 1071–1089.
65 D. X. Ban, Y. Liu, T. W. Cao and S. J. Gao, *Spinal Cord*, 2017, **55**(4), 411–418.
66 Y. C. Chen, R. N. Chen, H. J. Jhan, D. Z. Liu, H. O. Ho, Y. Mao and M. T. Sheu, *Tissue Eng. C Methods*, 2015, **21**(9), 971–986.
67 A. R. Narkar, Z. Tong, P. Soman and J. H. Henderson, *Biomaterials*, 2022, **283**, 121450.
68 A. B. Bloom and M. H. Zaman, *Physiol. Genom.*, 2014, **46**(9), 309–314.
69 S. Ozkan, D. M. Kalyon and X. Yu, *J. Biomed. Mater. Res., Part A*, 2010, **92**(3), 1007–1018.
70 R. Junka, C. M. Valmikinathan, D. M. Kalyon and X. Yu, *J. Biomim. Biomater. Tissue Eng.*, 2013, **3**(4), 494–502.
71 B. Sarker, R. Singh, R. Silva, J. A. Roether, J. Kaschta, R. Detsch and A. R. Boccaccini, *PLoS One*, 2014, **9**(9), e107952.
72 R. Jain and S. Roy, *ACS Biomater. Sci. Eng.*, 2020, **6**(5), 2832–2846.
73 Y. Long, L. Yan, H. Dai, D. Yang, X. Wu, X. Dong and Y. Chen, *Mater. Sci. Eng. C*, 2020, **116**, 111258.
74 Y. Huang, L. Tong, L. Yi, C. Zhang, L. Hai, T. Li and X. Yang, *Mol. Med. Rep.*, 2018, **17**(1), 250–256.
75 K. Pogoda, R. Bucki, F. J. Byfield, K. Cruz, T. Lee, C. Marcinkiewicz and P. A. Janmey, *Biomacromolecules*, 2017, **18**(10), 3040–3051.
76 X. Hong, K. Chedid and S. N. Kalkanis, *Int. J. Oncol.*, 2012, **41**(5), 1693–1700.
77 T. A. Ulrich, E. M. de Juan Pardo and S. Kumar, *Cancer Res.*, 2009, **69**(10), 4167–4174.
78 R. W. Style, C. Hyland, R. Boltyanskiy, J. S. Wettlaufer and E. R. Dufresne, *Nat. Commun.*, 2013, **4**(1), 1–6.
79 B. B. Tysnes, H. K. Haugland and R. Bjerkvig, *Invasion Metastasis*, 1997, **17**(5), 270–280.

STATEMENTS OF THE CO-AUTHORS

Oświadczenie doktoranta o udziale w publikacji naukowej

Niniejszym potwierdzam, że mój wkład w przygotowanie **publikacji nr 1** tj. Niemczyk B., Sajkiewicz P., Kołbuk D, Injectable hydrogels as novel materials for central nervous system regeneration, *Journal of Neural Engineering*, Vol.15, No.5, pp.051002-1-15, **2018,** obejmował zgromadzenie danych literaturowych odnoszących się do 145 publikacji oraz ich analizę. Dodatkowo odpowiedzialna byłam za napisanie przeglądu literaturowego, przygotowanie odpowiedzi dla recenzentów oraz pełniłam funkcję autora korespondencyjnego.

Podpis doktorantki

Podpis promotora

Podpis współautorów

- dr inż. D. Kołbuk-Konieczny

Oświadczenie doktoranta o udziale w publikacji naukowej

Niniejszym potwierdzam, że mój wkład w przygotowanie **publikacji nr 2** tj. Niemczyk-Soczyńska B., Gradys A., Kołbuk D., Krzton-Maziopa A., Sajkiewicz P., Crosslinking kinetics of methylcellulose aqueous solution and its potential as a scaffold for tissue engineering, *Polymers*, Vol.11, No.11, pp.1772-1-17, **2019,** obejmował wytworzenie różnych stężeń hydrożeli metylocelulozowych, pomiary reologiczne z wykorzystaniem dynamicznej analizy mechanicznej (DMA) oraz analizę uzyskanych wyników, jak również badanie morfologii komórek za pomocą skaningowej mikroskopii elektronowej (SEM). Dodatkowo brałam czynny udział w opracowaniu wyników i dyskusji, odpowiedzialna byłam za napisanie i redagowanie manuskryptu, przygotowanie wykresów oraz figur załączonych w tekście, przygotowanie odpowiedzi dla recenzentów i wprowadzenie odpowiednich poprawek do manuskryptu oraz pełniłam funkcję autora korespondencyjnego.

Beata Niemczyk-Soczyńska

Podpis doktorantki

Podpis promotora

Podpisy współautorów

- dr inż. A. Gradys — Arkadiusz Gradys
- dr inż. D. Kołbuk-Konieczny — Kołbuk
- dr hab. inż. A. Krztoń-Maziopa — Anna Krztoń-Maziopa

Oświadczenie doktoranta o udziale w publikacji naukowej

Niniejszym potwierdzam, że mój wkład w przygotowanie **publikacji nr 3** tj. Niemczyk-Soczyńska B., Gradys A., Sajkiewicz P., Hydrophilic surface functionalization of electrospun nanofibrous scaffolds in tissue engineering, *Polymers*, Vol.12, No.11, pp.2636-1-20, **2020,** obejmował koncepcję, zgromadzenie danych literaturowych odnoszących się do 111 publikacji oraz ich analizę. Ponadto odpowiedzialna byłam za napisanie i redagowanie przeglądu literaturowego, przygotowanie odpowiedzi dla recenzentów oraz pełniłam funkcję autora korespondencyjnego.

Beata Niemczyk-Soczyńska
Podpis doktorantki

Sajkiewicz
Podpis promotora

Podpis współautorów

- dr inż. A. Gradys Arkadiusz Gradys

Oświadczenie doktoranta o udziale w publikacji naukowej

Niniejszym potwierdzam, że mój wkład w przygotowanie **publikacji nr 4** tj. Niemczyk-Soczyńska B., Dulnik J., Jeznach O., Kołbuk D., Sajkiewicz P., Shortening of electrospun PLLA fibers by ultrasonication, *Micron*, Vol.145, pp.103066-1-8, **2021,** obejmował koncepcję, realizację i optymalizację metody wytwarzania krótkich włókien PLLA metodą elektroprzędzenia i fragmentacji ultradźwiękowej. Co więcej, przeprowadziłam badania morfologii włókien z wykorzystaniem skaningowej mikroskopii elektronowej (SEM), pomiary średniego rozkładu długości oraz średnic uzyskanych włókien, średniego rozkładu ciężaru cząsteczkowego PLLA przed i po procesie elektroprzędzenia oraz fragmentacji metodą chromatografii żelowej (GPC), jak również pomiary lepkości hydrożeli z dodatkiem krótkich włókien z wykorzystaniem wiskozymetru rotacyjnego. Ponadto, wykonałam analizę wyników, przygotowałam zdjęcia i wykresy umieszczone w publikacji, przygotowałam dyskusję, odpowiedzialna byłam za napisanie i redagowanie manuskryptu, opracowanie odpowiedzi dla recenzentów oraz wprowadzenie odpowiednich poprawek do tekstu.

Beata Niemczyk-Soczyńska

Podpis doktorantki

Podpis promotora

Podpis współautorów

- mgr inż. J. Dulnik Judyta Dulnik
- mgr inż. O. Jeznach Oliwia Jeznach
- dr inż. D. Kołbuk-Konieczny Kołbuk

Oświadczenie doktoranta o udziale w publikacji naukowej

Niniejszym potwierdzam, że mój wkład w przygotowanie **publikacji nr 5** tj. Niemczyk-Soczyńska B., Sajkiewicz P., Gradys A., Toward a Better Understanding of the Gelation Mechanism of Methylcellulose via Systematic DSC Studies, *Polymers*, Vol.14, No.9, pp.1810-1-13, **2022,** obejmował przygotowanie hydrożeli metylocelulozowych oraz częściowo pomiary efektów cieplnych z wykorzystaniem różnicowej kalorymetrii skaningowej (DSC). Ponadto brałam czynny udział w redagowaniu manuskryptu, interpretacji wyników i dyskusji na temat mechanizmu sieciowania metylocelulozy. Dodatkowo odpowiedzialna byłam za przygotowanie odpowiedzi dla recenzentów.

Beata Niemczyk-Soczyńska

Podpis doktorantki

Podpis promotora

Podpis współautorów

- dr inż. A. Gradys Arkadiusz Gradys

Oświadczenie doktoranta o udziale w publikacji naukowej

Niniejszym potwierdzam, że mój wkład w przygotowanie **publikacji nr 6** tj. Niemczyk-Soczyńska B., Gradys A., Kołbuk D., Krztoń-Maziopa A., Rogujski P., Stanaszek L., Lukomska B., Sajkiewicz P., A methylcellulose/agarose hydrogel as an innovative scaffold for tissue engineering, RSC Advances, Vol.12, No.41, pp.26882-26894, **2022**, obejmował przygotowanie hydrożeli metylocelulozowo-agarozowych, pomiary reologiczne z wykorzystaniem dynamicznej analizy mechanicznej (DMA) oraz analizę uzyskanych wyników, częściowo pomiary efektów cieplnych z wykorzystaniem różnicowej kalorymetrii skaningowej (DSC), przygotowanie i analiza trójwymiarowych zdjęć przestawiających rozkład komórek w hydrożelu z wykorzystaniem mikroskopii fluorescencyjnej, analizę statystyczną, jak również przygotowanie dyskusji do uzyskanych wyników. Ponadto, odpowiedzialna byłam za przygotowanie i redagowanie manuskryptu, opracowanie odpowiedzi dla recenzentów oraz pełniłam funkcję autora korespondencyjnego.

Podpis doktorantki Beata Niemczyk-Soczyńska

Podpis promotora Piotr Sajkiewicz

Podpisy współautorów

- dr inż. A. Gradys Arkadiusz Gradys
- dr inż. D. Kołbuk-Konieczny Kołbuk
- dr hab. inż. A. Krztoń-Maziopa Anna Krztoń-Maziopa
- mgr P. Rogujski Piotr Rogujski
- dr inż. L. Stanaszek Lucyna Stanaszek
- prof. dr hab. B. Łukomska Barbara Łukomska

Oświadczenie doktoranta o udziale w publikacji naukowej

Niniejszym potwierdzam, że mój wkład w przygotowanie **publikacji nr 7** tj. Niemczyk-Soczyńska B., Kołbuk D., Mikułowski G., Ciechomska I., Sajkiewicz P., Methylcellulose/agarose hydrogel loaded with short electrospun PLLA/laminin fibers as injectable scaffold for tissue engineering/3D cell culture model for tumour therapies, *RSC Advances*, Vol. 13, No.18, pp. pp.11889-11902, 2023, obejmował przygotowanie układu hydrożelowego napełnianego krótkimi elektroprzędzionymi włóknami, badania i analizę biodegradacji układu hydrożelowego, modyfikację włókien białkiem lamininą, badania zawartości białka na powierzchni włókien testem bicynchoninowym (BCA), charakterystykę zwilżalności włókien z wykorzystaniem goniometru, badania lepkości układów hydrożelowych z wykorzystaniem wiskozymetru rotacyjnego, częściowe przeprowadzenie testów wstrzykiwalności, badania morfologii układów hydrożelowych, analizę uzyskanych wyników oraz analizę statystyczną. Dodatkowo odpowiedzialna byłam za redagowanie manuskryptu oraz przygotowanie odpowiedzi dla recenzentów.

Beata Niemczyk-Soczyńska
Podpis doktorantki

Podpis promotora

Podpisy współautorów

- dr inż. D. Kołbuk-Konieczny
- dr inż. G. Mikułowski
- dr hab. I. Ciechomska